An Improved Understanding of the Yariv Reagent - A Plant Proteoglycan Binding Dye

By Raghuraj Hoshing

A Dissertation Submitted in Partial Fulfillment of the Requirements for the Degree of Doctor of Philosophy in the Department of Chemistry at Brown University

Providence, Rhode Island
February 2023

This dissertation by Raghuraj Hoshing is accepted in its present form by the Department of Chemistry as satisfying the dissertation requirement for the degree of Doctor of Philosophy.

Date_____ _____

Amit Basu, Ph.D., Advisor

Recommended to the Graduate Council

Date_____ _____

Sarah Delaney, Ph.D., Reader

Date_____ _____

Matthew Zimmt, Ph.D., Reader

Approved by the Graduate Council

Date_____ _____

Thomas Lewis, Ph.D.,
Dean of the Graduate School

CURRICULUM VITAE

Raghuraj Hoshing
Providence, RI
raghuraj_hoshing@brown.edu

Education:

Brown University, Providence, RI
Ph.D. Organic Chemistry, expected August 2022
Graduate Research (Advisor: Prof. Amit Basu)

- Synthesized and purified azo dyes used for plant proteoglycan imaging
- Structural and biophysical characterization of azo dyes via advanced NMR, UV/vis, Mass Spec and circular dichroism spectroscopy

Sheridan Center Reflective Teaching Certificate

- Completed readings on topics such as learning design, classroom communication and creating inclusive environments
- Completed assignments and took part in workshops to discuss experience of peers in implementing reflective teaching techniques in the classroom

Rose-Hulman Institute of Technology, Terre Haute, IN
B.S. Chemistry and Biochemistry and Molecular Biology (BCMB), May 2017
Undergraduate Research (Advisor: Prof. Ross Weatherman)

- Synthesized breast cancer drug (Tamoxifen) analogs conjugated to fluorophores to investigate mode of action
- Purified and characterized products using silica gel chromatography, thin layer chromatography and NMR

Professional Appointments:

Wheaton College, Massachusetts
Brown/Wheaton Faculty Fellow, January 2022-May 2022

- Instructed Organic Chemistry 1 (Chem 253) both online and in-person
- Prepared all course material including syllabus, schedule and exams
- Taught course in flipped classroom model

Brown University, Rhode Island
Teaching Assistant (Chem 0360; Organic Chemistry II), Sep 2021- Dec 2021

- Monitored and assisted students in the lab to ensure safety and proper execution of protocols
- Graded exams
- Held office hours to answer student inquiries about lab and coursework
- Performed all the head TA duties including organizing other TAs for proctoring, assigning grading duties, insuring timely return of exam grades to students

Teaching Assistant (Chem 0350; Organic Chemistry I), June 2021- Aug 2021

- Graded exams and lab reports
- Held office hours to answer student inquiries about lab and coursework

Teaching Assistant (Chem 0360; Organic Chemistry II), Sep 2018- Dec 2018

- Monitored and assisted students in the lab to ensure safety and proper execution of protocols
- Graded exams and lab reports
- Held office hours to answer student inquiries about lab and coursework

Teaching Assistant (Chem1450; Advanced Organic Chemistry), Jan 2021 – April 2021

- Generated answer keys for and graded homework assignments
- Held office hours to answer student inquiries about coursework

Teaching Assistant (Chem1450; Advanced Organic Chemistry), Jan 2019 – May 2019

- Researched synthetic protocols required to make target compound for laboratory component of the course
- Help setup lab by ensuring availability of glassware and other materials required to execute protocols
- Demonstrated safe and proper execution of lab protocols
- Monitored and assisted students in the lab to ensure safety and proper execution of protocols
- Graded in-class quizzes
- Held office hours to answer student inquiries about lab and coursework

Teaching Assistant (Chem 0360; Organic Chemistry II), Sep 2018- Dec 2018

- Monitored and assisted students in the lab to ensure safety and proper execution of protocols
- Graded exams and lab reports
- Held office hours to answer student inquiries about lab and coursework

Midwest-Compliance Laboratories, Terre Haute

Intern Chemist, June 2015-August 2015

- Performed analytical tests in a timely fashion following Quality protocols and Standard Operating Procedures
- Maintained proper documentations (including chain of custody, data sheets) and filled out timely
- Tests performed included Disintegrations, Identification tests, Assays, Dissolutions and HPLCs

Publications:

Hoshing, R.; Saladino, M.; Kuhn, H.; Caianiello, D.; Lusi, R. F.; Basu, A., An Improved Protocol for the Synthesis and Purification of Yariv Reagents. *J. Org. Chem* **2020,** *85* (24), 16236-16242.

Hoshing, R.; Leeber, B. W., 3rd; Kuhn, H.; Caianiello, D.; Dale, B.; Saladino, M.; Lusi, R.; Palaychuk, N.; Weingarten, S.; Basu, A., The Chirality of Aggregated Yariv Reagents Correlates with Their AGP-Binding Ability*. *Chembiochem* **2021**.

Presentations:

Oral Presentation, ACS National Meeting & Exposition, San Francisco, CA
"Synthesis and purification of the Yariv reagent; a plant proteoglycan binding dye", August 2020* Online due to COVID-19

Oral Presentation, ACS National Meeting & Exposition, San Francisco, CA
"Correlation between the chirality of supramolecular aggregates of an azo dye to its plant proteoglycan binding ability" August 2020* Online due to COVID-19

Poster Presentation, ACS National Meeting & Exposition, San Francisco, CA
"Tautomerism in a supramolecular triphenyl azo dye" August 2020* Online due to COVID-19

Flash Talk and Poster Presentation, 2020 New England Glyco-Chemistry Meeting, Brandeis University
"Synthesis, purification and characterization of the Yariv reagent – A plant proteoglycan binding dye", June 2020* Online due to COVID-19

Poster Presentation, 2019 New England Glyco-Chemistry Meeting, Northeastern University
"The importance of Yariv reagent's supramolecular chirality to its AGP binding ability", June 2019

Poster Presentation, Brown Graduate Student Poster Session, Brown University
"Correlation between the chirality of supramolecular aggregates of an azo dye to its plant proteoglycan binding ability", October 2019

Oral Presentation, ACS Spring 2020 National Meeting & Exposition, Philadelphia, PA
"Correlation between the chirality of supramolecular aggregates of an azo dye to its plant proteoglycan binding ability", March 2020* Cancelled due to COVID-19

Poster Presentation, 2016 Lilly Undergraduate Symposium, Eli-Lilly, Indianapolis
"Synthesis and Analysis of Tamoxifen Derivatives", August 2016

Oral Presentation, 2017 Butler Undergraduate Research Conference, Butler University
"Synthesis and Analysis of Tamoxifen Derivatives", April 2017

Oral Presentation, 13th Annual IRC Undergraduate Research Symposium, Rose-Hulman
"Synthesis and Analysis of Tamoxifen Derivatives", October 2016

Honors and Awards:

Brown/Wheaton Faculty Fellowship, January 2022-May 2022

Eli Lilly Undergraduate Research Grant, June 2016- August 2016

RHIT Global Scholarship, September 2013-2017

Dean’s List, Rose Hulman, 5 Times

Preface and Acknowledgements

Thank you to my advisor, Prof. Amit Basu who firstly gave me the opportunity to work with him on a fascinating project and the freedom to explore what I found interesting, and secondly guided me and helped me become a better scientist.

Thank you to Prof. Sarah Delaney for being constantly supportive and encouraging and Prof. Matthew Zimmt for several interesting conversations and thoughtful suggestions and thank you to both for being part of my committee.

Thank you to my wife Tina and my parents, my greatest supporters and best friends through this journey

Table of Contents

List of schemes and figures

List of Tables

Chapter 1- Introduction

1.1 The plant cell wall

1.1.1 The history of plant cell walls

We recognize today that cells are the most basic unit of life. The study of cells was first made possible thanks to the invention of the microscope. The term "cell" was coined by Robert Hooke in his 1665 book *Micrographia*, the first publication to report observations from the study of biological organisms using a microscope.[1] Hooke observed honeycomb like structures (Figure 1.1a) upon viewing a piece of cork under the microscope, and he called these structures "cells". This gave rise to some confusion as many people such as the English plant anatomist Nehemiah Grew didn't view the "cell" as the morphological unit of life.[2] Rather, Grew stated in his 1682 publication *The anatomy of plants*, "cells" were simply cavities (Figure 1.1b) created by "fibers woven together and layered on top of each other". Although others in the same period such as Marcello Malpighi, an Italian biologist, did state in his 1675 publication *Anatome Plantarum* that "cells" observed in plants were fluid filled sacs. However, it was only in the early 1800s that the likes of G.R. Treviranus and J.H.F Link showed without any doubt that plant "cells" are not simply cavities but individual units that contain the substances required for plant life. G.R. Treviranus used a needle to divide the buds of *Ranunculus Ficaria L.* into individual "bladders" and hypothesized that all living things are aggregates of these "little bladders". J.H.F Link and Karl Rudolphi provided evidence that the "cells" are separate by showing that no movement of colored fluids is seen from one "cell" to another and remarked on the existence of "double lines" between "cells". This showed that plant "cells" are separate units surrounded by cell walls. Therefore, the structures that Hooke termed "cells" in 1665 were in fact cell walls of dead plant cells.

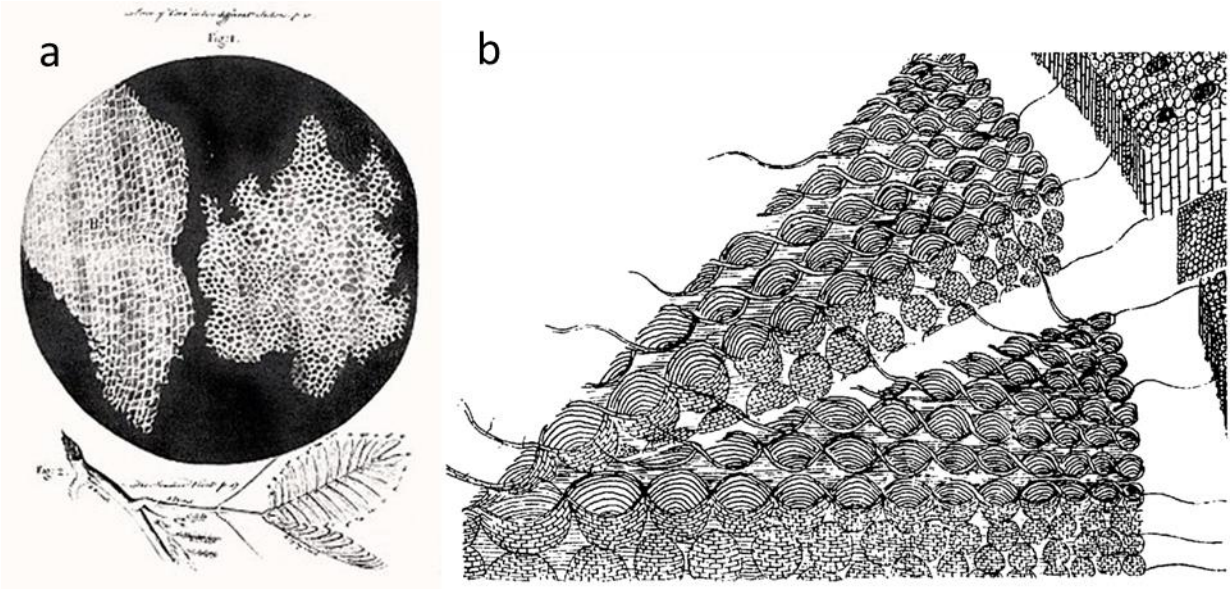

Figure 1.1 a) A drawing from Hooke's *Micrographia*[1] of his observation that led him to conclude the presence of "cells" in plants b) A part of the drawing from Grew's *The anatomy of plants* of the "fibers woven together and layered on top of each other", figure taken from *Journal of Cell Science* **1952,** *s3-93* (22), 157-190

Today we realize that cell walls are a distinguishing feature of plant cells from animal cells.[3] Cell walls may not be the "fundamental unit of life" in plants, but their components are known to play a variety of very important roles including 1) providing mechanical support against various challenges such as gravity, wind and turgor pressure; 2) cell signaling roles in cell growth, cell division, transport of material in and out of the cell, cell-cell communication, and plant-pathogen interactions; 3) providing stores for energy through carbohydrates. These large arrays of roles are made possible through the vast heterogeneity of the substances that compose the cell wall(Figure 1.2).[4] It was revealed early on, upon development of elemental analysis[5] by Gay-Lussac, that the composition of starch is very similar to that of wood extracts[6]. This clearly suggested the presence of carbohydrates in plant cell walls. It is now confirmed that the majority of plant cell wall is made up of carbohydrates, with some proteins (5-10%) and polyaromatics known as lignin (20-25%).[7]

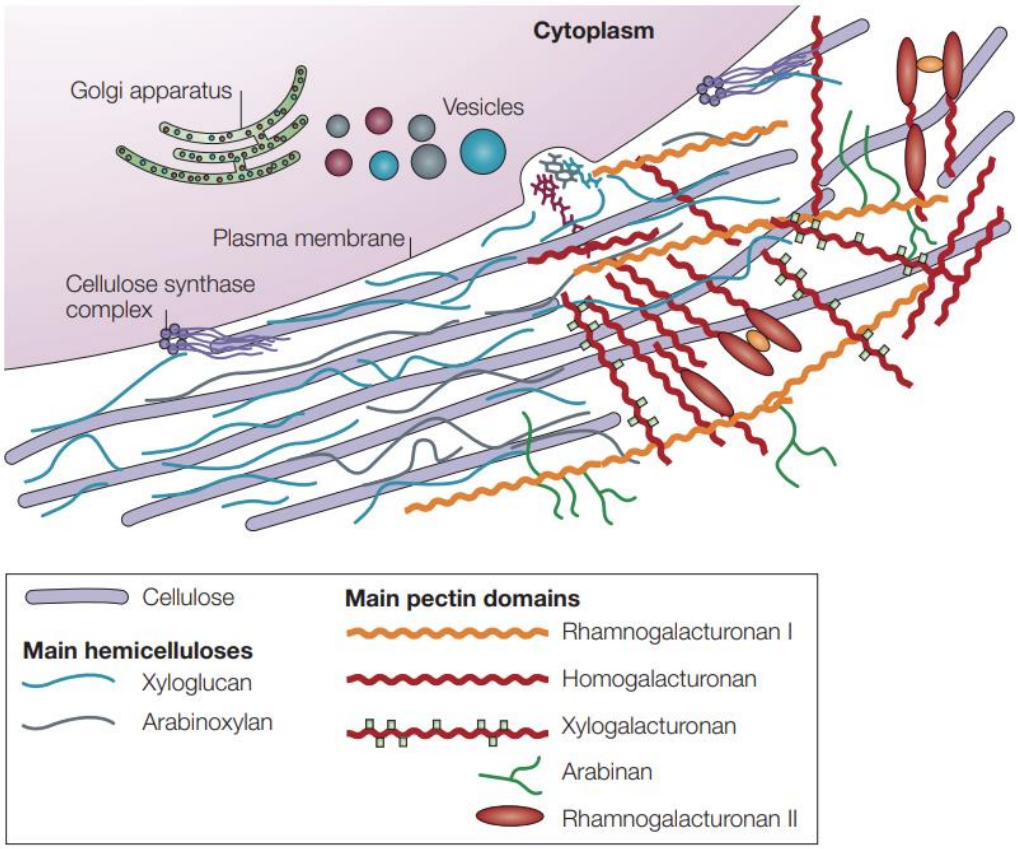

Figure 1.2 A cartoon representation of some cell wall polysacchrides, taken from *Nat Rev Mol Cell Biol* **2005,** *6* (11), 850-61

1.1.2 The composition of plant cell walls

The most abundant component among the carbohydrate polymers is cellulose, which is made up of (1,4)-β-D-glucan chains (Figure 1.3a) that are non-covalently linked to each other through inter- and intra-molecular hydrogen bonds to form a rigid network of cellulose microfibrils.[8] The plant cell wall contains three layers. The middle layer, known as the primary cell wall, contains the cellulose microfibrils and is the thickest. This middle layer also contains polymers known as hemicelluloses. The innermost layer of the cell wall, known as the secondary wall, contains celluloses, hemicelluloses, and lignin. Two major kinds of hemicelluloses are 1) xyloglucan, which contains the same backbone as cellulose but is decorated with xylose branches (Figure 1.3b) and 2) arabinoxylan which primarily consists of 1,4 β-D-xylan backbone decorated with arabinofuranosyl branches (Figure 1.3b). The hemicelluloses are linked to cellulose, but the exact

network formed between hemicelluloses and cellulose is still unclear. For example, it has been proposed that the hemicellulose could be directly linked to cellulose mircofibrils but it has also been proposed that the hemicellulose could be indirectly linked through another cell wall polysaccharide such as pectin.[8] Therefore, the exact morphology and molecular architecture of even the most commonly found components of cell walls is not well understood.

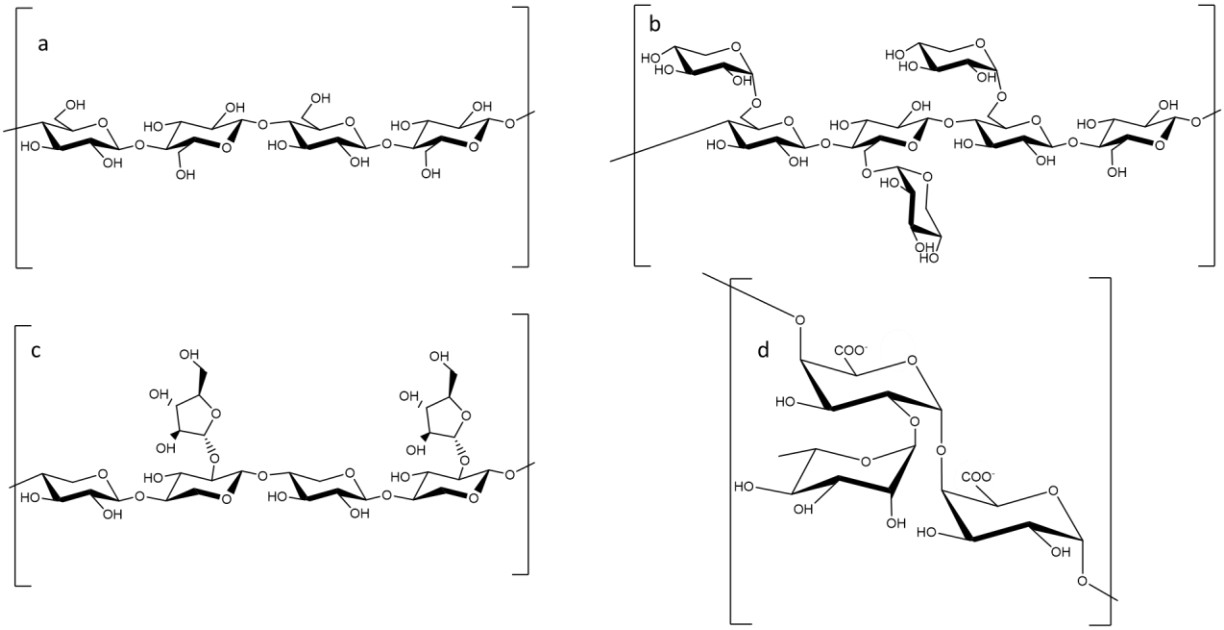

Figure 1.3 General structure of some plant polysaccharides a) cellulose b) xyloglucan c) arabinoxylan d) rhamnogalacturonan I

Pectins (Figure 1.2) are a heterogenous group of polysaccharides found in both the primary cell wall and the outermost layer known as middle lamella. Pectins may be composed of either alternating residues of galacturonic acid and rhamnose (rhamnogalacturonan I) (Figure 1.3d) or just galacturonic acid (homogalacturonan) which may or may not contain xylose branches. The carboxyl groups of pectins can be methyl esterified. Non-methyl esterified pectins undergo Ca^{2+}crosslinking which leads to formation of stiff gels. To allow for expansion during cell growth, pectins undergo methyl esterification which prevents cross linking and promotes cell wall loosening.[8] This is one of the many examples of the dynamic nature of cell wall composition.

Besides the polysaccharides, the cell wall also contains various proteins which are often glycosylated. For example, in dicots (flowering plants i.e. angiosperms whose seed contain two embryonic leaves or cotyledons) a family of hydroxyproline rich glycoproteins called extensins are found.[9] Extensins usually contain a repeating Ser-Hyp$_4$ pentapeptide motif. Most of the Hyp residues are glycosylated with arabinose residues while the Ser residues contain galactose units. However, exceptions exist such as the sugar beet which lacks the Ser-Hyp$_4$ pentapeptide motif. Monocots (angiosperms whose seed contains one embryonic leaf or cotyledon) contain different versions of extensins, which is rich in threonine and proline in addition to hydroxyproline and serine. Moreover, in monocots half of the hydroxyproline residues are not glycosylated. Further, the extensins found in green algae are different from those of monocots and dicots. Extensins thus exemplify the diversity in cell wall constituents that exists across the plant kingdom.

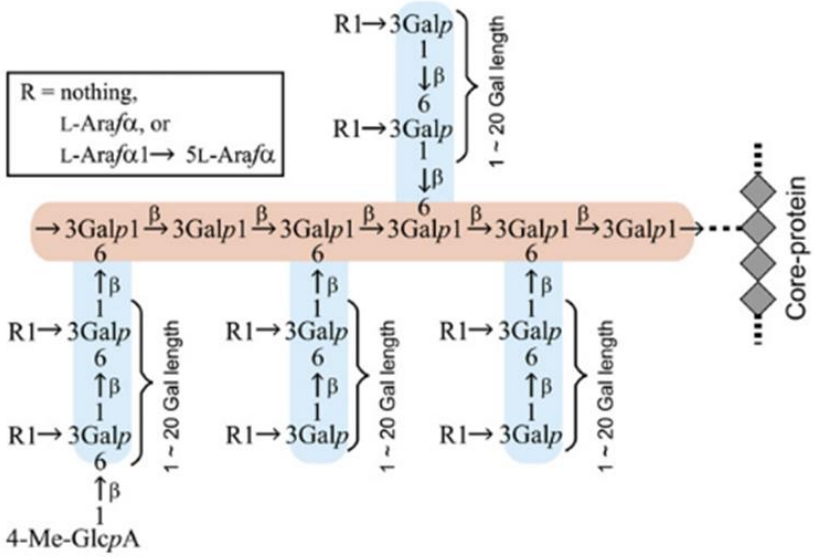

Figure 1.4 A schematic representation of radish root arabinogalactan protein (AGP) taken from *Plant Physiol* **2013,** *161* (3), 1117-26.

Another example of glycosylated proteins are the arabinoglactan proteins (AGPs).[9] AGPs are highly glycosylated proteoglycans with 90% of the molecular weight coming from glycans. AGPs consist of 1-3 linked β-D-galactopyranose residues branched with 1-6 linked β-D-galactopyranose residues, which are in turn further branched with arabinofuranosyl residues (Figure 1.4). AGPs

are also hydroxyproline rich proteins where the glycan moieties are attached to the Hyp residues. AGPs are anchored to plant cell membranes through a glycosylphosphatidylinositol (GPI) anchor.[10] AGPs are found ubiquitously in the plant kingdom. One study showed that AGPs were found in the seeds of 91 out of the 104 different species tested.[11] Out of the 104 species, 6 were gymnosperms (non-flowering plants that produce seeds), 11 were monocots and 87 were dicots. All 6 of the gymnosperms, 8 of the monocots and 78 of the dicots showed a positive result for AGP. It was also seen that the AGPs were found in various plant tissues such as the stem and leaves of the gymnosperms and every above ground part of the angiosperms.

AGPs play a wide variety of roles and are invovled in processes such as cell growth, cell division, programmed cell death, embryo pattern formation, pollen tube growth, plant microbe interactions, and cellulose deposition, to name a few.[10, 12-14] However, while AGPs are clearly very prevalent and important for plant biology, there is much unknown about them and the study of AGPs is still a vast area of research. For example, the exact mechanism of how AGP is involved in many of the abovementioned processes is not well understood and the involvement of AGPs in other processes are also being discovered.[15-19] Moreover, due to the structural heterogeneity of AGPs across species, the exact carbohydrate or protein composition in many cases is only now being studied.[20]

The above section highlights the diversity of the cell wall components. It has also been shown that the sugar composition varies not just between species but also within the different tissues and cell types of the same plant and at different stages of growth.[21] Moreover, various polysaccharides are shown to be insoluble upon extraction, but since they are synthesized in the Golgi, they must be soluble upon secretion and subsequently modified. Therefore, the exact modifications that these polysaccharides undergo and how they are then deposited to the cell wall remains unanswered. Another major challenge is understanding how the plant cell wall

polysaccharides are modified in order to allow for expansion and division. Answering these questions requires polysaccharides recognition tools that can accurately provide details about composition and spatiotemporal dynamics of cell wall polysaccharides. The various available tools will be discussed in the next section.

1.2 A summary of tools to study cell walls

1.2.1 Antibodies

The most popular tools for studying cell wall components are antibodies (Figure 1.5).[22] The procedure involves conjugating the target cell wall molecule to a carrier such as bovine serum albumin (BSA) followed by injection of these BSA conjugate to mice or rats for production of the antibodies. White blood cells that are then harvested from the mice or rat and fused with immortalized cells to create antibody producing hybridoma cells. The antibodies are then immobilized onto microarrays and the target of interest is incubated on the arrays. Binding is detected using fluorescent labelling of the target or a secondary detection reagent. The chosen monoclonal antibody can be used for imaging via transmission electron microscopy by combining with a nanogold conjugate of a secondary antibody. Using antibodies it was revealed that the pectin, homogalacturonan, is synthesized in a highly methyl esterified state in the Golgi and deposited to the cell wall and only subsequently de-methyl esterified.[23] Such information regarding pectin deposition was made possible because antibodies specific to either esterified or non-esterified homogalacturonan can be generated. However, there are various issues associated with antibodies. The first is that of epitope masking, which involves the target in its native form being hidden from the antibody because of interactions with other cell components. This can sometimes be a blessing in disguise as it may reveal more about the interactions between different components in the native context. For example, it was shown that pectins likely interact with and mask various hemicelluloses such as xyloglucan and mannans, because detection of these hemicelluloses through antibodies only occurred upon enzymatic removal of the pectin.[24] This

suggests an interaction between pectin and hemicelluloses. However, masking may also occur due to the large size of the antibody molecules compared to the target, in which cases smaller probes are required.[25] Another challenge with antibodies is that it's often difficult to find the pure version of the oligosaccharide targets to help generate antibodies. This can lead to either not finding an antibody for the target or not precisely determining the binding epitopes of the antibodies in use. For example, the most common cell wall polysaccharide, cellulose, does not have a known antibody.

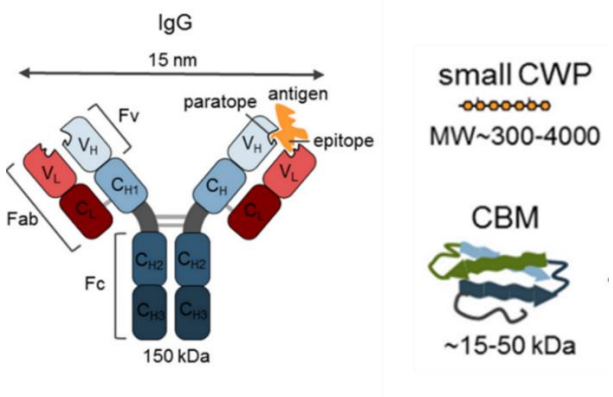

Figure 1.5 An illustration of various tools to study cell wall polysacchrides. CWP= Cell wall probe Edited version of a figure taken from *Front Plant Sci* **2018,** *9*, 581.

1.2.2 Carbohydrate binding modules

Another tool for detection of cell wall components are carbohydrate binding modules (Figure 1.5) (CBMs).[22] CBMs are non-catalytically active domains of carbohydrate active enzymes that bind carbohydrates and can be used as detection tools when expressed separately. CBMs are often expressed along with a His tag and then detected through immunolabeling using fluorescence or electron microscopy. CBMs can also be tagged with fluorescent proteins so antibodies are not required. CBMs have been utilized to show the diversity of polysaccharides present in a given cell. In collenchyma cells it was shown that primary cell walls contain a smaller proportion of cellulose microfibrils and higher amount of amorphous cellulose.[23] Challenges with CBMs are their broad specificity and difficulty in characterizing their ligand specificity in detail. Another disadvantage of CBMs, like antibodies, is that it can only be used for *in situ* imaging and not *in*

vivo imaging.[26] This can lead to loss of temporal information and fixation artefacts. In the future *in vivo* imaging maybe possible if CBMs with fluorescent proteins are expressed directly in plant cells.

1.2.3 Click Chemistry

Yet another strategy for imaging glycans is utilizing click chemistry.[23] For example, azide or alkyne modified sugar can be introduced and metabolically incorporated into a cell wall component of interest and then a fluorophore can be clicked on to the target. This method has been used to incorporate alkynylated fucose analogs into the pectin rhamnogalacturonan I followed by labelling with a membrane impermeable fluorophore. This technique was utilized to show the role of the kinesin FRA1 in rhamnogalacturonan I deposition. It was shown that mutants that lack FRA1 incorporated less rhamnogalacturonan I.[23] However, this technique has an important limitation that some modified sugars may not incorporated into the target polymer of interest. For example, no sugar analogs that can be incorporated into hemicelluloses have been discovered.[22]

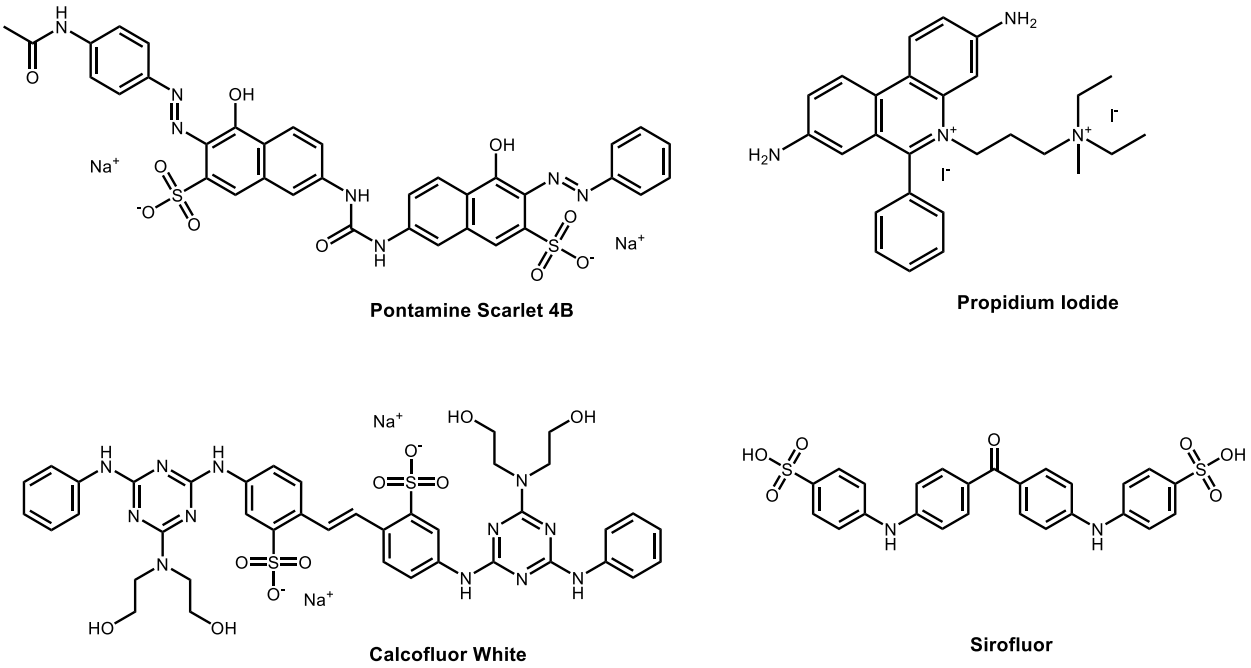

Figure 1.6 Examples of various small molecule dyes used in plant biology

1.2.4 Small Molecules Dyes

The cell wall visualization technique with the longest history is the use of small molecule dyes and stains (Figure 1.6).[26] These dyes are utilized in light microscopy or in the case of fluorescent dyes, are applicable in fluorescent microscopy. Several polysaccharide binding dyes are known. Calcofluor white (Figure 1.6) is popularly used as a cellulose stain I n immunohistological studies. Pontamine scarlet 4B (Figure 1.6) is another cellulose stain and is compatible with fluorescent imaging. Pontamine scarlet 4B was utilized to show that cellulose microfibril orientation changes with different stages of the cell's life.[26] While cellulose microfibrils were deposited perpendicular to the axis of growth in recently divided cells, in elongating cells the older cellulose fibrils reoriented to become diagonal, and in almost differentiated cells the fibrils reoriented along the axis of growth. The initial perpendicular orientation prevents the cell from growing radially, and the subsequent reorientation of cellulose prevents further expansion at late stages. Propidium iodide (PI) (Figure 1.6) is a fluorescent stain that is very useful to study de-esterified pectin.[23] PI binds negatively charged polymers, therefore can compete with $Ca^{2+}$for pectins. Ruthenium red (RR) (Figure 1.6) is another stain that similarly binds de-esterified pectins. Dyes and stains have been useful in the past for discovery of new plant cell wall polysaccharides. For example, certain parts of a plant such as pollen tubes were stained clear blue by the dye Sirofluor, a dye previously not known to stain any other cell wall polysaccharide.[27] This experiment suggested that a previously unidentified substance was present in the pollen tube. It was later shown that the substance stained by sirofluor was the polysaccharide callose, a 1-3-β-D-glucan.[28]

However, small molecule probes often suffer from specificity related issues. For example, calcofluor white binds all β-glucans, not just cellulose. Sirofluor has been shown to bind other polysacchrides such as amylopectin.[29] Propidium iodide strongly binds nucleic acids and prefers

them over any cell wall material in fixed samples, and is therefore limited to *in vivo* imaging. One small molecule dye however, the Yariv reagent, is well known for its strong specificity towards its target, the AGPs. The Yariv reagent and in particular its remarkable specificity towards AGP will be the focus of the thesis.

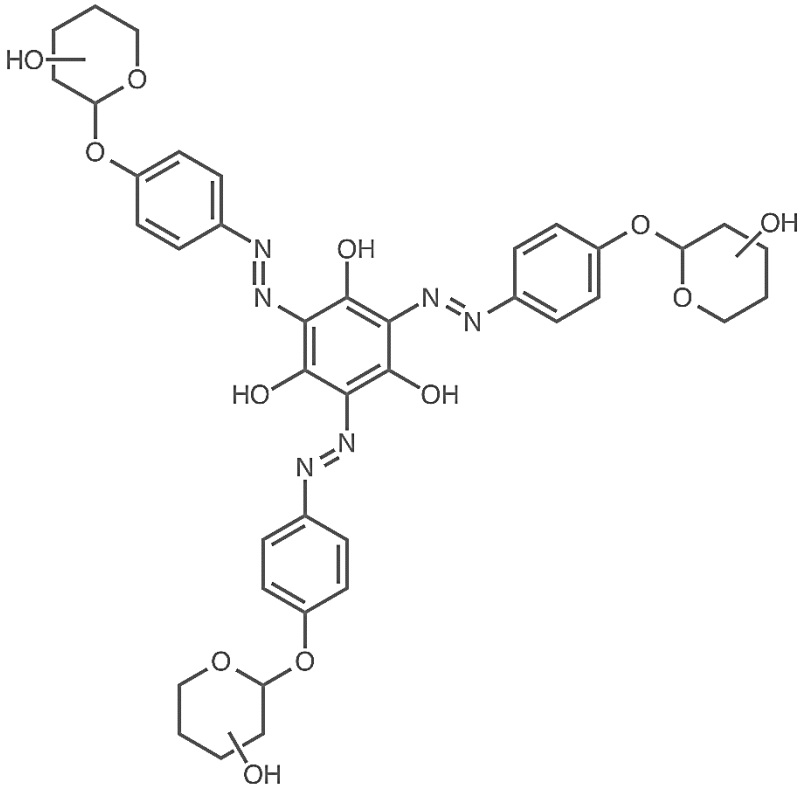

Scheme 1.1 Yariv reagent general structure

1.3 Yariv reagents – an important tool for studying AGPs

1.3.1 How Yariv reagents are utilized to study AGPs

The Yariv reagents are glycosylated tris-hydroxyazo dyes (Scheme 1.1). The Yariv reagents were first reported by Joseph Yariv in 1962 as reagents that precipitate carbohydrate binding antibodies.[30] In Joseph Yariv's initial study β-D-glucosyl (**1**), β-D-galactosyl (**2**) and β-lactosyl Yariv reagent were synthesized to precipitate and quantify glucose, galactose and lactose binding antibodies. It was later shown in another study by Joseph Yariv that the Yariv reagent **1** also precipitated a "polysaccharide" from seed extracts of the *Lotus tetragonolobus* plant.[31] TLC of

the hydrolysates confirmed that the "polysaccharide" contained galactose and arabinose residues. However, another study later showed that the "polysaccharide" could be precipitated from various seeds and was in fact a proteoglycan, which we now call AGPs.[11,32] . The AGP binding was tested for various Yariv reagents including β-D-glucosyl (**1**), β-D-galactosyl (**2**), β-D-xylosyl (**3**), β-D-mannosyl (**4**) and α-D-galactosyl Yariv reagent (**5**) to name a few (Scheme 1.2). Only β-D-sugars containing Yariv reagents were found to bind AGP. The only exception was β-D-mannosyl (**4**), which did not bind AGP.[33]

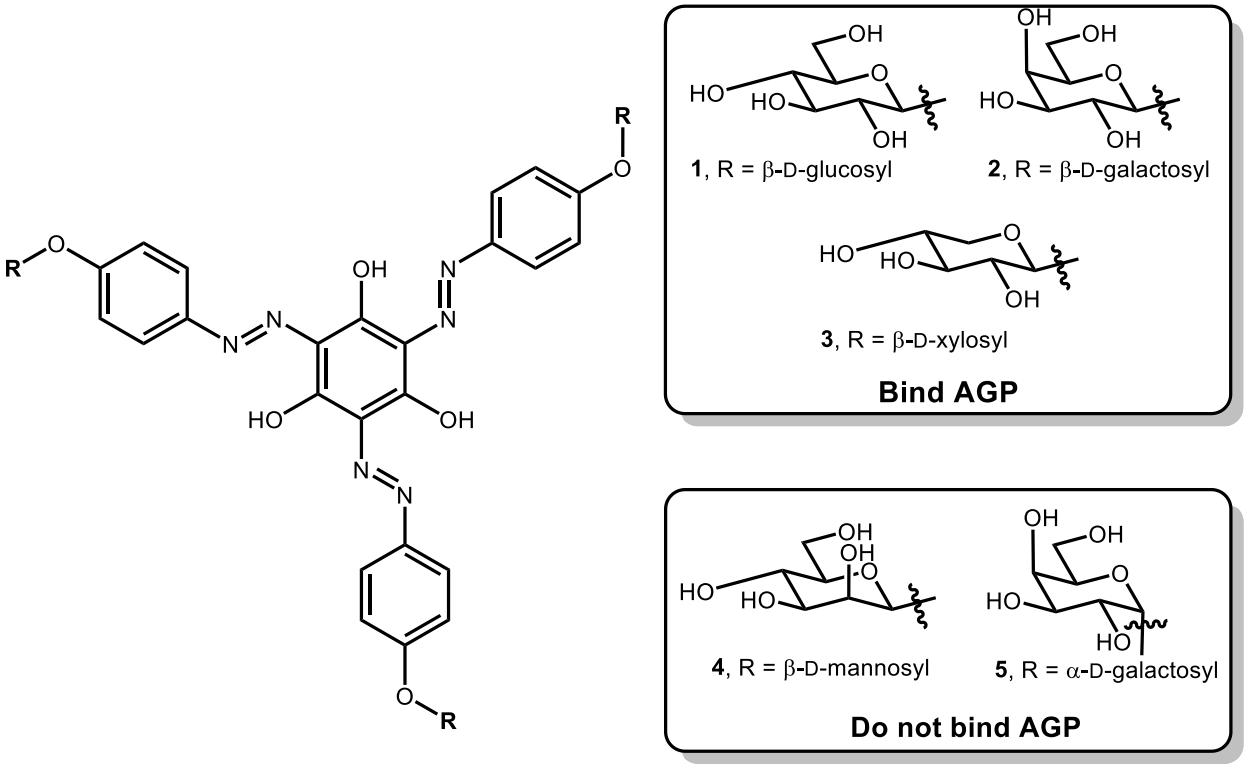

Scheme 1.2 Some examples of Yariv reagents whose AGP binding ability was reported in *Aust. J. Plant Physiol.* **1978,** *5* (5), 687-696

The Yariv reagents were soon utilized to stain AGPs and understand localization of AGPs in various plant parts using bright field microscopy.[34] For example, researchers wanted to understand the localization of AGPs in various parts of three different species of plants, *Hedera Helix*, *Zantedeschia* and *Alocasia*. They found that the phloem tissue of leaves and petals in each of the three species studied was stained by the Yariv reagent indicating the presence of AGPs.

Various part of reproductive tissues in the species *Gladiolus* such as pollen grains, style canals and the stigma surface were also stained by the Yariv reagents suggesting the presence of AGP in these parts as well.

The utility of the Yariv reagent extends beyond just imaging. A gel binding assay that utilized the Yariv reagent was developed that allowed quantification of AGP from whole plant extracts (Figure 1.7).[35] AGP extracts of various concentrations were added to agarose gels containing the Yariv reagents. A red halo formed upon incubation and the area of the halos were directly proportional to the AGP concentration.

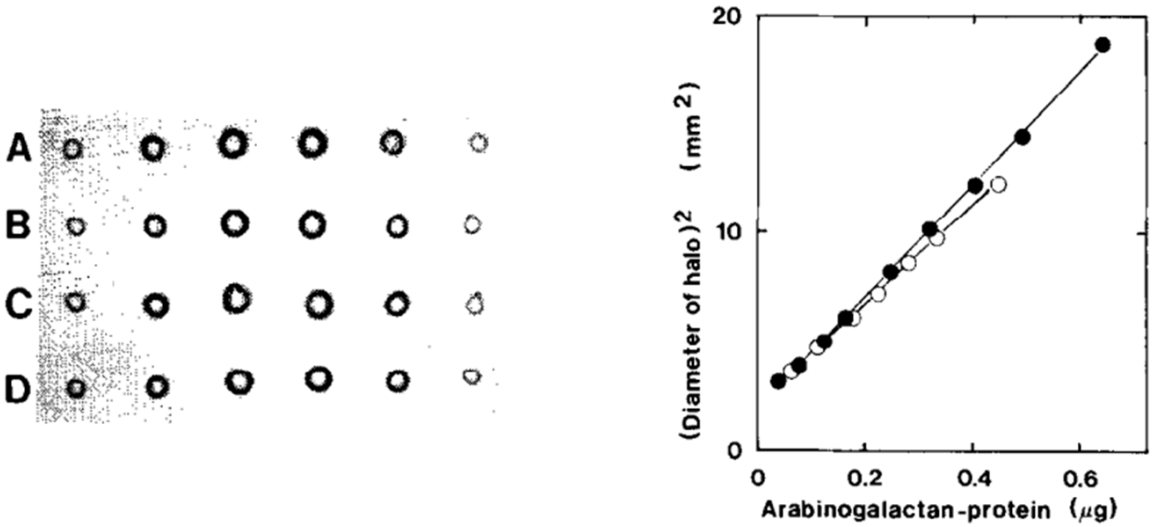

Figure 1.7 Left: An example of the gel diffusion assay. Gum arabic AGP added to the wells in row A and C, *Gladiolus* AGP added to wells in row B and D and Yariv reagent **1** in the gel. Right: A plot of halo area and quantity of AGP added to the wells. ○ *Gladiolus* AGP ● Gum arabic AGP. Figure taken from *Anal. Biochem* **1985,** *148* (2), 446-450

The Yariv reagents are also extremely useful in probing the role of AGPs by disrupting AGP functionality. The Yariv reagents that don't bind AGP such as β-D-mannosyl Yariv reagent (**4**) and α-D-galactosyl Yariv reagent (**5**) are often used as negative controls in such experiments. It was found that *Arabidopsis thaliana* seedlings grown in a medium containing the β-D-glucosyl Yariv reagent (**1**) showed impaired root growth. In the experiments with *Arabidopsis thaliana* seedlings, the α-D-galactosyl Yariv reagent (**5**) did not impact root growth. Finally, when the

stunted plants which were initially grown in a solution containing the Yariv reagent (**1**) were transferred to a regular medium, they grew back normally again. These experiments revealed that AGP has a function in root growth in *Arabidopsis thaliana*.[36] The role of AGP in lily pollen tube growth was also studied using Yariv reagent through such function disruption experiments.[37] Lily pollen tubes grown in presence of the β-D-glucosyl Yariv reagent (**1**) had enlarged tips with material accumulated beneath the tip. Visualization using antibodies revealed the presence of pectins and callose under the tip. The presence of pectins and callose suggested exocytosis was functioning normally (as these polymers are synthesized in the Golgi) but abnormal cell wall deposition of these materials was taking place. These experiments revealed a role for AGP in cell wall assembly of pollen tubes during pollen tube growth.

1.3.2 Yariv reagent specificity

The binding specificity of β-D-glucosyl Yariv (**1**) and α-D-galactosyl Yariv reagent (**5**) was evaluated in a study with variety of carbohydrate polymers.[38] For carbohydrate polymers that were insoluble in water, such as cellulose, a pellet of the polymer was suspended in a Yariv reagent solution and then washed. The Yariv reagent was then released from the pellet using DMF and the amount of Yariv reagent released was measured using UV/vis spectroscopy. In cases where Yariv reagent did not bind the polymer, the DMF step was not required as the Yariv reagent could simply be washed away. It was seen that DMF was required to release β-D-glucosyl Yariv (**1**) from cellulose, but DMF was also required for α-D-galactosyl Yariv reagent (**5**), i.e. both Yariv reagents bound cellulose. Moreover, the amount of both Yariv reagent released in each case was roughly equal. Similarly, both Yariv reagents were also shown to bind chitin, but 3.58 μmol of β-D-glucosyl Yariv reagent (**1**) per gram of chitin was bound in contrast with only 2.73 μmol of α-D-galactosyl Yariv reagent (**5**) per gram of chitin was required. Both Yariv reagents did not bind other non-water soluble polymers such as rayon, amylose, amylopectin and pachyman. For water soluble polymers, the polymers were incubated with Yariv reagents on a

membrane and then washed. The amount of Yariv reagent bound to the polymer was assessed subjectively by looking at the stain intensity. It was shown most polymers tested weren't bound to either Yariv reagent. However, it was seen that β-D-glucosyl Yariv reagent (**1**) did bind apple pectin, which the α-D-galactosyl Yariv reagent (**5**) did not bind. However, compared to AGP, the apple pectin stain was significantly weaker. Therefore, the above study suggested that β-D-glucosyl Yariv reagent (**1**) has a strong specificity towards AGPs. In few cases, where the β-D-glucosyl Yariv reagent (**1**) did bind other polymers, so did the α-D-galactosyl Yariv reagent (**5**) for the most part. Due to its strong specificity the Yariv reagent remains one of the most useful tools to study AGPs. However, it is not known exactly how the Yariv reagent binds AGP. Therefore, understanding exactly how the Yariv reagent binds AGP is of particular interest.

1.4 Yariv-AGP binding

In initial Yariv reagent-AGP binding studies a slightly different variation of the gel diffusion experiments described above was utilized to test the presence of binding.[11,33] Plant extracts were added to one well while the Yariv reagents or some analog was added to the neighboring well in agarose gels. When a red precipitate similar to the halo described above appeared, it was described as a "positive interaction" i.e. taken to mean that Yariv reagent-AGP binding had occurred.

This initial work also looked at the AGP binding ability of various other Yariv reagent analogs (Scheme 1.3) that provided structural requirements of the Yariv reagent for AGP binding ability. It was seen that O-glycosylation was not a necessity, as S-glycosylated Yariv reagents analogs of **1** and **2** also showed AGP binding ability. However, the N-glycosylated, C-glycosylated or CH_2-O-glycosylated variants of **1** did not show AGP binding ability. The importance of para substitution of -O-glycosyl moiety was also studied by testing the AGP binding ability of ortho and meta substituted variants. It was seen only Yariv reagents with para substituted -O-glycosyl

moieties bound AGP. Further, the importance of stereochemistry of sugar -OH groups was also analyzed. The lack of AGP binding ability in β-D-mannosyl Yariv (**4)** (which contains an axial 2-OH) and the 2-O-methylated glucosyl Yariv reagent indicates the importance of an equatorial 2-OH. Methylation or change in stereochemistry of other -OHs did not have an impact in the presence of AGP binding ability. For example, 3-O-methylation, 4-O-methylation and 6-O-methylation showed AGP binding ability. Although it must be noted that a 3-methyl substituted sugar containing Yariv reagent analog did not bind AGP. The β-D-galactosyl Yariv reagent (**2)** which contains an axial 4-OH and β-D-xylosyl Yariv (**3)** which does not contain a C6 also bind AGP. These results therefore suggest that the presence of an equatorial 2-OH is important and the presence of an oxygen on C3 may also be required. The AGP binding ability of mixed Yariv reagents was also tested. It was seen that the Yariv reagent with 2 β-D-glucosyl and 1 α-D-galactosyl residues had AGP binding ability whereas the Yariv reagent with 1 β-D-glucosyls and 2 α-D-galactosyl residues did not.

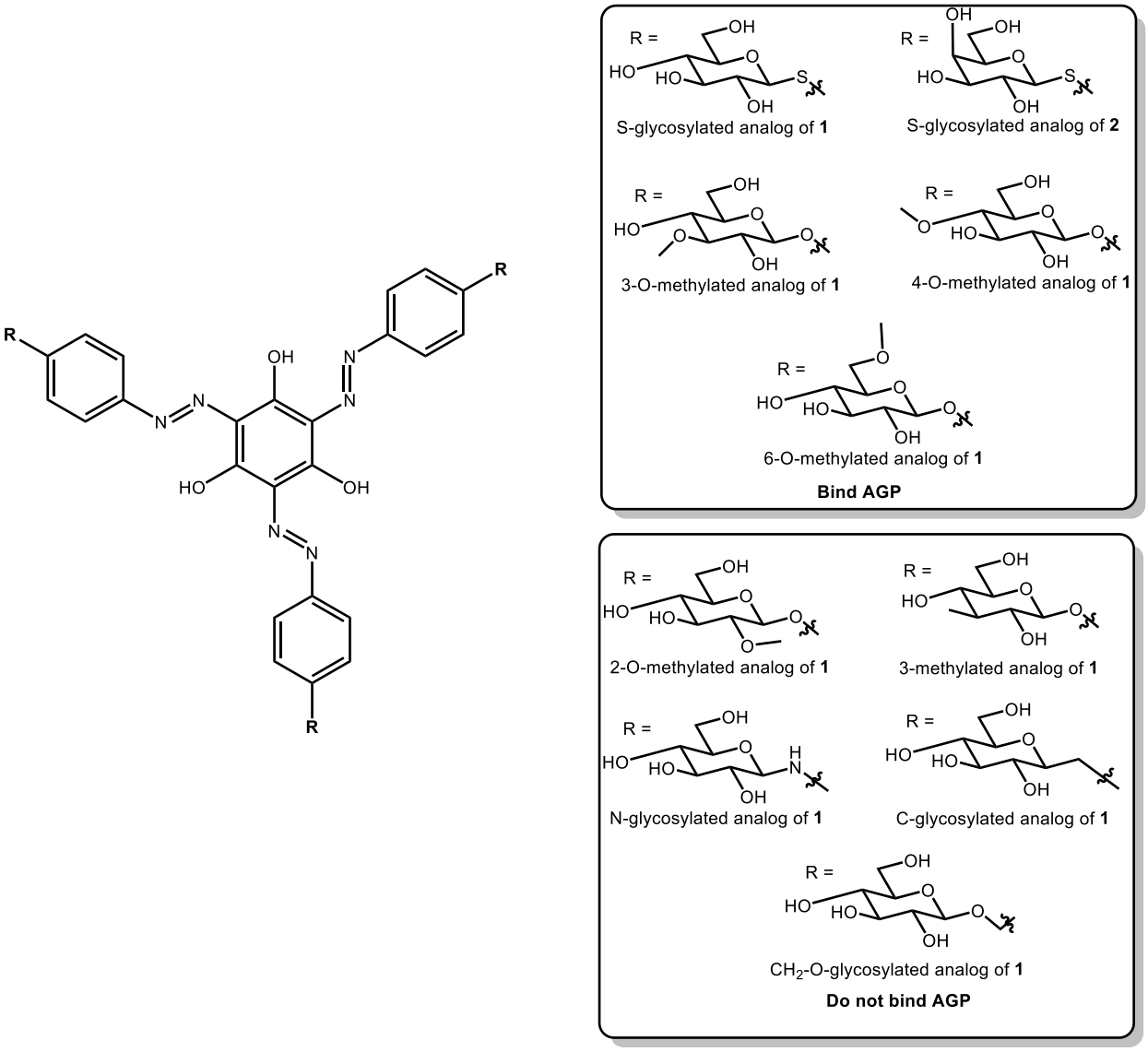

Scheme 1.3 Some examples of Yariv reagent analogs whose AGP binding ability was reported in *Aust. J. Plant Physiol.* **1978,** *5* (5), 687-696

1.5 Yariv reagent aggregation

1.5.1 Yariv reagent aggregate size

Based on the observation that the Yariv reagents in aqueous solutions do not pass through dialysis membranes it was speculated they are aggregated.[33] Since the Yariv-AGP binding takes place in aqueous conditions, the AGP binding unit is effectively the Yariv reagent aggregates. Therefore, understanding Yariv reagent aggregation is crucial to understanding Yariv-AGP binding. Analytical ultracentrifugation was utilized in the first major study of the Yariv reagent

aggregates.[39] In these experiments samples are loaded into sector-shaped cells and then centrifuged. The migration pattern of the species depends on their mass, with heavier species moving to a larger radius than lighter species. The concentration of sample at different radii of the cell upon centrifugation is calculated based on UV/vis absorption values at different radii. Average molecular weight in the cell is then calculated based on these concentration values. The experiment is repeated at different initial loading concentrations to obtain information such as association constant and other thermodynamic parameters. The authors claimed that the aggregation mechanism was isodesmic, i.e. the association constant and change in free energy remains the same regardless of how many monomers are present in the aggregate. The association constant per monomer addition was calculated to be 2.5 x 10^7 M^{-1} for β-D-glucosyl Yariv reagent (**1**), 0.9 x 10^7 M^{-1} for β-D-galactosyl Yariv reagent (**2**), 0.3 x 10^7 M^{-1} for α-D-galactosyl Yariv reagent (**5**) and 0.2 x 10^7 M^{-1} for β-D-mannosyl Yariv reagent (**4**). Therefore, while β-D-glucosyl Yariv (**1**) reagent aggregation was most favored, β-D-mannosyl Yariv (**4**) reagent was least aggregated. The apparent molecular weight of **1** was also determined in solutions of 6.2 M guanidine hydrochloride and 8.2 M urea. Molecular weight was found to be 1100 g/mol in guanidine hydrochloride and 2700 g/mol in urea while the molecular weight of the monomer is 973 g/mol i.e. almost no aggregation was seen in either solution.

The disaggregation of the Yariv reagent was also correlated to changes in the UV/vis spectrum. In water, two UV/vis peaks appeared at 398 and 485 nm, with the peak at 398 nm having the stronger intensity. In presence of guanidine hydrochloride, a decrease in the intensity of the 398 nm peak and increase in intensity and red shift of the long wavelength peak was seen. Therefore, in disaggregating conditions the long wavelength peak had a higher intensity, while in aggregating conditions the short wavelength peak had a higher intensity. The authors noted that similar changes in the UV/vis spectrum took place in the presence of sodium dodecyl sulfate (SDS).

The weaker aggregation of β-D-mannosyl Yariv reagent (**4**) as suggested by the above centrifugation experiments may explain its lack of AGP binding ability. Comparison of the interaction between AGP and the β-D-glucosyl Yariv reagent (**1**) vs the interaction between AGP and the β-D-mannosyl Yariv reagent (**4**) was studied using AFM.[40] "Nanopores" with ridged edges formed when the AGP reacted with either β-D-glucosyl (**1)** or β-D-mannosyl Yariv reagent (**4**) dried on graphite. The height of the ridges were pretty similar for β-D-glucosyl (**1**) or β-D-mannosyl Yariv reagent (**4**) but the diameters of the pores were significantly larger in the β-D-glucosyl experiment (**1**). Therefore, while there were clear differences in the size of these nanopores made by the two Yariv reagents, it is unclear if these differences are related to their AGP binding ability.

The thermodynamic parameters obtained from the ultracentrifugation studies mentioned above can be utilized to calculate the polymer size (number of monomers in the polymer) if the polymer shape is known. The Yariv reagents are structurally similar to several other molecules known to form supramolecular polymers, as they contain a hydrophobic core and hydrophilic peripheral molecules. The polymers formed in many of these cases are linear columnar supramolecular polymers, especially in those molecules that are C_3 symmetric such as the Yariv reagents.[41,42,43,44,45] In the case of linear polymers that stack with isodesmic association, the number of monomers in a polymer can be calculated using Equation 1.1.[46] Utilizing equation 1.1 for a 100 μM aqueous solution of β-D-glucosyl Yariv reagent (**1**) at 293 K would provide a N of 16 units if K = 2.5 x 10^7 M^{-1}as suggested by the centrifugation study.

$$N = ½ + (½)*(4*K*c+1)^{0.5}$$ – **Equation 1.1**

Where K is the association constant, and c is the concentration

Another study[47] utilized Dynamic Light Scattering (DLS), UV/vis spectroscopy and NMR spectroscopy to study aggregation of β-D-glucosyl (**1**) and α-D-galactosyl Yariv (**5**) reagent. The ^{1}H NMR spectra of β-D-glucosyl Yariv reagent (**1**) was obtained in three different solvents, D_2O, DMSO-d_6 and DMF-d_7. While the spectrum in D_2O only showed two very broad peaks confirming aggregation in aqueous solution, the spectra in DMSO and DMF had sharp peaks, confirming disaggregation in DMSO and DMF. DLS measurements of hydrodynamic radii were obtained for **1** in water (both in the presence and absence of NaCl), DMF, 8 M urea. For **1**, the radius in water was found to be 122 nm while in both 10% NaCl and 8 M urea it was 50 nm, and the radius in DMF was 0.4 nm. For **5**, radii in water and DMF were obtained. In water the hydrodynamic radius of **5** was 82 nm and in DMF it was 0.5 nm. UV/vis spectra showed similar results to those obtained in the centrifugation studies, as addition of either urea or SDS red shifted and increased the intensity of the long wavelength peak, with the long wavelength peak having a higher intensity than the short wavelength peak in disaggregating conditions. An aggregate size of 305 units was calculated using the DLS data for **1** at 100 μM. Therefore, there is clear discrepancy between the centrifugation (16 units) and DLS study (305 units) with regards to the size of the aggregate and therefore this question is still unresolved.

The centrifugation study showed that an increase in temperature lead to lower molecular weight aggregates. The authors claimed that since an increase in temperature strengthens hydrophobic interactions, it can be inferred that hydrophobic interactions are not the dominant reason for Yariv reagent aggregation. A positive entropy change was found to be associated with the Yariv reagent aggregation process, which the authors conclude arises from increased order in solvent molecules around monomers compared to aggregates. A molecular modelling study[48] which looked at Yariv reagent **2** dimers suggested that the dimers are stabilized predominantly by π-π stacking between its aromatic moieties. The same study also modeled tetramers of **2**, but these were found to be irregularly shaped and interacted via π-π as well as CH/π interactions.

1.5.2 Yariv reagent aggregate helicity

To learn what part of the AGP binds the Yariv aggregates, degradation studies were performed where residues of the AGP are selectively removed and the binding of trimmed AGPs to Yariv reagents is tested. Upon cleavage of protein residues of the AGP in radish root using base treatment, the binding of the various fractions with Yariv reagents was retained.[49] Subsequently, enzymatic treatment removed the various carbohydrate moieties sequentially. When the arabinofuranosyl and the 1,6-galactan side chain residues were removed from the AGPs, binding to Yariv reagent was still observed. However, binding ability was lost upon cleavage of 1,3-galactan main chain residues. This suggests that the 1,3 galactan chain is the main Yariv reagent binding epitope of the AGP. This was backed by another study[50] which showed that having extensive 1,6 substitution leads to diminished interaction with Yariv reagent, probably due to the Yariv reagents – 1,3 main chain interaction being blocked by the extensive substitution. Synthetic 1,3- and 1,6-galactan oligomers containing 4 to 9 glycosyl residues were also prepared. It was seen that binding only occurred with 1,3- chains containing more than seven residues. Computational modeling showed that the 1,3- chain adopts a right-handed helical structure with each helical turn containing 7-8 residues. Based upon the finding that the Yariv reagents bind a helical polysaccharide, we hypothesized that the Yariv aggregates in turn may adopt helical architectures.

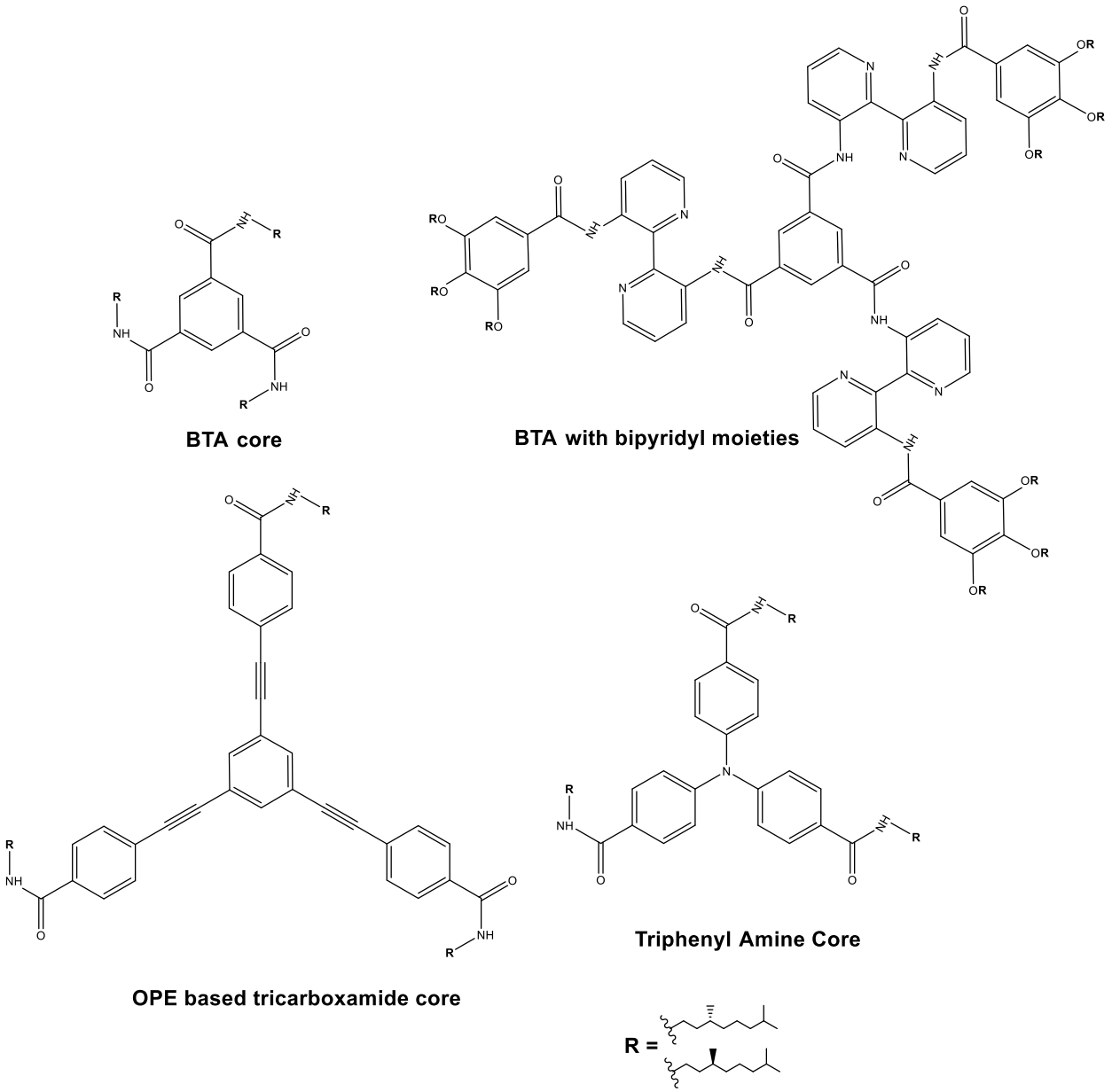

Figure 1.8 Structures of various common C_3-symmetrical building blocks for helical supramolecular polymers

Yariv reagents are C_3-symmetrical molecules containing aromatic cores. Such molecules have previously been extensively studied and very commonly utilized as building blocks for helical supramolecular polymers.[51] The most studied of such C_3-symmetrical molecules are those with benzene-1,3,5-tricarboxamide (BTA) cores (Figure 1.8). X-ray structures have shown that these BTA monomers self-assemble by formation of intermolecular H-bonds between the N-H groups of one BTA and the C=O groups of the adjacent BTA. However, in other cases where a bipyridyl

moiety is present, the intermolecular was replaced with an intramolecular hydrogen bond between amide N-H and pyridine N (Figure 1.8). In either case, with or without the presence of a bipyridyl moiety, when CD spectra was acquired in apolar solvents, it was seen that those BTAs with chiral enantiopure sidechains produced a strong CD signal with bisignate CD couplets.

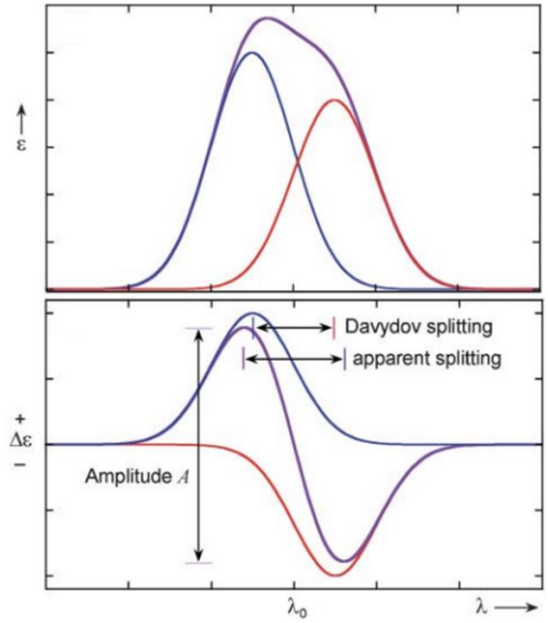

Figure 1.9 Theoretical UV/vis (top) and bisignate CD spectra (bottom) expected when helical supramolecular aggregation induced exciton coupling takes place. Blue spectra represent contribution form E+V state and red spectra represent contribution from E-V state. Overall spectra shown in purple. Figure taken from *Chem Soc Rev* ***2007,*** *36 (6), 914-31*

Such bisignate CD couplets (Figure 1.9) are often observed when molecules form helical aggregates.[52] The sign of the CD couplet is dependent on the helicity of the dipole transtion moments associated with the UV/vis. This phenomenon is due to exciton coupling, which involves splitting of an excited state into two different excited states upon interactions of transition dipole moments.[53] The new excited states are separated from the original excited state by the interaction energy V i.e. if the difference between the ground state energy and original excited state energy is E, then the two new excited states will have the energies E+V and E-V. The CD signals associated with these excited states are equal in magnitude and opposite in sign. Moreover, the exact sign of the CD signal associated with the two states, depends on the cross

product of the two dipole transition moments. When a right-handed helix is formed, the cross product is positive, and the sign of the CD signal associated with E-V state is positive while the sign of the CD signal associated with the E+V state is negative. However, when a left-handed helix is formed, the sign of the CD signal associated with the E-V state is negative and E+V state is positive. This gives rise to the exciton coupling rule, where a positive couplet i.e. the shorter wavelength region is negative, and longer wavelength region is positive, is associated with a right handed helix and vice versa (Figure 1.10). It was shown that BTA monomers that are enantiomers of each other, form helical aggregates of opposite helical sense, whereas those with achiral sidechains did not produce a CD signal.

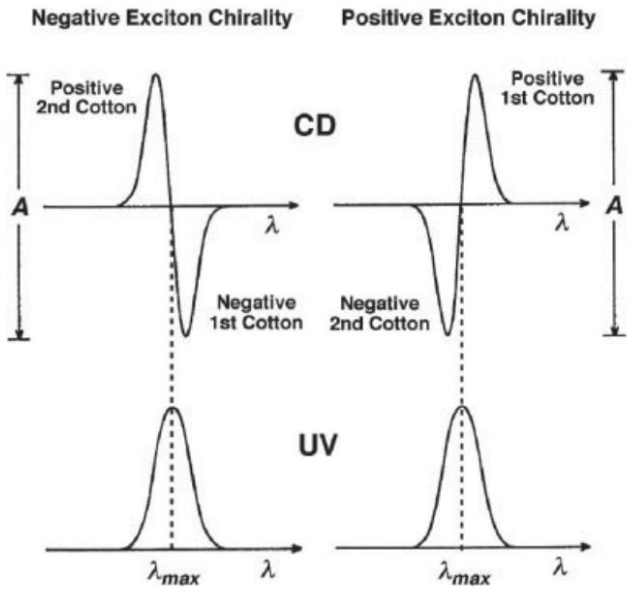

Figure 1.10 A depiction of negative and positive CD couplets. Figure taken from *Comprehensive Chiroptical Spectroscopy, Volume 2: Applications in Stereochemical Analysis of Synthetic Compounds, Natural Products, and Biomolecules*. **2012**

Another example of C_3-symmetrical building blocks are oligo-(phenyleneethynylene) (OPE) based molecules such as OPE based tricarboxamides (Figure 1.8). These molecules showed a CD signal with bisignate couplets in methylcyclohexane indicative of helical aggregates. The CD signal was eliminated at higher temperatures upon disaggregation. Computational calculations showed that in these OPE based tricarboxamides adjacent molecules in the columnar stack are

separated by 3.725 Å and rotated by 18.0°, while the amide moieties are rotated out of the plane by 34.9°. Other methods by which these systems have been characterized include TEM and small-angle X-ray scattering (SAXS). For example, BTAs with oligopeptide sidechains have been characterized with TEM and SAXS to show formation of nanorods. Helical aggregates with monomers containing triphenyl amine cores (Figure 1.8) have been characterized via AFM to show the presence of columnar aggregates. Overall, it is clear that C_3-symmetric molecules with aromatic cores and chiral peripheral moieties often form helical supramolecular aggregates.

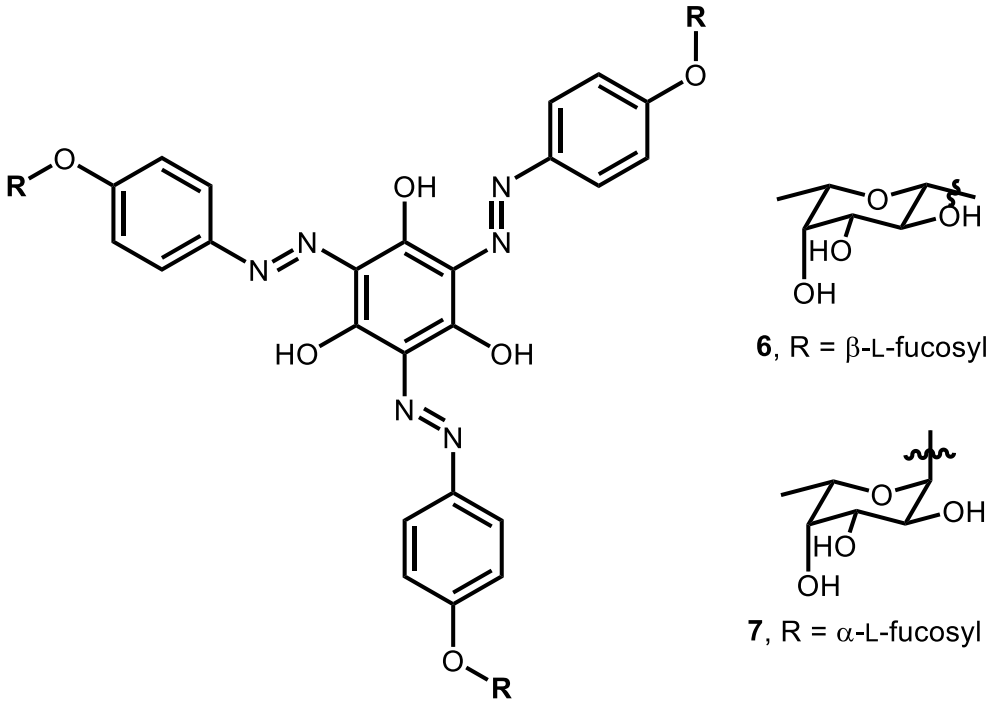

Scheme 1.4 The structure of Yariv reagents **6** and **7**

To see if the Yariv reagents also form helical aggregates like other C_3-symmetrical molecules containing aromatic cores and chiral peripheral moieties, we previously used CD. The CD spectra of **1**-**5** has been previously acquired in water. Additionally, two more Yariv reagents, **6** and **7** (Scheme 1.4) were also synthesized and the CD spectra of these Yariv reagents was also acquired. In each case the CD spectrum contained two bisignate couplets (Figure 1.11), one associated with the shorter wavelength 398 nm transtion and the other with the longer wavelength 487 nm transtion seen in the UV/vis spectra of each of these Yariv reagents in water (Figure

1.12). Each of the β-D-Sugar containing Yariv reagents (**1**-**4**) showed positive couplets. Assigning the absolute configuration of the aggregates requires further knowledge of their morphology[54] i.e. stacked on top of each other (H aggregates) vs offset (J aggregates). Comparison of the Yariv reagent structure to C_3-symmetric molecules described above suggests that the Yariv reagent aggregates are likely H-type. If the Yariv reagents are indeed H-type aggregates, it would suggest that the β-D-sugar containing Yariv reagents (**1**-**4**) form right-handed helical structures. Although qualitatively the spectra for **1**-**4** look similar with two positive couplets, there are significant differences in intensity. The quantitative parameter of a CD spectrum represents the difference in absorbance of left and right-handed circularly polarized light and is described in terms of ellipticity, θ (mdeg) or molar ellipticity, Δε deg $M^{-1}cm^{-1}$. The ellipticities of the CD spectra of **2** are comparable to **1**, while those for **3** and **4** are significantly lower. The lower intensity CD spectra of **4** is consistent with its lower amount of aggregation.

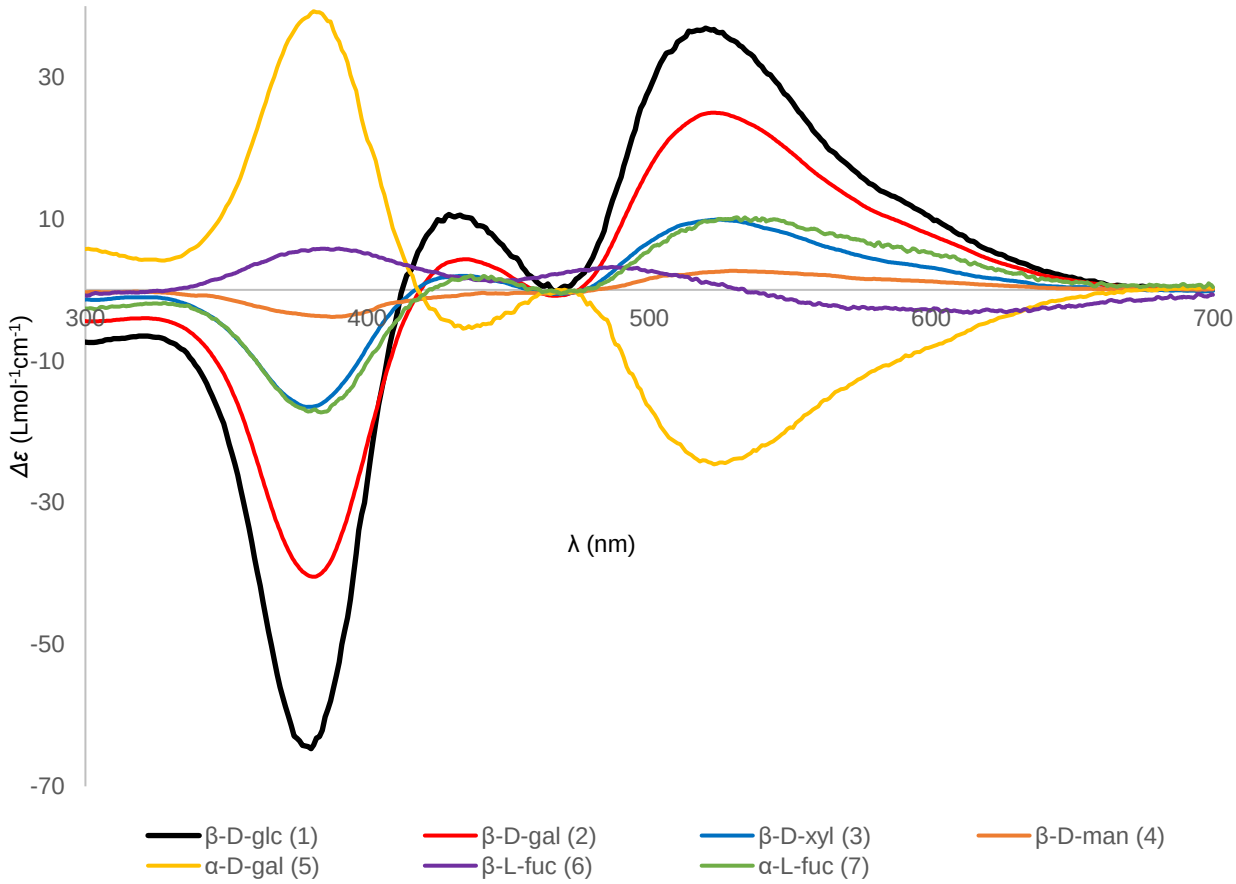

Figure 1.11 CD spectra of various Yariv reagents previously obtained in the Basu Lab (300 μM in water)

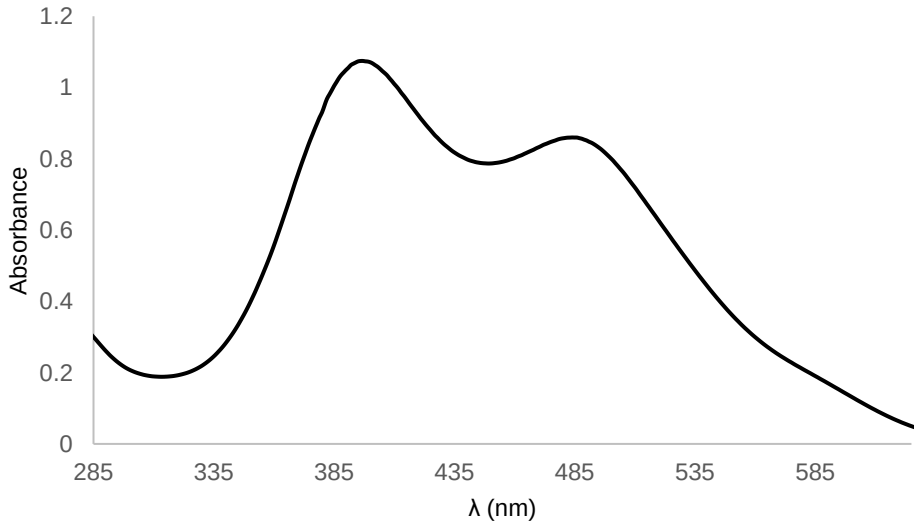

Figure 1.12 UV/vis spectrum of **1** in water (30 μM)

The effect of anomeric configuration on the helicity of the Yariv reagent aggregates can be seen by comparing the CD spectra of α-D-galactosyl (**5**) with the β-D-sugar containing Yariv reagents. While two bisignate couplets are still seen, the sign of each couplet is negative. The negative sign of these Cotton effects indicates an inversion of helicity in the aggregates. The effect of switching from D to L enantiomers can been seen in the CD spectrum of β-L-fucosyl (**6**). A negative cotton effect is seen in the CD spectrum of β-L-fucosyl (**6**) as well. Finally, the CD spectrum of α-L-fucosyl Yariv (**7**) was obtained and found to exhibit positive exciton couplets. These results indicate that a change in the D or L configuration, as well as a change in the anomeric configuration, causes a reversal in helicity in the Yariv reagent aggregates. To ensure that the CD signal arises only because of aggregation and is not an inherent property of the monomer, the CD signal of **1** was also acquired in disaggregating conditions such as in the presence of SDS or in DMSO. A significantly weaker CD spectra was seen in presence of 1%SDS. In DMSO no CD signal was seen (Figure 1.13).

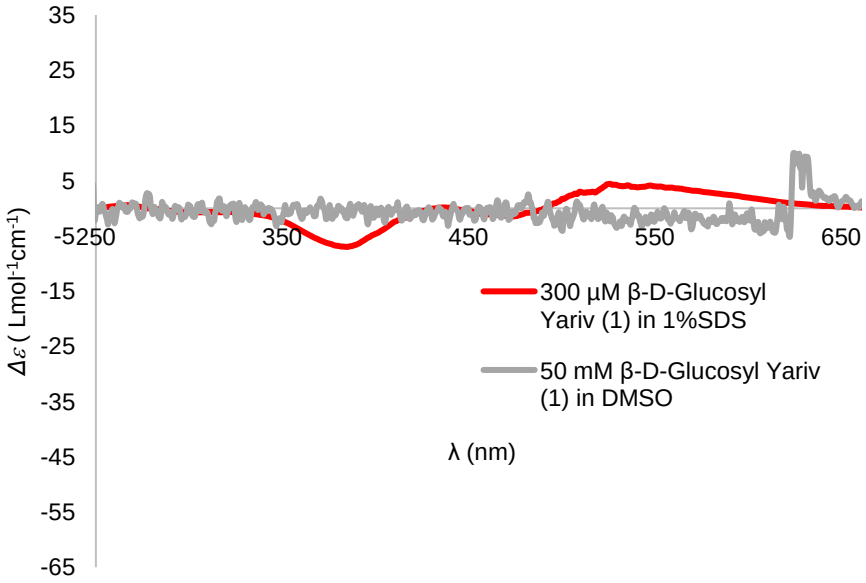

Figure 1.13 CD Spectra of **1** in disaggregating conditions

Comparison of the helicity of aggregates with their AGP binding ability shows that all the Yariv reagents that were known in literature to bind AGP (**1**, **2** and **3**) also form right-handed helical

structures alongside containing β-D-sugars. The only β-D-sugar containing Yariv reagent that does not bind AGP, **4**, showed a very weak right-handed CD signal. These results suggested the importance of right-hand helicity of the Yariv aggregates to their AGP binding ability. Support for this hypothesis has been provided by the modelling study as well. It was shown that the stacks formed by the dimers of **1** in the study had a right-handed rotation.[48]

1.6 Work presented in this thesis

Despite significant development in our understanding of the Yariv reagents, several unaddressed issues remain. In this thesis, our work on three aspects of the Yariv reagents is presented-

1) Synthesis and Purification of Yariv reagents: The first synthesis of Yariv reagents was reported in 1962. Several subsequent synthetic protocols provided additional details such as partial ^{1}H NMR characterization**.** However, a detailed purification protocol and complete NMR characterization data had not been reported. In our attempts to synthesize the Yariv reagents we found that the isolated crude products often contaminated with impurities and exhibited peak broadening in their NMR spectra. In this chapter the reasons for these issues which hindered complete characterization are presented in brief. Further, optimization and development of protocols that help resolve these problems are presented.
2) Characterization of Yariv reagent-AGP Binding and Yariv reagent aggregation: This chapter elaborates upon our previous work on the helicity of Yariv reagent aggregates and its correlation of AGP binding ability. The CD spectra and AGP binding ability of additional Yariv reagents and the bis and mono analogs of **1** is discussed. The development and results of a modified version of the Yariv-AGP binding detection gel assay that allows comparison of AGP binding ability of different Yariv reagents is also presented. This allowed us to see more clearly the correlation between the helicity of the Yariv reagent aggregates and AGP binding ability. The Yariv reagent aggregates are

further studied using a variety of experiments such as the soldiers and sergeants phenomenon and variable temperature experiments.

3) Identification of the chromophore(s) in the Yariv reagent UV/vis spectra: The UV/vis spectra of Yariv reagents exhibit two major transitions (Figure 1.12). However, the exact chromophore(s) that give rise to these transitions have not been determined. In this chapter, we evaluate if some commonly hypothesized identities of the chromophore for hydroxy-azo dyes are applicable to the Yariv reagents.

References

1. Hooke, R., *Micrographia, or, Some physiological descriptions of minute bodies made by magnifying glasses : with observations and inquiries thereupon*. 1665.
2. Baker, J. R., The Cell-Theory: A Restatement, History, and Critique. *Journal of Cell Science* **1952,** *s3-93* (22), 157-190.
3. Doblin, M. S.; Pettolino, F.; Bacic, A., Plant cell walls: the skeleton of the plant world. *Functional Plant Biology* **2010,** *37* (5), 357.
4. Burton, R. A.; Gidley, M. J.; Fincher, G. B., Heterogeneity in the chemistry, structure and function of plant cell walls. *Nat Chem Biol* **2010,** *6* (10), 724-32.
5. Holmes, F. L., Elementary Analysis and the Origins of Physiological Chemistry. *Isis* **1963,** *54* (1), 50-81.
6. Hon, D. N. S., Cellulose: a random walk along its historical path. *Cellulose* **1994,** *1* (1), 1-25.
7. Zeng, Y.; Himmel, M. E.; Ding, S. Y., Visualizing chemical functionality in plant cell walls. *Biotechnol Biofuels* **2017,** *10*, 263.
8. Cosgrove, D. J., Growth of the plant cell wall. *Nat Rev Mol Cell Biol* **2005,** *6* (11), 850-61.
9. Showalter, A. M., Structure and function of plant cell wall proteins. *Plant Cell* **1993,** *5* (1), 9-23.
10. Nothnagel, E. A., Proteoglycans and Related Components in Plant Cells. **1997,** *174*, 195-291.
11. Jermyn, M. A.; Yeow, Y. M.; Woods, E. F., A Class of Lectins Present in the Tissues of Seed Plants. *Functional Plant Biology* **1975,** *2* (4), 501.
12. Lin, S.; Miao, Y.; Huang, H.; Zhang, Y.; Huang, L.; Cao, J., Arabinogalactan Proteins: Focus on the Role in Cellulose Synthesis and Deposition during Plant Cell Wall Biogenesis. *Int J Mol Sci* **2022,** *23* (12).
13. Seifert, G. J.; Roberts, K., The biology of arabinogalactan proteins. *Annu Rev Plant Biol* **2007,** *58*, 137-61.
14. Su, S.; Higashiyama, T., Arabinogalactan proteins and their sugar chains: functions in plant reproduction, research methods, and biosynthesis. *Plant Reprod* **2018,** *31* (1), 67-75.

15. Ajayi, O. O.; Held, M. A.; Showalter, A. M., Glucuronidation of type II arabinogalactan polysaccharides function in sexual reproduction of Arabidopsis. *Plant J* **2022,** *109* (1), 164-181.
16. Deng, Y.; Wan, Y.; Liu, W.; Zhang, L.; Zhou, K.; Feng, P.; He, G.; Wang, N., OsFLA1 encodes a fasciclin-like arabinogalactan protein and affects pollen exine development in rice. *Theor Appl Genet* **2022,** *135* (4), 1247-1262.
17. Kaur, D.; Moreira, D.; Coimbra, S.; Showalter, A. M., Hydroxyproline-O-Galactosyltransferases Synthesizing Type II Arabinogalactans Are Essential for Male Gametophytic Development in Arabidopsis. *Front Plant Sci* **2022,** *13*, 935413.
18. Plachno, B. J.; Kapusta, M.; Stolarczyk, P.; Swiatek, P., Arabinogalactan Proteins in the Digestive Glands of Dionaea muscipula J.Ellis Traps. *Cells* **2022,** *11* (3).
19. Zhou, D.; Zou, T.; Zhang, K.; Xiong, P.; Zhou, F.; Chen, H.; Li, G.; Zheng, K.; Han, Y.; Peng, K.; Zhang, X.; Yang, S.; Deng, Q.; Wang, S.; Zhu, J.; Liang, Y.; Sun, C.; Yu, X.; Liu, H.; Wang, L.; Li, P.; Li, S., DEAP1 encodes a fasciclin-like arabinogalactan protein required for male fertility in rice. *J Integr Plant Biol* **2022**.
20. Nguyen, H. T.; Herrmann, F.; Konig, S.; Goycoolea, F. M.; Hensel, A., Structural characterization of the carbohydrate and protein part of arabinogalactan protein from Basella alba stem and antiadhesive activity of polysaccharides from B. alba against Helicobacter pylori. *Fitoterapia* **2022,** *157*, 105132.
21. Somerville, C.; Bauer, S.; Brininstool, G.; Facette, M.; Hamann, T.; Milne, J.; Osborne, E.; Paredez, A.; Persson, S.; Raab, T.; Vorwerk, S.; Youngs, H., Toward a Systems Approach to Understanding Plant Cell Walls. *Science* **2004,** *306* (5705), 2206-2211.
22. Rydahl, M. G.; Hansen, A. R.; Kracun, S. K.; Mravec, J., Report on the Current Inventory of the Toolbox for Plant Cell Wall Analysis: Proteinaceous and Small Molecular Probes. *Front Plant Sci* **2018,** *9*, 581.
23. Voiniciuc, C.; Pauly, M.; Usadel, B., Monitoring Polysaccharide Dynamics in the Plant Cell Wall. *Plant Physiol* **2018,** *176* (4), 2590-2600.
24. Lee, K. J.; Marcus, S. E.; Knox, J. P., Cell wall biology: perspectives from cell wall imaging. *Mol Plant* **2011,** *4* (2), 212-9.
25. DeVree, B. T.; Steiner, L. M.; Glazowska, S.; Ruhnow, F.; Herburger, K.; Persson, S.; Mravec, J., Current and future advances in fluorescence-based visualization of plant cell wall components and cell wall biosynthetic machineries. *Biotechnol Biofuels* **2021,** *14* (1), 78.
26. Wallace, I. S.; Anderson, C. T., Small molecule probes for plant cell wall polysaccharide imaging. *Front Plant Sci* **2012,** *3*, 89.
27. Smith, E. F.; Mangin, L., Sur la callose, nouvelle substance fondamentale existant dans la membrane. *The Journal of Mycology* **1892,** *7* (2), 140.
28. Currier, H. B.; Strugger, S., Aniline blue and fluorescence microscopy of callose in bulb scales ofAllium cepa L. *Protoplasma* **1956,** *45* (4), 552-559.
29. Evans, N. A.; Hoyne, P. A.; Stone, B. A., Characteristics and specificity of the interaction of a fluorochrome from aniline blue (sirofluor) with polysaccharides. *Carbohydrate Polymers* **1984,** *4* (3), 215-230.
30. Yariv, J.; Rapport, M. M.; Graf, L., The interaction of glycosides and saccharides with antibody to the corresponding phenylazo glycosides. *Biochem J* **1962,** *85*, 383-8.

31. Yariv, J.; Lis, H.; Katchalski, E., Precipitation of arabic acid and some seed polysaccharides by glycosylphenylazo dyes. *Biochem J* **1967,** *105* (1), 1C-2C.
32. Anderson, R. L.; Clarke, A. E.; Jermyn, M. A.; Knox, R. B.; Stone, B. A., A Carbohydrate-Binding Arabinogalactan-Protein From Liquid Suspension Cultures of Endosperm From <I>Lolium multiflorum</I>. *Functional Plant Biology* **1977,** *4* (1), 143-158.
33. Jermyn, M. A., Comparative specificity of concanavalin A and the beta lectins. *Aust. J. Plant Physiol.* **1978,** *5* (5), 687-696.
34. Clarke, A. E.; Gleeson, P. A.; Jermyn, M. A.; Knox, R. B., Characterization and Localization of β-Lectins in Lower and Higher Plants. *Functional Plant Biology* **1978,** *5* (5), 707.
35. van Holst, G.-J.; Clarke, A. E., Quantification of arabinogalactan-protein in plant extracts by single radial gel diffusion. *Anal. Biochem* **1985,** *148* (2), 446-450.
36. Willats, W. G.; Knox, J. P., A role for arabinogalactan-proteins in plant cell expansion: evidence from studies on the interaction of beta-glucosyl Yariv reagent with seedlings of Arabidopsis thaliana. *Plant J* **1996,** *9* (6), 919-25.
37. Roy, S.; Jauh, G. Y.; Hepler, P. K.; Lord, E. M., Effects of Yariv phenylglycoside on cell wall assembly in the lily pollen tube. *Planta* **1998,** *204* (4), 450-458.
38. Triplett, B. A.; Timpa, J. D., β-Glucosyl and α-Galactosyl Yariv Reagents Bind to Cellulose and Other Glucans. *Journal of Agricultural and Food Chemistry* **1997,** *45* (12), 4650-4654.
39. E.F. Woods, G. G. L., M.A. Jermyn, The Self-Association of Glycosyl Phenylazo Dyes (Yariv Antigens). *Aust. J. Chem.* **1978,** *31* (10), 2225-2238.
40. Zhou, L. H.; Weizbauer, R. A.; Singamaneni, S.; Xu, F.; Genin, G. M.; Pickard, B. G., Structures formed by a cell membrane-associated arabinogalactan-protein on graphite or mica alone and with Yariv phenylglycosides. *Ann Bot* **2014,** *114* (6), 1385-97.
41. Leenders, C. M.; Jansen, G.; Frissen, M. M.; Lafleur, R. P.; Voets, I. K.; Palmans, A. R.; Meijer, E. W., Monosaccharides as Versatile Units for Water-Soluble Supramolecular Polymers. *Chemistry* **2016,** *22* (13), 4608-15.
42. Huang, Y.; Hu, J.; Kuang, W.; Wei, Z.; Faul, C. F., Modulating helicity through amphiphilicity-tuning supramolecular interactions for the controlled assembly of perylenes. *Chem Commun (Camb)* **2011,** *47* (19), 5554-6.
43. Hendrikse, S. I. S.; Su, L.; Hogervorst, T. P.; Lafleur, R. P. M.; Lou, X.; van der Marel, G. A.; Codee, J. D. C.; Meijer, E. W., Elucidating the Ordering in Self-Assembled Glycocalyx Mimicking Supramolecular Copolymers in Water. *J Am Chem Soc* **2019,** *141* (35), 13877-13886.
44. Van Gorp, J. J.; Vekemans, J. A.; Meijer, E. W., C3-symmetrical supramolecular architectures: fibers and organic gels from discotic trisamides and trisureas. *J Am Chem Soc* **2002,** *124* (49), 14759-69.
45. Buendia, J.; Calbo, J.; Garcia, F.; Arago, J.; Viruela, P. M.; Orti, E.; Sanchez, L., Helical supramolecular polymerization of C3-symmetric amides and retroamides: on the origin of cooperativity and handedness. *Chem Commun (Camb)* **2016,** *52* (42), 6907-10.
46. Smulders, M. M.; Nieuwenhuizen, M. M.; de Greef, T. F.; van der Schoot, P.; Schenning, A. P.; Meijer, E. W., How to distinguish isodesmic from cooperative supramolecular polymerisation. *Chemistry* **2010,** *16* (1), 362-7.

47. Paulsen, B. S.; Craik, D. J.; Dunstan, D. E.; Stone, B. A.; Bacic, A., The Yariv reagent: behaviour in different solvents and interaction with a gum arabic arabinogalactan-protein. *Carbohydr Polym* **2014,** *106*, 460-8.
48. Prerovska, T.; Pavlu, A.; Hancharyk, D.; Rodionova, A.; Vavrikova, A.; Spiwok, V., Structural Basis of the Function of Yariv Reagent-An Important Tool to Study Arabinogalactan Proteins. *Front Mol Biosci* **2021,** *8*, 682858.
49. Kitazawa, K.; Tryfona, T.; Yoshimi, Y.; Hayashi, Y.; Kawauchi, S.; Antonov, L.; Tanaka, H.; Takahashi, T.; Kaneko, S.; Dupree, P.; Tsumuraya, Y.; Kotake, T., beta-galactosyl Yariv reagent binds to the beta-1,3-galactan of arabinogalactan proteins. *Plant Physiol* **2013,** *161* (3), 1117-26.
50. Sato, K.; Hara, K.; Yoshimi, Y.; Kitazawa, K.; Ito, H.; Tsumuraya, Y.; Kotake, T., Yariv reactivity of type II arabinogalactan from larch wood. *Carbohydr Res* **2018,** *467*, 8-13.
51. Dorca, Y.; Matern, J.; Fernández, G.; Sánchez, L., C3-Symmetrical π-Scaffolds: Useful Building Blocks to Construct Helical Supramolecular Polymers. *Israel Journal of Chemistry* **2019,** *59* (10), 869-880.
52. Berova, N.; Di Bari, L.; Pescitelli, G., Application of electronic circular dichroism in configurational and conformational analysis of organic compounds. *Chem Soc Rev* **2007,** *36* (6), 914-31.
53. Kobayashi, N.; Muranaka, A., Chapter 1. Theory of Optical Spectroscopy. **2011**, 1-41.
54. Swathi, K.; Sissa, C.; Painelli, A.; George Thomas, K., Supramolecular chirality: a caveat in assigning the handedness of chiral aggregates. *Chem Commun (Camb)* **2020,** *56* (59), 8281-8284.

Chapter 2- Synthesis and purification of Yariv reagents

Some findings from this chapter are published: Hoshing, R.; Saladino, M.; Kuhn, H.; Caianiello, D.; Lusi, R. F.; Basu, A., An Improved Protocol for the Synthesis and Purification of Yariv Reagents. *J. Org. Chem* **2020,** *85* (24), 16236-16242

2.1 Introduction

The first synthesis of Yariv reagents was reported in 1962.[1] The synthesis involved reduction of 4-nitrophenyl glycosides into 4-aminophenyl glycosides using a heterogeneous catalyst (platinum oxide) and molecular hydrogen at atmospheric pressure, followed by diazotization of 4-aminophenol glycosides and coupling to phloroglucinol (Figure 2.1). The dye was isolated from the coupling reaction by precipitation from ethanol (for the gluco and lactoside) or methanol (for the galactoside). Subsequently, two more synthetic protocols for the Yariv reagent were published. [2,3] In each of these subsequent protocols, modifications were made only to the first step

i.e. reduction of the 4-nitrophenyl glycosides into 4-aminophenyl glycosides. The first of these subsequent protocols described the use of either a Parr shaker and Pd/C catalyst to reduce the 4-nitrophenyl glycosides or an alternate reduction technique which involved transfer hydrogenation using ammonium formate. In the second protocol, an easier method to remove the excess ammonium formate was described. Another set of reports claimed increased yield upon minimizing the amount of water utilized during diazotization.[4-5]

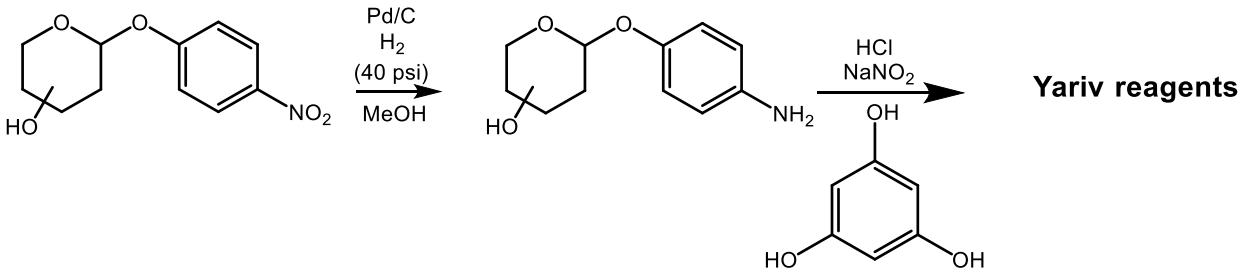

Figure 2.1 General synthetic scheme of Yariv reagents

Previous reports[6] stated that the isolated crude product can contain significant amount of impurities. The only report[6] of a purification technique addressed the impurities by an extensive procedure involving dialysis, lyophilization, redissolution followed by reprecipitation by methanol, with this procedure repeated seven times and yielding 10% of the original material. Therefore, a simple and straightforward purification protocol of the Yariv reagents had never been reported. Besides the issue of a lack of purification protocol, there was also a lack of NMR characterization data for the Yariv reagents. The first publication to report NMR characterization data of the Yariv reagent **1** only reported the resonances corresponding to the aromatic protons on the peripheral aromatic rings.[2] These protons appear as doublets at 7.16 and 7.66 ppm. Based on analogy with other C_3 symmetric hydroxyazo dyes,[7] the 7.66 ppm doublet corresponds to the protons which are ortho to the azo group and the 7.16 ppm doublet corresponds to the protons ortho to the *C*-O-Sugar carbon. Another publication[8] reported the partial NMR spectra of **1** in DMF and assigned the peak at 4.94 ppm to the sugar anomeric proton.

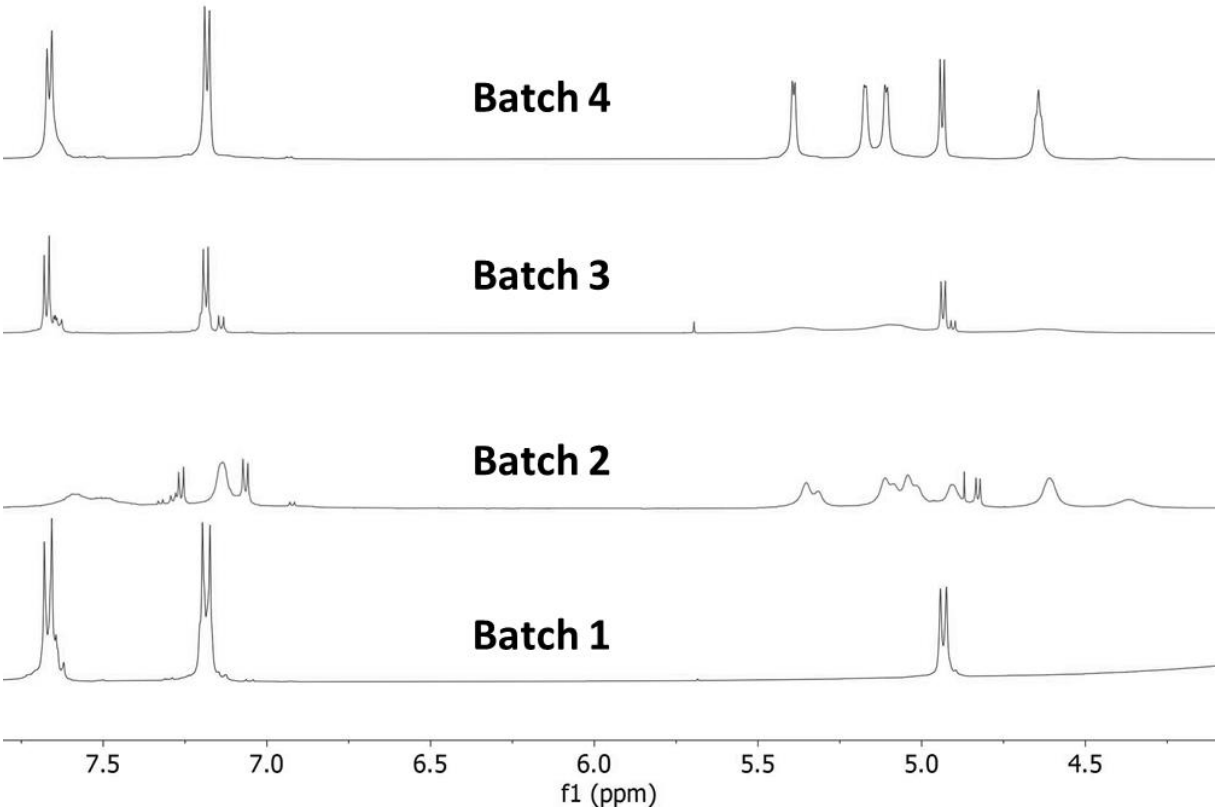

Figure 2.2 NMR spectra of the crude product from multiple batches of β-D-glucosyl Yariv reagent (**1**) syntheses. Spectra were obtained in DMSO-d_6.

We began the synthesis of **1**, first using the literature protocols.[3] We utilized the Parr shaker procedure to hydrogenate 4-nitrophenyl glucoside at 40 psi for 7 hours. A spot-to-spot conversion, and the NMR spectra of the crude product suggested that 4-aminophenyl glucoside was obtained. The first batch of the β-D-glucosyl Yariv reagent (**1**) was synthesized and the ^{1}H NMR spectrum of the crude product was obtained in DMSO-d_6 (Figure 2.2). Although resonances corresponding to the peripheral aromatic protons and the anomeric proton could clearly be seen, the sugar -OH protons were not visible. However, when a second batch of **1** was synthesized using the same protocol the ^{1}H NMR of batch 2 crude product showed significantly more peaks than expected. Additional peaks in the aromatic region (7-7.5 ppm) and the sugar -OH region (4.5-5.5 ppm) suggested batch 2 crude contained significantly more impurities compared to batch 1. The sugar – OH protons could be seen more clearly in batch 2, although these were still quite broad. To understand the extent of the batch-to-batch variation that can

occur, several batches were synthesized. A set of partial ^{1}H NMR spectra of four representative batches of crude products of **1** are displayed in Figure 2.2. Resonances at 7.16 and 7.66 ppm corresponding to the protons of the p-azophenoxy moiety were observed in each spectrum, but these resonances were occasionally poorly resolved (e.g., batch 2). Several spectra exhibit additional peaks in the aromatic region, indicating the presence of impurities in these batches. Also observed in Figure 2.2 are variations in the peak shapes of the sugar −OH resonances between 4.5 and 5.5 ppm, with many, but not all, of these spectra exhibiting peak broadening. Thus, peak broadening made characterization of Yariv reagents more challenging. Also, the impurities could potentially interfere with Yariv-AGP binding, therefore for Yariv-AGP binding studies having pure Yariv reagents would be useful.

2.2 Identification of the major impurity

Woods et al observed increases in the molecular weight distribution of the Yariv reagent aggregates upon repeated redissolution of **1** in water, followed by precipitation from methanol.[6] They suggested that the increase in molecular weight was due to removal of incomplete diazo coupling products, i.e., bis- and mono-azo adducts, from the aggregates. Our observation of a peak corresponding to the bis azo variant (**8**) of the **1** in the mass spectrum of the crude product of **1** suggests the presence of the bis azo variant of **1** is likely (Peak observed on mass spec: 691.1, MW of M+H of **8**, 691.2). We synthesized the bis azo analog of **1**, **8.** The synthesis of **8** was originally carried out to study the difference between having three vs two peripheral aromatic and carbohydrate moieties on aggregation and AGP binding ability. These studies of aggregation and AGP binding ability of **8** are provided in Chapter 3. But beyond understanding the AGP binding ability and aggregation of **8**, we were able to able to use it to verify the identity of the main impurity.

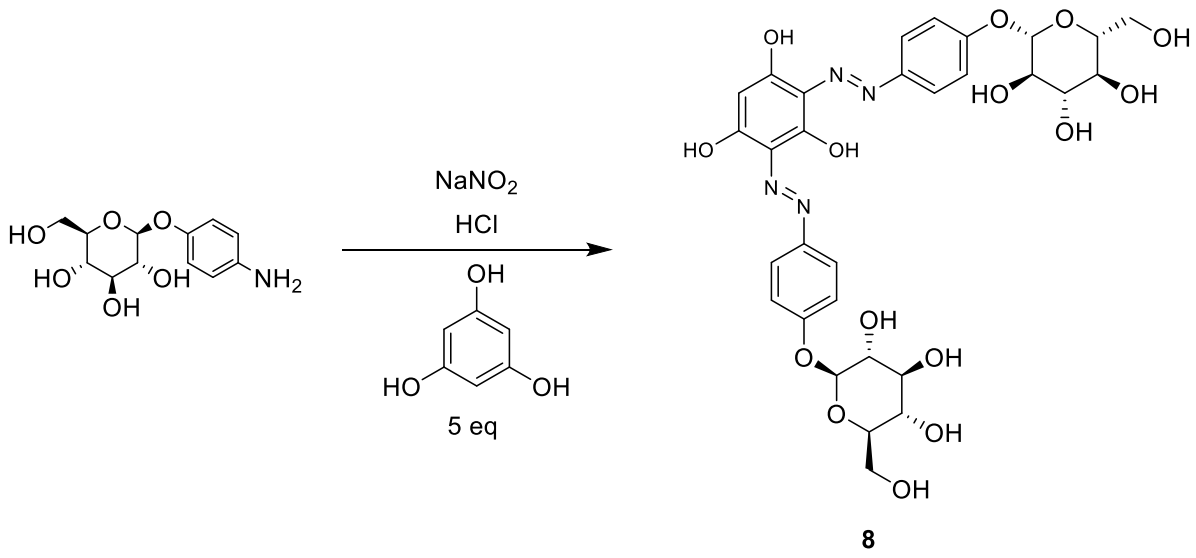

Figure 2.3 Synthesis of bis azo Yariv reagent **8**

To synthesize the bis azo Yariv **8** the Yariv reagent synthesis protocol described above was utilized, except 5 equivalents of phloroglucinol was used instead of 0.34 equivalents (as is done in the synthesis of **1**). A representative spectrum of a crude product is shown in Figure 2.4. Peaks corresponding to the bis azo Yariv reagent **8** can be seen in the 4.5-8 ppm region. Doublets in the 7.1-7.7 ppm region correspond to aromatic protons on the peripheral rings. The doublet at 4.9 ppm corresponds to the anomeric sugar protons. Upon setting the integration values of the aromatic protons to 4, the doublet at 4.9 ppm integrates to 2 as would be expected for the anomeric sugar proton. The spectra also show two singlets in the 5.6-5.8 ppm region. The more downfield singlet at 5.79 ppm integrates to 1 and likely corresponds to the central aromatic proton. The more upfield singlet around 5.69 ppm corresponds to the aromatic hydrogen of one of the starting materials, phloroglucinol.[9] A peak at 15.58 ppm is seen in the NMR spectra of the bis azo **8** crude product, corresponding to the -O*H*/N*H* proton. The peak at 15.58 ppm integrates to 1, which is lower than the expected value of 2. A slightly altered synthetic protocol of the bis azo variant, where it was precipitated at neutral pH instead of being precipitated at an acidic pH gave rise to a crude product which had a slightly different ^{1}H NMR spectrum. In this alternate form,

the upfield aromatic peak at 7.62 ppm is observed at 7.26 ppm and the aromatic peak at 7.13 is observed at 7.06 ppm. Further, the peak at 5.79 corresponding to the central aromatic proton, is observed at 4.87 ppm. The two forms of **8** can be interchanged by varying the pH. Addition of 1 equivalent of triethyl amine (TEA) gives rise to the ^{1}H spectra obtained by precipitating at a higher pH value (Fig 2.5). This suggested that the ^{1}H spectra of **8** at a higher pH corresponds to an anion of **8.** However, the exact structure of either form, the form at lower pH or higher pH has not been confirmed but is discussed further in chapter 4.

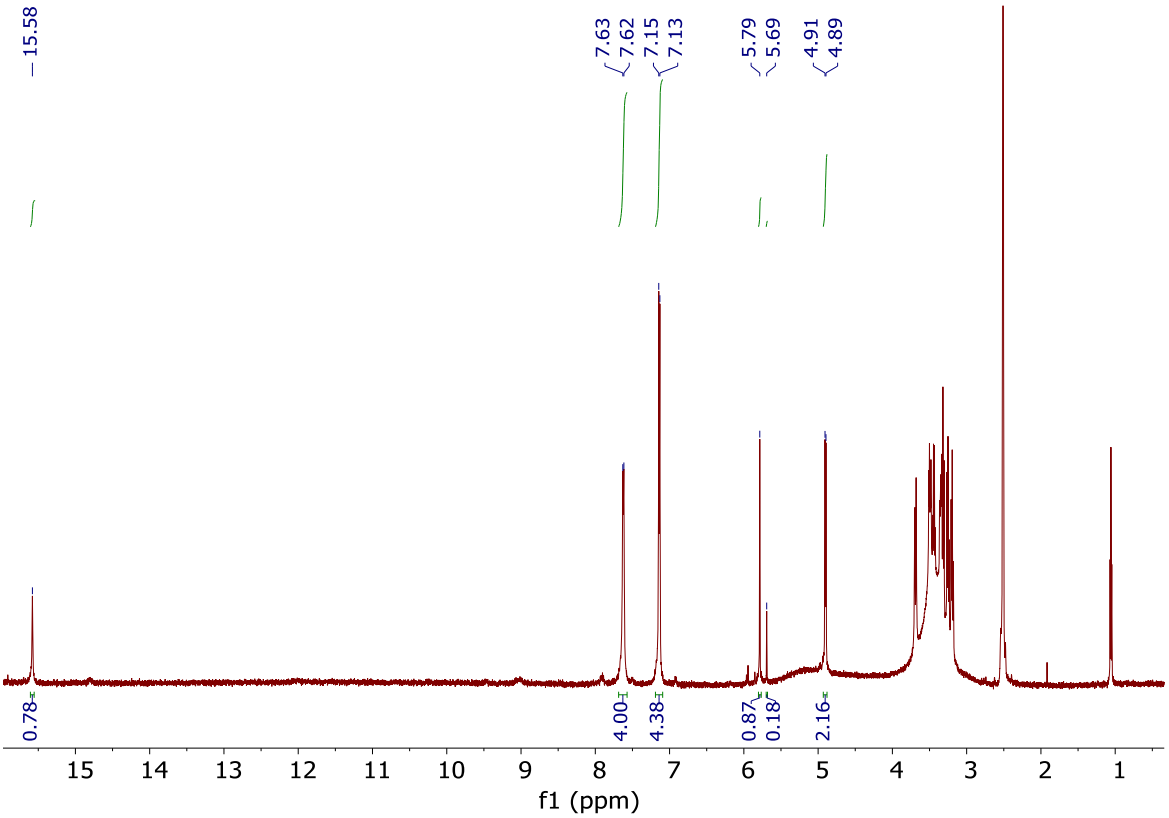

Figure 2.4 ^{1}H NMR of crude product from synthesis of bis azo Yariv reagent **8**, isolated at an acidic pH value**.** Spectra were obtained in DMSO-d^{6}

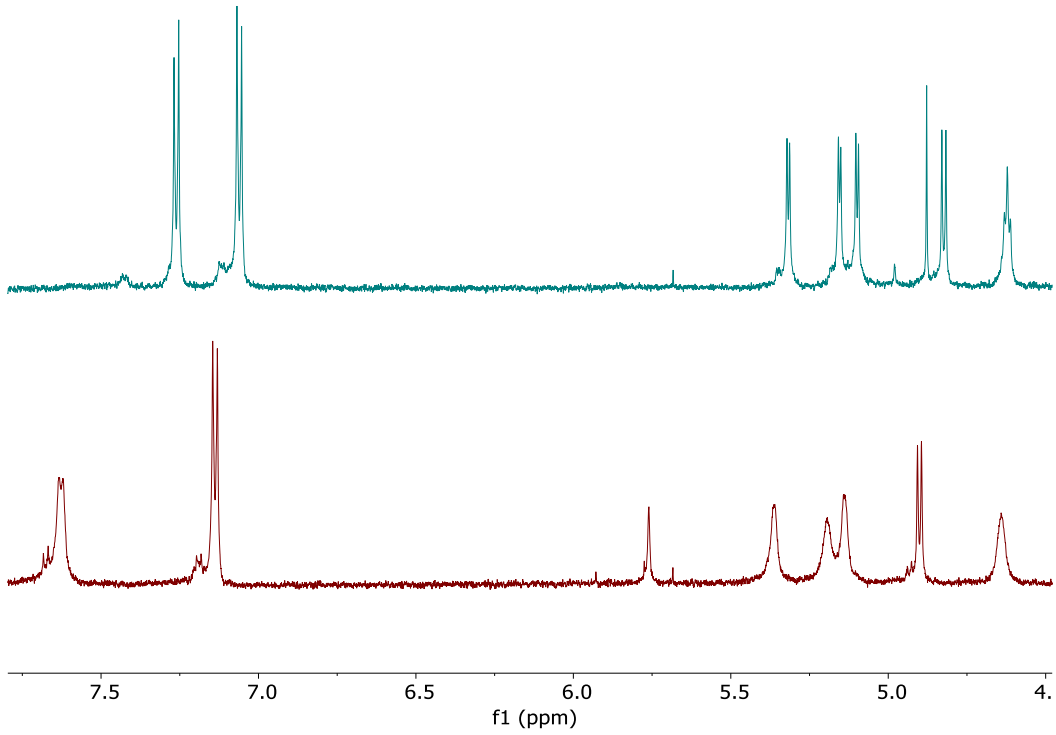

Figure 2.5 Comparison of ^{1}H NMR of the two bis azo Yariv reagent **8** forms. Before (bottom) and after (top) addition of 1 equivalent of TEA. Spectra were obtained in DMSO-d_6

A comparison of the proton spectra (Figure 2.6) from a preparation of **1** (batch 2) with the proton spectra of **8** shows the presence of **8** in the crude product of **1**. The aromatic region (6.8-7.7 ppm) shows the presence of sharp doublets at 7.05 and 7.26 ppm in each spectrum. Similarly, every peak in the 4.5-5.5 ppm of ^{1}H NMR of **8** also appears in the **1** batch 2 crude spectra. For example, the peak at 4.89 corresponding to the core aromatic proton appears in both spectra and so do the broad peaks in 4.5-5.5 ppm region corresponding to the sugar -OHs. Figure 2.7 shows the comparison of **1** Batch 3 with bis azo Yariv reagent **8** at lower pH values. Peaks corresponding to bis azo Yariv reagent **8** such as the aromatic protons at 7.14 and 7.63 ppm as well as the anomeric at 4.9 ppm clearly appear in the Batch 3 spectra. In summary, the main impurity appearing in the tris azo Yariv reagent crude **1** can be either form of the bis azo Yariv reagent **8**.

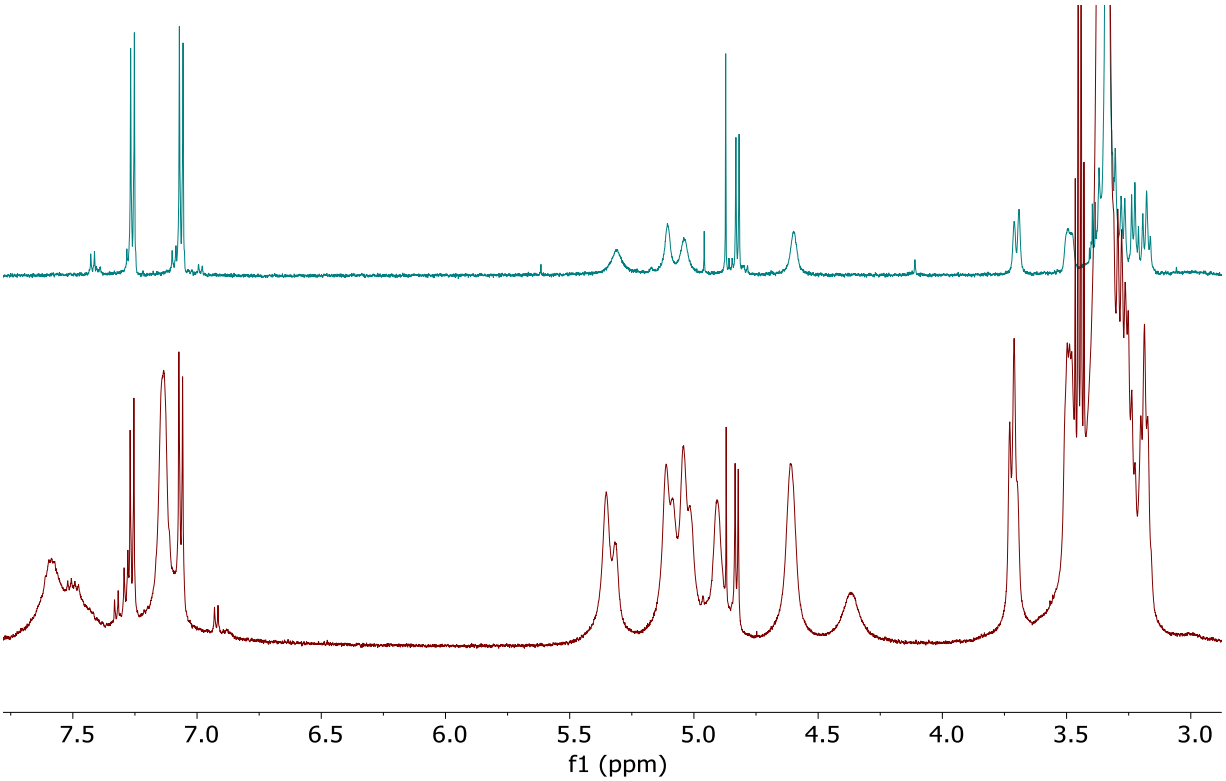

Figure 2.6 Comparison of ^{1}H NMR of bis azo Yariv reagent **8** after addition of 1 equivalent of TEA (top) and tris Yariv **1** crude batch 2 (bottom). Spectra were obtained in DMSO-d_6

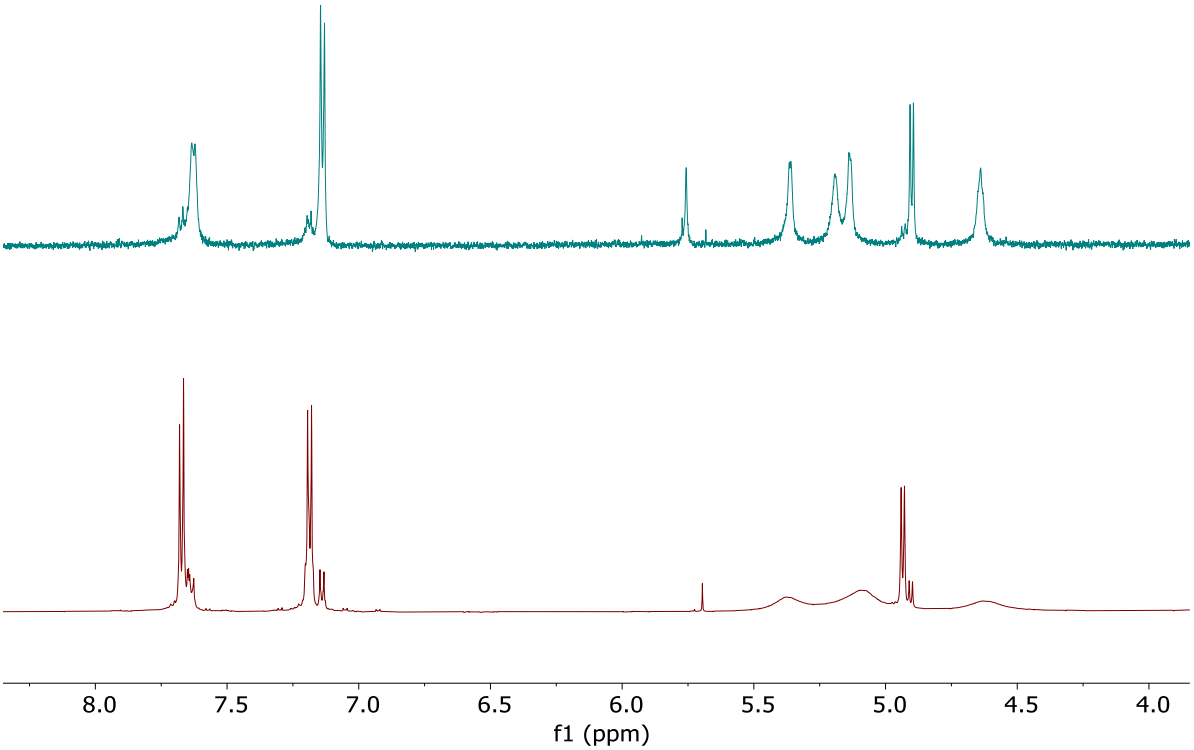

Figure 2.7 Comparison of ^{1}H NMR of bis azo Yariv reagent **8** (top) and tris Yariv reagent **1** crude batch 3. Spectra were obtained in DMSO-d_6

2.3 Development of purification protocol

Our attempts at removing the impurities focused on using the redissolution and reprecipitation protocol mentioned by Woods et al.[6] To evaluate if redissolution− reprecipitation is effective in removing these impurities, the crude product of **1** (batch 2) was dissolved in water and reprecipitated from ethanol to provide a material that we designate R1X. The ^{1}H NMR spectrum of R1X does not contain the doublets at 7.05 ppm and 7.26 ppm corresponding to the peripheral aromatic protons of **8** or the peak at 4.89 ppm corresponding to the core aromatic proton in **8** (Figure 2.8). The NMR spectrum of **1** R1X therefore indicates a significant reduction in the amount of **8** compared to the crude product of **1**. Thus, one round of redissolution-reprecipitation protocol was clearly effective in significantly reducing the bis azo **8** impurities.

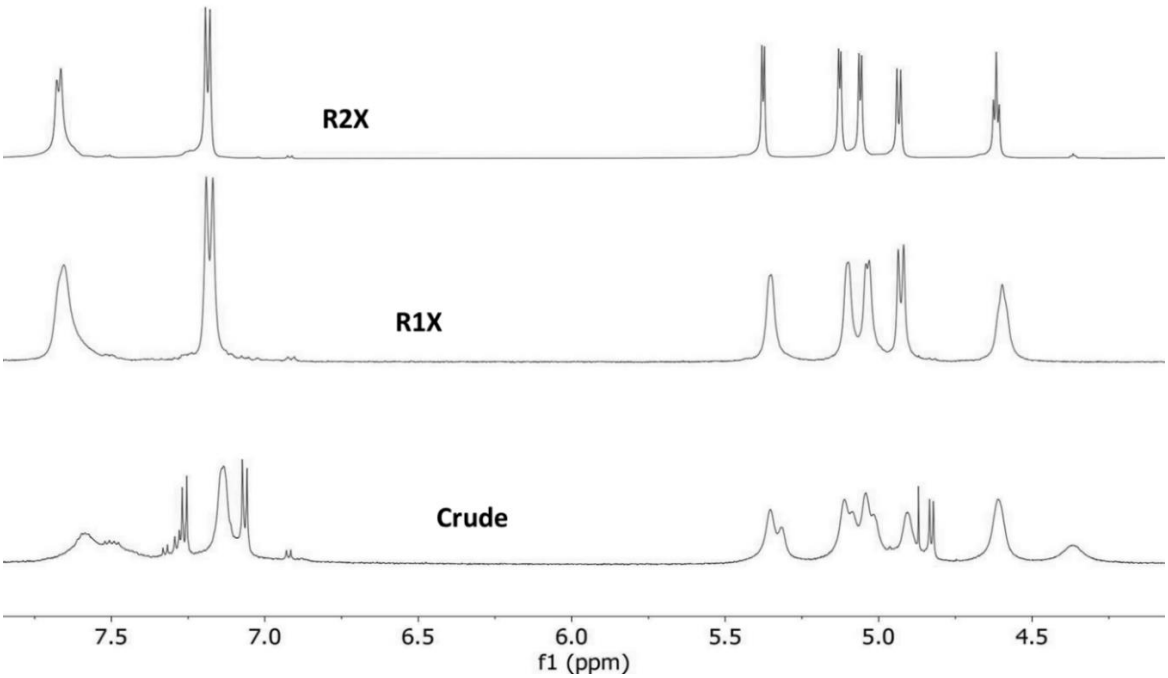

Figure 2.8 Purification of the β-D-glucosyl Yariv reagent (**1**) batch 2 crude showing, from bottom to top, the crude, the reprecipitated once (R1X), and the reprecipitated twice (R2X) spectra. Spectra were obtained in DMSO-d_6

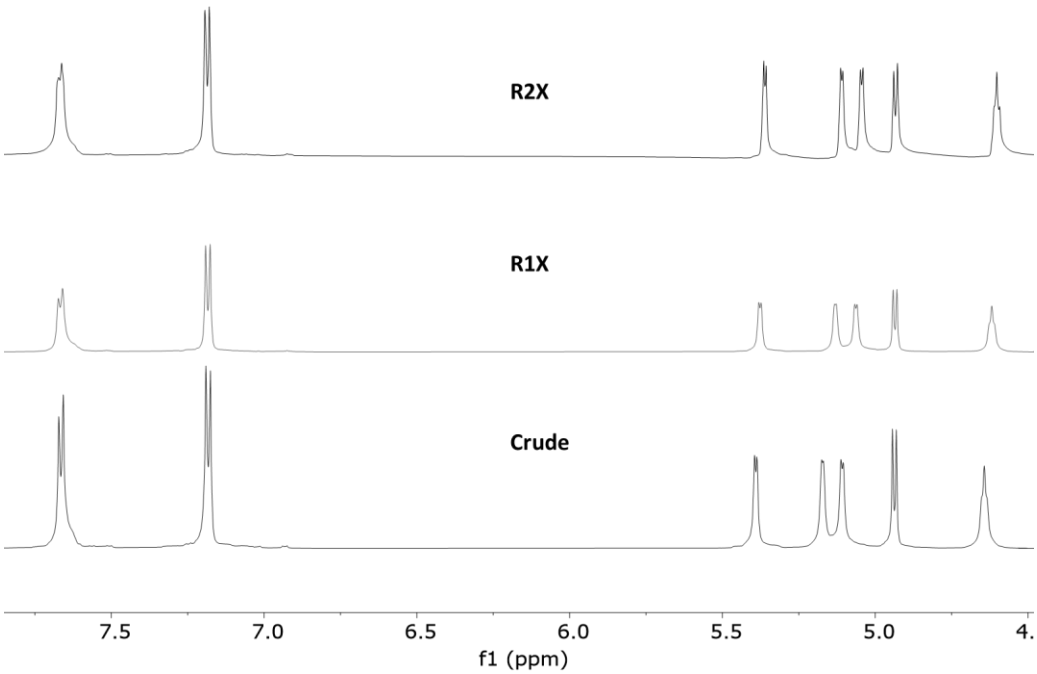

Figure 2.9 Purification of the β-D-glucosyl Yariv reagent (**1**) batch 4 crude showing, from bottom to top, the crude, the reprecipitated once (R1X), and the reprecipitated twice (R2X) spectra. Spectra were obtained in DMSO-d_6

The ^{1}H spectra of Batch 2 R1X does not suggest the presence of any bis azo **8** impurities. However, the Woods et al protocol had claimed that the molecular weights of the Yariv reagent aggregates increased with repeated reprecipitation. Therefore, it was hypothesized that any further reduction in impurities by reprecipitation could be examined by CD spectroscopy. Another redissolution and reprecipitation was therefore performed to give batch 2 R2X. No presence of the bis azo **8** contents could be discerned in batch 2 R2X as well (Fig 2.8). Further, the crude product of batch 4 had negligible bis azo **8** (Fig 2.2). There the batch 4 sample was also useful in examining effects of redissolution-reprecipitation on sample that do not contain the bis azo **8** impurity. The redissolution- reprecipitation protocol was performed twice on the batch **4** crude sample to obtain batch 4 R1X and batch 4 R2X and no significant change in the ^{1}H NMR was noticed (Figure 2.9).

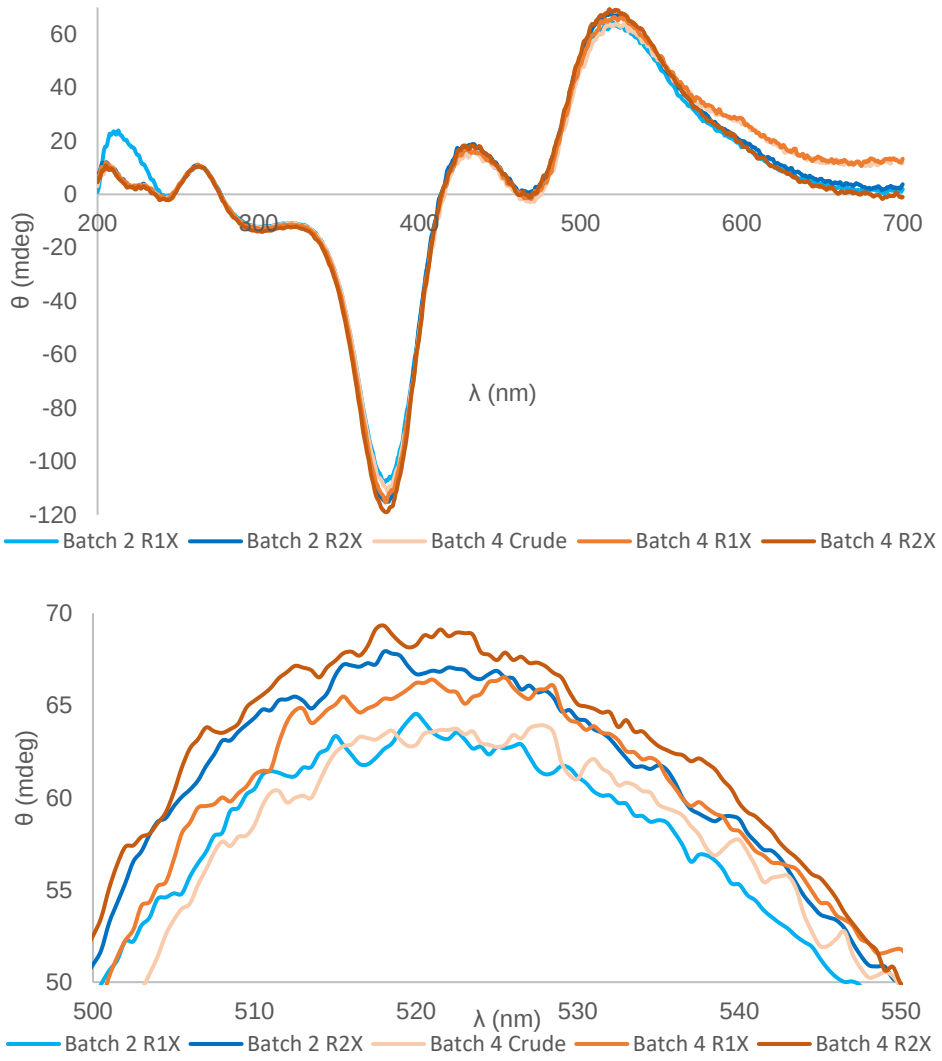

Figure 2.10 CD spectra upon purification of the β-D-glucosyl Yariv reagent (**1**). Spectra acquired in water (300 μM)

The CD spectra of the various samples of **1** was obtained. When the CD signal at the maxima (527 nm) for the R1X sample of Batch 2 is compared to the R2X sample of Batch 2, an increase of 4 mdeg can be seen (Figure 2.10). This increase is interesting because it demonstrates that even though there seems to be little difference in the ^{1}H NMR spectra of batch 2 R1X and R2X with respect to the amount of the bis azo impurity **8**, a slight increase in CD signal is noticed. Comparison of the crude, R1X and R2X of batch 4 also shows a clear increase in CD signal at

527 nm (Figure 2.10). Therefore, even if the ^{1}H spectra suggests that Yariv reagent **1** is mostly pure, the redissolution− reprecipitation protocol is useful to perform.

2.4 Resolving the -OH peak broadening

The sugar -OH peaks at 5.37 ppm, 5.11 ppm, 5.05 ppm and 4.61 ppm in the crude of Batch 2 (Figure 2.8) are broad and the coupling is unresolved. Besides, the reduction of impurities another goal of developing a purification protocol was to resolve the peak broadening associated with the sugar -OH resonances. Having well resolved -OH peaks which allow calculation of the coupling constants would enable better characterization of the Yariv reagents. Comparison of the ^{1}H NMR spectrum of **1** crude product with the spectrum of **1** R1X at 4.61 ppm and 5.05 ppm indicates some sharpening of the sugar -OH peaks (Figure 2.8). A second round of redissolution and reprecipitation to generate batch R2X resulted in further sharpening of the sugar −OH peaks, and the coupling to the backbone C−H protons was observed (Figure 2.8). This indicates that the redissolution-reprecipitation protocol is effective in reducing the broadening associated with the sugar- OH peaks.

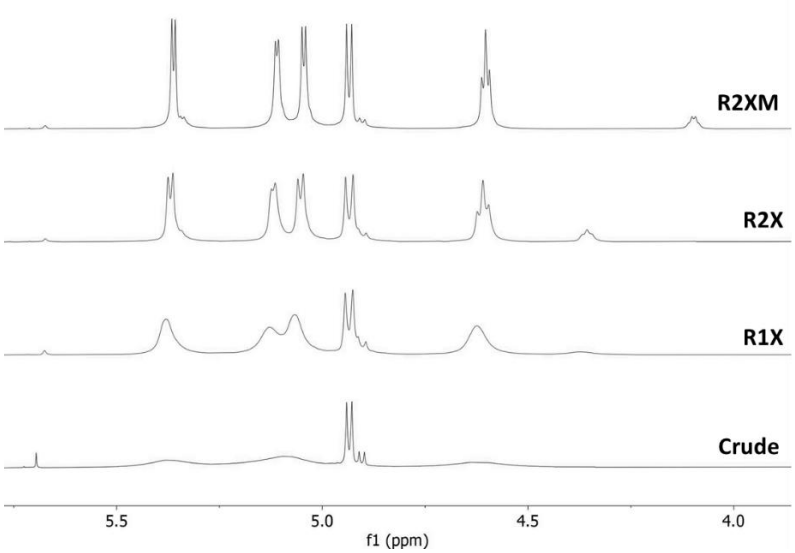

Figure 2.11 Purification of the β-D-glucosyl Yariv reagent (**1**) batch 3 crude showing, from bottom to top, the crude, the reprecipitated once (R1X), and the reprecipitated twice (R2X), triturated with methanol (R2XM) spectra. Spectra were obtained in DMSO-d_6

However, in some cases additional processing beyond redissolution and reprecipitation was required to observe sharp −OH peaks. For example, as seen in Figure 2.11, the crude product from batch 3 was subject to two rounds of redissolution and reprecipitation to give R1X and R2X. This procedure successfully resolved individual −OH proton resonances that were not visible in the crude product, but these resonances remained slightly broadened even in the R2X sample. Peak broadening of labile protons can occur due to hydrogen exchange with water present in DMSO.[10] Such exchange would lead to peak broadening in the water peak at 3.33 ppm as well. Evaluating peak width at half height in the batch 3 R1X and batch R2X samples for the 3.33 ppm peak shows that water peak in R1X (peak width at half height = 9.23 Hz) is significantly broader than R2X (peak width at half height = 3.6 Hz). Given that the sugar -OH peaks are also broader in R1X than in R2X, it suggests that the peak broadening is due to water.

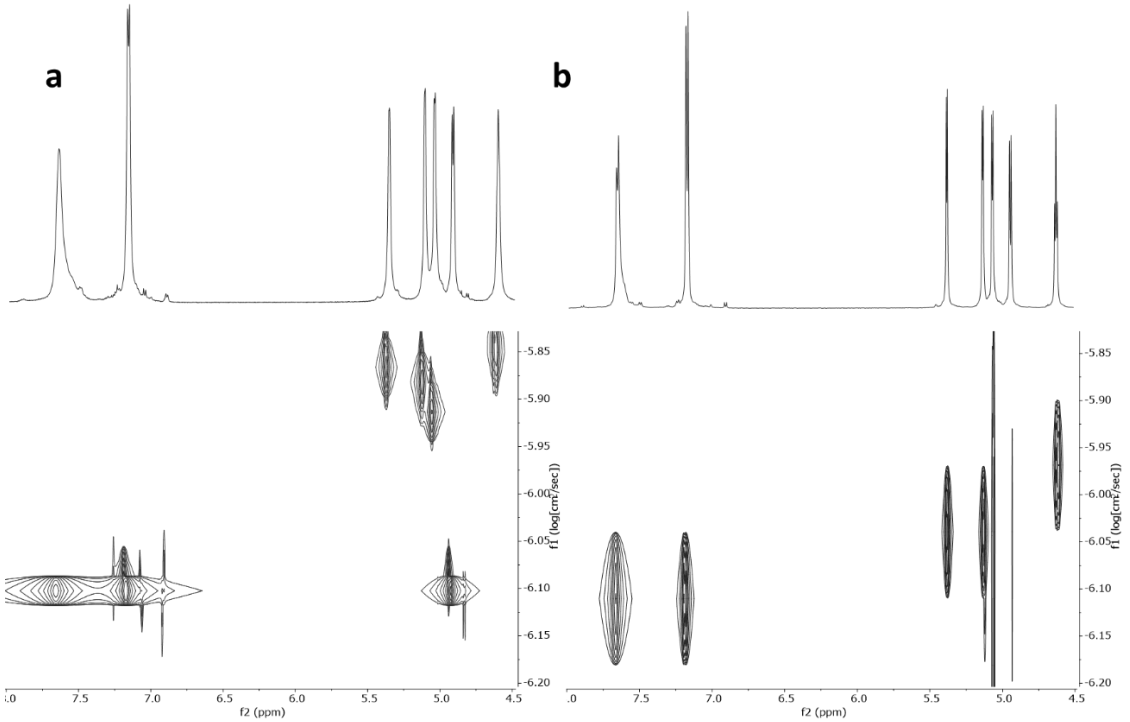

Figure 2.12 Comparison of ^{1}H NMR and DOSY NMR spectra and of a β-D-glucosyl Yariv reagent (**1**) batch 2 sample containing (a) broad−OH peaks vs a sample containing (b) sharp −OH peaks

Next, DOSY NMR experiments were carried out using two different samples of **1**, one with batch 2 R1X and the batch 2 R1X. The log of the diffusion coefficient (D) was recorded for the various sugar -OH resonances as well as for the resonance for water in each sample. A more positive log D for a resonance indicates that the proton associated with the peaks is diffusing faster. The diffusion coefficient of the sugar −OH resonances was greater (logD = −5.9) in the samples containing broad peaks (R1X) compared to the sharp −OH peak (R2X) samples (logD = −6.0), indicating that the R1X -O*H*s are diffusing faster (Figure 2.12). The logD values for the nonexchangeable aromatic protons of both samples displayed the same diffusion coefficients (logD = −6.1). The differences in the diffusion coefficient values of the sugar −OH resonances between the two samples are consistent with an increased exchange of these protons with water in the sample with broader sugar -OH resonances. An examination of the level of trace water observed in the DMSO-d_6 sample before and after the dissolution of the Yariv reagent indicates an increase after analyte addition (Figure 2.13), establishing that the excess water observed in the NMR spectra originates from water associated with the Yariv reagent and not solely from adventitious moisture in the NMR solvent. This was corroborated by the observation of a smaller diffusion constant for water in the sample exhibiting broad Yariv −OH peaks (Table 2.1).

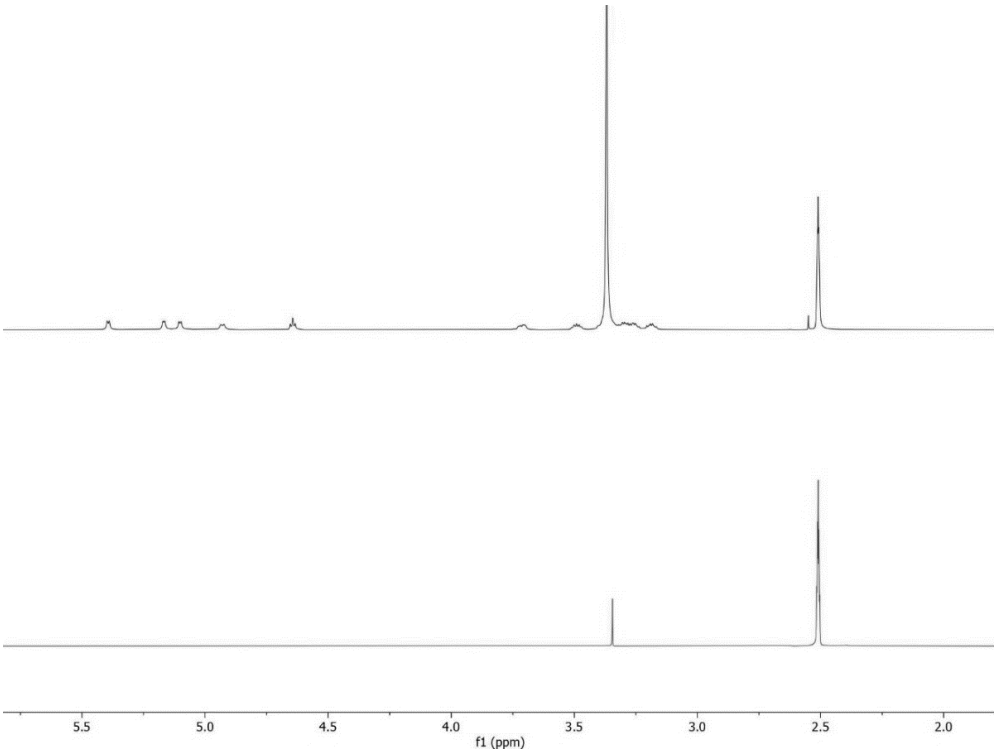

Figure 2.13 β-D-glucosyl Yariv reagent (**1**) NMR (top) and the solvent DMSO-d_6 NMR (bottom)

Finally, ^{1}H spectra of batch 4 of **1** was acquired at various temperatures. Increase in temperature resulted in significant peak broadening in both sugar -OH NMR peaks and water NMR peak as well as upfield shifts in each of these peaks (Figure 2.14). The upfield shifts along with peak broadening seen in the variable temperature NMR experiment matched exactly what was seen upon increasing temperature in another system where a labile proton exchanged with the water in DMSO.[10] It was clear now that the peak broadening was due to exchange with water.

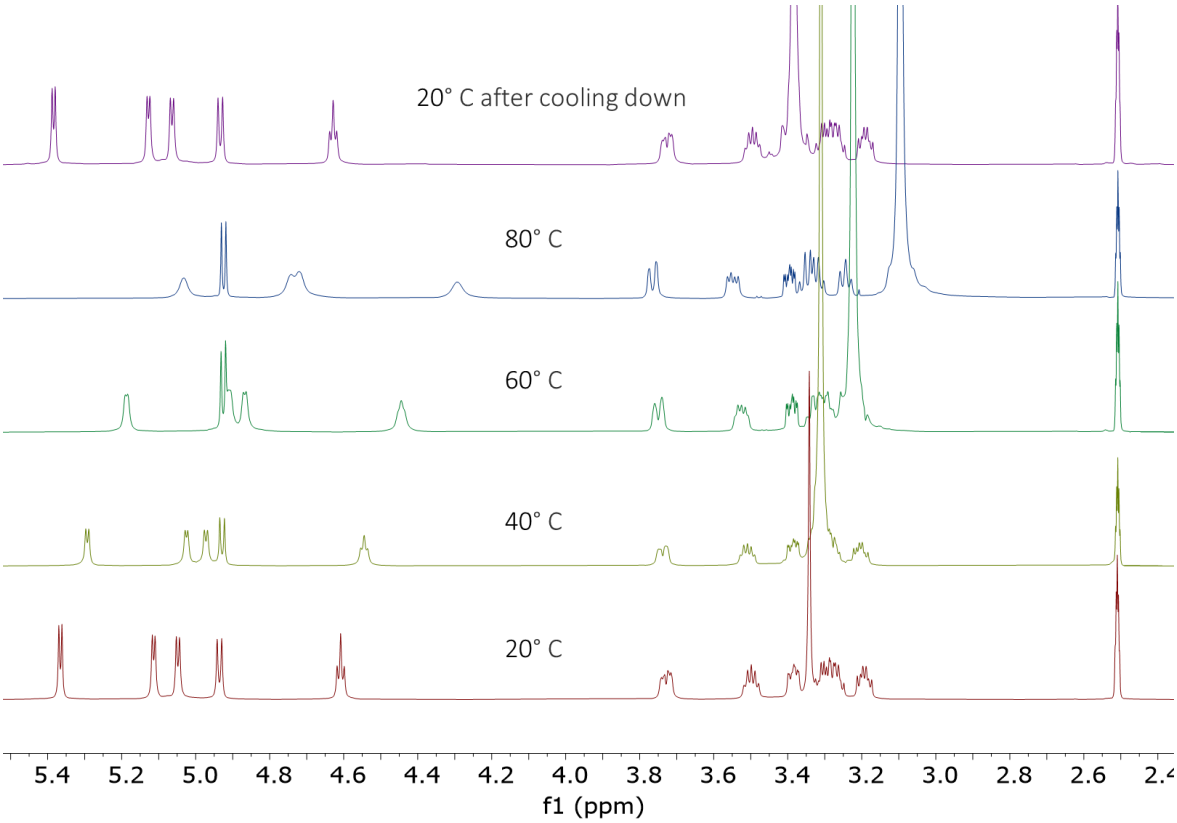

Figure 2.14 Partial ^{1}H spectra of batch 4 of **1** at various temperatures

Table 2.1. Diffusion constants (-Log D) of β-D-glucosyl Yariv reagent (**1**) samples containing either sharp or broad -sugar OH peaks

Proton resonance (*ppm*) / **Sample Log D**	ArH *7.66*	ArH *7.18*	2-OH *5.37*	3-OH *5.11*	4-OH *5.05*	H1 *4.94*	6-OH *4.61*	Water *3.35*
Sharp -OH	6.11	6.11	6.04	6.04	6.09	6.04	5.97	4.59
Broad -OH	6.10	6.10	5.87	5.88	5.91	6.10	5.85	5.34
Difference	0.01	0.01	0.17	0.16	0.17	-0.06	0.12	-0.75

2.5 Development and optimization of drying protocol

Table 2.2 Results of various drying conditions tested, X represents broad OH and √ indicates sharpened OH peaks

β-D-Gal Yariv 10 mg samples in DMSO-d_6	Column 1	Column 2	Column 3	Column 4	Column 5	Column 6	Column 7
Incubation conditions/ Time Period of incubation	+Vacuum (high vac)	+Dessicator +Drierite	+Dessicator +P_2O_5 +Drierite	+Methovaped +Dessicator +Drierite	+Methovaped +Dessicator +Drierite +P_2O_5	+Methovaped +Vacuum (high vac)	+Methovaped +Dessicator +Drierite outside +Vacuum
1 hr						X -Broadness in the 3.6-4.6 ppm region lost -3.3-3.6 ppm becomes broad -methanol peak appears -Ethanol peak lost	
24 hr	X -Broadness in the 3.6-4.6 ppm region lost -Ethanol peak remains	X -Broadness in the 3.6-4.6 ppm region lost -Ethanol peak remains	X -Broadness in the 3.6-4.6 ppm region lost -Ethanol peak remains		X -Broadness in the 3.6-4.6 ppm region lost -Ethanol peak lost -Methanol peak present	X -Same as above	X -Broadness in the 3.6-4.6 ppm region lost -Ethanol peak lost -Methanol peak present
72 hr		X -Same as above	X -Same as above	√ -Water peak present -Broadness in the 3.6-4.6 ppm region lost -Ethanol peak lost -methanol peak present	√ -Water peak present	X -Same as above	√ -Water peak present

Upon determining the cause of peak broadening to be exchange with water, the β-D-galactose Yariv reagent **2** was subjected to several conventional drying techniques such as drying over P_2O_5 or Drierite or under high vacuum for various time periods, and the peak broadness of the sugar -OH peaks were monitored. In the first experiment, 10 mg of the crude product from the synthesis of **2** was placed under high vacuum for 24 hrs. Next, two 10 mg samples of the crude product of **2** in scintillation vials were placed in a dessicator containing Drierite. One of the samples was incubated for 24 hrs while the other was incubated for 72 hrs. Finally, another set of

two 10 mg samples of the crude product of **2** were placed in the dessicator, this time alongside P_2O_5. Again, one of the samples was incubated for 24 hrs while the other was incubated for 72 hrs. At the end of each period, the NMR spectrum for each sample was recorded. In each case the resonances for the sugar-OH's were not sharpen (Table 2.2, Column 1,2,3) and (Figure 2.15). Therefore, conventional drying techniques failed to help resolve the peak broadening issue.

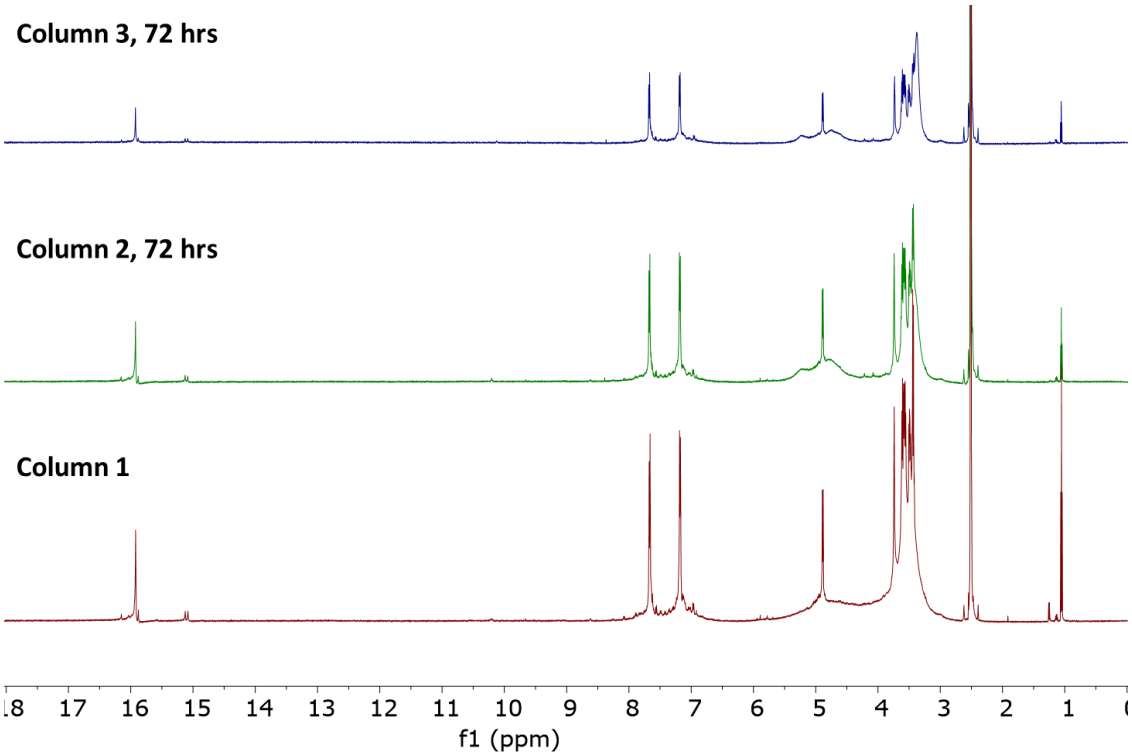

Figure 2.15 ^{1}H NMR spectra corresponding to samples processed with conditions described in Column 1, Column 2 and Column 3 (See Table 2.2)

The Yariv reagents are amphiphilic molecules as a result of the fact they contain a hydrophobic aromatic core and hydrophilic peripheral moieties (sugars). Challenges in characterization due to poor resolution of sugar-OH peaks in ^{1}H NMR spectra is a phenomenon seen in other amphiphilic glycoconjugates as well. In several cases where glycoconjugates were precipitated out of methanol or washed with methanol after precipitation, well resolved −OH resonances were observed, indicating the utility of processing glycoconjugates with methanol during purification.[11-14] Therefore, various treatments with methanol were attempted. Each of the above

conventional drying experiments was repeated. However, prior to incubation each 10 mg sample was first washed with methanol, and then subsequently the methanol was removed by rotary evaporation (a process which we termed "methovaping"). After 24 hrs, none of the samples showed any sharpening of the OH peaks compared to the conventional methods. However, samples incubated in the desiccator for 72 hrs after methovaping showed well resolved and sharpened sugar -OH peaks (Table 2.2, Column 4 and 5) and (Figure 2.16). Moreover, in samples where the sugar OH peaks are sharpened, the peak corresponding to water at 3.3 ppm is also sharpened, corroborating that the peak broadening was due to exchange with water. In summary, a simple methanol wash-evaporation procedure with methanol (methovaping) followed drying in the desiccator with Dririte seemed to be an effective protocol to sharpen sugar -OHs.

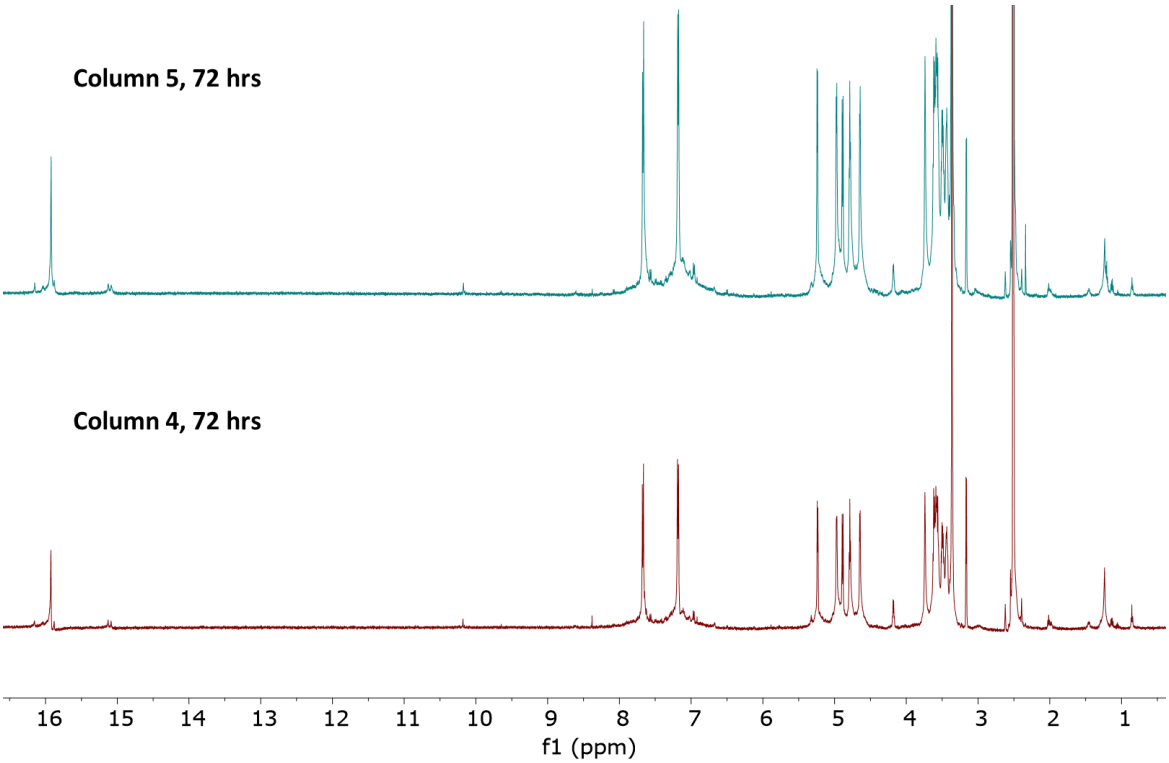

Figure 2.16 ^{1}H NMR spectra corresponding to samples processed with conditions described in Column 4 and Column 5 (See Table 2.2)

Curiously, the sugar OH peaks of the sample dried under high vacuum did not show sharpening after 72 hrs even after methovaping (Table 2.2, Column 6) and (Figure 2.17). To understand if

this had something to do with the vacuum itself, two 10 mg crude samples of **2** were methovaped and then placed in a desiccator containing Drierite which was put under vacuum. After 24 hrs, this sample did not show sharpening of sugar OHs but the sugar OH's were sharpened after 72 hrs (Table 2.2, Column 7) and (Figure 2.17).

To evaluate which of the 3 protocols that provided sharp sugar -OHs worked best, the % excess integration ((experimental integration – expected integration)/expected integration)*100 was plotted for each of the sugar -OHs (Figure 2.18). For each sugar -OH, the lowest value of integration is for the sample dried in the desiccator without vacuum or P_2O_5 after methovaping. Interestingly, in 3 out 4 OHs the highest %excess was seen in the case where desiccator was under high vacuum. This along with the fact that under direct high vacuum sugar OH sharpening is not seen, suggests that high vacuum somehow impedes the drying process.

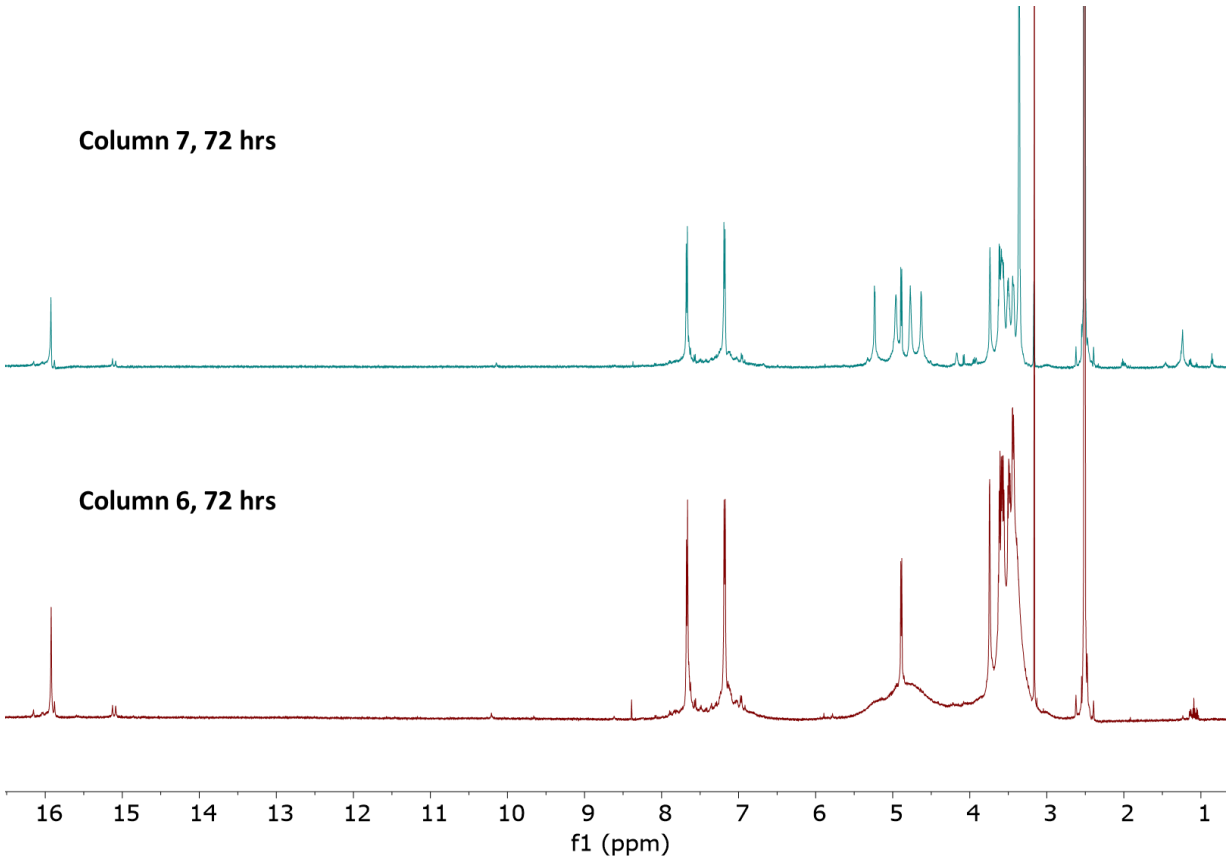

Figure 2.17 ^{1}H NMR spectra corresponding to samples processed with conditions described in Column 6 and Column 7 (See Table 2.2)

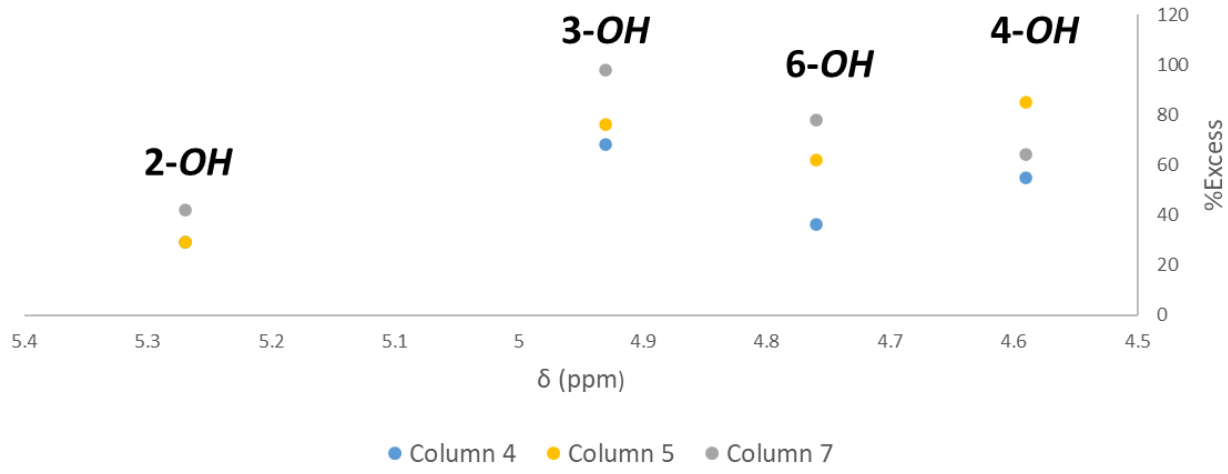

Figure 2.18 % Higher than expected integration values for various -OHs after methovaping

For larger amounts (>40 mg) it was seen that methovaping gave inconsistent results. Therefore, a slightly different protocol was used in these cases. For example, batch 3 of **1** which was subject to two rounds of redissolution and reprecipitation to give batch 3 R2X did not show completely sharpened peaks. Therefore, R2X Batch 3 of **1** was further processed by washing with methanol and subsequent incubation in a vacuum oven at 75 °C for 24 hrs, to give a methanol-processed batch, referred to as R2XM (Figure 2.11). This procedure successfully sharpened the −OH resonances in larger samples. Besides sharpening the −OH peaks, the methanol washing process also effectively removed ethanol from the sample.

In summary, we observed that sugar -OH resonances in the Yariv reagent ^{1}H NMR spectrum are often broad. We ascribed this broadening phenomenon to exchange with water and provided multiple lines of evidence consistent with the hypothesis in this section. Finally, we found that processing the Yariv reagent with methanol is effective in reducing peak broadening as well as residual ethanol.

2.6 Synthesis and purification of other Yariv reagents

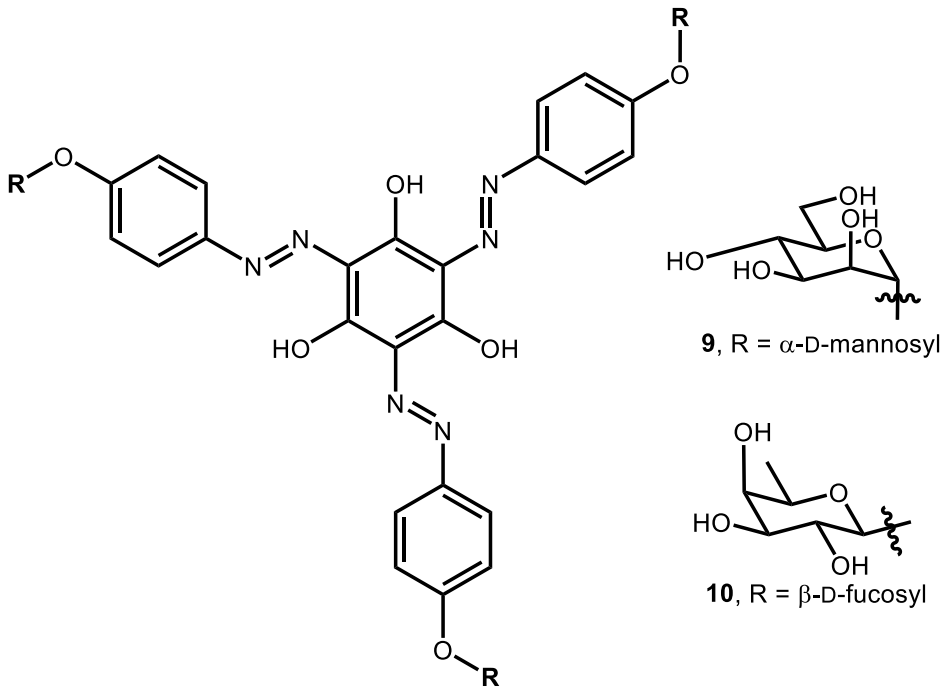

Scheme 2.1 Structures of Yariv reagents **9** and **10**

To study Yariv reagent-AGP binding it would be useful to have samples of the various Yariv reagents that are pure and well characterized. Therefore, several Yariv reagents (**1**−**7**) were resynthesized using these optimized protocols. Additionally, new Yariv reagents **9** and **10** were also synthesized. The diazotization of the cognate 4-aminophenyl glycoside and the coupling to phloroglucinol were carried out in the same manner as that for the glucosyl derivative **1**. Several of the resulting crude products exhibited significant −OH broadening. In each case, redissolution and reprecipitation effectively sharpened the −OH resonances. To remove the additional residual ethanol, the β-D-xylosyl analog **3** and both L-fucosyl compounds **6** and **7** were methovaped. Purified compounds were obtained in good yields. Yields of the crude product ranged from 72 to 93%, and mass balances of the final product after redissolution−reprecipitation and methanol processing ranged from 41 to 99% (Table 2.3). The number in the "crude" row in Table 2.3 represents (mass of crude/theoretical mass of product)*100. The number in the "R1X" row represents (mass of the sample obtained upon first redissolution-reprecipitation/mass of crude)* 100 i.e. mass balance after R1X. The numbers in the "R2X" row represent mass balance after

second redissolution reprecipitation. Numbers in the "R2XM" and "R2XM2" represent mass balance after first time methovaping and second time methovaping respectively. The improved purification protocols allowed the complete characterization of these Yariv reagents by ^{1}H and ^{13}C NMR.

Table 2.3 Crude yield (%); mass balance (%) for each purification step

Yariv / **Purification Step Yield/Mass Balance***	β-D-glc (**1**) Batch 3	β-D-glc (**1**) Batch 4	β-D-gal (**2**)	β-D-xyl (**3**)	β-L-fuc (**6**)	α-L-fuc (**7**)	β-D-fuc (**10**)
Crude	87	86	quant.	77	80	93	72
R1X	77	81	60	53	73	54	59
R2X	92	85	77	82	84	68	41
R2XM	78	95	99	92	90	92	
R2XM2				90			

* *Crude yield refers to the percent yield of the crude product from the synthesis reaction. Subsequent values are mass balances for % recovery of material from each purification step. Not all of the product of a given step was carried forward to each subsequent step.*

The purification protocol was not effective for all Yariv reagents. The ^{1}H NMR spectrum of the crude product for **4** and **5** exhibited impurities that were similar to other Yariv reagents (Figure 2.19). For example, alongside peaks corresponding to the desired product, the spectra of both **4** and **5** contain smaller peaks around the aromatic region (7-7.8 ppm) as well as the sugar -OH region (4.3-5.7 ppm). However, when mass spectrometry results of the crude products were obtained, they did not show evidence for the bis azo variant in either crude product. The redissolution-reprecipitation protocol was attempted to remove these non-bis azo impurities. However, in each case the procedure was unsuccessful, and the impurities remained. Similarly, even the ^{1}H NMR spectra of the crude product of **7** and **9** suggests the presence of minor amount of impurities. The mass spectrometry results of the crude product of **9** do suggest the presence of the bis variant. However, the impurities in **7** and **9** could also not be removed through the redissolution-reprecipitation product.

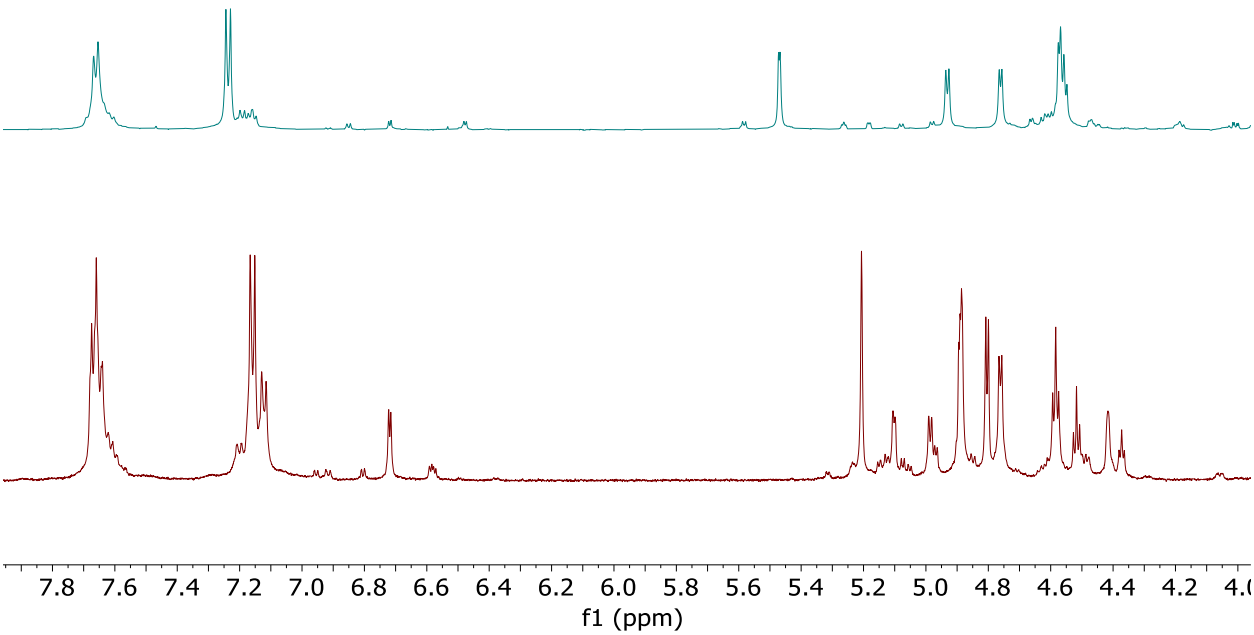

Figure 2.19 ^{1}H NMR spectra of **4** (bottom) and **5** (top)

2.7 Characterization of impurities in 4

To get a better understanding of what the impurities in **4** might be, further characterization of the crude sample of **4** was required. Mass spectrometry results of **4** indicated that a prominent peak appeared at 811.2403. This matched the $[M+H]^+$ fragment of **4** lacking a sugar (Scheme 2.2). The presence of this ion suggests that the impurity could be the fragment of **4** or the free D-mannopyranose formed from hydrolysis of **4**.

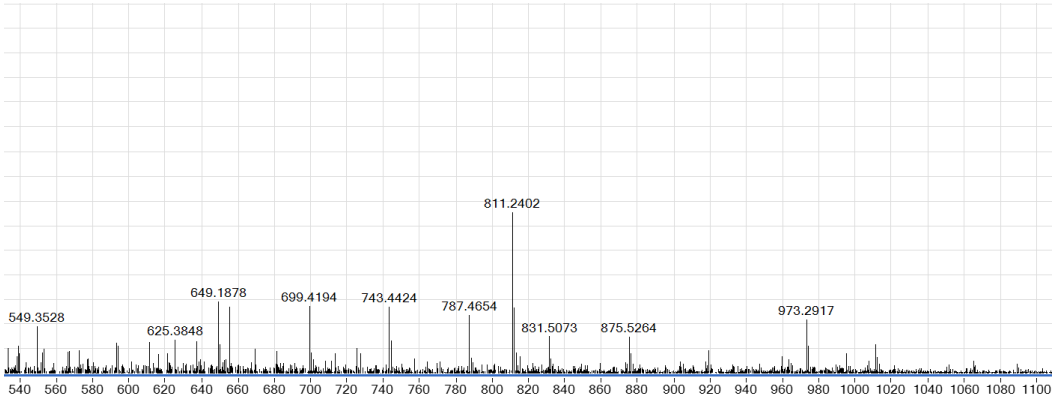

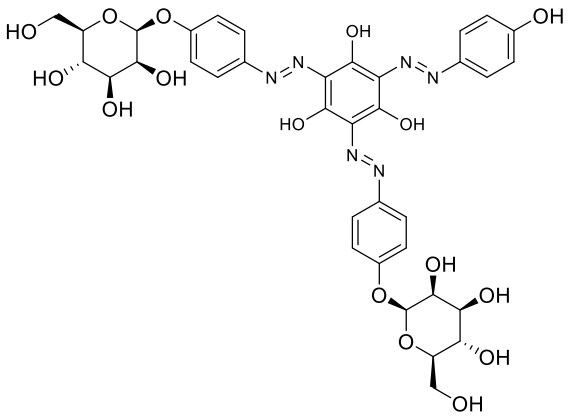

[M + H]+ found: 811.2402

Scheme 2.2 The fragment of **4** with calculated [M+H]+ corresponding to 811.2423 (below) and the mass spec results (above, y axis: ion count, x axis: m/z ratio of the ion)

Upon inspecting the ^{13}C spectrum of **4** we see that each sugar carbon peak has a clear corresponding "impurity" peak (Figure 2.20). The C1' peak appears at 90.7 ppm and has an HSQC correlation to the proton at 5.1 ppm, suggesting this is the anomeric proton of the impurity. It is seen that the anomeric proton of the impurity is a doublet with coupling constant of 5 Hz. COSY spectrum of the crude product shows that the anomeric proton of the impurity is coupled to a proton at 6.7 ppm. Comparison of various spectra of crude products from synthesis of **4**, some of which have broad -OHs and some that have sharp -OH peaks shows that the peak at 6.7 ppm is only observed when other sugar -OHs are observed as well (Figure 2.21). The fact that the peak at 6.7 ppm is sharp only when other peaks corresponding to exchangeable protons are, suggests that the proton corresponding to the 6.7 ppm peak is an exchangeable proton. More importantly, the proton at 6.7 ppm does not have an HSQC correlation to any carbon peaks, again suggesting the proton at 6.7 ppm is connected to a heteroatom. The fact that the anomeric proton of the impurity is coupled to an exchangeable proton suggested that the impurities in the sugar region might correspond to from free D-mannose.

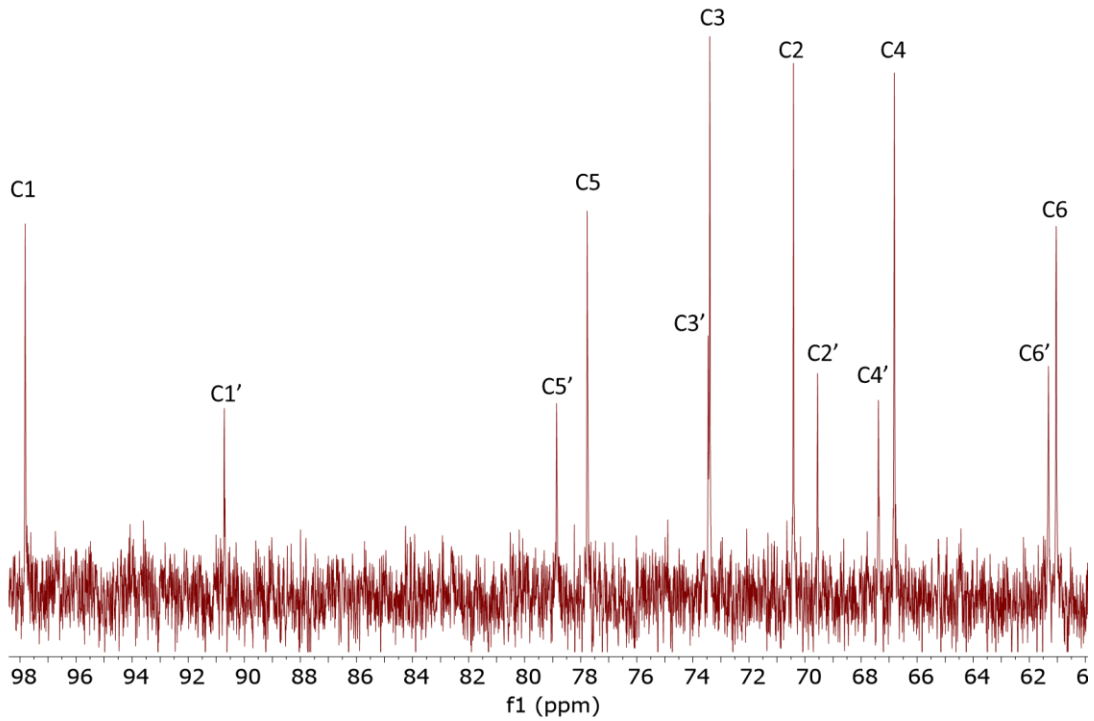

Figure 2.20 ^{13}C NMR spectrum of **4**

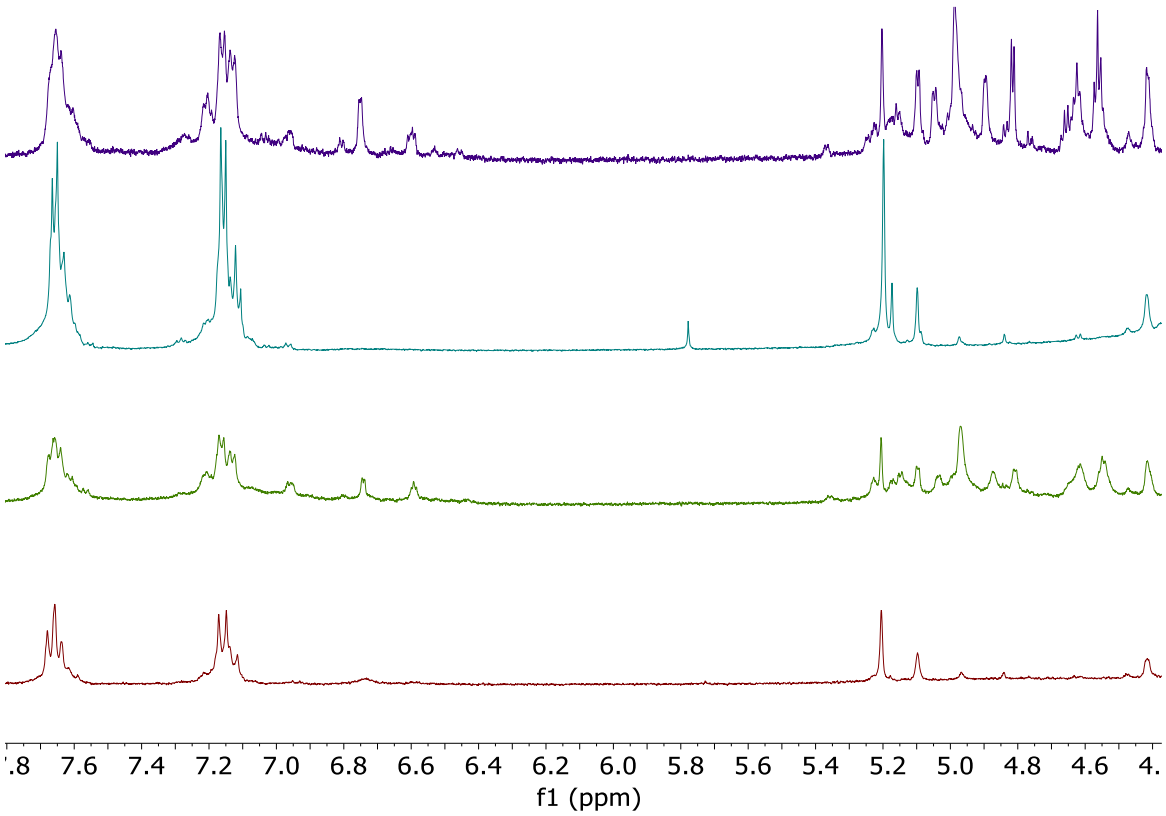

Figure 2.21 ^{1}H NMR spectra of various crude products of **4**

To confirm if the impurity in the sugar region is D-mannose, the literature NMR characterization data of D-mannose[15] was compared to the impurity NMR data. However, the literature values did not match. Further, D-mannose was added to a solution of **4**, the impurity peaks didn't match the D-mannose peaks (Figure 2.22). However, the added D-mannose's peaks also didn't match the literature values. For example, the chemical shift reported in DMSO for the anomeric proton of D-mannose is 4.68 ppm, however this does not match the 5.1 ppm we found for the chemical shift of the impurity anomeric proton. Further, a proton coupled carbon spectra was acquired for **4** and the C-H coupling constant of C1' was recorded and compared to the C-H coupling constant of C1 in β- and α-D mannose.[16] The C-H coupling constant of C1' was found to be 166.3 Hz. The corresponding J_{CH} is 160 Hz for β-D mannose and 170 Hz for α-D mannose, therefore not precisely matching either. DOSY spectra was also acquired to evaluate the differences in hydrodynamic radii of the impurity peaks compared to **4**. It was seen that the aromatic impurities, the anomeric impurity, as well as the Yariv reagent all had similar diffusion constants (Figure 2.23). This could mean that the impurity peaks all come from one molecule which is around the same size as the Yariv reagent or that the various impurities and the Yariv reagent are aggregated and thus have the same hydrodynamic radii. To test if aggregation is occurring, the DOSY spectrum was reacquired at 80° C (Figure 2.24). However, the diffusion constants of the impurities in both the aromatic and anomeric region were still similar to the Yariv reagent impurities suggesting that the impurity might actually be a molecule with a size similar to the Yariv reagent **4**.

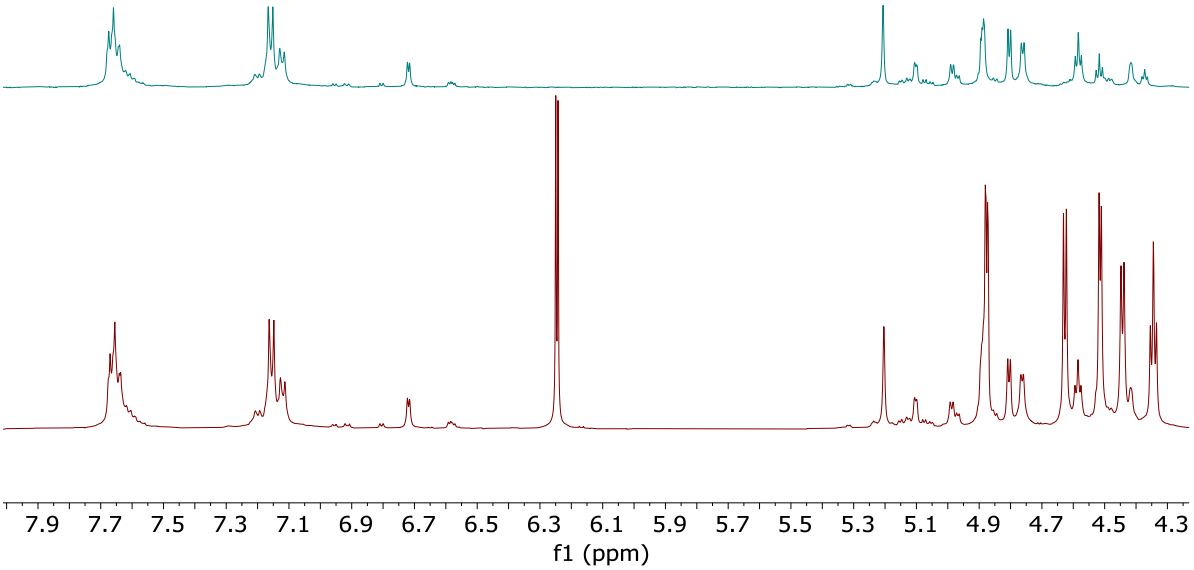

Figure 2.22 ^{1}H NMR spectra of **4** before (top) and after addition of D-mannose (bottom)

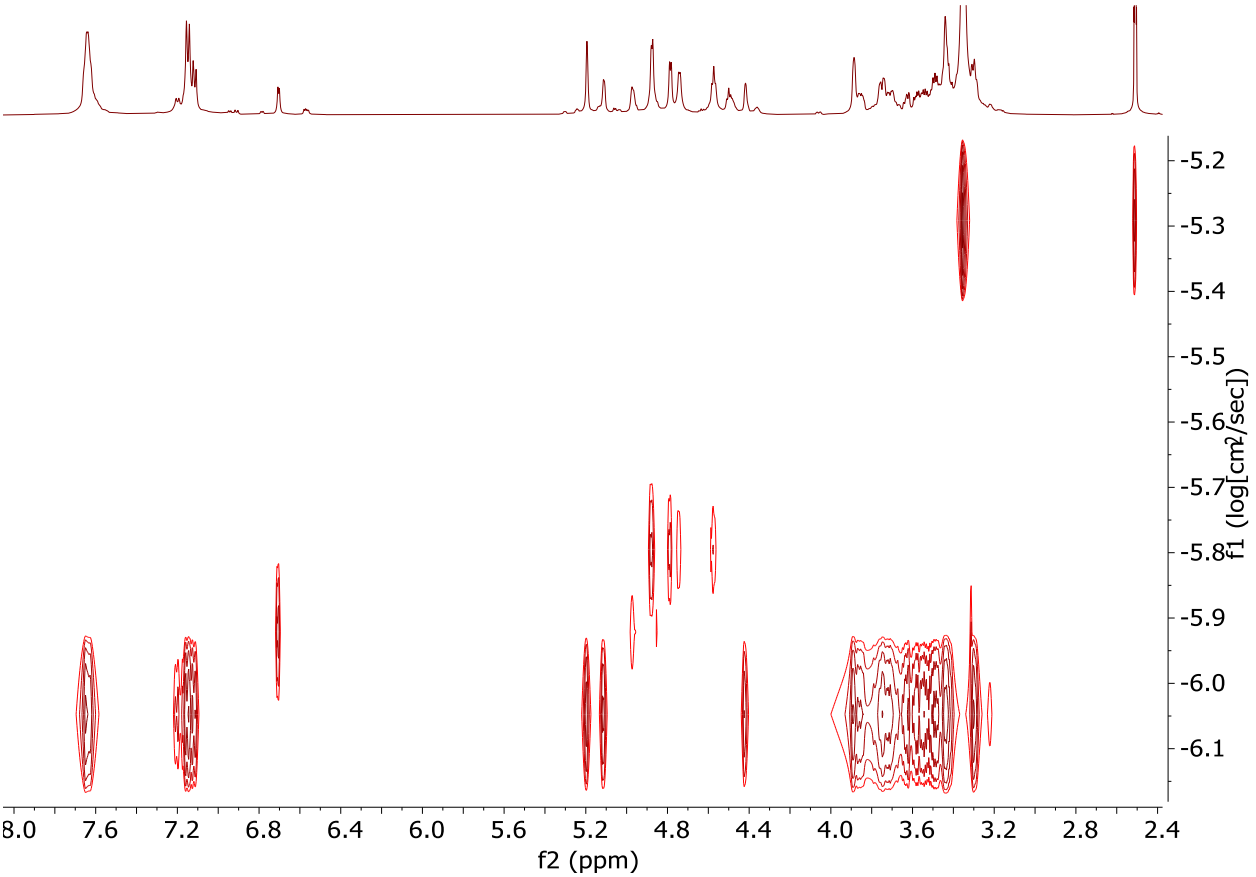

Figure 2.23 DOSY spectrum of **4**

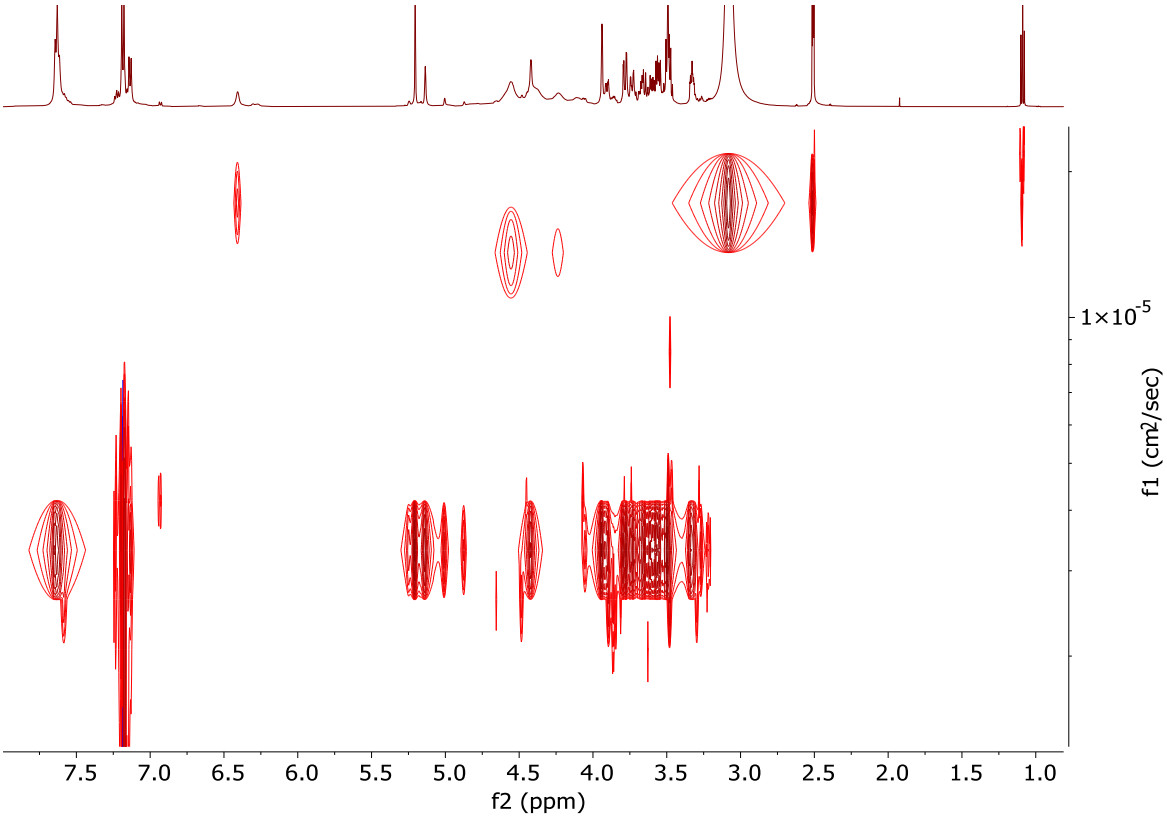

Figure 2.24 DOSY spectrum of **4** at 80° C

2.8 Conclusion

In summary, to achieve our goal to study the Yariv reagent-AGP binding interactions, we required pure and well characterized Yariv reagents. We first utilized synthetic protocols published in literature to try and synthetize these dyes, however we encountered several issues that have been described in this section. These issues included presence of impurities in the crude product, and difficulty in NMR characterization due to peak broadening. While several Yariv reagent synthetic protocols had previously been published, there was a lack of a simple and straightforward purification protocol for the Yariv reagent in any of these. We devised a simple protocol which involves dissolution of the crude product and precipitation by addition of ethanol. This dissolution-precipitation protocol is repeated twice to get rid of what was found to be the biggest source of impurity in most cases, the lower homologs such as the bis azo variant. This redissolution-reprecipitation protocol also helped reduce the peak broadening that was associated with the sugar-OH resonances in the Yariv reagent ^{1}H NMR. The peak broadening was found to

be due to exchange with water. This peak broadening could be eliminated by processing the Yariv reagent samples with methanol. The Yariv reagents **1**-**7** and **9-10** were synthesized and characterized using this optimized synthetic protocol. We could now proceed with our Yariv reagent AGP binding studies, as well as characterization of other Yariv reagent properties which will be described in the next two chapters.

Supplemental Information

Experimental

General Protocols: Thin layer chromatography was carried out on Merck silica gel 60 F_{254} precoated glass plates. Compounds were visualized under a UV lamp. All NMR spectra were recorded on a Bruker Avance III HD Ascend 600 MHz instrument using DMSO-d_6 as the solvent. ^{1}H NMR and ^{13}C NMR spectra were referenced to residual solvent peaks. Coupling constants are given in hertz (Hz), and chemical shifts are given in parts per million (ppm). Electrospray ionization (ESI) mass spectra were obtained using a Thermo LCQ Deca XP Max ion trap mass spectrometer. Purified water was obtained from an EMD Millipore Direct-Q 3 Tap to Pure and Ultrapure Water Purification system. A vacuum oven set at 75 °C was used to dry the Yariv reagents after the final purification.

Circular Dichroism: Circular dichroism (CD) measurements were performed in triplicate using a Jasco J-815 spectropolarimeter. Temperature was controlled by a JASCO Peltier temperature control unit. Unless otherwise noted the concentration and volume of the Yariv reagent samples was 300 µM and 600 µL, respectively. The sample cell was kept at 20 °C. CD measurements were obtained in a Hellma analytics 2mm pathlength stoppered cuvette and corrected against a purified water standard. Wavelength readings ranged from 200 to 700 nM and were obtained at a speed of 100 nM/minute. The measured ellipticity θ was converted to molar ellipticity $\Delta\varepsilon = \theta$ /

32980•*c*•*l*, where ellipticity is given in mdeg, *c* is the concentration in mol•L^{-1} and *l* is the optical path length in cm.

Synthesis of β-D-glucosyl Yariv reagent (**1**): A Parr shaker bottle was charged with 4-nitrophenyl β-D-glucopyranoside (2.5 g, 8.3 mmol) and methanol (250 mL) and a stir bar were added to the bottle. The mixture was stirred while sparging for 20 minutes with N_2 introduced via a needle. 10% Pd/C (40 mg) was added to the Parr bottle, which was put on a Parr shaker and shaken under 40 psi H_2 for 7 hours. TLC showed complete conversion (2:1 dichloromethane /isopropyl alcohol). The reaction mixture was filtered through Celite into a 1000 mL flask and then concentrated in vacuo to about 100 mL. Solution was transferred into a 250 mL preweighed flask and concentrated in vacuo and placed under high vacuum. The amino sugar was obtained as a pale yellow/clear crystalline solid (2.20 g, 8.1 mmol, 97 %). This material was directly used in the next step.

^{1}H NMR (600 MHz, DMSO-d_6) δ 6.77 (d, *J* = 8.8 Hz, 2H), 6.49 (d, *J* = 8.5 Hz, 2H), 5.23 (s, 1H), 5.07 (d, *J* = 4.6 Hz, 1H), 5.00 (d, *J* = 4.9 Hz, 1H), 4.69 (s, 2H), 4.57 (d, *J* = 7.7 Hz, 1H), 4.55 (t, *J* = 5.8 Hz, 1H, 1H), 3.71 – 3.65 (m, 1H), 3.46 (dt, *J* = 11.5, 5.4 Hz, 1H), 3.25 – 3.09 (m, 4H).

A solution of cold freshly prepared 1.2 M HCl (17 mL, 2.5 eq) was added to 4-aminophenyl β-D-glucopyranoside (2.2 g, 8.11 mmol, 1 eq) in a 250 mL round bottom flask. This solution was cooled in an ice bath while stirring. $NaNO_2$ (616 mg, 8.9 mmol, 1.1 eq) was dissolved in 1 mL of cold water in an Eppendorf tube. The $NaNO_2$ solution was added to a 5 mL syringe with a 4 inch x 22 gauge needle which was clamped above the reaction flask, leading to a gravity assisted dropwise addition. The reaction was stirred at 0 °C for 3 hrs. Phloroglucinol (348 mg, 2.8 mmol, 0.34 eq) was dissolved in a minimal amount of cold 5 M NaOH (1~2 ml) and added dropwise to the reaction. 5 M NaOH was added until the pH was basic as indicated by pH paper, at which point the ice bath

was removed. The pH was maintained at ~11 (dark blue on pH strip) by addition of 5 M NaOH as necessary. The reaction was stirred overnight. Cold 100% ethanol (200 mL) was added to the reaction, which was neutral at this point as determined by pH paper. 1.2 M HCl was added until the solution was acidic as indicated by pH paper. The reaction flask was placed in a freezer for at least 24 hours until a dark red/brown precipitate was observed. The precipitate was filtered through a Hirsch funnel to provide the crude Yariv reagent **1** as a glossy red, sticky powder which clumped together. This solid was air dried for a few hours, at which point it hardened to a solid mass which became a powder when crushed. The powder was transferred to a pre-weighed scintillation vial and dried in a vacuum oven with at 75 °C for 24 hours. This crude product (2.31 g, 2.4 mmol), was obtained in 86% yield as a dark red powder. Some of this material was further purified twice using the redissolution – reprecipitation protocol followed by trituration.

Redissolution - reprecipitation (representative protocol)

To 0.6 g of the crude product (β-D-glucosyl Yariv reagent (**1**)), 20 mL of water was added, the mixture was heated and vortexed until complete dissolution. 130 mL of cold 100% ethanol was added to the solution. The mixture was filtered through a Hirsch funnel and the precipitate was allowed to air dry and then transferred to a pre weighed vial. The precipitate was then allowed to dry in a vacuum oven overnight. 0.5 g of material R1X (81%) was obtained. A second redissolution – reprecipitation with (**1**) R1X (0.4 g) provided 0.35 g of β-D-glc (**1**) batch 4 R2X (85%).

Trituration (representative protocol)

0.19 g of the β-D-glucosyl Yariv reagent (**1**) R2X was weighed out into an Erlenmeyer flask. The material was then rinsed with 10 mL of boiling methanol 5 times and filtered through a Hirsch funnel. It was then dried in a vacuum oven overnight to afford 0.18 g (95%) of β-D-glc (**1**) batch 4 R2XM as a mixture of dark red and black pellets which were crushed into a powder.

^{1}H NMR (600 MHz, DMSO-d_6) δ 15.91, 15.86 15.11 and 15.06 (s, 3H, core Ar-O*H*), 7.66 (d, *J* = 8.6 Hz, 6H, Ar*H ortho* to azo), 7.18 (d, *J* = 8.7 Hz, 6H, Ar*H ortho* to sugar), 5.37 (d, *J* = 5.0 Hz,

3H, 2-O*H*), 5.11 (d, *J* = 4.7 Hz, 3H, 3-O*H*), 5.05 (d, *J* = 5.3 Hz, 3H, 4-O*H*), 4.94 (d, *J* = 7.4 Hz, 3H, *H1*), 4.61 (t, *J* = 5.8 Hz, 3H, 6-O*H*), 3.73 (ddd, *J* = 12.0, 5.3, 2.1 Hz, 3H, $H6_a$), 3.50 (dt, *J* = 11.9, 6.0 Hz, 3H, $H6_b$), 3.38 (ddd, *J* = 9.7, 5.7, 2.3 Hz, 3H, *H5*), 3.34 – 3.23 (m, 6H, *H3 & H2*), 3.19 (td, *J* = 9.0, 4.9 Hz, 3H, *H4*);

^{13}C NMR (151 MHz, DMSO-d_6) δ 178.1(core Ar, *C*-O), 156.8(Ar *C*-O-sugar), 136.6(Ar *C*-N), 128.9(core Ar, *C*-N), 119.0(Ar *C*-C-N), 118.0(Ar *C*-C-O-sugar), 101.0(*C1*), 77.6(*C5*), 77.1(*C3*), 73.7(*C2*), 70.2(*C4*), 61.2(*C6*) HRMS (ESI) m/z: $[M + H]^+$ calcd for $C_{42}H_{49}N_6O_{21}$ 973.2951; found 973.2927.

Synthesis of β-D-Galactosyl Yariv reagent (**2**) : 4-nitrophenyl β-D-galactopyranoside (0.7 g, 2.4 mmol) and 10% Pd/C 42 mg) were used to prepare the aniline using the same procedure used for 4-aminophenyl β-D-glucopyranoside. TLC showed complete conversion (2:1 dichloromethane /methanol). The product was dried in vacuo overnight to give the aniline as a pale-yellow powder (0.6 g, 2.2 mmol, 91 %). This material was directly used in the next step.

^{1}H NMR (600 MHz, DMSO-d_6) 6.76 (d, *J* = 9 Hz, 2H), 6.49 (d, *J* = 9.1 Hz, 2H), 5.07 (d, *J* = 5.1 Hz, 1H), 4.79 (d, *J* = 6.2 Hz, 1H), 4.78 (s, 2H), 4.62 (t, *J* = 5.4 Hz, 1H), 4.54 (d, *J* = 7.7 Hz, 1H), 4.45 (d, *J* = 4.6 Hz, 1H), 3.67 (t, *J* = 3.9 Hz, 1H), 3.55 (dt, *J* = 10.3, 5.4 Hz, 1H), 3.47 (m, 3H), 3.37 (m, 1H).

1.2 M HCl (5 mL, 2.5 eq) and 4-aminophenyl β-D-galactopyranoside (608 mg, 2.24 mmol, 1 eq) was used to synthesize Yariv reagent **2** using largely the same procedure used for **1**. However, basification of the reaction was done using 2M NaOH instead of 5M NaOH. The crude product (0.8 g, 0.76 mmol), was obtained in 100% yield. Some of this material was further purified using the redissolution – reprecipitation protocol twice followed by methovaping - 0.66 g of the crude product was reprecipitated from 20 mL of water and 130 mL of ethanol to give 0.4 g of β-D-

galactosyl Yariv reagent (**2**) R1X product (60%). The second redissolution – reprecipitation with R1X (300 mg) from 20 mL of water and 130 mL of ethanol provided 0.23 g of β-D-galactosyl Yariv reagent (**2**) R2X (77%). (**2**) R2X was purified by rotary evaporation from methanol (methovaping).

Methovaping (representative protocol)

0.055 g of β-D-gal (**2**) R2X was weighed out into a scintillation vial. 3 mL of methanol was added to the vial and then evaporated using a rotovap. The vial was incubated in a vacuum oven overnight at 75° C overnight to afford 0.054 g (99%) of β-D-gal R2XM as a mixture of dark red and black pellets which could be crushed into a powder. The vial containing the product was stored in a dessicator containing Drierite for several days.

Procedures of the various treatments from Table 2.2

Column 1 protocol: 10 mg of β-D-gal (**2**) crude was weighed out into a scintillation vial. The vial was then put into high vacuum for 24 hrs.

Column 2 protocols: 10 mg of β-D-gal (**2**) crude was weighed out into a scintillation vial. The vial was then incubated in a desiccator containing Drierite for either 24 hrs or 72 hrs.

Column 3 protocols: 10 mg of β-D-gal (**2**) crude was weighed out into a scintillation vial. The vial was then incubated in a desiccator containing Drierite and a scintillation vial full of P_2O_5 for either 24 hrs or 72 hrs.

Column 4 protocol: 10 mg of β-D-gal (**2**) crude was weighed out into a scintillation vial. 3 mL of methanol was added to the vial and then evaporated using a rotovap. The vial was then incubated in a desiccator containing Drierite for 72 hrs.

Column 5 protocols: 10 mg of β-D-gal (**2**) crude was weighed out into a scintillation vial. 3 mL of methanol was added to the vial and then evaporated using a rotovap. The vial was then incubated in a desiccator containing Drierite and a scintillation vial full of P_2O_5 for either 24 hrs or 72 hrs.

Column 6 protocols: 10 mg of β-D-gal (**2**) crude was weighed out into a scintillation vial. 3 mL of methanol was added to the vial and then evaporated using a rotovap. The vial was then put into high vacuum for either 1 hr, 24 hrs or 72 hrs.

Column 7 protocols: 10 mg of β-D-gal (**2**) crude was weighed out into a scintillation vial. 3 mL of methanol was added to the vial and then evaporated using a rotovap. The vial was then incubated in a desiccator under vacuum attached to a trap containing Drierite for either 24 hrs or 72 hrs.

^{1}H NMR (600 MHz, DMSO) δ 15.91 and 15.53-14.77 (s, 3H, core Ar-O*H*), 7.60 (d, *J* = 8.4 Hz, 6H, Ar*H ortho* to azo), 7.15 (d, *J* = 8.6 Hz, 6H, Ar*H ortho* to sugar), 5.27 (d, *J* = 5.1 Hz, 3H, 2-O*H*), 4.93 (d, *J* = 5.1 Hz, 3H,3-O*H*), 4.89 (d, *J* = 7.5 Hz, 3H, *H1*), 4.76(t, *J* = 5.1 Hz, 3H, 6-O*H*), 4.59 (d, *J* = 4.5 Hz, 3H, 4-O*H*), 3.73 (t, *J* = 3.3 Hz, 3H, *H4*), 3.60 (m, 12H, *H2*, *H5*, *H6*), 3.45 (s, 3H, *H3*);

^{13}C NMR (151 MHz, DMSO-d_6) δ 177.9 (core Ar, *C*-O), 156.9(Ar *C*-O-sugar), 136.5(Ar *C*-N**)**, 128.8 (core Ar, *C*-N), 119.0(Ar *C*-C-N), 117.9(Ar *C*-C-O-sugar), 101.5(*C1*), 76.1(*C2*), 73.7(*C3*), 70.8(*C5*), 68.7(*C4*), 60.9(*C6*). HRMS (ESI) m/z: $[M + H]^+$ calcd for $C_{42}H_{49}N_6O_{21}$ 973.2951; found 973.2920.

Synthesis of β-D-xylosyl Yariv reagent (**3**): 4-nitrophenyl β-D-xylopyranoside (1.0 g, 3.7 mmol) and 10% Pd/C (36 mg) were used to prepare the aniline using the same procedure used for 4-aminophenyl β-D-glucopyranoside. TLC showed complete conversion (5:1 dichloromethane /methanol). The amino sugar was obtained as a pale yellow/clear crystalline solid (0.9 g, 3.6 mmol, 97 %). This material was directly used in the next step.

^{1}H NMR (600 MHz, DMSO-d_6) δ 6.72 (d, *J* = 8.8 Hz, 2H), 6.49 (d, *J* = 8.7 Hz, 2H), 5.26 (s, 1H), 5.10 (s, 1H), 5.04 (s, 1H), 4.70 (s, 2H), 4.56 (d, *J* = 7.2 Hz, 1H), 3.70 (dd, *J* = 11.2, 5.3 Hz, 1H), 3,38 (m, 1H), 3.22 – 3.08 (m, 3H).

4-aminophenyl β-D-xylopyranoside (0.89 g, 3.7 mmol, 1 eq) used to synthesize Yariv reagent **3** using the same procedure used for **1**. However, basification of the reaction was done using 2M NaOH instead of 5M NaOH. The crude product (0.84 g, 0.9 mmol), was obtained in 77% yield. This material was further purified twice using redissolution – reprecipitation protocol followed by methovaping (see below): 0.8 g of the crude product was reprecipitated from 30 mL of water and 80 mL of ethanol to give 0.45 g of β-D-xylosyl Yariv reagent (**3**) R1X (53%). A second redissolution – reprecipitation with (**3**) R1X (0.45 g) reprecipitated from 30 mL of water and 80 mL of ethanol provided 0.36 g of β-D-xyl (**3**) R2X (82%). 0.36 g of β-D-xyl (**3**) R2X was then triturated to afford 0.33 g of β-D-xyl (**3**) R2XM (92%). 0.037 g of β-D-xyl (**3**) R2XM sample was methovaped and dried in a vacuum oven overnight at 75° C overnight to afford 0.033 g (90%) of β-D-xyl R2XM2 as a mixture of dark red and black pellets which was crushed into a powder.

^{1}H NMR (600 MHz, DMSO-d_6) δ 15.91, 15.86, 15.09 and 15.05 (s, 3H, core Ar-O*H*), 7.64 (d, *J* = 8.7 Hz, 6H, Ar*H ortho* to azo), 7.15 (d, *J* = 8.5 Hz, 6H, Ar*H ortho* to sugar), 5.40 (d, *J* = 3.8 Hz, 3H, 2-O*H*), 5.14 (d, *J* = 3.2 Hz, 3H, 3-O*H*), 5.10 (d, *J* = 4.6 Hz, 3H, 4-O*H*), 4.94 (d, *J* = 6.3 Hz, 3H, *H1*), 3.79 (dd, *J* = 10.9, 5.1 Hz, 3H, $H5_a$), 3.40 (dq, *J* = 9.1, 4.3 Hz, 3H, *H4*), 3.32 (d, *J* = 10.9 Hz, 3H, $H5_b$), 3.27 (m, 6H, *H3* and *H2*).

^{13}C NMR (151 MHz, DMSO-d_6) δ 178.1(core Ar, *C*-O), 156.5(Ar *C*-O-sugar), 136.6(Ar *C*-N), 128.9(core Ar, *C*-N), 119.0(Ar *C*-C-N), 118.0(Ar *C*-C-O-sugar), 101.5(*C1*), 76.9(*C3*), 73.5(*C2*), 69.8(*C4*), 66.2(*C5*) HRMS (ESI) m/z: $[M + H]^+$ calcd for $C_{39}H_{43}N_6O_{18}$ 883.2634; found 883.2644.

Synthesis of β-D-fucosyl Yariv reagent (**10**): 4-nitrophenyl β-D-fucopyranoside (0.5 g, 1.7 mmol) and 10% Pd/C (37 mg) were used to prepare the aniline using the same procedure used for 4-aminophenyl β-D-glucopyranoside. The amino sugar was obtained as a pale yellow/clear crystalline solid (0.4 g, 1.6 mmol, 99 %). This material was directly used in the next step.

^{1}H NMR (600 MHz, DMSO-d_6) δ 6.72 (d, *J* = 8.6 Hz, 2H), 6.48 (d, *J* = 8.8 Hz, 2H), 5.06 (s, 1H), 4.85 (s, 1H), 4.67 (s, 2H), 4.55 (d, *J* = 7.6 Hz, 1H), 4.47 (s, 1H), 3.63 (q, *J* = 6.6 Hz, 1H), 3.49 – 3.40 (m, 2H), 3.40 – 3.34 (m, 1H), 1.13 (d, *J* = 6.4 Hz, 3H).

4-aminophenyl β-D-fucopyranoside (0.4 g, 1.73 mmol, 1 eq) was used to synthesize Yariv reagent **4** using the same procedure used for **1**. The crude product (0.39 g, 0.4 mmol) was obtained in 72% yield. Some of this material was further purified twice using redissolution – reprecipitation: 0.27 g of the crude product was reprecipitated from 20 mL of water and 150 mL of ethanol to give 0.16 g of β-D-fucosyl Yariv reagent (**4**) R1X product (59%). The second redissolution – reprecipitation with R1X (0.09 g) from 20 mL of water and 150 mL of ethanol provided 0.035 g of β-D-fucosyl Yariv reagent (**4**) R2X (41%) to provide a dark red, sticky powder.

^{1}H NMR (600 MHz, DMSO-d_6) δ 15.94,15.89, 15.11 and 15.08 (s, 3H, core Ar-O*H*), 7.65 (d, *J* = 9.0 Hz, 6H, Ar*H ortho* to azo), 7.15 (d, *J* = 9.0 Hz, 6H, Ar*H ortho* to sugar), 5.18 (d, *J* = 5.2 Hz, 3H, 2-O*H*), 4.90 (d, *J* = 7.6 Hz, 3H, *H1*), 4.84 (d, *J* = 5.8 Hz, 3H, 3-O*H*), 4.57 (d, *J* = 4.9 Hz, 3H, 4-O*H*), 3.81 (q, *J* = 6.6 Hz, 3H, *H5*), 3.56 (m, 3H, *H2*), 3.50 (t, *J* = 4.3 Hz, 3H, *H4*), 3.44 (m, 3H, *H3*), 1.18 (d, *J* = 6.4 Hz, 9H, *H6*);

^{13}C NMR (151 MHz, DMSO-d_6) δ 178.0(core Ar, *C*-O), 156.8(Ar *C*-O-sugar), 136.3(Ar *C*-N), 128.8(core Ar, *C*-N), 119.0(Ar *C*-C-N), 117.8(Ar *C*-C-O-sugar), 101.1(*C1*), 73.9(*C3*), 71.4(*C4*), 70.8(*C5*), 70.4(*C2*), 17.1 (*C6*). HRMS (ESI) m/z: $[M + H]^+$ calcd for $C_{42}H_{48}N_6O_{18}$ 925.3103; found 925.3091.

Synthesis of α-L-fucosyl Yariv reagent (**7**)

4-nitrophenyl α-L-fucopyranoside (1 g, 3.38 mmol) and 10% Pd/C (36 mg) were used to prepare the aniline using the same procedure used for 4-aminophenyl β-D-glucopyranoside. The amino sugar was obtained as a pale yellow/clear crystalline solid (0.9 g, 3.35 mmol, 99 %). This material was directly used in the next step.

^{1}H NMR (400 MHz, DMSO-d_6) δ 6.74 (d, *J* = 8.8 Hz,2H), 6.49 (d, *J* = 8.6 Hz, 2H), 5.08 (d, *J* = 3.5 Hz, 1H), 4.68 (d, *J* = 6.5 Hz, 1H), 4.68 (s, 2H), 4.61 (d, *J* = 5.5 Hz, 1H), 4.50 (d, *J* = 4.4 Hz, 1H), 4.00 – 3.90 (m, 1H), 3.68 (m, 2H), 3.55 (s, 1H), 1.07 (d, *J* = 6.5 Hz, 3H).

4-aminophenyl α-L-fucopyranoside (0.85 g, 3.34 mmol, 1 eq) was used to synthesize Yariv reagent **5** using the same procedure used for **1**. This crude product (0.97 g, 1 mmol), was obtained in 93% yield. This material was further purified twice using redissolution – reprecipitation followed by methovaping: 0.97 g of the (**5**) crude product was reprecipitated from 20 mL of water and 180 mL of ethanol to give 0.52 g of α-L-fuc R1X (**5**) product (59%). The second redissolution – reprecipitation with (**5**) R1X (0.5 g) from 20 mL of water and 180 mL of ethanol provided 0.35 g

of α-L-fuc (**5**) R2X (68%). Methovaping 33.8 mg of (**5**) R2X using 3 mL of methanol gave 31.1 mg of (**5**) R2XM (92%) as dark red pellets which was crushed into a powder.

^{1}H NMR (600 MHz, DMSO-d_6) δ 15.95, 15.90, 15.11 and 15.07 (s, 3H, core Ar-O*H*), 7.63 (d, *J* = 8.1 Hz, 6H, Ar*H ortho* to azo), 7.18 (d, *J* = 8.1 Hz, 6H, Ar*H ortho* to sugar), 5.46 (d, *J* = 3.2 Hz, 3H, *H1*), 4.90 (d, *J* = 5.7 Hz, 3H, 2-O*H*), 4.71 (d, *J* = 5.2 Hz, 3H, 4-O*H*), 4.60 (d, *J* = 4.4 Hz, 3H, 3-O*H*), 3.92 (q, *J* = 6.7 Hz, 3H, *H5*), 3.80 (m, 6H, *H4* and *H2*), 3.60 (t, *J* = 3.8 Hz, 3H, *H3*), 1.09 (d, *J* = 6.5 Hz, 9H, *H6*).

^{13}C NMR (151 MHz, DMSO-d_6) δ 178.1(core Ar, *C*-O), 156.7(Ar *C*-O-sugar), 136.3(Ar *C*-N), 128.8(core Ar, *C*-N), 119.0(Ar *C*-C-N), 118.4(Ar *C*-C-O-sugar), 98.8(*C1*), 71.8(*C3*), 69.9(*C4*), 68.1(*C2*), 67.9(*C5*), 17.0(*C6*) HRMS (ESI) m/z: $[M + H]^+$ calcd for $C_{42}H_{48}N_6O_{18}$ 925.3103; found 925.3092.

Synthesis of β-L-fucosyl Yariv reagent (**6**)

4-nitrophenyl β-L-fucopyranoside (0.8 g, 2.82 mmol) and 10% Pd/C (35 mg) were used to prepare the aniline using the same procedure used for 4-aminophenyl β-D-glucopyranoside. The amino sugar was obtained as a pale yellow/clear crystalline solid (0.72 g, 2.8 mmol, 99 %). This material was directly used in the next step.

^{1}H NMR (600 MHz, DMSO-d_6) δ 6.73 (d, *J* = 8.7 Hz, 2H), 6.49 (d, *J* = 8.9 Hz, 2H), 5.03 (s, 1H), 4.76 (s, 1H), 4.67 (s, 2H), 4.55 (d, *J* = 7.6 Hz, 1H), 4.47 (s, 1H), 3.63 (qd, *J* = 6.4, 1.1 Hz, 1H), 3.48 – 3.42 (m, 2H), 3.40 – 3.34 (m, 1H), 1.13 (d, *J* = 6.4 Hz, 3H).

4-aminophenyl β-L-fucopyranoside (0.72 g, 2.8 mmol, 1 eq) was used to synthesize Yariv reagent **6** using largely the same procedure used for **1**. However, basification of the reaction was done using 2M NaOH instead of 5M NaOH. This (**6**) crude product (0.71g, 1 mmol), was obtained in 80% yield. This material was further purified twice using redissolution – reprecipitation followed

by methovaping: 0.71 g of the crude product was reprecipitated from 20 mL of water and 180 mL of ethanol to give 0.52 g of β-L-fuc (**6**) R1X product (73%). The second redissolution – reprecipitation with (**6**) R1X (0.5 g) from 20 mL of water and 180 mL of ethanol provided 0.44 g of β-L-fuc (**6**) R2X (84%). Methovaping 31 mg of (**6**) R2X using 3 mL of methanol gave 28 mg of (**6**) R2XM (90%) as a mixture of dark red and black pellets which was crushed into a powder.

^{1}H NMR (600 MHz, DMSO-d_6) δ 15.94, 15.88, 15.10 and 15.06 (s, 3H, core Ar-O*H*), 7.62 (d, *J* = 8.7 Hz, 6H, Ar*H ortho* to azo), 7.14 (d, *J* = 8.5 Hz, 6H, Ar*H ortho* to sugar), 5.19 (d, *J* = 5.0 Hz, 3H, 2-O*H*), 4.90 (d, *J* = 7.6 Hz, 3H, *H1*), 4.84 (m, 3H, 3-O*H*), 4.57 (s, 3H, 4-O*H*), 3.80 (q, *J* = 6.5 Hz, 3H, *H5*), 3.57 (m, 3H, *H2*), 3.51 (s, 3H, *H4*), 3.45 (d, *J* = 10.2 Hz, 3H, *H3*), 1.18 (d, *J* = 6.5 Hz, 9H, *H6*).

^{13}C NMR (151 MHz, DMSO-d_6) δ 178.1 (core Ar, *C*-O), 156.9(Ar *C*-O-sugar), 136.3(Ar *C*-N), 128.8(core Ar, *C*-N), 119.0(Ar *C*-C-N), 117.8(Ar *C*-C-O-sugar), 101.2(*C1*), 73.9(*C3*), 71.4(*C4*), 70.8(*C5*), 70.4(*C2*), 17.1(*C6*). HRMS (ESI) m/z: $[M + H]^+$ calcd for $C_{42}H_{48}N_6O_{18}$ 925.3103; found 925.3068.

Synthesis of α-D-galactosyl-Yariv reagent (**5**)

p-aminophenyl-α-D-galactopyranoside (218 mg, 0.81 mmol) was dissolved in 0.5 M HCl (4.7 mL) and cooled to 0 °C. A freshly prepared cold aqueous solution of 0.3 M $NaNO_2$ (2.7 mL) was added with an addition funnel over a period of 5 min, and the solution was stirred for 2 h. The reaction mixture was cooled to 0 °C and a solution of phloroglucinol (31 mg, 0.25 mmol, 0.3 eq.) in cold water (10 mL), was added dropwise with an addition funnel over a period of 15 min. The pH of the reaction mixture was adjusted to 9 with 0.5M NaOH. The reaction mixture was stirred for an additional 2 h, while readjusting the pH to 9 if necessary. After 2 h MeOH (25 mL) was added to the reaction mixture and the reaction mixture was placed in a freezer overnight. The pH was adjusted to neutral with 1 M HCl and the reaction mixture was placed in a freezer overnight. The

formed precipitate was collected using a Hirsch-funnel and rinsed with cold methanol, and dried under high vacuum overnight to provide **7** as a deep red powder (186 mg 0.19 mmol, 76 % yield).

^{1}H NMR (600 MHz, DMSO-d_6) δ = 15.94 (s, 3H, core Ar-OH), 7.66 (d, *J*=8.9, 6H, ArH ortho to azo), 7.24 (d, *J*=8.5, 6H, ArH ortho to sugar), 5.47 (d, *J*=3.2, 3H, H1), 4.93 (d, *J*=6.0, 3H, 2-OH), 4.76 (d, *J*=5.2, 3H, 3-OH), 4.57 (d, *J*=3.4, 3H, 4-OH), 4.56 (t, *J*=5.9, 3H, 6-OH), 3.78 (m, 9H, H2, H3, H4), 3.73 (t, *J*=6.3, 3H, H5), 3.55 (m, 3H, H6), 3.42 (m, 3H, H6).

^{13}C NMR (151 MHz, DMSO-d_6) δ 178.0(core Ar, C−O), 156.8(Ar, C-O-Sugar), 136.1(Ar C-N), 128.5(Core Ar C-N), 118.9(Ar, C−C−N), 118.6(Ar, C−C−O−sugar), 98.8(C1), 72.8(C2), 69.8(C5), 69.1(C4), 68.4(C3), 60.9(C6**)**

HRMS Calc. for $C_{42}H_{49}N_6O_{21}$ [M+H]: 973.2951, Obsd. 973.2925

Synthesis of β-D-mannosyl-Yariv reagent (**4**)

A solution of cold freshly prepared 1.2 M HCl (4 mL, 2.5 equiv) was added to 4-aminophenyl β-D-mannopyranoside (541 mg, 2 mmol, 1 equiv) in a 250 mL round-bottom flask. This solution was cooled in an ice bath while stirring. $NaNO_2$ (151 mg, 2.2 mmol, 1.1 equiv) was dissolved in 0.5 mL of cold water in an Eppendorf tube. The $NaNO_2$ solution was added to a 1 mL syringe with a 4 in. × 22 gauge needle that was clamped above the reaction flask, leading to a gravity-assisted dropwise addition. The reaction was stirred at 0 °C for 2 h. Phloroglucinol (86 mg, 0.7 mmol, 0.34 equiv) was dissolved in a minimal amount of cold 5 M NaOH (1−2 mL) and added dropwise to the reaction mixture. To the mixture was added 5 M NaOH until the pH was basic as indicated by a pH paper. The pH was maintained at∼11 (dark blue on the pH strip) by the addition of 5M NaOH as necessary. The reaction mixture was stirred overnight. Cold 100% ethanol (200 mL) was added to the reaction mixture, which was neutral at this point as determined by the pH paper. To the mixture was added 12 M HCl until the solution was acidic as indicated by a pH paper. The reaction flask was placed in a freezer for at least 24 h until a dark red-brown precipitate was observed. The

precipitate was filtered through a Hirsch funnel and air dried. 0.89 g crude was obtained (quantitative). To 0.49 g of the crude product was added 5 mL of water, and the mixture was vortexed until complete dissolution. To the solution was added 150 mL of 100% ethanol. The mixture was filtered through a Hirsch funnel, and the precipitate was allowed to air-dry and then transferred to a preweighed vial. 200 mg of R1X was obtained and air dried.

^{1}H NMR (600 MHz, DMSO-d_6) δ 15.91 (s, 3H, core Ar−OH), 7.65 (m, 6H, ArH ortho to azo), 7.16 (d, J = 8.9 Hz, 6H, ArH ortho to sugar), 5.2 (s, 3H, H1), 4.89 (d, J = 5.08 Hz, 3H, 4-OH), 4.8 (d, J = 5.01 Hz, 3H, 2-OH), 4.76 (d, J = 4.96 Hz, 3H, 3-OH), 4.58 (t, J = 6 Hz, 3H, 6-OH), 3.88 (d, J = 3.03 Hz, 3H, H2), 3.74 (dd, J = 10.1 Hz, 4.6 Hz, 3H, H6$_a$), 3.48 (m, 3H, H6$_b$), 3.43 (m, 6H, H3 and H4), 3.29 (m, 3H, H5)

^{13}C NMR (151 MHz, DMSO-d_6) δ 177.6(core Ar, C−O), 156.0(Ar, C-O-Sugar), 135.7(Ar C-N), 128.4(Core Ar C-N), 118.5(Ar, C−C−N), 117.3(Ar, C−C−O−sugar), 97.8(C1), 77.8(C5), 73.4(C3), 70.4(C2), 66.8(C4), 61.04(C6**)**

HRMS (ESI) m/z: $[M + H]^+$ calcd for $C_{42}H_{49}N_6O_{21}$ 973.2951; found 973.2948

Synthesis of α-D-mannosyl-Yariv reagent (**9**)

A solution of cold freshly prepared 1.2 M HCl (7 mL, 2.5 equiv) was added to 4-aminophenyl α-D-mannopyranoside (880 mg, 3.3 mmol, 1 equiv) in a 250 mL round-bottom flask. This solution was cooled in an ice bath while stirring. $NaNO_2$ (247 mg, 3.6 mmol, 1.1 equiv) was dissolved in 0.5 mL of cold water in an Eppendorf tube. The $NaNO_2$ solution was added to a 1 mL syringe with a 4 in. × 22 gauge needle that was clamped above the reaction flask, leading to a gravity-assisted dropwise addition. The reaction was stirred at 0 °C for 2 h. Phloroglucinol (140 mg, 1.1 mmol, 0.34 equiv) was dissolved in a minimal amount of cold 5 M NaOH (1−2 mL) and added dropwise to the reaction mixture. To the mixture was added 5 M NaOH until the pH was basic as indicated by a pH paper. The pH was maintained at∼11 (dark blue on the pH strip) by the addition of 5M NaOH as necessary. The reaction mixture was stirred overnight. Cold 100% ethanol (200 mL) was

added to the reaction mixture, which was neutral at this point as determined by the pH paper. To the mixture was added 12 M HCl until the solution was acidic as indicated by a pH paper. The reaction flask was placed in a freezer for at least 24 h until a dark red-brown precipitate was observed. The precipitate was filtered through a Hirsch funnel and air dried. 0.94 g crude was obtained (87%). To 0.65 g of the crude product was added 5 mL of water, and the mixture was vortexed until complete dissolution. To the solution was added 150 mL of 100% ethanol. The mixture was filtered through a Hirsch funnel, and the precipitate was allowed to air-dry and then transferred to a preweighed vial. 300 mg of R1X was obtained and air dried.

^{1}H NMR (600 MHz, DMSO-d_6) δ 15.90, 15.86, 15.11 and 15.06(s, 3H, core Ar-OH), 7.64(d, *J* = 8.8 Hz, 6H, ArH *ortho* to azo), 7.23(d, *J* = 8.4 Hz, 6H, ArH *ortho* to sugar), 5.43(s, 3H, *H1*), 5.08(s, 3H, *2-OH*), 4.87(s, 3H, 4-*OH*), 4.79(s, 3H, *3-OH*), 4.50(s, 3H, *6-OH*), 3.86(s, 3H, *H2*), 3.70(d, *J* = 9.4 Hz, 3H, *H3*), 3.62(d, *J* = 11.5 Hz, 3H,*H6*) , 3.50-3.20(m,9H, *H6*,*H4*,*H5*)

^{13}C NMR (151 MHz, DMSO-d_6) δ 177.7(core Ar, C−O), 155.3(Ar, C-O-Sugar), 136.2(Ar C-N), 128.4(Core Ar C-N), 118.6(Ar, C−C−N), 118.1(Ar, C−C−O−sugar), 99.1(C1), 75.1(C5), 70.7(C3), 70.0(C2), 66.8(C4), 61.1(C6).

HRMS (ESI) m/z: $[M + H]^+$ calcd for $C_{42}H_{49}N_6O_{21}$ 973.2951; found 973.2957

Synthesis of bis β-D-glucosyl Yariv reagent (**8**)

A solution of cold freshly prepared 1.2 M HCl (3 mL, 2.5 eq) was added to 4-aminophenyl β-D-glucopyranoside (0.36 g, 1.3 mmol, 1 eq) in a 250 mL round bottom flask. This solution was cooled in an ice bath while stirring. $NaNO_2$ (97 mg, 1.4 mmol, 1.1 eq) was dissolved in 0.5 mL of cold water in an Eppendorf tube. The $NaNO_2$ solution was added to a 5 mL syringe with a 4 inch x 22 gauge needle which was clamped above the reaction flask, leading to a gravity assisted dropwise

addition. The reaction was stirred at 0 °C for 2 hrs. Phloroglucinol (830 mg, 6.5 mmol, 5 eq) was dissolved in a minimal amount of cold 5 M NaOH (5 ml) and added dropwise to the reaction. 5 M NaOH was added until the pH was basic as indicated by pH paper, at which point the ice bath was removed. The pH was maintained at ~11 (dark blue on pH strip) by addition of 5 M NaOH as necessary. The reaction was stirred overnight. Cold 100% ethanol (150 mL) was added to the reaction, which was neutral at this point as determined by pH paper. 1.2 M HCl was added until the solution was acidic as indicated by pH paper. The reaction flask was placed in a freezer for at least 24 hours until a red precipitate was observed. The precipitate was filtered through a Hirsch funnel to provide the crude Yariv reagent **1** as a glossy red, sticky powder which clumped together. This solid was air dried for a few hours, at which point it hardened to a solid mass which became a powder when crushed. The powder was transferred to a pre-weighed scintillation vial and dried in a vacuum oven with at 75 °C for 24 hours. This crude product (0.8 g, 1.2 mmol) was obtained in 88% yield as a dark red powder. 121 mg of the crude was washed with water and filtered through a Hirsch funnel. 30 mg of filtered product was obtained.

^{1}H NMR (600 MHz, DMSO-d_6) δ 15.58 (s, 2H, core Ar-O*H*), 7.64 (d, *J* = 7.2 Hz, 4H, Ar*H ortho* to azo), 7.14 (d, *J* = 9 Hz, 4H, Ar*H ortho* to sugar), 5.7 (s, 1H, Core-ArH), 5.37 (d, *J* = 4.8 Hz, 2H, 2-O*H*), 5.15 (d, *J* = 3.9 Hz, 2H, 3-O*H*), 5.09 (d, *J* = 4.9 Hz, 2H, 4-O*H*), 4.90 (d, *J* = 7.5 Hz, 2H, *H1*), 4.63 (t, *J* = 5.6 Hz, 2H, 6-O*H*), 3.71 (ddd, *J* = 11.7, 6.0, 2.5 Hz, 2H, $H6_a$), 3.48 (dt, *J* = 12.0, 5.9 Hz, 2H, $H6_b$), 3.39-3.18 (m, 8H, *H5, H3, H2 & H4*)

^{13}C NMR (151 MHz, DMSO-d_6) δ 177.3(core Ar, *C*-O), 156.2(Ar *C*-O-sugar), 136.6(Ar *C*-N), 127.0(core Ar, *C*-N), 118.5(Ar *C*-C-N), 117.8(Ar *C*-C-O-sugar), 102.1(*C1*), 101.0(*C1*), 77.5(*C5*), 77.1(*C3*), 73.7(*C2*), 70.1(*C4*), 61.1(*C6*) HRMS (ESI) m/z: $[M + H]^+$ calcd for $C_{42}H_{49}N_6O_{21}$ 690.1996; found 690.2021.

DOSY NMR Protocol

DOSY experiments were performed using the ledbpg2s pulse sequence. The experiments were conducted with an exponential gradient stepped between 2% and 95%. 16 1D ^{1}H spectra were collected with a gradient duration of 1.5 ms and an echo delay of 100 ms.

References

1. Yariv, J.; Rapport, M. M.; Graf, L., The interaction of glycosides and saccharides with antibody to the corresponding phenylazo glycosides. *Biochem J* **1962,** *85*, 383-8.
2. Ganjian, I.; Basile, D. V., Reductive syntheses of p-aminophenyl-beta-D-glucoside and its conversion to beta-glucosyl Yariv reagent. *Anal Biochem* **1997,** *246* (1), 152-5.
3. Basile, D. V.; Ganjian, I., β-d-Glucosyl and α-d-Galactosyl Yariv Reagents: Syntheses from p-Nitrophenyl-d-glycosides by Transfer Reduction Using Ammonium Formate. *Journal of Agricultural and Food Chemistry* **2004,** *52* (25), 7453-7456.
4. Zhang, J.; Li, M.; Chen, C.; Xu, Y.; Tian, X. Method for preparing β-glucosyl-yariv reagent from 4-nitrophenyl glucoside. CN101691450B, April 07, 2010.
5. Zhang, J.; Li, M.; Chen, C.; Xu, Y.; Tian, X. One-step process for preparation of β-glucosyl-Yariv reagent. CN101525358A, Sep 09, 2009.
6. E.F. Woods, G. G. L., M.A. Jermyn, The Self-Association of Glycosyl Phenylazo Dyes (Yariv Antigens). *Aust. J. Chem.* **1978,** *31* (10), 2225-2238.
7. Liu, X.; Luo, X. S.; Fu, H. X.; Fan, W.; Chen, S. L.; Huang, M. H., Irreversible tautomerization as a powerful tool to access unprecedented functional porous organic polymers with a tris(beta-keto-hydrazo)cyclohexane subunit (TKH-POPs). *Chem Commun (Camb)* **2020,** *56* (14), 2103-2106.
8. Paulsen, B. S.; Craik, D. J.; Dunstan, D. E.; Stone, B. A.; Bacic, A., The Yariv reagent: behaviour in different solvents and interaction with a gum arabic arabinogalactan-protein. *Carbohydr Polym* **2014,** *106*, 460-8.
9. Elbagary, R. I.; Fouad, M. A.; Ezzeldin, M. I., Quantitative Nuclear Magnetic Resonance Spectroscopic Analysis of Two Commonly Used Gastrointestinal Tract Drugs. *J AOAC Int* **2020,** *103* (5), 1208-1214.
10. Zhu, H.; Yang, H.; Li, J.; Barlow, K. J.; Kong, L.; Mecerreyes, D.; MacFarlane, D. R.; Forsyth, M., Proton-Exchange-Induced Configuration Rearrangement in a Poly(ionic liquid) Solution: A NMR Study. *J Phys Chem Lett* **2017,** *8* (21), 5355-5359.
11. Chan, Y. T.; Moorefield, C. N.; Newkome, G. R., Synthesis, characterization, and self-assembled nanofibers of carbohydrate-functionalized mono- and di(2,2':6',2''-terpyridinyl)arenes. *Chem Commun (Camb)* **2009,** (45), 6928-30.
12. Lee, D. W.; Kim, T.; Park, I. S.; Huang, Z.; Lee, M., Multivalent nanofibers of a controlled length: regulation of bacterial cell agglutination. *J Am Chem Soc* **2012,** *134* (36), 14722-5.
13. Wang, K. R.; An, H. W.; Wu, L.; Zhang, J. C.; Li, X. L., Chiral self-assembly of lactose functionalized perylene bisimides as multivalent glycoclusters. *Chem Commun (Camb)* **2012,** *48* (45), 5644-6.

14. Yu, G.; Ma, Y.; Han, C.; Yao, Y.; Tang, G.; Mao, Z.; Gao, C.; Huang, F., A sugar-functionalized amphiphilic pillar[5]arene: synthesis, self-assembly in water, and application in bacterial cell agglutination. *J Am Chem Soc* **2013,** *135* (28), 10310-3.
15. Zhang, T.; Pan, Z.; Qian, C.; Chen, X., Isolation and purification of D-mannose from palm kernel. *Carbohydr Res* **2009,** *344* (13), 1687-9.
16. Bock, K.; Lundt, I.; Pedersen, C., Assignment of anomeric structure to carbohydrates through geminal13C-H coupling constants. *Tetrahedron Letters* **1973,** *14* (13), 1037-1040.

Chapter 3 - Characterization of Yariv reagent-AGP Binding and Yariv reagent aggregation

Some findings from this chapter are published: Hoshing, R.; Leeber, B. W., 3rd; Kuhn, H.; Caianiello, D.; Dale, B.; Saladino, M.; Lusi, R.; Palaychuk, N.; Weingarten, S.; Basu, A., The Chirality of Aggregated Yariv Reagents Correlates with Their AGP-Binding Ability*. *Chembiochem* **2021**

3.1 Introduction

Even though the Yariv reagents are one of the most used tools to study AGPs, the precise nature of interaction between AGPs and the Yariv reagents is poorly defined. As noted previously (Chapter 1), the main Yariv reagent binding epitope in AGPs is the core 1,3-β-D-galactan main chain of AGP, which is proposed to adopt a helical conformation.[1] Also, we previously showed that the Yariv aggregates adopt helical architectures. To show that Yariv reagents form helical aggregates CD spectroscopy was utilized (Figure 1.11). The CD spectra of **1**-**7** also indicated that a change in the D or L configuration, as well as a change in the anomeric configuration, causes a reversal in helicity in the Yariv reagent aggregates. Previous reports had shown that **1**-**3** bind

AGP and **4-7** do not bind AGP. Comparison of the CD spectra show that besides containing β-D-sugars, Yariv reagents that bind AGP also exhibit positive CD couplets.

Given the fact that the Yariv reagent is highly aggregated[2] in conditions where it binds AGP, it is important to study Yariv reagent aggregation to understand Yariv-AGP binding. In this chapter, various aspects of Yariv reagent aggregation, are studied in more detail. The relationship between helicity of aggregates and AGP binding ability is explored further. We synthesized additional Yariv reagents such as **9** and **10**, which were also analyzed for their aggregation and AGP binding properties. The CD spectra of the resynthesized Yariv reagents **1-7** were reobtained. The AGP binding ability of the resynthesized Yariv reagents was analyzed, and these results are presented in this chapter as well. The soldiers and sergeants phenomenon[3] in the context of various Yariv reagents is also detailed here. Finally, aggregation of various Yariv reagents is analyzed via variable temperature experiments.

3.2 Helical chirality of Yariv reagent aggregates

As shown in chapter 2 (Figure 2.10), even in cases where the ^{1}H NMR spectra of the Yariv reagents did not show evidence of significant presence of impurities, using the purification protocol gave rise to an increase in the CD signal of the Yariv reagents. Therefore, it was important reevaluate the CD spectra of the resynthesized Yariv reagents. Besides β-D- sugar containing Yariv reagents, the CD spectra of other Yariv reagents such as **6** and **7**, which contain β-L and α-L fucosyl moieties respectively were also reacquired for the sake of completeness. The CD spectra of other reagents such as **9** and **10** had never been previously acquired and therefore also needed to be acquired.

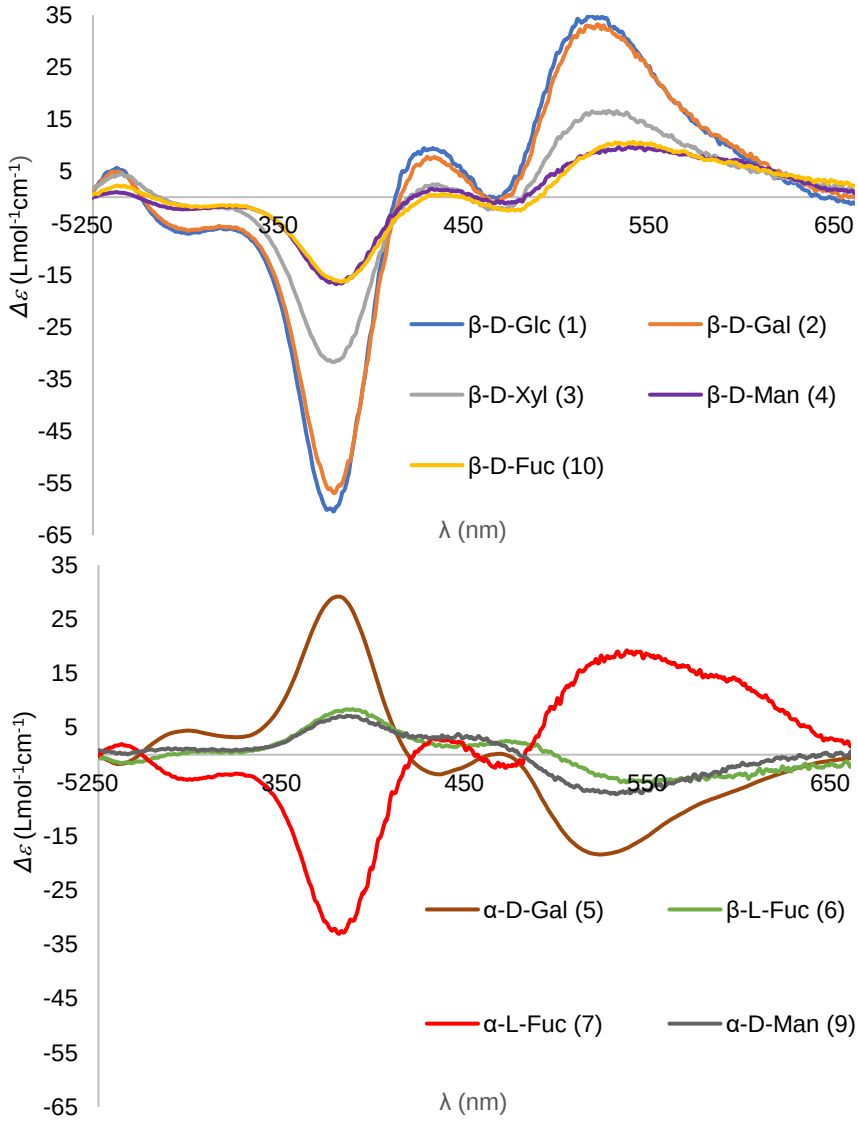

Figure 3.1 CD spectra (in water (300 μM)) of Yariv reagents: β-D-sugar analogs (top) and Non-β-D-sugar analogs (bottom)

The reacquired CD spectra (Figure 3.1) for each Yariv reagent was qualitatively consistent with the previously acquired CD spectra (Figure 1.11). For all the Yariv reagents **1**-**9**, we see the presence of two overlapping bisignate cotton effects with $\lambda_{min/max} \approx 380$ nm for the couplet at the lower wavelength and $\lambda_{max/min} \approx 527$ nm for the couplet at higher wavelength (Table 3.1). As discussed previously in chapter 1, the exciton-coupling induced Cotton effects likely arise from two distinct transitions with a UV/vis maxima at 398 nm and 487 nm. For Yariv reagents with β-D-sugars (**1**-**4** and **10**) and α-L-fucosyl (**7**) we see two positive couplets, i.e., each couplet has a

positive cotton effect at higher wavelengths and negative cotton effect at lower wavelengths. The opposite is true for Yariv reagents containing α-D-sugars (**5** and **9**) and β-L-fucosyl (**6**) where we see two negative couplets, i.e., negative cotton effect at higher wavelengths and positive cotton effect at lower wavelengths for each couplet. These results suggest that the β-D-sugars (**1**-**4** and **10**) and α-L-fucosyl (**7**) Yariv reagents form right-handed aggregates, and α-D-sugars (**5** and **9**) and β-L-fucosyl (**6**) form left-handed aggregates. Therefore, the CD spectra of the resynthesized Yariv reagents were qualitatively similar to the CD spectra of the Yariv reagents synthesized without the optimized protocol. Although, qualitatively the CD results of the resynthesized Yariv reagents were the same as the CD results of originally synthesized Yariv reagents, there were large quantitative differences in many cases (Table 3.1).

Table 3.1. $\Delta\varepsilon_{\lambda max}$ ($mol^{-1}cm^{-1}$) of Yariv reagents synthesized by previous lab members compared to Yariv reagents synthesized by optimized protocol

Yariv Reagent	λ_{max} (nm)	$\Delta\varepsilon_{\lambda max}$ ($mol^{-1}cm^{-1}$) for Yariv reagents synthesized by original protocol	$\Delta\varepsilon_{\lambda max}$ ($mol^{-1}cm^{-1}$) for Yariv reagents synthesized with optimized protocol	λ_{min} (nm)	$\Delta\varepsilon_{\lambda min}$ ($mol^{-1}cm^{-1}$) for Yariv reagents synthesized by original protocol	$\Delta\varepsilon_{\lambda min}$ ($mol^{-1}cm^{-1}$) for Yariv reagents synthesized by optimized protocol
β-D-glc (**1**)	527	36.65	34.46	378	-64.38	-60.42
β-D-gal (**2**)	524	24.97	32.28	380	-40.38	-56.91
β-D-xyl (**3**)	527	9.84	16.09	380	-16.44	-31.68
β-D-man (**4**)	525	2.68	8.95	387	-3.79	-16.41
α-D-gal (**5**)	380	39.28	29.13	524	-24.48	-18.34
β-L fuc (**6**)	380	5.80	8.02	588	-2.64	-3.89
α-L-fuc (**7**)	527	9.98	17.71	384	-17.23	-32.47
α-D-man (**9**)	527		7.04	588		-6.81
β-D-fuc (**10**)	527		10.03	380		-15.94

Comparison of the CD spectra of various samples of β-D-Glc Yariv reagent (**1**) showed that the previously synthesized sample had a slightly higher CD signal. However, in all other cases the CD signal was significantly higher for the optimized method. Yariv reagents **9** and **10** were

excluded from comparison because these were never synthesized via the previous method. Yariv reagent **5** is included but the optimized synthetic and purification protocol were not as useful for **5** i.e., ^{1}H NMR suggests that the previous sample was significantly purer (Chapter 2). Yariv reagent **4** is included but there are two important caveats i) the previous sample was purchased commercially and due to lack of enough sample ^{1}H NMR spectra of the original sample of **4** could not be acquired, therefore purity of previous sample is not known and ii) the optimized purification protocol like for **5**, was not very effective for **4**. Nevertheless, it must be pointed out that the CD signal of the commercially obtained **4** was significantly weaker than the CD signal of the sample that we synthesized. For example, the commercially obtained spectra of **4** had a $\Delta\varepsilon_{\lambda max}$ of 2.68 $mol^{-1}cm^{-1}$. The sample of **4** synthesized by us had a $\Delta\varepsilon_{\lambda max}$ of 8.95 $mol^{-1}cm^{-1}$. The relative CD signal of the β-D-sugar containing Yarivs did change significantly in some cases and remained similar in other. The ellipticities of the CD spectra of **2** are comparable to **1** now whereas previously, **2** was significantly lower. Those for **3** and **4** remain significantly lower than **1** and **2**. **10** is a new molecule, and its CD was found to be very similar to the new CD signal of **4**. Overall, it can be concluded that the optimized synthetic and purification protocol gave rise to Yariv reagent samples with significantly stronger CD signals.

3.3 Correlation between Yariv reagent-AGP binding ability and aggregate helicity

3.3.1 Regular gel binding assays

Next, the AGP binding ability of the Yariv reagents was evaluated. AGP binding ability of the Yariv reagents β-L (**6**) and α-L fucosyl (**7**) had not been previously evaluated by us. Therefore, the classic AGP binding evaluation assay known as the gel binding assay Yariv reagents were utilized to evaluate the AGP binding ability of **6** and **7**. In the classical gel assay, Yariv reagent is present in the gel and AGP is added to wells in the gel. The presence of a red halo indicates the presence of AGP binding ability. For example, positive results in the regular gel assay can be seen for β-D-glc (**1**) and β-D-xyl (**3**) in Figure 3.2. The regular gel assay results showed that

neither **6** nor **7** bound to AGP (Figure 3.3). These results were consistent with the previously obtained data that had shown that only β-D-sugar containing Yariv reagents bind AGP.

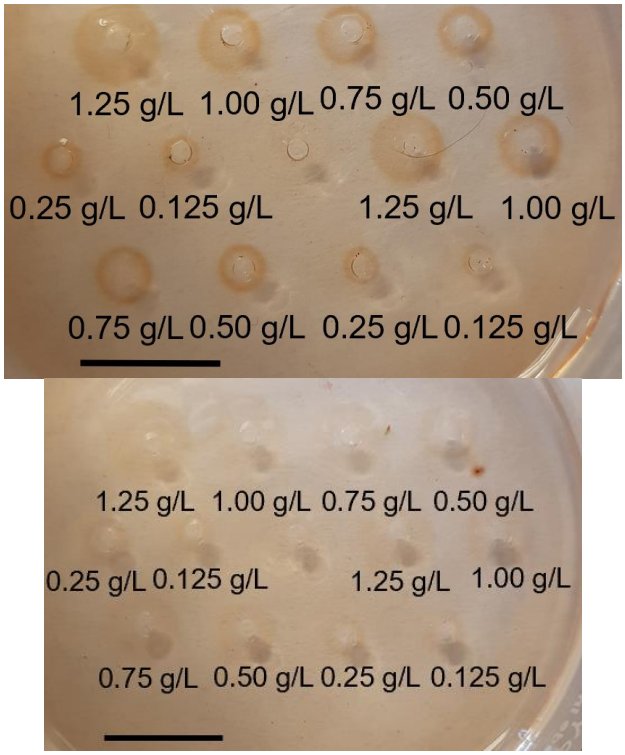

Figure 3.2 Regular gel assay containing a) β-D-glc (**1**) b) β-D-xyl (**3**) Yariv reagents with gum arabic AGP added to the wells. Concentration of the added AGP solution shown. Scale Bar – 1 cm

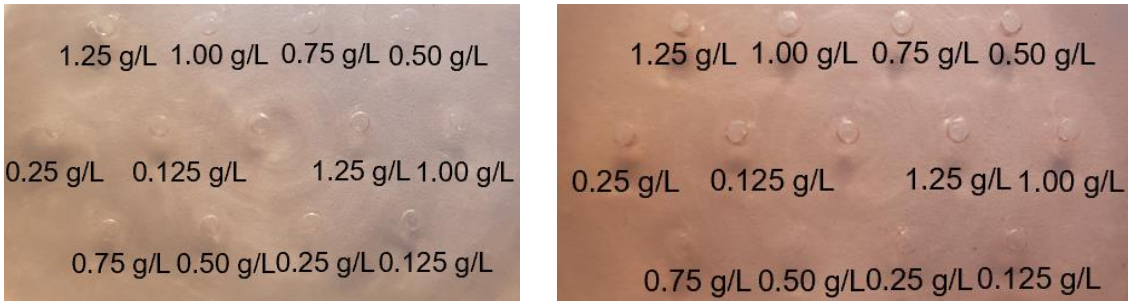

Figure 3.3 Regular gel assay containing a) β-L-fuc (**6**) b) α-L-fuc (**7**) Yariv reagents with gum arabic AGP added to the wells. Concentration of the added AGP solution shown.

The most significant difference between the gel containing **1** vs **3** was that the halos formed in the regular gel assay of β-D-glc (**1**) were significantly smaller but darker than those formed in the regular gel assays containing β-D-xyl (**3**) (Figure 3.2 and Figure 3.4). Two possible reasons for the differences in the regular assay of **1** and **3** could include the fact that the interaction between **1**

and AGP could be stronger than between **3** and AGP, causing slower diffusion of AGP to occur when added to a gel with **1**, thus leading to the halos in gel assay containing (**1**) being smaller. Alternatively, it could be that there is a "critical amount" of AGP that a given Yariv aggregate can bind before it precipitates. This critical amount could be higher for the β-D-Glc Yariv than β-D-Xyl Yariv. The ability for **1** to bind more AGP before it precipitates means that less amount of **1** would be required to bind the same amount of AGP leading to a smaller halo.

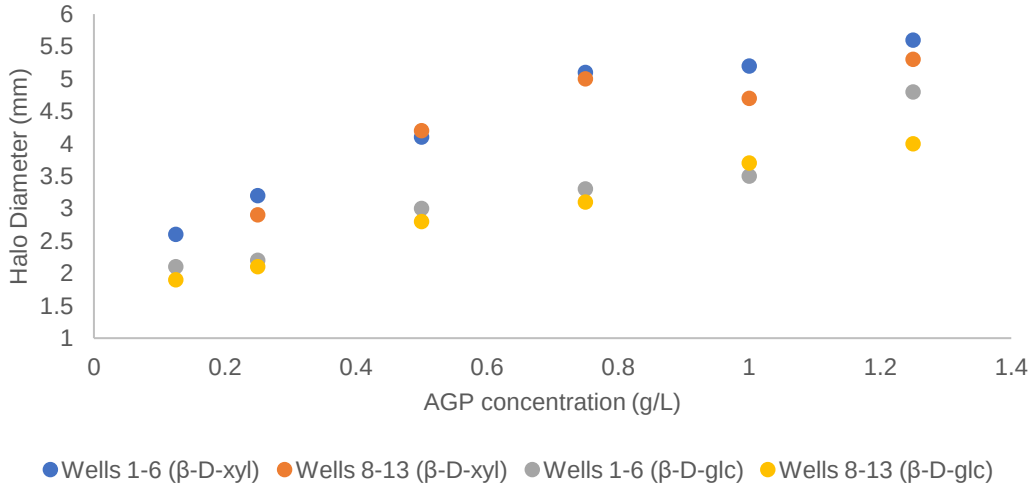

Figure 3.4 The halo diameters produced in the gels shown in Figure 3.2 plotted against the AGP concentrations added to the wells

3.3.2 Reverse gel assay

The regular assay does not readily allow one to compare the AGP binding ability of different Yariv reagents due to subtle gel to gel variations. Therefore, we inverted the standard assay such that different dyes could be injected into a single AGP-infused gel. This method, which we term a 'reverse-gel assay', allows easy comparison of AGP binding ability of various Yariv reagents on the same gel.

In order to develop this reverse gel assay, the exact amount of various materials required had to be optimized. The optimization of the reverse gel assay was required to identify AGP and Yariv reagent concentrations which would produce halos upon binding that are large and dark enough to be easily visible. An optimized reverse gel assay should provide halo sizes that ensure good

resolution of the various halos produced in a gel without being too small. To prepare the reverse gel assay, the concentrations of various reagents such as water, NaCl, NaN_3 and agarose in the gel was kept the same as the regular gel assays. However, gum arabic was added to the gel mixture instead of Yariv reagent. To determine what concentration of gum arabic and Yariv reagent works best, six different reverse gels were prepared with gum arabic concentrations of 0.75 g/L, 0.5 g/L, 0.25 g/L, 0.125 g/L, 0.075 g/L and 0.05 g/L. Just like in the regular gels, molds were used to prepare gels that contained 13 wells. Various concentrations of **1** ranging from 0.26 mM to 1.04 mM, a range in which most Yariv reagents are typically soluble, were then added to the wells. It was seen that when using gum arabic concentrations of 0.05g/L gum arabic and 1.04 mM Yariv reagent **1** the sizes of the halos produced were well resolved and also not too small to measure (Figure 3.5). Therefore, conditions for reverse gel assay were optimized and this assay could now be used for comparing AGP binding ability.

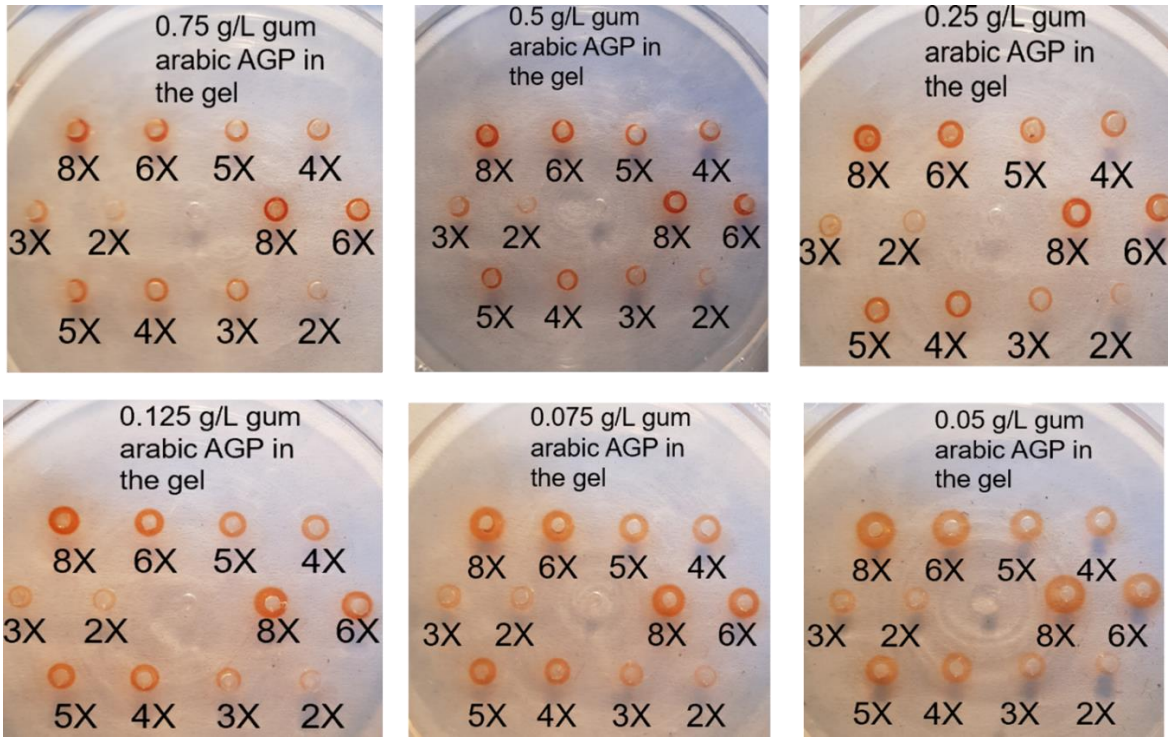

Figure 3.5 'Reverse' gel assay optimization; Gum Arabic AGP in the gel, **1** in the wells, concentrations of **1** range from 2X to 8X where X=0.13 mM

The β-D-glucosyl and galactosyl Yariv reagents **1** and **2** both formed intense red halos upon addition (Figure 3.6). This result confirms previous reports and is consistent with their wide use for AGP staining and isolation. The Yariv reagents with negative CD couplets (**5**, **6**, and **9**) do not show any evidence of binding. Precipitated Yariv reagent can be seen in wells with **6** and **9**, consistent with the poorer solubility of these compounds, while wells with the α-D-galactosyl derivative **5** generates diffuse halos without a clearly defined precipitate halo. These results indicate a direct correlation between the observation of intense positive CD couplets and strong AGP binding.

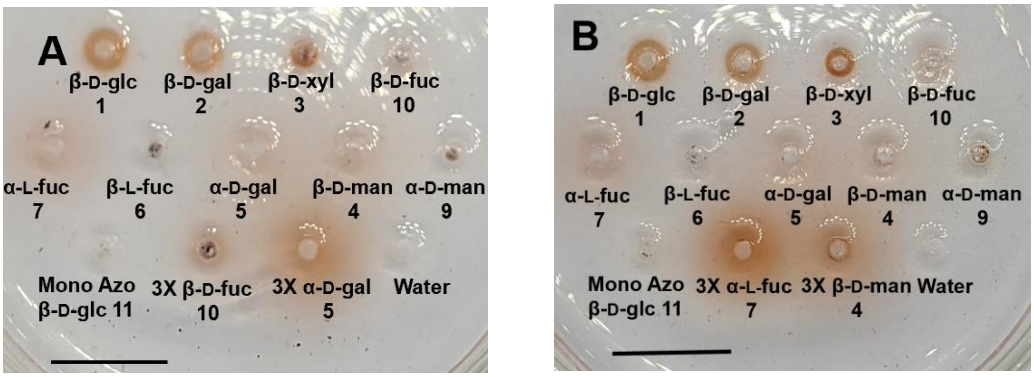

Figure 3.6. Reverse gel assay with Yariv reagents **1**-**7** and **9**-**11** added to individual wells. Scale bar – 1 cm

Wells corresponding to the three other β-D-Yariv reagents that exhibit less intense positive CD couplets - the β-D-xylosyl **3**, β-D-fucosyl **10**, and β-D-mannosyl **4** analogs do not generate halos indicative of strong AGP binding. The β-D-xylosyl derivative **3** forms well defined precipitate halos, but of smaller diameter than **1** and **2**. The AGP binding ability of **10** is very weak, as evidenced by the very faint halos that were observed for **10.** Use of threefold more Yariv reagent **10** in the well (3x) results in formation of a more defined precipitation halo (Figure 3.6A), albeit still much fainter than those seen with **1**, **2**, and even **3**. Furthermore, precipitate is visible in the well, consistent with the poor solubility of **10**. For comparison, a 3x experiment with **5** or **7** intensifies the diffuse color (Figure 3.6) but does not generate a characteristic precipitate halo. Interestingly, **4** shows a very thin precipitate halo when examined at 3x (Figure 3.6B). While it

cannot rule out the possibility that the binding seen in the 3x experiment arises from the impurities present in the synthesized sample of **4**, but even so, this would indicate that **4** does not bind AGP very strongly. While the concentrations used for the reverse gel are significantly higher than the 30 μM typically used for staining plant tissue, these results suggest that the α-D-galactosyl reagent (**5)** might serve as better negative control than the β-D-mannoside (**4**) in these types of experiments. Others have also noted potential concerns about the use of **4** as a negative control.[4] The CD spectrum of **7** is similar to the β-D-sugars i.e. shows two positive bisignate couplets. Therefore **7** also self-assembles into right-handed helical aggregates. However, **7** does not exhibit any halo formation in the reverse gel assay, even at 3x. Therefore, right-handed helicity alone is clearly not enough for APG binding ability.

When the gel-binding assay results are considered in conjunction with the CD spectra, the AGP binding ability correlates strongly with the CD couplet intensity. The two largest halos were formed by the β-D-glucosyl and β-D-galactosyl reagents **1** and **2** which also exhibit the most intense CD signals. Other β-D-sugar containing analogs bind with varying affinities ranging from the clear halo observed with the β-D-xylosyl analog **3**, to the marginal and inconclusive result with β-D-fucosyl derivative **10** and the β-D-mannosyl derivative **4** respectively. The CD signal in these cases is also correlated, as **3** has a significantly stronger CD signal than **10** and **4** but weaker than **1** and **2**, just like the AGP binding ability of **3** is significantly stronger than **10** and **4** but weaker than **1** and **2** in the reverse gel assay. Our results conclusively show that all Yariv reagents that bind AGP contain β-D-sugars and exhibit positive CD couplets. Further, these results show that the strength of AGP binding ability of β-D-sugar containing Yariv reagents in gel binding assays is correlated to the magnitude of their CD signal. We also demonstrate that the observation of a positive CD couplet and β-D-sugars is a necessary, but not sufficient, feature for the AGP binding ability of a Yariv reagent. Our observations are consistent with prior studies showing that the substituent and stereochemistry at C1 and C2 of the pyranoside are critical for AGP-binding, but changes at C3,

C4 and C6 do not perturb binding.[5] For example, the 6-MeO-, 4-MeO-, and 3-MeO- analogs of **1** all precipitate AGP, but the 2-MeO- derivative does not. However, the strength of the AGP binding ability does vary with the stereochemistry and presence/absence of hydroxyls at positions other than C1 and C2. The importance of stereochemistry for AGP binding can now be explained by the observation that changes at various positions result in changes in the sign and magnitude of the exciton couplets. However, correlation is not causation, and more insights into the Yariv-AGP complex and the Yariv reagent aggregates themselves are required to elucidate the specific binding mode of the Yariv-AGP complex.

3.3.3 Yariv-AGP binding studies using CD

To test if AGP binding can be detected using other methods, we have previously used CD. This experiment involves monitoring changes in CD signals of various Yariv reagents in presence of increasing AGP concentrations. Previously, when this experiment was done using β-D-glc Yariv (**1**), an increase in the CD signal was seen with increasing amount of AGP, until the CD signal saturated at around 0.5 mg/ml of AGP. Moreover, no increase in CD signal was seen for Yariv reagents that do not bind AGP such as **5**. These results suggested that AGP binding ability can be detected through this experiment if an increase in CD signal is seen upon AGP addition. This could potentially be either due to shortening of distance between two monomers or an increase in size of the aggregates upon AGP binding. We decided to retry the AGP titration experiment with the "weaker" AGP binders from the gel assay such as **3** and **10.** The CD spectra of 300 μM solutions of **3** and **10** in water containing various amounts of gum arabic AGP was acquired. An increase in CD signal with increasing amounts of AGP was seen for both **3** and **10**. The CD signal at 378 nm was plotted against amount of AGP added (Figure 3.7). The results were striking since the saturation of change in CD signal occurred at the same concentration for **3** and **10** as **1**. Therefore, it is important to note that the difference in halo sizes may not reflect inherent difference in AGP binding ability but rather simply in conditions that allow precipitation.

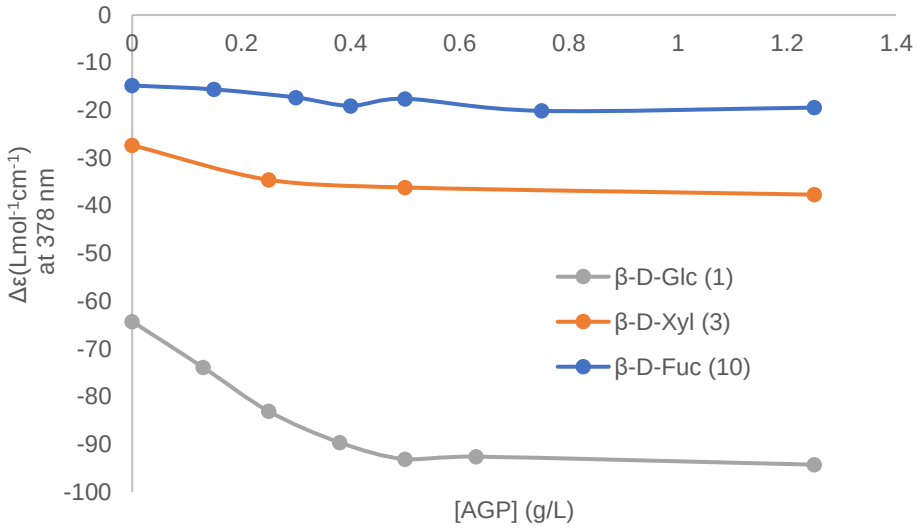

Figure 3.7 Comparison of increase in CD signal upon gum arabic addition for **1**,**3** and **10**

3.4 Other important factors for Yariv-AGP binding

3.4.1 Aggregation

Besides looking at the correlation between magnitude of exciton couplets of β-D-sugar containing Yariv reagents and AGP binding ability, the importance of aggregation to AGP binding ability was also tested using a variety of β-D-glc Yariv reagent analogues and gel conditions. For example, the binding of **1** to gum arabic was examined using a modified version of the regular gel assay in which the agarose gel containing the Yariv reagent was prepared in the presence of 1% SDS or 50% DMSO (Figure 3.10). As shown previously, the Yariv reagent **1** has a negligible CD signal in disaggregating conditions such as in 1% SDS or DMSO (Figure 1.12). No halo formation was observed in the presence of SDS, indicating that aggregation of **1** is required for AGP binding. Results in the 50% DMSO were somewhat unclear, while halos appear, these are significantly fainter than in the regular gel containing **1**, consistent with weaker binding in disaggregating conditions. However, the size of the halos appears to be smaller, contrary to what is expected from weaker binding in a regular gel. A reverse gel experiment with gum arabic AGP in the gel and Yariv reagent **1** dissolved in either 1% SDS or DMSO added to wells was also performed (Figure

3.11). Here, clear red halos indicating Yariv-AGP binding in each case was seen. This highlights the limitations of the reverse gel assay, as the DMSO and SDS likely diffused faster than the Yariv reagent in the gel, therefore Yariv aggregate formation and Yariv-AGP binding took place.

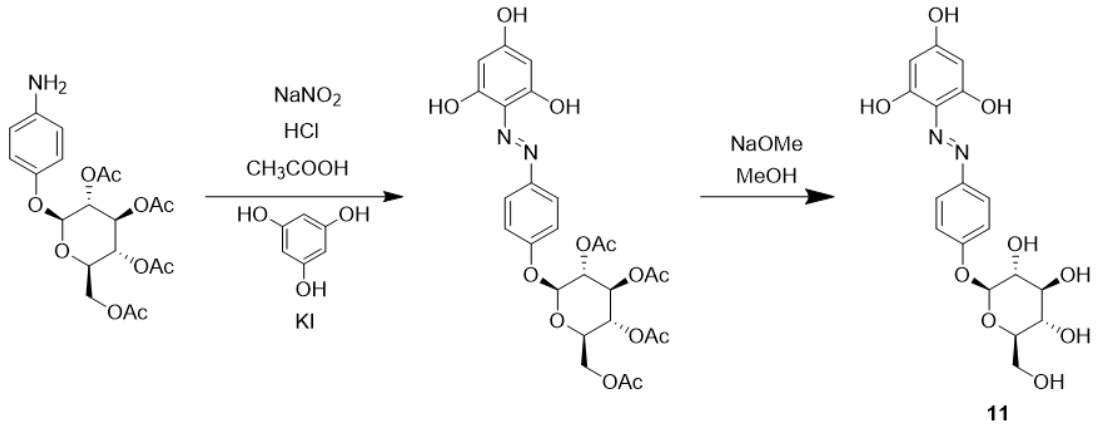

Scheme 3.1 Synthesis of **11**, the mono azo variant of the β-D-Glc Yariv reagent **1**

A mono azo analogue of the Yariv reagent **1** (**11**, Scheme 3.1) was synthesized. The synthesis of **11** involved using an acetyl protected 4-aminophenylglucoside which was diazotized and added to 10 equivalents of phloroglucinol to give the diazotization coupling product, an acetyl protected version of **11**. Upon purification of the diazotization coupling product using column chromatography, the acetyl groups were removed using sodium methoxide to give **11**.

When the regular tris azo Yariv reagent **1** is dissolved in water and ^{1}H NMR spectrum is acquired, we see the presence of only 2 broad peaks indicating aggregation (Figure 3.8). Therefore, for **1** the various sugar-H peaks and the two aromatic-H peaks are broadened to the extent that only one broad peak associated with each of these set of protons is seen. Further, compared to ^{1}H NMR spectrum in DMSO-d_6, the aromatic peaks are significantly upshifted for **1**. However, while the ^{1}H NMR of mono azo variant **11** also shows broad peaks, individual peaks for the various hydrogens are well resolved (Figure 3.8). The sharper peaks in water for the mono azo variant **11** indicates that it does not aggregate in water as much as the tris azo variant. Further, the aromatic peaks of

mono azo variant **11** are not upshifted compared to their chemical shifted in DMSO-d_6 (data presented in chapter 4).

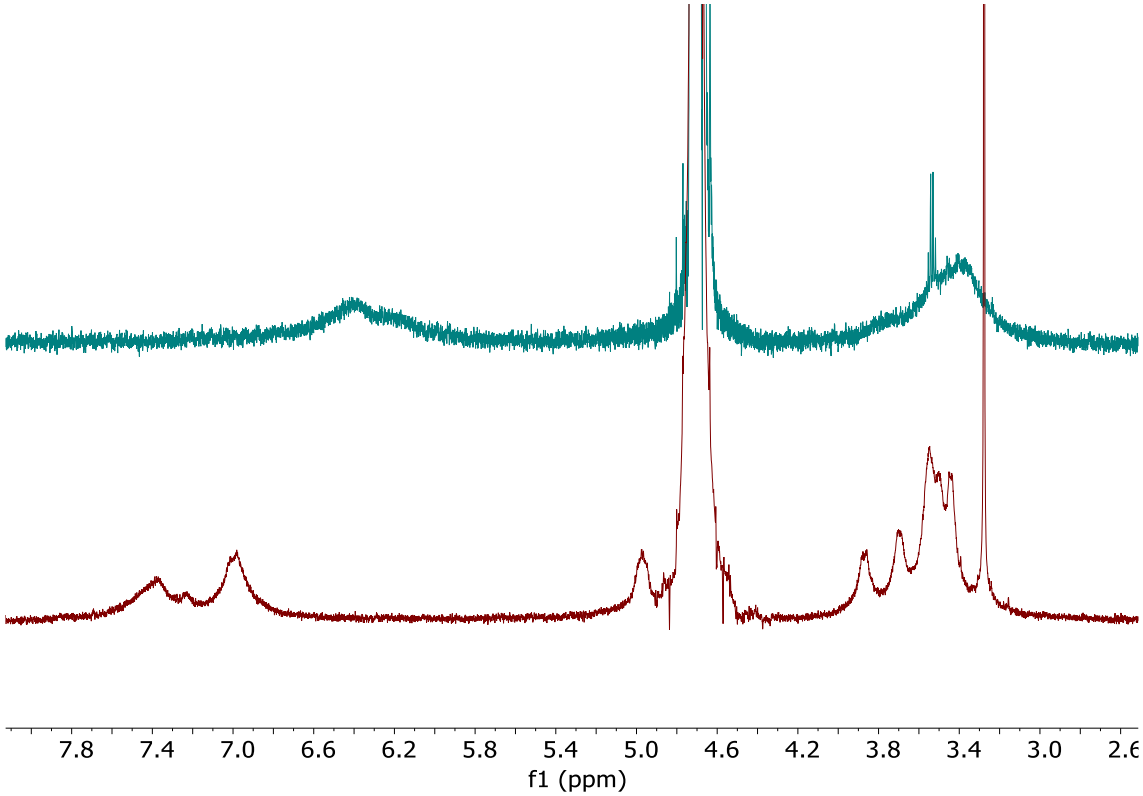

Figure 3.8 Comparison of ^{1}H NMR spectra of **1** (Top) and **11** (Bottom) in water

The CD signal of the mono azo variant was also found to be negligible (Figure 3.9). The mono azo variant does not bind AGP in the reverse gel assay (Figure 3.6). This lack of AGP binding ability could be due to having just one arm but also due to lack of aggregation.

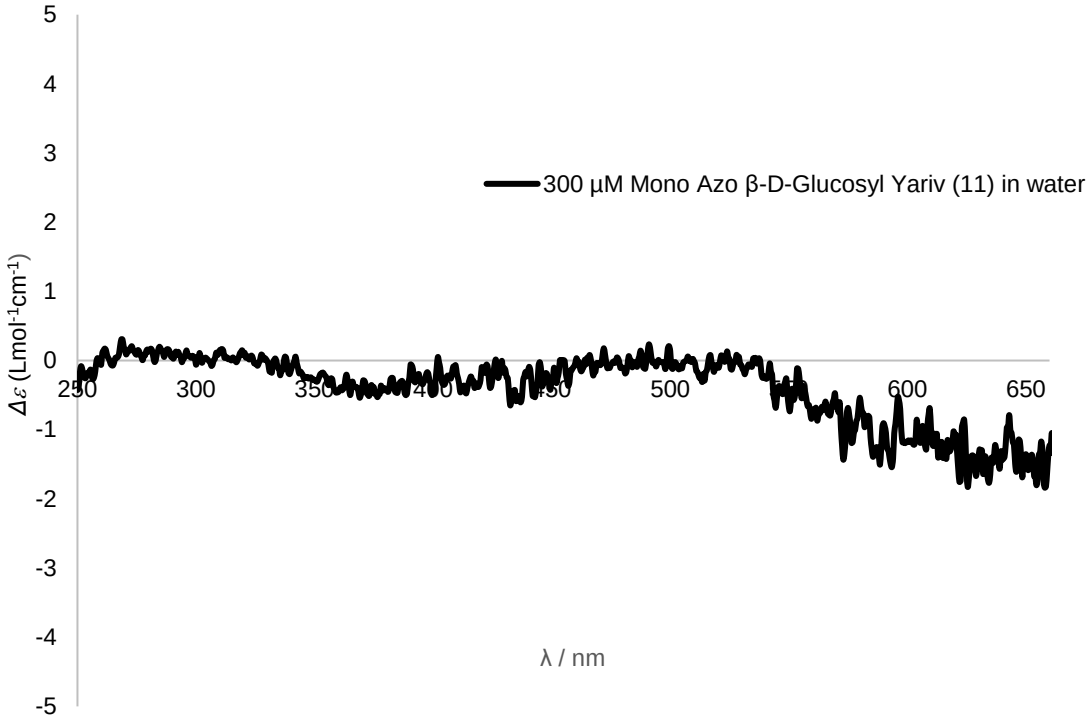

Figure 3.9 CD spectra of **11**

Overall, lack of binding seen in the modified regular gel experiments in 1% SDS or 50% DMSO and with **11** in the reverse gel assay indicated that aggregation is required for AGP binding.

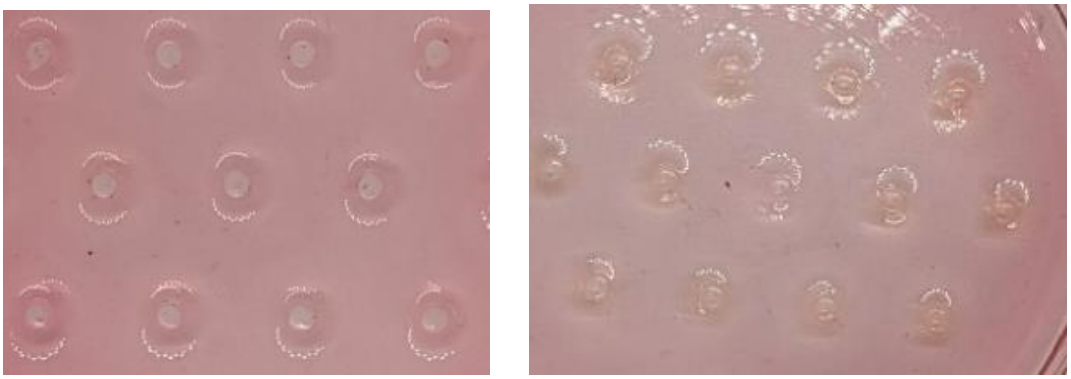

Figure 3.10 Gel assay containing **1** in 1% SDS (left) and **1** in 50% DMSO (right) in the gel and AGP added to the wells (1.25 mg/mL)

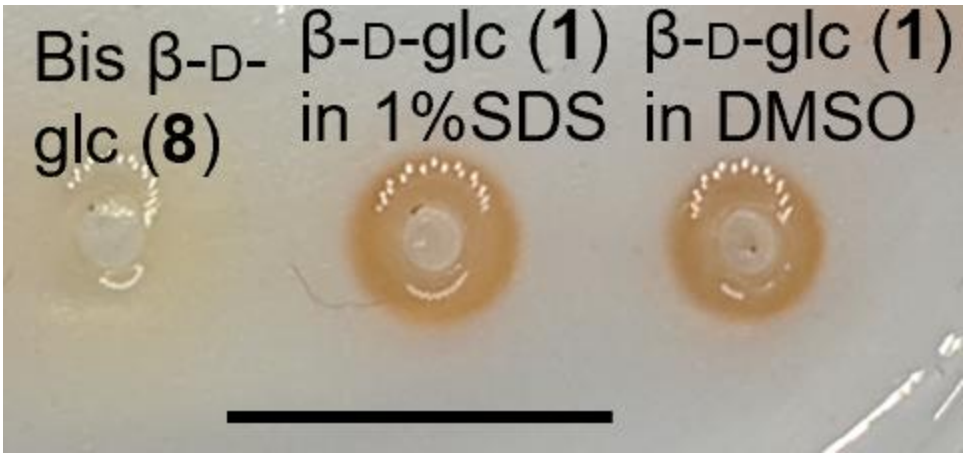

Figure 3.11 Reverse gel assay with AGP in the gel Yariv reagents added to the well; Scale bar 1-cm

3.4.2 Number of arms

A bis azo variant of **1** was also synthesized (**8**, Figure 2.3). It has been reported that mixed Yariv analogues containing two binding units such as β-D-glc and one non-binding unit such as α-D-gal can bind AGP.[5] However, it is not clear if a Yariv reagent with two β-D-glc units that is lacking a third arm is enough for aggregation and AGP binding. The ^{1}H NMR spectra of **8** in D_2O was shows broad peaks (Figure 3.12), indicating that the bis azo analogue **8** is aggregated in water.

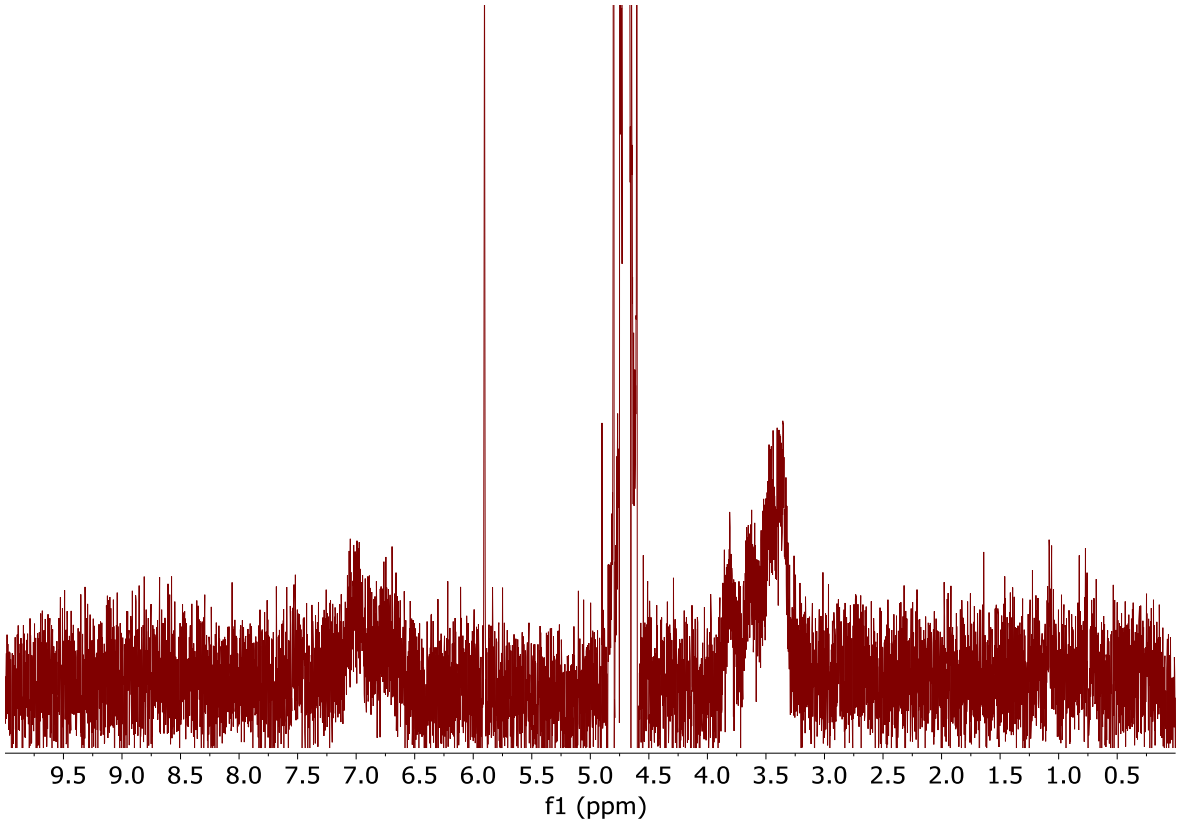

Fig 3.12 ^{1}H NMR spectrum of **10** in D_2O

A CD spectrum in water was obtained for the bis azo Yariv reagent **8** and showed a large CD couplet. Unlike the tris azo Yariv reagents which show two overlapping couplets, **8** only exhibits only one major couplet (Figure 3.13). The positive sign of the couplet indicates the presence of a right-handed aggregate just like the tris azo Yariv reagent (**1**). The UV/Vis spectrum in water also shows only one major transition corresponding to this couplet (Figure 3.13). The presence of a large CD couplet in water as well as broad peaks in ^{1}H NMR indicates that the biz azo variant **8** forms a helical aggregate.

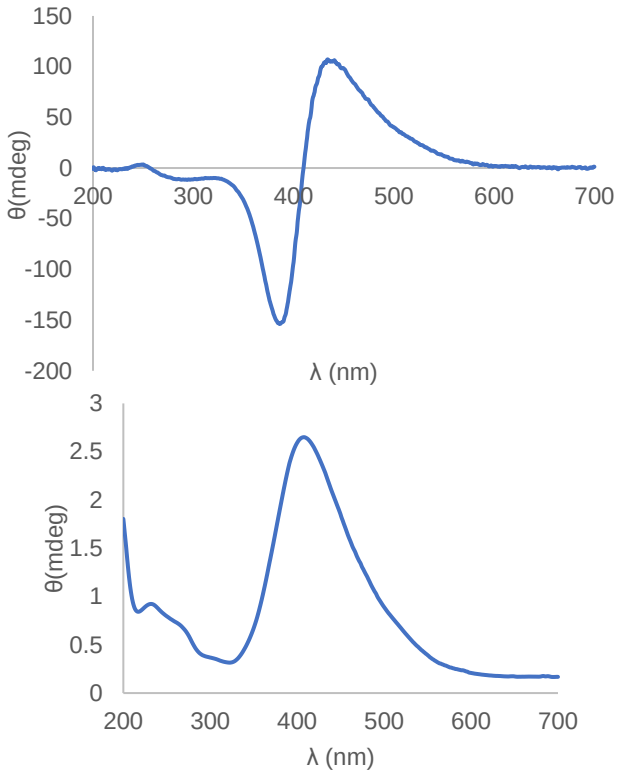

Fig 3.13 CD (left) and UV/vis spectrum (right) of 300 μM bis azo β-D-glc **8** in water

The AGP binding ability was first tested using a regular gel assay with bis azo **8** in the gel and AGP added to wells (Figure 3.14). No precipitation was seen in the regular assay indicating lack of AGP binding ability. The AGP binding ability of **8** was also tested using the reverse gel assay (Figure 3.11) and here too no AGP binding ability was seen. To ensure this is a valid result, the AGP binding ability was tested via the CD titration method. Gum Arabic AGP was added to a solution of bis azo Yariv reagent **8**, and the CD signal was measured. No increase in CD signal was noticed with addition of AGP (Figure 3.14)

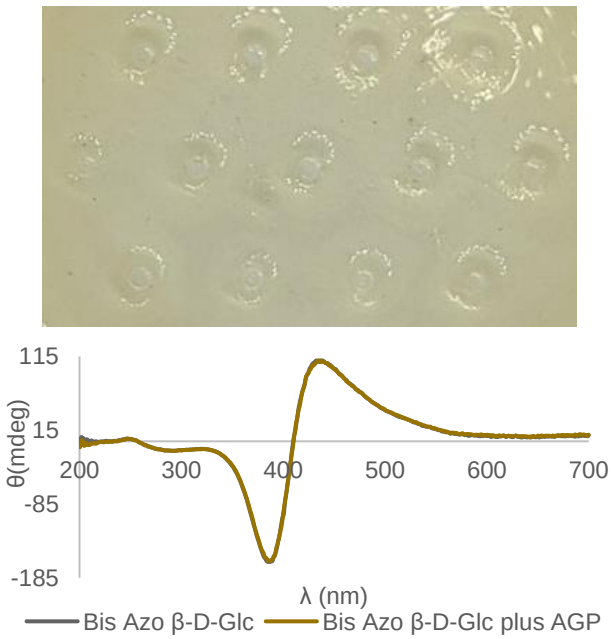

Figure 3.14 Left**:** Regular gel assay with bis azo β-D-glc **8** in the gel and gum arabic AGP added to the wells. Right: CD spectra of 300 μM bis azo β-D-glc **8** in water with (1.25 mg/mL) and without AGP

3.5 Soldiers and Sergeants Phenomenon

3.5.1 Introduction

A well-known phenomenon in supramolecular aggregation is "the soldiers and sergeant effect" through which the helicity of supramolecular aggregates can be manipulated.[3] In a soldiers and sergeant experiment a chiral molecule that aggregates with a preferred sense of helicity is introduced into a solution containing an achiral molecule that does not have a preferred sense of helicity. A soldiers and sergeants phenomenon is said to occur if upon introduction of the chiral molecule, the CD signal increases non-linearly. This is attributed to the fact that when a chiral molecule is introduced to the solution, the achiral monomers aggregate with the preferred helicity of the chiral molecule. It has previously been shown that even a solution containing 2.5% chiral "sergeant" showed the same CD signal as 100% "sergeant", while a achiral 100% "soldier" solution did not have CD signal.[6] The Yariv reagents could be said to display soldiers and sergeants

phenomenon if a Yariv reagent with higher ellipticity values such as **1** when added to a solution of a Yariv reagent with lower ellipticity values such as **3** or **10** increases the CD signal non-linearly.

The importance of helicity for AGP binding can be tested if soldiers and sergeant phenomenon is seen to occur. For example, if the AGP binding ability of the "soldiers and sergeants" mixture is seen to increase disproportionately compared to the amount of "sergeant" in the "soldier and sergeant mixture" then it would indicate that helicity of the Yariv reagents aggregates is related to the amount of AGP it can bind before it precipitates.

3.5.2 Experiments with **1** and **3**

A soldiers and sergeant experiment with β-D-glc Yariv (**1**) and β-D-xyl Yariv (**3**) was attempted. CD spectra of various mixtures of **1** and **3** were obtained. The mixtures ranged from 100% **3**, 50-50 mixture of **3** and **1**, 25-75 mixture of **3** and **1**, and 100% **1**. A soldiers and sergeant effect is said to take place if a strong non-linear increase in CD signal is seen upon increasing the amount of **1**. Therefore, if either the 25-75 or 50-50 mixture have CD signals of similar magnitude to 100% **1,** it would be considered a strong soldiers and sergeant effect. However, plotting the CD signal (mdeg) showed that only a slight non-linear increase is seen (Figure 3.15). This indicates that the β-D-glc Yariv reagent (**1**) does not strongly affect the helicity of the β-D-xyl (**3**) aggregates and argues against a strong soldiers and sergeant effect.

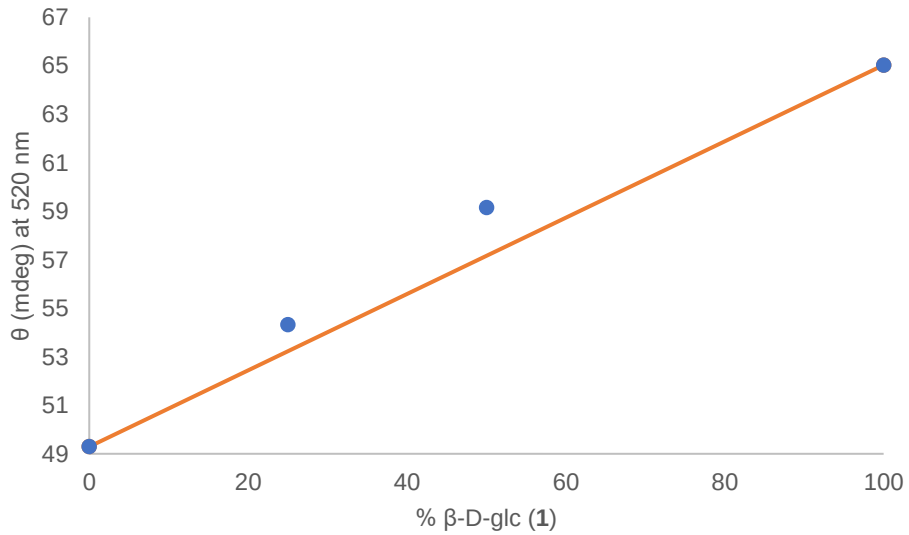

Figure 3.15 CD signal (mdeg) of 300 μM solutions of various mixtures of **1** and **3** in water at 520 nm vs % **1**. Orange line is a guide line that shows what completely linear increase would look like.

Even though CD experiments provide evidence of a very weak soldier and sergeant effect with mixtures of **1** and **3**, we decided to check whether any increase in AGP binding ability is seen using a reverse gel assay. Four different types of Yariv reagent samples were injected into the gel containing gum arabic AGP (Figure 3.16). Three trials of each type of Yariv reagent sample was injected into the reverse gel. First, the three trials of samples containing 1 μL 0.78 mM β-D-xyl (**3**) were injected. Then solutions containing the "soldiers and sergeant mixture" i.e. a mixture of 0.5 μL of 0.78 mM β-D-xyl (**3**) and 0.5 μL of 0.78 mM β-D-glc (**1)** were injected. Next, samples containing 1 μL of 0.78 mM β-D-glc (**1**) were injected. Finally, three trials of a "control experiment" solution containing 1 μL of 0.38 mM β-D-glc (**1**) was also injected. It was expected that if AGP binding ability is increased due to soldiers and sergeant effect, the "mixture" halos should be comparable to 0.78 mM **1** halos. The 0.39 mM **1** control allows determination of the contribution from **1** in the "mixture" halos since both the control and "mixture" contain the same amount of **1**. Halo sizes produced by each Yariv solution in the reverse gel was evaluated. It was seen that the halo sizes produced in by 0.78 mM **3** were on average significantly smaller halos than either the 50/50 mixture or 0.78 mM **1.** The increase in halo size produced by the 50/50 mixture as compared

to 0.78 mM **3** be either due to formation of mixed aggregates with increased helicity via soldiers and sergeants effect or simply to due presence of self-sorted stacks of **1** which inherently have a higher AGP binding ability as compared to **3**. To determine if the increased halos size in the mixture compared to **3** alone is due to soldiers and sergeant effect, the theoretical halo size produced by a mixture of self-sorted stacks was compared to the actual halo size of the 50/50 mixture. The theoretical halo size of a mixture of self-sorted stacks was calculated to be:

½*(Average halo area produced by 0.79 mM **3**) + (Average halo area of 0.39 mM 1) = ½*(4) + (3.13) = 4.63 mm^2

A caveat in this analysis is that the first term in the above equation assumes linearity of halo area with concentration. However, observing the halo areas produced by 0.39 mM vs 0.78 mM **1** (Table 3.2), this relationship does not hold. Despite the lack of linearity, the analysis was performed as large differences in the predicted theoretical halo size from self-sorted stacks vs measured halo sizes of the mixture may still be somewhat informative. The average halo size produced in the soldiers and sergeant mixture was found to be 5.81 mm^2 (Table 3.2) which is significantly larger than the calculated theoretical halo size produced by a mixture of self-sorted stacks (4.63 mm^2) and comparable to the average halo size produced by 0.78 mM β-D-glucose Yariv (6.10 mm^2). Since the halo sizes produced by the mixture are more comparable to the 0.78 mM β-D-glc Yariv rather than the theoretical mixture of self-sorted stacks, the increase in AGP binding ability could be due to an increase in the slight helicity induced by soldiers and sergeants phenomenon.

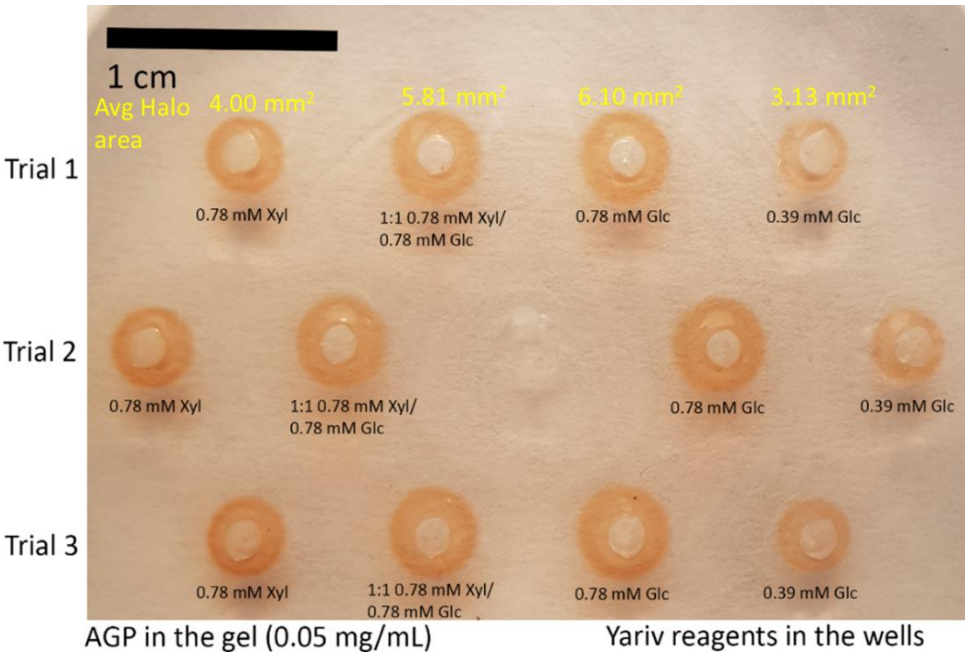

Figure 3.16 Reverse gel assay with four different kinds of samples injected into the wells

Table 3.2 Measured areas (in mm^2) of halos produced from various Yariv-AGP reverse gel experiments shown in Figure 3.16

Sample/Trial	0.78 mM **3**	S&S mixture	0.78 mM **1**	0.39mM **1**
Trial 1	3.93	5.72	5.91	3.29
Trial 2	4.11	6.05	6.28	2.95
Trial 3	3.94	5.66	6.10	3.14
Average	3.99	5.81	6.10	3.13

3.5.3 Experiments with **1** and **10**

The soldiers and sergeant CD experiment was then repeated with β-D-glc (**1**) and β-D-fuc (**10**). To check if introduction of **1** can lead into increase chirality of aggregates of **10**, CD spectra of various mixtures of **1** and **10** were obtained. The θ (mdeg) at 520 nm vs % β-D-glc (**1**) was plotted again. Although it was seen that CD signal of the pure sample of **1** was weaker than expected (50 mdeg at 520 nm instead of the usual 70 mdeg) it was significantly stronger than **10** (20 mdeg), and therefore could still potentially be used as the "sergeant". The CD results were very similar to the experiments with **3**, as a slightly non-linear increase in the CD signal was seen (Figure 3.17). Therefore, a slight amplification of chirality was seen. Next, the AGP binding experiment was repeated with **1** and **10**.

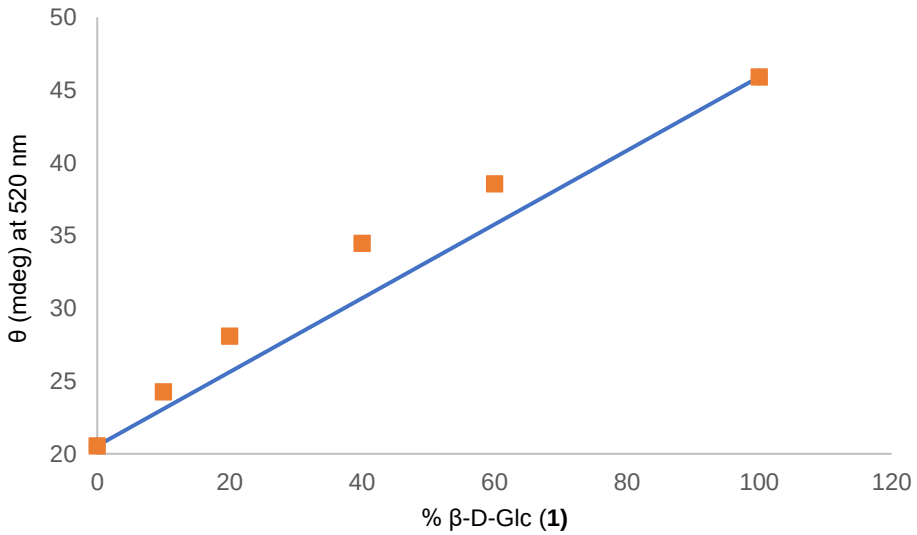

Figure 3.17 CD signal (mdeg) of 300 μM solutions of various mixtures of **1** and **10** in water at 520 nm vs % **1**. Blue line is a guide line that shows what completely linear increase would look like.

Halo sizes produced by each Yariv solution in the reverse gel was evaluated again (Figure 3.18, Table 3.3). The halo size of 0.78 mM **10** was 2.85 mm^2, the "soldiers and sergeant mixture" was 4.06 mm^2, 0.78 mM **1** was 5.1 mm^2 which is significantly smaller than the halo size seen in the experiment with **3** where the halo size of 0.78 mm **1** was 6.1 mm^2, however it was consistent with the weaker CD signal, and finally the control value was 2.93 mm^2. Here the expected theoretical halo size for self-sorted stacks were being formed is 4.36 mm^2 which is close to the actual halo size found for the **1**-**10** mixture (4.06 mm^2). This indicates lack of soldiers and sergeants induced increase in AGP binding ability. These AGP binding results combined with CD results of both the β-D-xyl (**3**) and β-D-fuc (**10**) experiments indicate that low amounts of chiral amplification in the Yariv reagents with β-D-glc (**1**) as the sergeant and **3** and **10** as soldiers. The lack of observed chiral amplification could be due to lack of chirality transfer because of formation of mostly self-sorted stacks rather than mixed aggregates. It may also be possible that an already chiral "soldier" may not lend itself well to the transfer of chirality due to changes in intermolecular interactions among chiral soldiers required for such an amplification to take place.

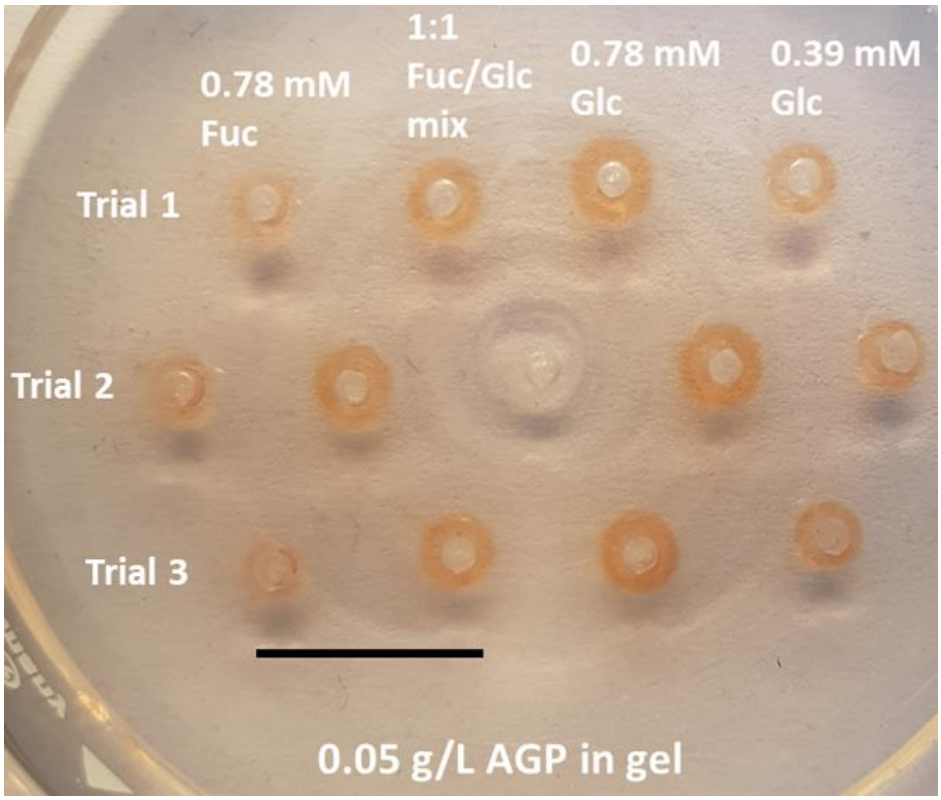

Figure 3.18 Reverse gel assay with four different kinds of samples injected into the wells. Scale Bar – 1 cm

Table 3.3 Measured areas (in mm^2) of halos produced from various Yariv-AGP reverse gel experiments shown in Figure 3.18

Sample/Trial	0.78 mM **10**	S&S mixture	0.78 mM **1**	0.39 mM **1**
Trial 1	2.40	3.79	5.22	3.10
Trial 2	3.80	4.46	5.32	2.87
Trial 3	2.35	3.95	4.76	2.82
Average	2.85	4.07	5.10	2.93

3.5.4 Experiments with **1** and **5**

To analyze if Yariv reagents can form mixed aggregates consisting of Yariv reagents with opposing chiral preferences, a reverse gel assay was utilized. In each well either purely β-D-glc (**1**) was added or mixtures of β-D-glc (**1**) and α-D-gal (**5**) was added (Figure 3.19). The mixtures consisted of increasing amounts of α-D-gal (**5**) while the keeping β-D-glc (**1**) amount constant. It was seen that the sizes of the halos produced did not change with the increasing amounts of **5**. If α-D-gal Yariv/β-

D-glc Yariv mixtures were producing non-helical or left-handed mixed aggregates, it would be expected that smaller halos would be produced with increasing α-D-gal Yariv (**5**) because as we've established, right handed helical aggregates are required for AGP binding. Since halo sizes remain constant it indicates that mixing **5** and **1** produces self-sorted stacks. To further analyze the nature of aggregates produced by mixing **5** and **1**, UV/vis spectroscopy was utilized. It is possible that if supramolecular co-polymers were being produced, the UV/vis spectra of the α-D-gal Yariv/β-D-glc Yariv mixture may starkly differ from the sum of the UV/vis spectra of pure α-D-gal Yariv and β-D-glc Yariv solutions. Therefore, the UV/vis spectra of 15 uM α-D-gal Yariv, 15 uM β-D-glc Yariv solutions and 1:1 mixture of 30 uM α-D-gal Yariv and β-D-glc Yariv was acquired (Figure 3.20). It was found that the sum of absorbances from the 15 uM solutions was almost equal to the absorbance from the 1:1 mixture. Like the gel results, the UV/vis results suggest the presence of self-sorted stacks as well. Lack of evidence of formation of mixed aggregates in the case of β-D-glc (**1**) and α-D-gal (**5**) suggests opposing chiral preferences are not conducive to formation of mixed aggregates.

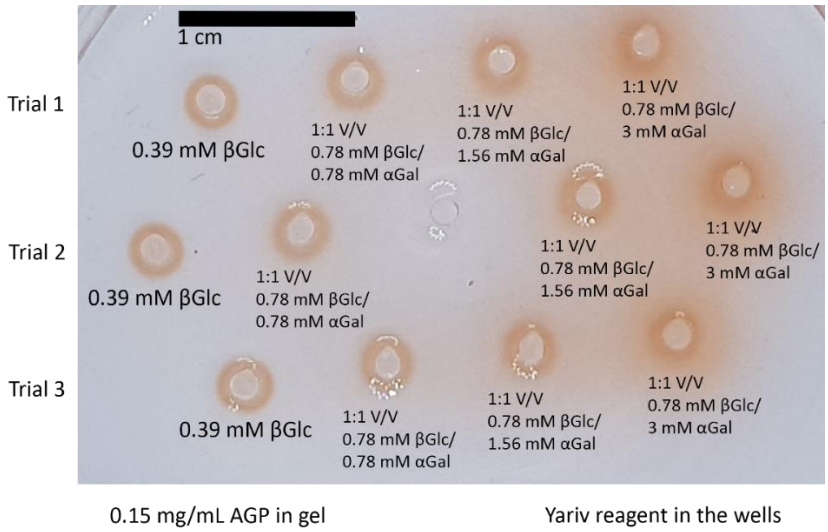

Figure 3.19 Reverse gel assay with four different kinds of samples injected into the wells

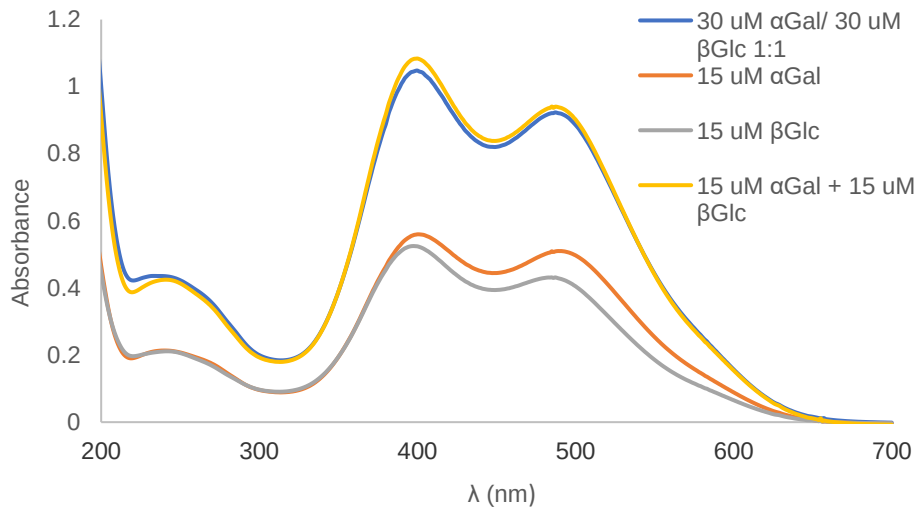

Figure 3.20 UV/vis spectra of mixture of **5** and **1** compared to sum of individual UV/vis spectra of **5** and **1**

3.5.5 Achiral Yariv reagent synthesis

A true "achiral Yariv reagent" might be required for formation of mixed aggregates that undergo chiral amplification via soldiers and sergeants effect because an achiral Yariv reagent would have no preference for helicity in its aggregates. Efforts to prepare an achiral Yariv reagent have been largely unsuccessful. My first attempt at synthesis of an achiral Yariv reagent was the "phenol Yariv reagent" (**12**). While this was easily synthesized by diazo coupling of 4-aminophenol with phloroglucinol (Scheme 3.2), the phenol Yariv reagent was largely insoluble in water, therefore not useful for soldiers and sergeant experiments. My next attempt at synthesizing an achiral Yariv reagent was the "glycerol Yariv reagent" (Scheme 3.3) which could potentially be water soluble. A general version of the synthetic protocol utilized to attempt the synthesis of "glycerol Yariv reagent" involved using either 4-nitrophenol or 4-aminophenol to substitute the bromine on a diethyl bromomalonate, followed by reduction of the ester to alcohol and then diazo coupling to give the achiral Yariv reagent. However, the substitution step was largely unsuccessful. A summary of the attempts and results is provided in Table 3.4. To circumvent the substitution step, another achiral Yariv reagent was proposed, the trimethylolmethane Yariv reagent (Scheme 3.4). The plan here was that the substitution would be circumvented by an addition of the 4-nitrophenol on to a

methylene malonate analog. However, the reflux conditions required for the addition reaction resulted in the polymerization of the methylene malonate analog. The achiral Yariv reagent synthesis was subsequently abandoned.

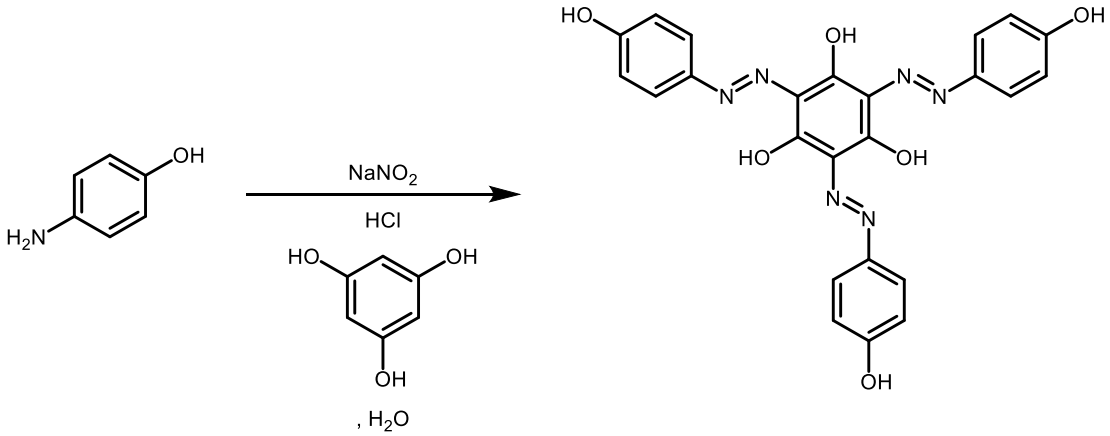

Scheme 3.2 Synthesis of **12**, The Phenol Yariv reagent

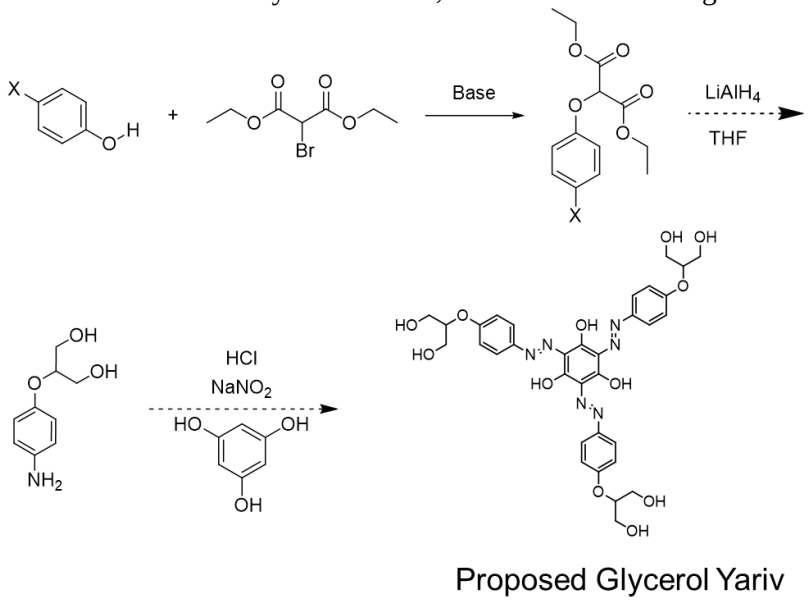

Scheme 3.3 Proposed synthesis of "Glycerol Yariv reagent". Solid arrows represent steps that were attempted and dashed arrows were not attempted. For identity of X and Base, see Table 3.4

Table 3.4. Summary of results from the attempted substitution reaction shown in Scheme 3.3

X=NO_2/NH_2	Base	Result
NH_2	NaH	Too many side products
NH_2	K_2CO_3	Imine formation (Mass spec, NMR)

NO_2	NaH	No evidence of desired product
NO_2	NaOH	Desired product formed (mass spec, NMR), separation difficult
NO_2	K_2CO_3	No evidence of desired product

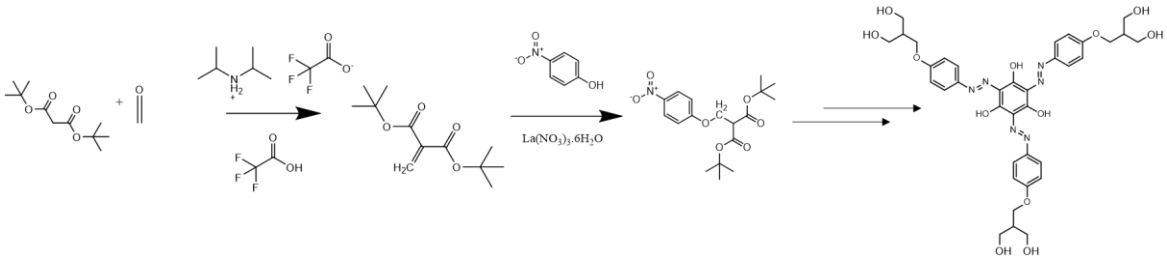

Scheme 3.4 Proposed synthesis of the "trimethylolmethane Yariv reagent"

3.6 Yariv reagent aggregation mechanism

Obtaining the thermodynamic parameters of the polymerization process could allow determination of polymer length, which would be important to understanding the Yariv-AGP binding process.[7] However, to obtain the thermodynamic parameters, it is important to understand the polymerization mechanism.[7] There are two major types of supramolecular polymerization mechanisms that give rise to linear supramolecular polymers. The first type is isodesmic, which can be characterized by the presence of just one association constant which isn't affected by the number of monomers present in the polymer. In the isodesmic association mechanism, there is lack of any critical temperature or concentration required for polymerization. On the other hand, self-assembly can also proceed through the cooperative mechanism which invovles significant polymerization after a critical temperature or concentration. The cooperative mechanism is characterized by the presence of an activation step with a significantly lower association constant compared to the polymerization step which happens subsequently. The first step in identifying whether the polymerization process is isodesmic or cooperative often invovles temperature dependent measurements. A sigmoidal

transition upon polymerization is indicative of an isodesmic mechanism whereas a non-sigmoidal transition with a nucleation phase indicates a cooperative mechanism.

In the case of Yariv reagents, ultracentrifugation experiments have shown that Yariv reagents aggregate through the isodesmic mechanism.[2] Further, thermodynamic parameters have been calculated for the association process using the ultracentrifugation data. However, these results haven't been confirmed through temperature dependent CD spectroscopy. We have previously attempted temperature dependent CD experiments. However, the mechanism of aggregation was unclear from these CD experiments. For example, variable temperature CD data was obtained for 300 μM α-D-gal (**5**) in water. The intensity of the CD signal was recorded at λ_{max} (381 nm for **5**). However, a significantly large CD signal was seen even at the highest recorded temperature indicating lack of complete disaggregation. To obtain information about aggregation mechanism, we need complete disaggregation so that the presence or absence of a sigmoidal curve can be determined. Further, the temperature dependent CD curve was completely linear. However, to calculate the thermodynamic parameters, it is necessary that at lowest recorded temperatures, the CD approaches a horizontal asymptote. The variable temperature CD approach was also repeated for **5** in various other solvent mixtures. The idea was that by using a co-solvent in which Yariv reagents are known to disaggregate, we may see complete disaggregation at higher temperatures in some solvent mixture. Various water-alcohol mixtures were utilized (containing MeOH, EtOH, and iPrOH), however an unexpected result was obtained in these cases. CD spectra for the samples containing methanol and ethanol are inverted when compared to the spectrum of the sample with pure water, whereas the CD spectrum for the isopropyl alcohol sample exhibits a large increase in CD signal reaching beyond detection limit of the instrument. The alcohol results suggested the formation of higher order aggregates that are irrelevant to AGP-Yariv binding. Variable temperature experiments were also previously attempted in water-DMF mixtures. While a 300 μM α-D-gal (**5**) solution in 40% DMF-water mixtures did show almost complete attenuation of CD

signal upon heating and a non-linear temperature dependent CD curve, my experiments have revealed that the Yariv reagents are likely in an anionic state in DMF. When triethyl amine is added to Yariv reagent **1** dissolved in DMSO, the two peaks in the Yariv reagent UV/vis spectra are gradually replaced with one major peak at 450 nm and one shoulder peak around 370 nm (Figure 3.21). This change in UV/vis is also noticed when other bases such as 1,8-diazabicyclo[5.4.0]undec-7-ene (DBU) are added to **1** in DMSO (Figure 3.22). The UV/vis signal in DMF matches with the UV/vis signal obtained by adding 6 equivalents of triethyl amine to Yariv reagent **1** dissolved in DMSO (Figure 3.23). The reason for this is likely the presence of trace dimethyl amine in DMF due to hydrolysis. Therefore, previously our experiments have been unable to confirm the ultracentrifugation results of an isodesmic mechanism due to lack of complete disaggregation or formation of species that are different from the regular Yariv reagent aggregates such as anions.

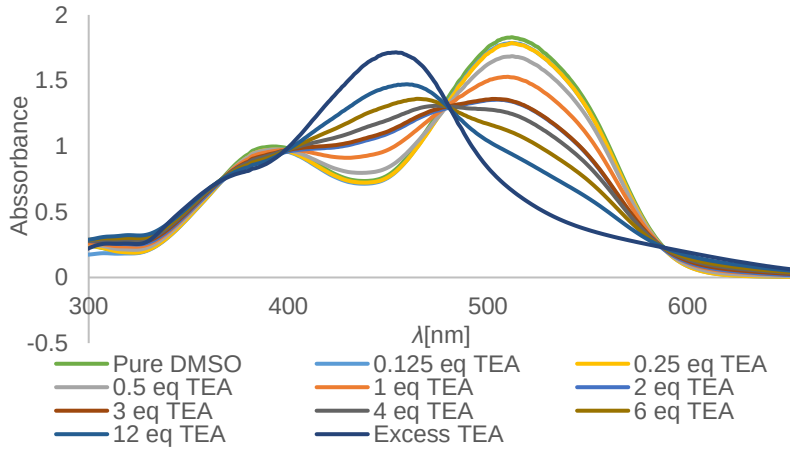

Figure 3.21 UV/vis spectra of **1** in DMSO (30 μM) in presence of varying amounts of triethyl amine (TEA)

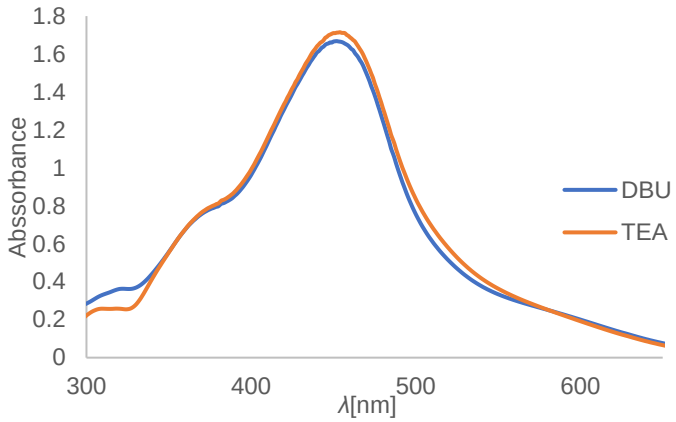

Figure 3.22 UV/vis spectra of **1** in DMSO (30 μM) in presence of TEA and DBU

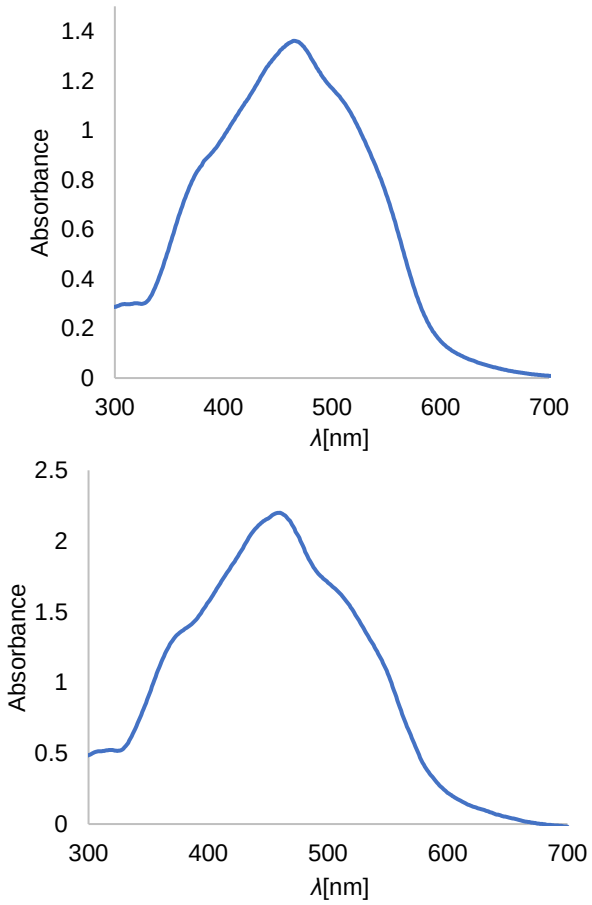

Figure 3.23 UV/vis spectra of 300 μM solution of **1** in DMF (right) compared to 30 μM solution of **1** in DMSO with 6 equivalents of Triethyl Amine (TEA) added (left)

To understand the aggregation mechanism, we first repeated the variable temperature CD experiments with β-D-glc (**1**) Yariv reagent. The variable temperature CD experiment was

attempted with 300 μM β-D-glc (**1**) in water. The CD signal was monitored at λ_{max} (520 nm for **1**) from 20-90 °C. The result was very similar to the one obtained for **5** previously under these conditions. A linear decrease in CD signal was noticed that did not attenuate significantly (Figure 3.24). Next, the concentration of **1** was reduced to 100 μM in order to see if this would allow for complete dissociation. The variable temperature CD was acquired from 20 deg to 95 °C for 100 μM sample of **1.** While complete attenuation was not seen, the graph looks non-linear and almost reaches a horizontal asymptote at 20 °C (Figure 3.25). Moreover, the lowest CD signal (9 mdeg) reached is below the half of the maximum recorded CD signal (20 mdeg). The temperature at which the degree of aggregation is 0.5 (T_m) is required to calculate the enthalpy release (ΔH) for the aggregation step in an isodesmic aggregation process. Since the horizontal asymptote is almost reached at 20 °C, it can be assumed that the "maximum possible" CD signal is very close to the CD signal recorded at 20 °C. Therefore, if the aggregation process is truly isodesmic, we now have enough information to calculate ΔH as well as the association constant K for the aggregation process in these conditions for **1**. However, since we do not see complete disaggregation, it is hard to know if the aggregation process is truly isodesmic.

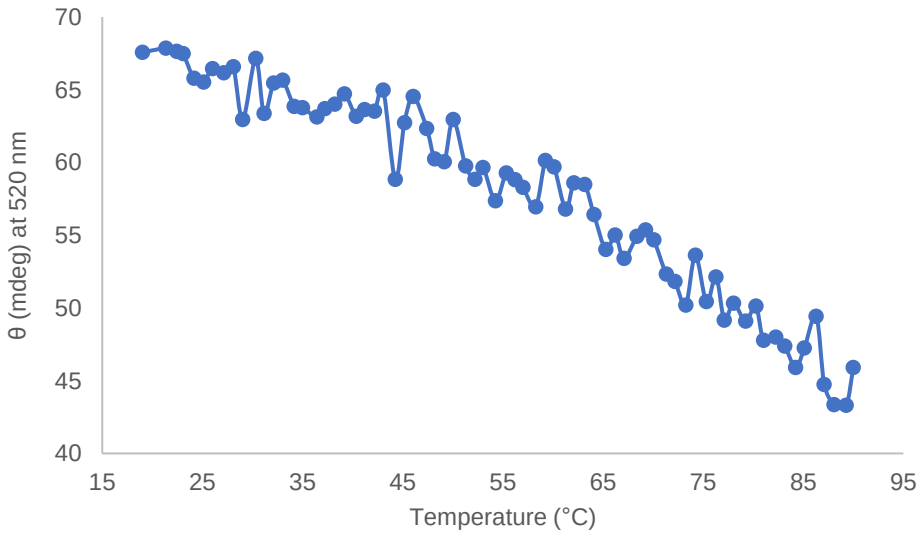

Figure 3.24 CD signal monitored at λ_{max} for 300 μM β-D-glc (**1**) in water at various temperatures

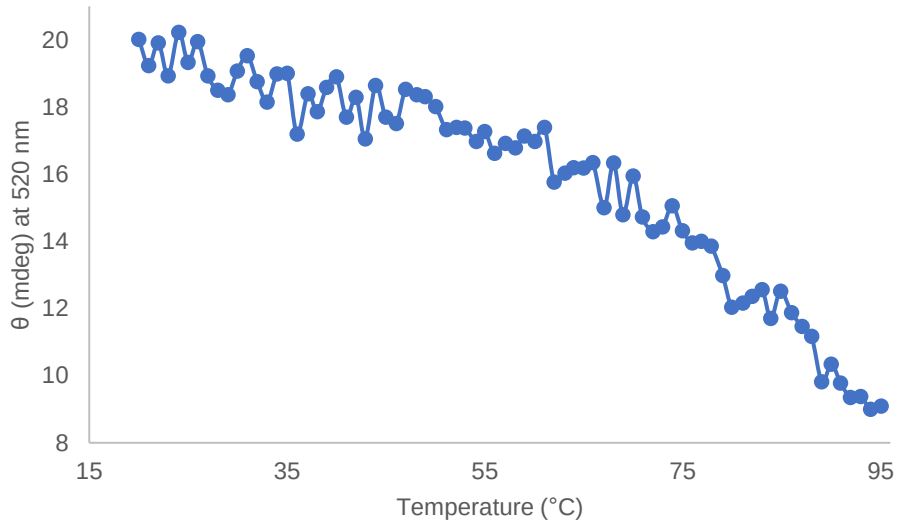

Figure 3.25 CD signal monitored at λ_{max} for 100 μM β-D-glc (**1**) in water at various temperatures

Next, we tried to obtain complete disaggregation by using the co-solvent strategy that was previously employed with DMF. However, we chose to use DMSO instead. The UV/vis spectra in DMSO-water mixtures show two peaks and look very similar to the UV/vis spectra in pure water (Figure 3.26). Therefore, it is more likely that the Yariv reagent aggregate has a similar morphology and aggregation mechanism in DMSO-water solvent mixture than in DMF-water. For this experiment, instead of recording the CD signal at one wavelength for various temperatures, the entire CD spectrum of 300 μM β-D-glc (**1**) in 75% water-25% DMSO was recorded at intervals of 10 °C from 20-90°C and then another CD spectrum was recoded at 95 °C. This is because it was noticed from previous CD experiments that the λ_{max} of the CD spectra of Yariv reagents shows significant changes with disaggregation. These changes are relatively minor in pure water but much more significant in more disaggregating conditions such as in the presence of urea or guanidinium Chloride. Therefore, as a precaution the entire CD spectra of 300 μM β-D-glc (**1**) was recorded in DMSO-water mixtures for the variable temp CD experiment. It was noticed that while a significant change in the λ_{max} is seen, the λ_{min} of the lower wavelength exciton couplet remains largely the same (Figure 3.27). Therefore, the CD signal at 382 nm was plotted against the temperature. A large dynamic range is seen, the CD signal attenuates very significantly to 6 mdeg starting from -

82 mdeg however does not reach complete disaggregation (Figure 3.28). However, the CD signal does almost reach a horizontal asymptote at 95 °C, this suggests that at slightly higher DMSO content, complete disaggregation might be reached at these temperatures. However, no asymptote is seen at 20 °C, which suggests that to obtain the "maximum possible" CD signal, slightly lower temperatures are required in these conditions. Overall, these conditions look somewhat promising and more variable temperature experiments with slightly higher amount of DMSO and starting with lower temperatures is required.

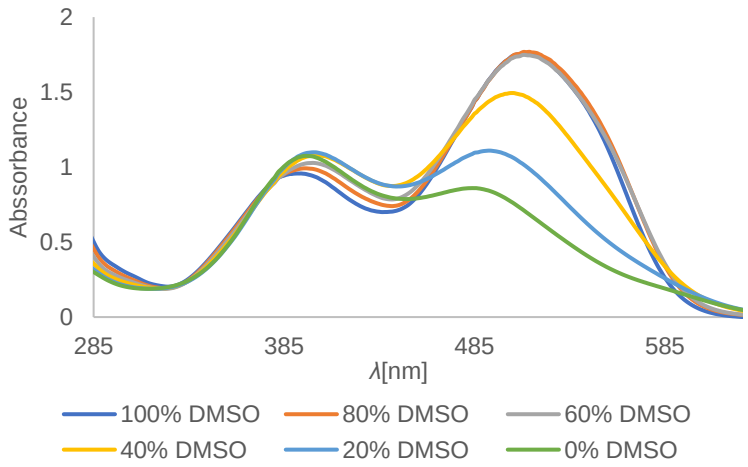

Figure 3.26 UV/vis of 30 μM β-D-glc (**1**) in various DMSO-water mixtures

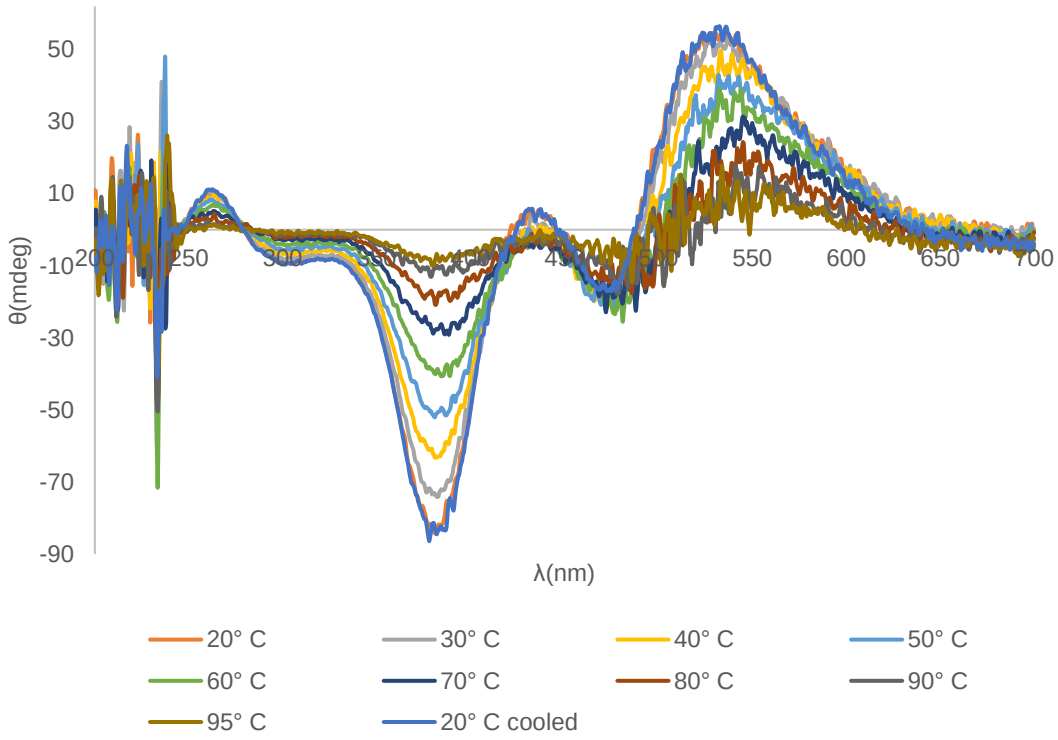

Figure 3.27 CD spectra (mdeg) of 300 μM β-D-glc (**1**) in 25/75 DMSO-water at various temperatures

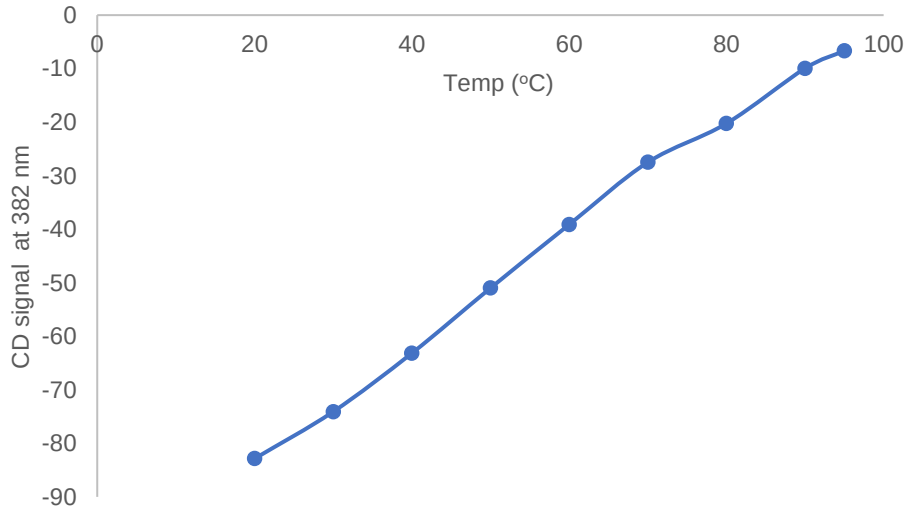

Figure 3.28 CD signal at 382 nm of 300 μM β-D-glc (**1**) in 25/75 DMSO-water at various temperatures

Variable temperature CD experiments were also performed with non-canonical Yariv reagents that typically show weaker CD signals such as β-D-xyl (**3**) and β-D-fuc (**10**). It was hypothesized

that **3** and **10** might show complete disaggregation because the lower CD signal for these might arise from the formation of weaker aggregates. First, the CD signal of 300 μM β-D-xyl (**3**) at 520 nm was recorded from 5-90 °C in water. The plot was linear (Figure 3.29). The linearity indicates that at the lowest temperature, the CD signal was not close to the maximum possible value as no asymptote was seen. Further, the CD signal was not attenuated to 0. Therefore, the mechanism of aggregation could not be deciphered from the β-D-xyl (**3**) CD melttemp data. Next, the CD signal of 300 μM β-D-fuc (**10**) at 520 nm was recorded over a temperature range of 5-95 °C. Interestingly, instead of a steady decline in CD signal, we only see the CD signal reduce until 70 °C. After 70 °C, we see the CD signal increase again (Figure 3.30). To see if this effect is real, the actual CD spectra was recorded at 20, 78 and 95 °C. The CD signal is slightly lower at 78 °C compared to 20 °C but at 95 °C it is almost equal to 20 °C (Figure 3.31). This unexpected result could possibly be due to presence of undissolved β-D-fuc (**10**), which only dissolves at higher temperatures. In conclusion both β-D-xyl (**3**) and β-D-fuc (**10**) were not suitable for understanding the aggregation mechanism in these conditions.

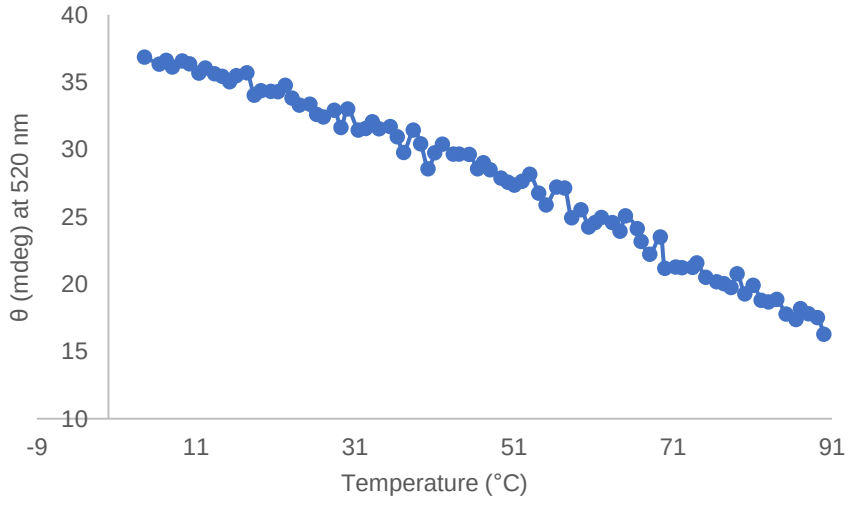

Figure 3.29 CD signal monitored at λ_{max} for 300 μM β-D-xyl (**3**) in water at various temperatures

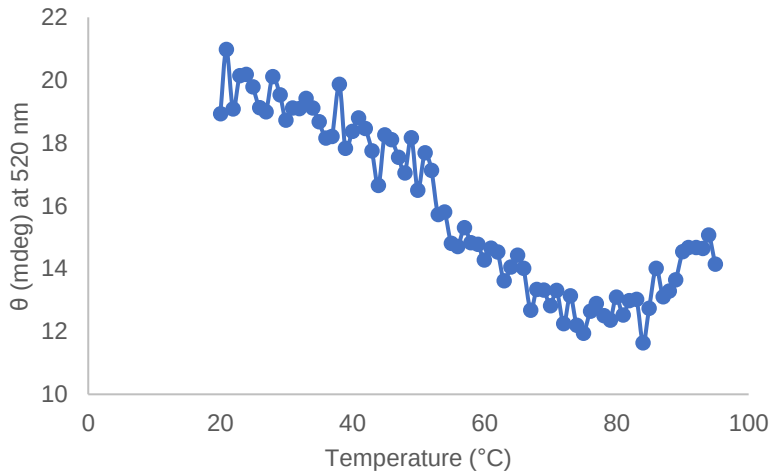

Figure 3.30 CD signal monitored at λ_{max} for 300 μM β-D-fuc (**10**) in water at various temperatures

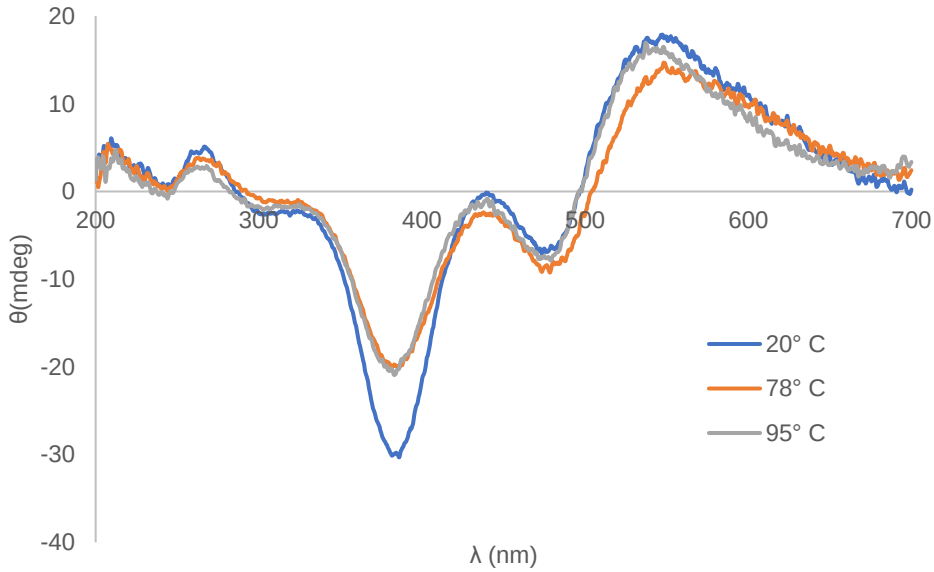

Figure 3.31 CD spectra of 300 μM β-D-fuc (**10**) in water at various temperatures

3.7 Conclusion and future work

In this chapter various aspects affecting Yariv reagent-AGP binding were studied. It was found that besides β-D-sugars the presence of right-handed Yariv reagent aggregates with three arms is a requirement for AGP binding ability. Further, strength of the right-handed aggregation (i.e. CD signal with positive couplets) is proportional to the AGP binding ability. The Yariv reagent aggregation was also studied in more detail. First, the ability of two different Yariv reagents to form a co-polymer and undergo chiral amplification via soldiers and sergeant phenomenon was studied. No evidence was found for formation of co-polymers in the case of Yariv reagents with

opposite helicity preference (**5** and **1**). Evidence consistent with very weak soldiers and sergeant phenomenon and therefore formation of co-polymers was seen when **1** and **3** or **10** were mixed. However, chiral amplification only led to increase in AGP binding ability in the case of the mixture between **1** and **3**. The thermodynamic parameters of Yariv reagent aggregation is another important piece of information that needs to be obtained. This would require finding conditions that allow complete disaggregation so the supramolecular polymerization mechanism of the Yariv reagents can be deciphered. Obtaining the thermodynamic parameters could allow determination of the polymer length required for Yariv reagent-AGP binding. Here, we used variable temperature experiments in a variety of conditions, but none of these showed complete disaggregation. However, some experimental conditions such as 75/25 water/DMSO mixture as solvent seemed promising and less concentrated solutions or more higher proportions of DMSO could potentially be utilized in future experiments to obtain complete disaggregation.

Supplemental Information

General Protocols and CD spectroscopy: Refer to chapter 2 SI for general and CD spectroscopy protocols. For variable temperature experiments, the CD signal was recorded at the wavelength shown, upon varying from 20-95° C at 4° C per min and 76 data points were collected.

UV/vis spectroscopy: UV/vis spectroscopy measurements were acquired using an Agilent 8453 UV/vis spectroscopy system in a 5 mm cuvette at room temperature. Background correction was made using a purified water standard or DMSO depending on which solvent was used for the sample.

Gel Assay Representative protcol: A solution of 0.15 M NaCl (10 mL) was added to 0.10 g agarose, followed 0.1 ml of 1.04 mM solution of Yariv reagent. The mixture was heated until boiling (~30 secs) in the microwave. Immediately after, 0.02% w/v NaN_3 (0.1 mL) was added to

the solution and mixed gently. 4 mL of this solution was quickly dispersed into a glass petri dish using a pipet. Once the solution was added to each dish, a custom-made well-mold with 13 pins of 1.5 mm diameter was inserted into the dish to create the wells in which gum arabic (GA) solution could be added into the gel. The well molds were removed after the gels set for 10 minutes, leaving a gel with 13 wells that could be used to house GA. GA was the inserted into each well using a 10 µL Hamilton Microliter™ PGC syringe; 1 µl of GA solution was added into each well. The gels were placed on a platform in a large basin filled with water and covered with foil, to create a moist environment that would prevent the gels from drying out overnight. The gels were left undisturbed for approximately 16 hours before imaging the next day.

Reverse Gel Assay Optimized Protocol: To create the gel mixture, a freshly prepared gum arabic solution (of appropriate concentration) is added to an Erlenmeyer flask. 10 mL of gel mixture per gel assay is prepared, however only 4 mL is required for each gel, the extra solution prevents formation of air bubbles while transferring the solution using pipette later. To the gum arabic solution, NaCl is added to obtain a 0.15 M NaCl solution. Agarose is then added to the gel mixture (0.01 g per 1 mL of gel mixture). A watch glass is placed on top of the Erlenmeyer flask (to prevent evaporation), following which the Erlenmeyer flask is microwaved until the contents are boiling (~10 seconds for a 10 mL mixture). Immediately after, 0.02% w/v NaN_3 (0.01 mL per 1 mL of gel mixture) was added to the flask. The solution is then dispensed into petri dishes using a p1000 pipet (4 mL of gel mixture for each gel). Once the solution was added to each dish, a custom-made well-mold was inserted into each dish to create the wells in which Yariv reagents are to be added. The well molds were removed after the gels set for 10 minutes, leaving a gel with 13 wells that could be used to house the Yariv reagent. The appropriate Yariv reagent was then inserted into each well using a 10 µL Hamilton Microliter™ PGC syringe; 1 µl of 1.04 mM Yariv reagent solution was added into each well. The gels were placed on a platform in a large basin filled with water and covered with foil, to create a moist environment that would prevent the gels

from drying out overnight. The gels were left for approximately 16 hours before imaging the next day.

Synthesis of mono azo β-D-glucosyl Yariv reagent (**11)**: 2,3,4,6-Tetraacetyl-p-aminophenyl-β-D-glucopyranoside (1.2 g, 1.8 mmol) was dissolved in glacial acetic acid (20 ml) and cooled to 0 °C. Hydrochloric acid (12.1 M, 0.7 ml) was added, followed by 320 mg of $NaNO_2$ dissolved in 0.5 mL of cold water and the solution was stirred for 70 min. A cold aqueous solution of phloroglucinol (3.4 g, 10 eq) was prepared in 250 mL water. The diazo compound was then rapidly added to the phloroglucinol, with vigorous stirring. Stirring was continued for 10 min, at which point potassium iodide (0.68 g) was added, and the reaction was stirred for an additional 10 minutes. The reaction mixture was diluted with dichloromethane (200 ml) and washed with water (40 ml). The aqueous layer was re-extracted with dichloromethane (40 ml). The combined organic layers were washed once with saturated sodium bicarbonate, and once with brine. The organic layer was dried (magnesium sulfate) and filtered. TLC showed 2 major spots (60-40 EtOAc/Hex). Column chromatography (60-40 EtOAc/Hex) was used to isolate product as a red powder (Rf=0.49,0.84 g, 50%).

^{1}H NMR (600 MHz, DMSO-d_6) δ 12.02 (s, 2H), 10.49 (s, 1H), 7.93 (d, *J* = 9.0 Hz, 2H), 7.11 (d, *J* = 9.1 Hz, 2H), 5.84 (s, 2H), 5.70 (d, *J* = 7.9 Hz, 1H), 5.43 (t, *J* = 9.6 Hz, 1H), 5.10 (dd, *J* = 9.8, 8.0 Hz, 1H), 5.03 (t, *J* = 9.7 Hz, 1H), 4.34 – 4.29 (m, 1H), 4.22 (dd, *J* = 12.3, 5.6 Hz, 1H), 4.10 (dd, *J* = 12.3, 2.4 Hz, 1H), 2.06 – 1.98 (12H)

^{13}C NMR (151 MHz, DMSO) δ 170.48, 170.09, 169.81, 169.62, 165.23, 158.52, 157.61, 146.11, 123.56, 122.89, 117.37, 97.32, 95.39, 72.43, 71.42, 71.17, 68.51, 62.12, 21.00, 20.89, 20.86, 20.79.

500 mg of above product was dissolved in methanol (10 mL). Sodium (80 mg, 4 eq) was added and the solution was stirred at room temperature. The reaction mixture was monitored by TLC (5:1 Dichloromethane/methanol). The solution was stirred for 2 hours, at which TLC showed full conversion. The solution was diluted with methanol (60 mL) and neutralized with Amberlite™ IR120 ion exchange resin (monitored by pH paper). The mixture was filtered and washed with methanol. Concentration in vacuo provided product as a red crystalline substance **11** (0.29 g, 82%)

^{1}H NMR (600 MHz, DMSO-d_6) δ 12.03 (Broad s, 1H, Core -OH next to unsubstituted carbons), 7.84 (d, *J* = 8.6 Hz, 2H, ArH ortho to azo), 7.13 (d, *J* = 8.6 Hz, 2H, ArH ortho to sugar), 5.75 (s, 2H, Core-ArH), 5.35 (s, 1H, 2-OH), 5.10 (s, 1H, 3-OH), 5.04 (s, 1H, 4-OH), 4.95 (d, *J* = 7.4 Hz, 1H, H1), 4.6 (s, 1H, 6-OH), 3.7 (d, *J* = 11.7 Hz, 1H, H6), 3.48 (dd, *J* = 5.8 Hz,11.9 Hz, 1H, H6), 3.42 – 3.17 (m, 4H, H5, H4, H3 and H2)

^{13}C NMR (151 MHz, DMSO-d_6) δ 167.00 (Core Ar C-OH, 2C), 158.5(Core C-OH, 1C), 157.8 (Ar, C-O-Sugar), 144.5(Ar C-N), 122.5 (Core C-N), 122.3 (ArC, C−C−N), 117.0 (ArC, C−C−O−sugar), 100.3 (C1), 95.5 (Core ArC-H), 77.1 (C5), 76.6 (C3), 73.2 (C2), 69.7 (C4), 60.7 (C6**)**

HRMS (ESI) m/z: $[M + H]^+$ calcd for $C_{18}H_{20}N_2O_9$ 409.1247; found 409.1258

Synthesis of phenol Yariv reagent (**12)**: A solution of cold freshly prepared 2.4 M HCl (3.5 mL, 2.5 eq) was added to 4-aminophenyl (0.37 g, 3.4 mmol, 1 eq) in a 100 mL round bottom flask. This solution was cooled in an ice bath while stirring. $NaNO_2$ (0.29 mg, 4.2 mmol, 1.2 eq) was dissolved in 0.7 mL of cold water in an Eppendorf tube. The $NaNO_2$ solution was added to a 5 mL syringe with a 4 inch x 22 gauge needle which was clamped above the reaction flask, leading to a gravity assisted dropwise addition. The reaction was stirred at 0 °C for 2.5 hrs.

Phloroglucinol (0.15 g, 1.2 mmol, 0.34 eq) was dissolved in a minimal amount of cold 2 M NaOH (1~2 ml) and added dropwise to the reaction. 2 M NaOH was added until the pH was basic as indicated by pH paper, at which point the ice bath was removed. The pH was maintained at ~9 by addition of 2 M NaOH as necessary. The reaction was stirred for two hours. Cold 100% ethanol (50 mL) was added to the reaction. 1.2 M HCl was added until the solution was neutral as indicated by pH paper. The reaction flask was placed in a freezer for at least 24 hours until a dark precipitate was observed. The precipitate was filtered through a Hirsch funnel to provide the crude Yariv reagent **12** as a black solid clump together. The wet solid was transferred to a pre-weighed scintillation vial and dried in a vacuum oven at 75 °C for few hours and then lyophilized. This crude product (0.11 g, 0.23 mmol), was obtained in 20% yield as a dark powder.

References

1. Kitazawa, K.; Tryfona, T.; Yoshimi, Y.; Hayashi, Y.; Kawauchi, S.; Antonov, L.; Tanaka, H.; Takahashi, T.; Kaneko, S.; Dupree, P.; Tsumuraya, Y.; Kotake, T., beta-galactosyl Yariv reagent binds to the beta-1,3-galactan of arabinogalactan proteins. *Plant Physiol* **2013,** *161* (3), 1117-26.
2. E.F. Woods, G. G. L., M.A. Jermyn, The Self-Association of Glycosyl Phenylazo Dyes (Yariv Antigens). *Aust. J. Chem.* **1978,** *31* (10), 2225-2238.
3. Palmans, A. R.; Meijer, E. W., Amplification of chirality in dynamic supramolecular aggregates. *Angew Chem Int Ed Engl* **2007,** *46* (47), 8948-68.
4. Zhou, L. H.; Weizbauer, R. A.; Singamaneni, S.; Xu, F.; Genin, G. M.; Pickard, B. G., Structures formed by a cell membrane-associated arabinogalactan-protein on graphite or mica alone and with Yariv phenylglycosides. *Ann Bot* **2014,** *114* (6), 1385-97.
5. Jermyn, M. A., Comparative specificity of concanavalin A and the beta lectins. *Aust. J. Plant Physiol.* **1978,** *5* (5), 687-696.
6. Brunsveld, L.; Schenning, A. P. H. J.; Broeren, M. A. C.; Janssen, H. M.; Vekemans, J. A. J. M.; Meijer, E. W., Chiral Amplification in Columns of Self-AssembledN,N′,N″-Tris((S)-3,7-dimethyloctyl)benzene-1,3,5-tricarboxamide in Dilute Solution. *Chemistry Letters* **2000,** *29* (3), 292-293.
7. Smulders, M. M.; Nieuwenhuizen, M. M.; de Greef, T. F.; van der Schoot, P.; Schenning, A. P.; Meijer, E. W., How to distinguish isodesmic from cooperative supramolecular polymerisation. *Chemistry* **2010,** *16* (1), 362-7.

Chapter 4- Identification of the chromophore(s) in the Yariv reagent UV/vis spectra

4.1 Introduction

As stated in chapter 1, the exact chromophore(s) which give rise to the two major transitions in the UV/vis spectra (Figure 4.1) of Yariv reagents are not known. For **1**, in aqueous solution, one of these transitions is observed at 398 nm while the other is centered at 487 nm. In DMSO these transitions are observed at 383 nm and 530 nm. It has previously been suggested in other hydroxy-azo dyes that the two transitions in the UV/vis are associated with the azo and hydrazone tautomeric forms (Figure 4.2a) .[1-4] Alternatively it has also been proposed that the two peaks represent contributions from the monomeric and aggregated forms of the Yariv reagent (Figure 4.2b).[5] In this chapter, each of these hypotheses will be evaluated in the context of Yariv reagents.

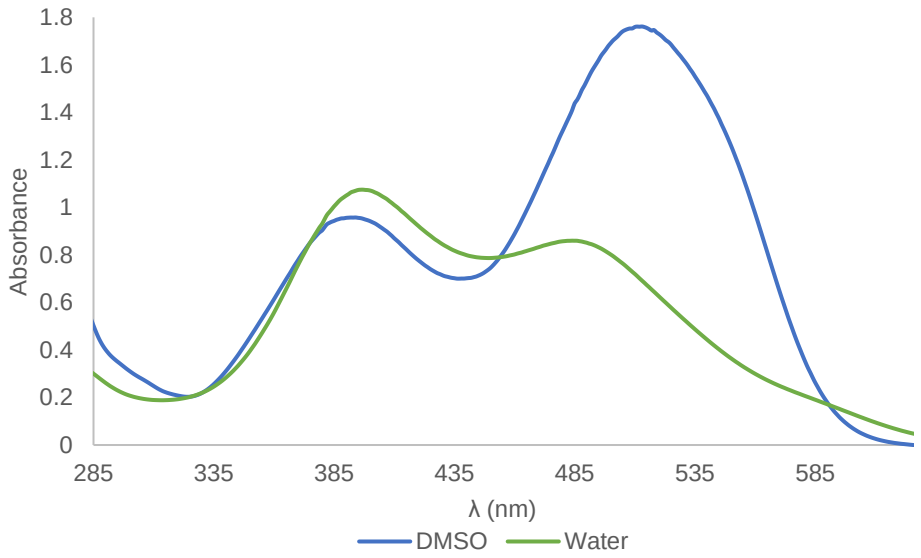

Figure 4.1 UV/vis spectra of **1** in water and DMSO (30 μM)

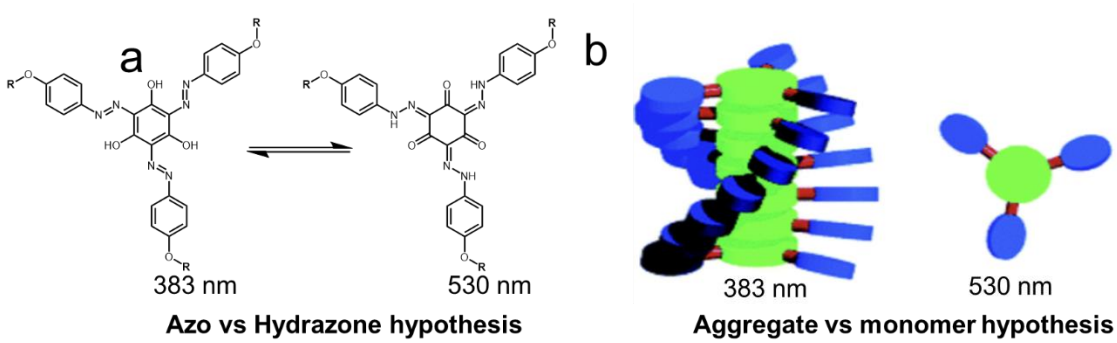

Figure 4.2 The two hypotheses we experimentally examined for the identity of the chromophores that give rise to the two major transitions in the Yariv reagent UV/vis spectra. Fig 4.2b adopted from *J Am Chem Soc* **2002,** *124* (49), 14759-69

4.1.1 Tautomeric hypothesis

The tautomeric hypothesis was based on studies of "locked" tautomeric versions of hydroxyazo dyes.[6] For example, the N methylation of 1-azophenyl-4-napthol (**13**) give rise to **14** (Figure 4.3) which locks it into the hydrazone tautomeric state and O-methylation give rise to **15** (Figure 4.3) which locks it into the azo state. The UV/vis spectrum of 1-azophenyl-4-napthol (**13**), the N-methylated analog (**14**) and the O-methylated analog (**15**) was acquired. While 1-azophenyl-4-napthol (**13**) in benzene had two major UV/vis transitions, both the N-methylated (**14**) and an O-methylated analog (**15**) of 1-azophenyl-4-napthol had only one major transition (Figure 4.3). The peak for the N-methylated analog **14** appeared around the same wavelength as the longer

wavelength peak of 1-azophenyl-4-napthol. The O-methylated variant (**15**)'s UV/vis peak appeared at the same wavelength as the short wavelength peak of 1-azophenyl-4-napthol. The shorter wavelength peak in the UV/vis of **13** was thus assigned to the azo tautomer and the longer wavelength peak was assigned to the hydrazone tautomer.

For 1-azophenyl-4-napthol (**13**), change in solvents gave rise to either a major peak at longer wavelengths or a major peak at shorter wavelengths which corresponded with changes in carbon spectra.[3, 7] For example, in acetone one major transtion at 400 nm and a small shoulder peak at around 460 nm is seen (Figure 4.4). The ^{13}C shift for the C-OH/C=O carbon in acetone was found to be 158 ppm, which corresponds more to *C*-OH. In chloroform the major transition is at 460 nm with a shoulder at 400 nm and the ^{13}C shift for the C-OH/C=O carbon was found to be 173 ppm which corresponds more to a *C*=O. These results support the idea that the peak at longer wavelengths correspond to hydrazone tautomer and the short wavelength peak corresponds to the azo tautomer.

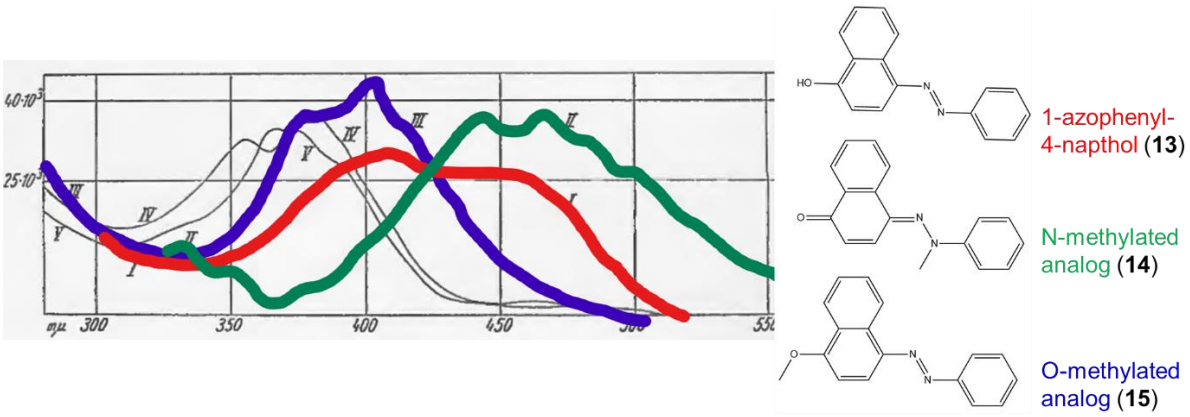

Figure 4.3 The UV/vis spectra (in benzene) of 1-azophenyl 4-napthol **(13)**, the N-methylated analog of **13** (**14)**, and the O-methylated analog of **13** (**15)**. Figure adopted from *Justus Liebig's Annalen der Chemie* **1935,** *516* (1), 143-155

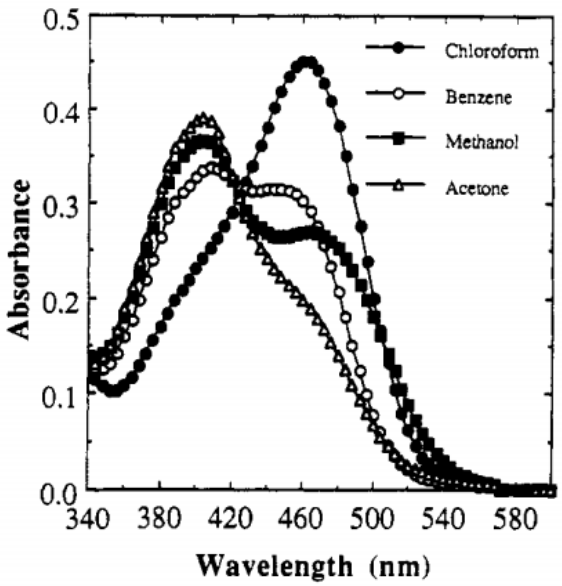

Figure 4.4 The UV/vis spectra of **13** in various solvents. Figure taken from *The Journal of Physical Chemistry* **2002,** *95* (20), 7863-7867

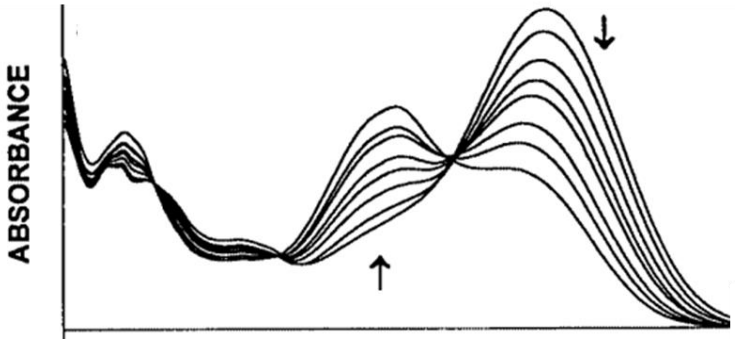

Figure 4.5 Absorption spectra of 1-azophenyl-4-naphthol (**13**) in different water/ethanol compositions (arrows show the decrease of water contents). Figure taken from *Chemical Society Reviews* **2000,** *29* (3), 217-227

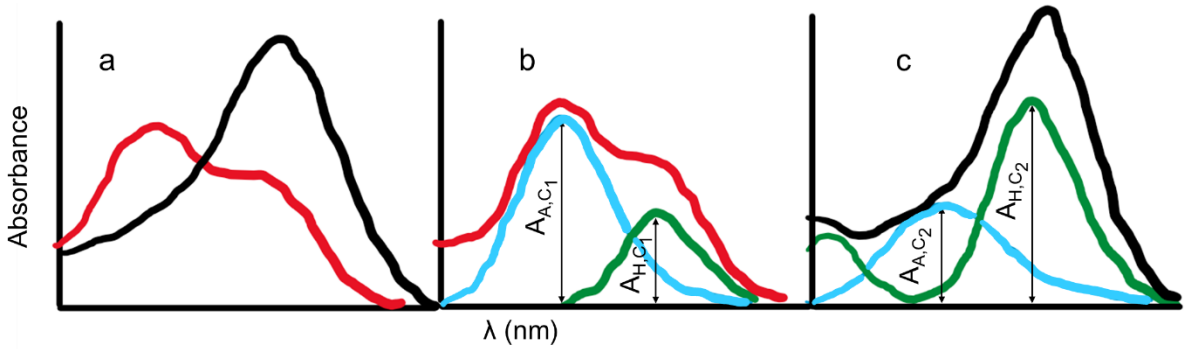

Figure 4.6 a) An imaginary set of UV/vis spectra for a hydroxyazo dye in condition 1 (Red) and condition 2 (Black). Deconvolution of the UV/vis spectra into 2 gaussian curves representing the individual contributions of azo (blue) and hydrazone (green) tautomers in **b)** condition 1 and **c)** condition 2. See **Equation 4.1**

In many cases, so called "semi-quantitative" methods have been applied to evaluate the tautomeric constant K_T (concentration of hydrazone divided by concentration of the azo tautomer in a given solution) (equation 1) to calculate the amount of azo and hydrazone tautomer present. One such method is the deconvolution of UV/vis spectra.[8] In this method, conditions such as either temperature or solvent are varied and the UV/vis spectrum in each condition is obtained. If the ratio of the intensity of the two peaks in the UV/vis spectra changes with the conditions and an isosbestic point is obtained then this method is applicable, an example of such a set of spectra is shown (Figure 4.5). It is assumed that the extinction coefficient for the two tautomers do not change with conditions and that the overall UV/vis spectra is a result of the sum of individual UV/vis spectra of the tautomers represented as gaussian curves (Figure 4.6). First, deconvolution of spectra at two different conditions is performed using either a software that can do this or manually through excel to obtain the "individual contributions" from each tautomer towards the overall UV/vis spectra. Next, the tautomeric constant in the condition of interest can be evaluated using equation 4.1. The azo to hydrazone equilibrium constant K_T was evaluated for 1-azophenyl-2-napthol (**16**) (Scheme 4.1) in chloroform (1.46) and dichloromethane (0.838) using the deconvolution method.[9]

$$K_{T,C1} = [\text{Hydrazone}]/[\text{Azo}] = (-\Delta A_A/\Delta A_H)*(A_{H,C1}/A_{A,C1}) - \textbf{Equation 4.1}$$

Where $K_{T,C1}$ is the ratio of concentration of the hydrazone and azo tautomers in condition 1 (see Figure 4.5).$A_{H,C1}$ and $A_{A,C1}$ are the individual absorbance of the hydrazone and azo tautomer respectively in condition 1, obtained through the deconvolution. Also $\Delta A_A = A_{A,C1}-A_{A,C2}$ and $\Delta A_H = A_{H,C1}-A_{H,C2}$

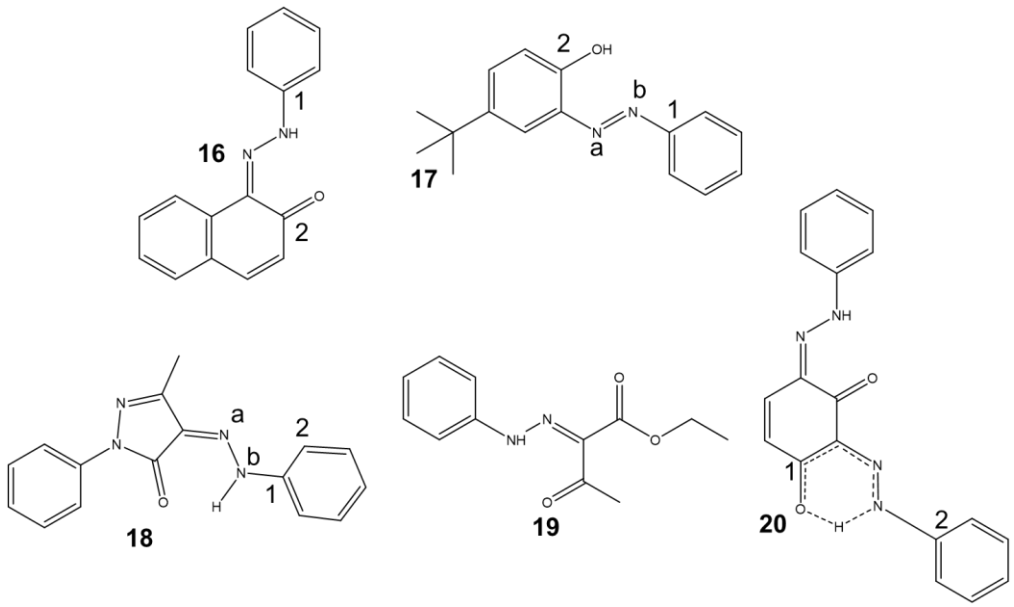

Scheme 4.1 1-azophenyl-2-napthol **16**; Pure azo model **17**; Pure hydrazone model **18**; Pure hydrazone model **19**; An example of an hydroxyazo dye studied using DIS **20**

Another "semi-quantitative" methodology to evaluate K_T is using NMR techniques such as ^{15}N and ^{13}C NMR.[9] Such techniques require the use of "pure" tautomer models, assigned based on their UV/vis spectra. The pure azo model (**17**), and two of the pure hydrazone models (**18**) and (**19**) utilized to evaluate the tautomeric equilibrium of 1-azophenyl-2-napthol (**16**) are shown (Scheme 4.1). Various types of NMR signals such as ^{13}C chemical shifts of the C=O/C-OH carbon, ^{15}N chemical shifts and ^{1}J (^{15}N,^{1}H) for the pure azo model, pure hydrazone model and hydroxyazo dye of interest are obtained. Linear regression is utilized to calculate the K_T. For example, in $CDCl_3$ the ^{1}J (^{15}N,^{1}H) of the pure azo model (**17**) was calculated to be 0[10], the ^{1}J (^{15}N,^{1}H) of the pure hydrazone model (**19**) was calculated to be 96 Hz[11] and the ^{1}J (^{15}N,^{1}H) of 1-azophenyl-2-napthol (**16**) was calculated to be 68 Hz[10] at 290 K. The % hydrazone for 1-azophenyl-2-napthol (**16**) was calculated by assuming that ^{1}J (^{15}N,^{1}H) of hydroxyazo dyes changes linearly with % hydrazone. Therefore % hydrazone for **16** was found to be (68/96)*100 = 71% and thus K_T would be 2.42.[9]

^{15}N NMR can also be applied to calculate K_T. It is assumed that chemical shifts change linearly with % tautomer. % Hydrazone can be calculated using equation 4.2. For example, **17** was utilized as a pure azo model and **18** was utilized as pure hydrazone model to determine % hydrazone in **16** using equation 4.2.[9] When chemical shift of nitrogen "a" in $CDCl_3$ was used for reference, % hydrazone was found to be (22.8-126.9/-17.3-126.9)*100 = 72% therefore K_T was 2.57. When chemical shift of nitrogen "b" in $CDCl_3$was used for reference, % hydrazone was found to be (-126.2-69.4/-205.2-69.4)*100 = 71% therefore K_T was 2.47. Using ^{13}C NMR (assuming 147 ppm for pure azo and 180 ppm for pure hydrazone) gave a K_T of 2.59 in $CDCl_3$. ^{13}C NMR in CD_2Cl_2 provided a K_T of 2.69. The K_T obtained in $CDCl_3$ through the various NMR techniques are very similar and self-consistent (2.57, 2.47 and 2.59). However, when the K_T values from the UV/vis deconvolution experiment are compared to the NMR experiment values there are some large differences. For example, NMR in CD_2Cl_2 suggests that for 1-azophenyl-2-napthol (**16**), hydrazone tautomer is prevalent whereas the UV/vis method suggests that azo tautomer is dominant. These inconsistencies in data suggests that UV/vis assignment of the two peaks as azo and hydrazone is not necessarily correct in all cases.

$$\%\text{Hydrazone} = ((\delta(^{15}N) - \delta(^{15}N)_A)/(\delta(^{15}N)_H - \delta(^{15}N)_A))*100 \quad \textbf{Equation 4.2}$$

where $\delta(^{15}N)$ is chemical shift of the nitrogen of interest in the molecule of interest, $\delta(^{15}N)_A$ is the chemical shift of the corresponding nitrogen in the pure azo model and $\delta(^{15}N)_H$ is the chemical shift of the corresponding nitrogen in the pure hydrazone model

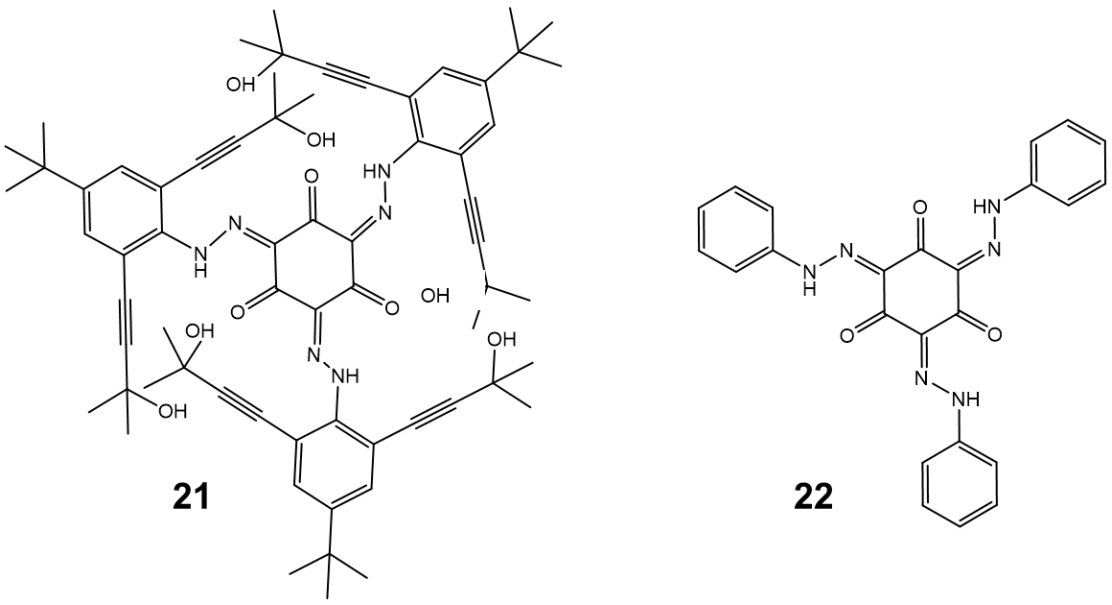

Scheme 4.2 Examples of two tris hydroxyazo dyes whose tautomeric state has been studied and reported in literature

Yariv reagents are classified as tris-hydroxyazo dyes.[12] In several cases, only evidence for presence of the hydrazone tautomer has been found in tris-hydroxyazo dyes. For example, it was shown that the bond lengths obtained from the crystal structure for the tris-hydroxyazo dye **21** (Scheme 4.2) matched those for the DFT calculated bond lengths of the hydrazone tautomer but not the azo tautomer.[12] Also, both the proton and carbon NMR spectra of this molecule in DMSO-d_6 showed the presence of three minor peaks, all with the same integrations values (Figure 4.7). The three minor peaks in the ^{1}H NMR spectrum are associated with the N*H*/O*H* proton while the minor peaks in the ^{13}C NMR spectrum are associated with the *C*=O/*C*-OH carbon. These minor peaks suggests three inequivalent N*H*/O*H* protons and *C*=O/*C*-OH carbons as a result the presence of the C_s conformer of hydroxyazo dyes (Figure 4.8). The fact that the peaks corresponding to both conformers are present suggests lack of fast equilibrium between the two conformers. The authors claimed that the slow equilibrium between C_{3h} and C_s conformations would only be possible in the hydrazone tautomer and not the azo tautomer.[12]

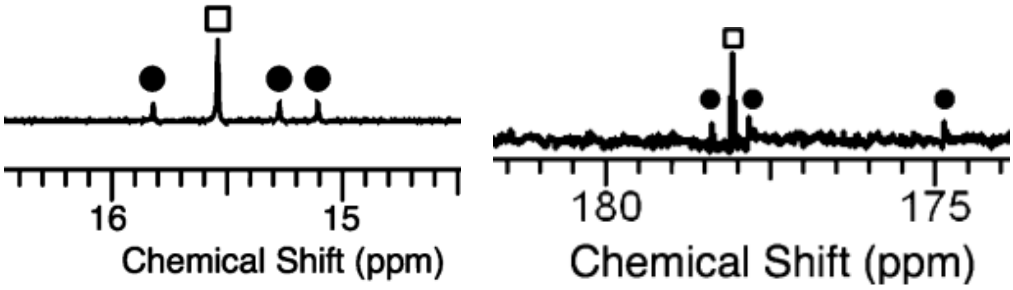

Figure 4.7 Partial ^{1}H (left) and ^{13}C NMR (right) spectrum of **21** in DMSO-d_6. Figure adopted from *J Am Chem Soc* **2010,** *132* (34), 12133-44

^{15}N NMR of another tris-hydroxyazo dye **22** (Scheme 4.2) has shown that the two nitrogens vary dramatically in chemical shift (8 ppm (=N) and -180 ppm (N-H) in solid state NMR and -10 ppm (=N) and -234 ppm (N-H) in $CDCl_3$.[13,14] The dramatic difference in chemical shift of the two nitrogens indicate the hydrazone tautomer is dominant. In azo tautomers the chemical shifts of the chemical shifts of the two nitrogens generally differ by ~50 ppm in $CDCl_3$.[9] Moreover, N-H HSQC also showed a strong N-H coupling in this molecule. Computational calculations have also shown that the hydrazone tautomer is more energetically stable. Finally, all reported tris-hydroxyazo dyes have a ^{13}C chemical shift for the *C*=O/*C*-OH of above 175 ppm which is more indicative of a C=O rather (hydrazone) than a C-OH (azo).[12,13-15] Therefore, while there is ample evidence for the presence of hydrazone tautomer in tris-hydroxyazo dyes, there is no evidence for the presence of significant amounts of azo tautomer. Since the azo-hydrazone hypothesis would require the presence of substantial amount of both tautomers, this hypothesis for the identity of the chromophores is unlikely to be true for the Yariv reagents. In this chapter we present results that show that in DMSO, we only see presence of the hydrazone tautomer for the Yariv reagents as well.

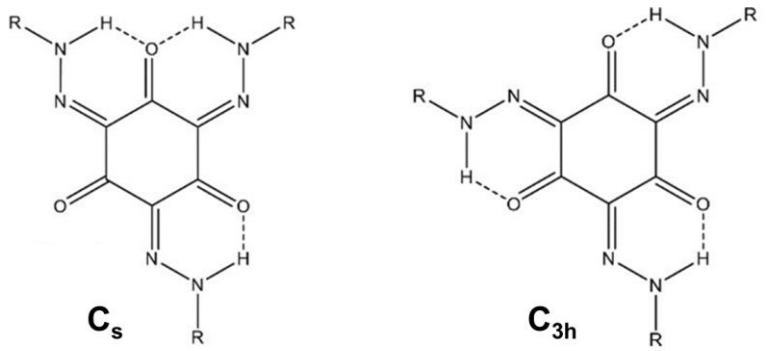

Figure 4.8 The two conformations in C_3 symmetric hydrazone dyes, R=Phenyl

4.1.2 Monomer-Aggregate Hypothesis

Alternatively, it has also been suggested by Paulsen et al that the two peaks in the Yariv reagent UV/vis spectra arise from the aggregated (short wavelength peak) and monomeric forms (long wavelength peak) of the Yariv reagents.[5] Since some other C_3 symmetric molecules with hydrophobic cores and hydrophilic peripheral moieties form H-aggregates, the Yariv reagent may also form H-aggregates.[16-18] The UV/vis spectra of H-aggregates show a blue shift compared to monomers.[19] A similar phenomenon could be happening for Yariv reagents, where in aggregating conditions such as water, the short-wavelength peak is of higher intensity and the long wavelength peak intensity is of lower intensity (Figure 4.1). Meanwhile, in disaggregating conditions the such as in DMSO, the short-wavelength peak is of lower intensity and the long wavelength peak intensity is of higher intensity. However, if the aggregate-monomer hypothesis is true, it would suggest that aggregates are present in significant amount in what we previously considered non-aggregating conditions such as DMSO, since the short wavelength peak has a significantly strong absorbance value in DMSO. Although no CD signal is seen in DMSO even at very high concentrations (Figure 1.13), this lack of CD signal could potentially be due to presence of either non-helical aggregates in DMSO or an equal mixture of left and right handed aggregates. This phenomenon where lack of optical activity is seen in some solvents even with presence of aggregates but presence of CD signal in other solvents has previously been observed in other supramolecular systems.[20] In this chapter, the validity of this aggregate-monomer

hypothesis was also evaluated. Here, we show that we do not see the presence of significant amount of aggregates in DMSO. Finally, alternatives to the azo-hydrazone and aggregate-monomer hypothesis are discussed.

4.2 Analysis of tautomeric state of 1 in DMSO

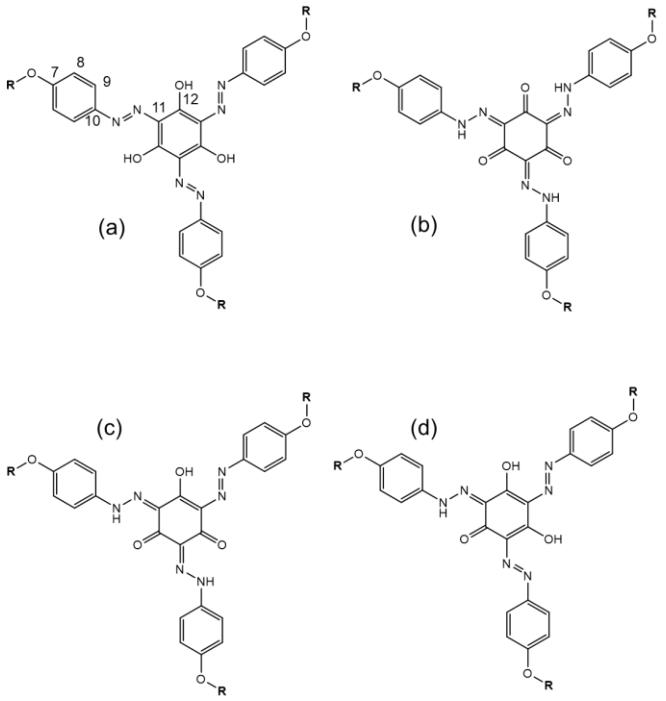

Scheme 4.3 The tautomeric forms of the tris azo Yariv reagents

To evaluate whether the azo-hydrazone hypothesis for the UV/vis spectra is possible, we wanted to determine the tautomeric composition of the Yariv reagent. The Yariv reagents can exist in various tautomeric forms (Scheme 4.3). For example, Yariv reagents could be completely in the azo state (Scheme 4.3a) or hydrazone state (Scheme 4.3b). Yariv reagents could also be in a mixture of azo and hydrazone states (Scheme 4.3c and d). The chromophore(s) could be anyone or a combination of these different tautomeric states. Our studies were carried out in DMSO but it must be noted that the identity of the chromophore(s) is more pertinent in water because the Yariv-AGP binding, and Yariv reagent aggregation takes places in water. However, evaluating the tautomeric state in water by looking at ^{13}C NMR chemical shifts is impossible due to aggregation related peak broadening.

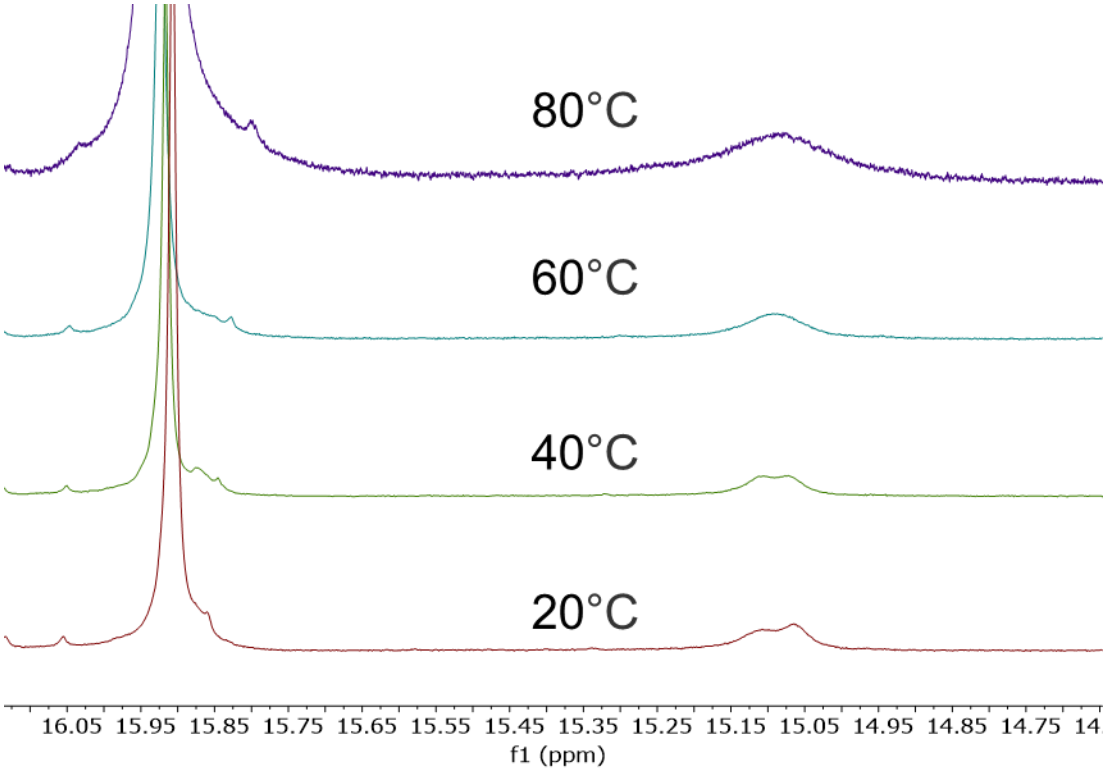

Figure 4.9 Partial ^{1}H NMR of **1** in DMSO-d_6 at various temperatures

First, the ^{1}H NMR of **1** in DMSO-d_6 was examined. A chemical shift of 15.9 ppm is assigned to the N*H*/O*H* proton by analogy to **21** and **22**. At 15.88 ppm, 15.11 ppm and 15.06 ppm minor peaks in the ^{1}H NMR can be seen (Figure 4.8). These are very similar to the minor peaks (Figure 4.7) which have previously been assigned to N*H*/O*H* peaks of the minor C_s conformer (Figure 4.8). The minor peaks at 15.11 and 15.06 are resolved well enough to integrate individually and each have an integration of 0.22 relative to the 3 anomeric protons. An equal value of integration for these protons is consistent with the idea that they are both N*H*/O*H* protons. The total sum of the integrations of the various N*H*/O*H* peaks adds up to 2.86 which is very close to the expected value of 3. This clearly suggests that the minor peaks arise from the C_s conformer (Figure 4.8). Further, increasing the temperature to 80 °C does not cause the minor peaks to coalesce (Figure 4.9). The integrations of the peaks also do not change upon increasing temperature. The lack of

coalescence suggests that the barrier to rotation between the C_s and C_{3H} conformations is high. It has previously been shown that the mechanism of switching between *E* and *Z* forms in hydrazone based rotary switches is through tautomerization, i.e. rotation does not occur in the hydrazone form, but occurs when tautomerization to azo form occurs.[21] A lack of free rotation as shown by our variable temperature data is therefore consistent with lack of the azo form.

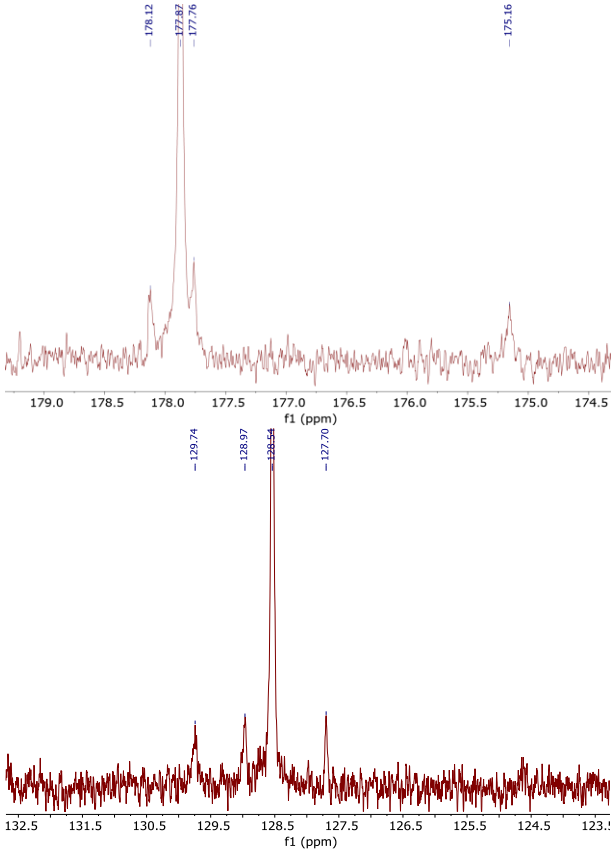

Figure 4.10 Partial ^{13}C NMR spectra of **1** in DMSO-d_6

Next, the ^{13}C NMR spectrum was evaluated. The ^{13}C NMR spectrum was very similar to the other tris hydroxyazo dyes such as **21** and **22,** which have been shown to be in the hydrazone tautomeric state. The most down field carbon with a chemical shift of 177.9 ppm (Figure 4.10) especially stands out, because in **21** and **22**, the corresponding peak also appears at 178 ppm and was assigned to C12 the *C*=O carbon (Scheme 4.3).[12, 14] Hydroxyazo dyes in the azo tautomeric form such as **17** (Scheme 4.1) show a chemical shift of 150 ppm for the *C*-OH/*C*=O carbon. The minor peaks are also present in the ^{13}C NMR spectrum. Minor peaks can be seen at 178.1, 177.8

and 175.2 ppm corresponding to the *C*=O/*C*-OH carbons of the C_s form (Figure 4.10). For **22**, the peak at 128.7 was assigned to the C11, the *C*=N carbon (Scheme 4.3). **1** has a corresponding peak at 128.5 which can thus also be assigned to the *C*=N/*C*-N carbon. Further, minor peaks associated with the *C*=N/*C*-N carbon of the C_s form can also be seen at 129.7, 129.0 and 127.7 ppm (Figure 4.10). The existence of the minor peaks in ^{13}C NMR spectrum is also consistent with slow exchange between the minor C_s conformation and regular C_{3H} conformation indicative of the hydrazone tautomer.

The HMBC NMR spectrum of 1 was also acquired. The presence of cross peaks in HMBC NMR indicate long range coupling between carbon and hydrogen atoms. Therefore, hydrogens that are 2 or 3 bonds away from a carbon show a cross peak to that carbon. Looking at the HMBC NMR for **1** (Figure 4.11), the hydrogen at 15.9 ppm corresponding to the N*H*/O*H* peak shows three cross peaks. These cross peaks are to the aromatic carbon C9 at 117 ppm, the *C*=N/*C*-N carbon C11 at 128 ppm and the C-NH/C-N carbon C10 at 135 ppm (Figure 4.11). The cross peaks to 128 ppm and 117 ppm would be expected for the hydrazone tautomer but not the azo tautomer. Finally, the cross peak to the carbon at 178 ppm (C=O/C-OH) is missing. The presence of a cross peak between the O*H* hydrogen and *C*-OH carbon would be expected if any azo tautomer was present. Overall, these NMR results only indicate the presence of the hydrazone tautomer.

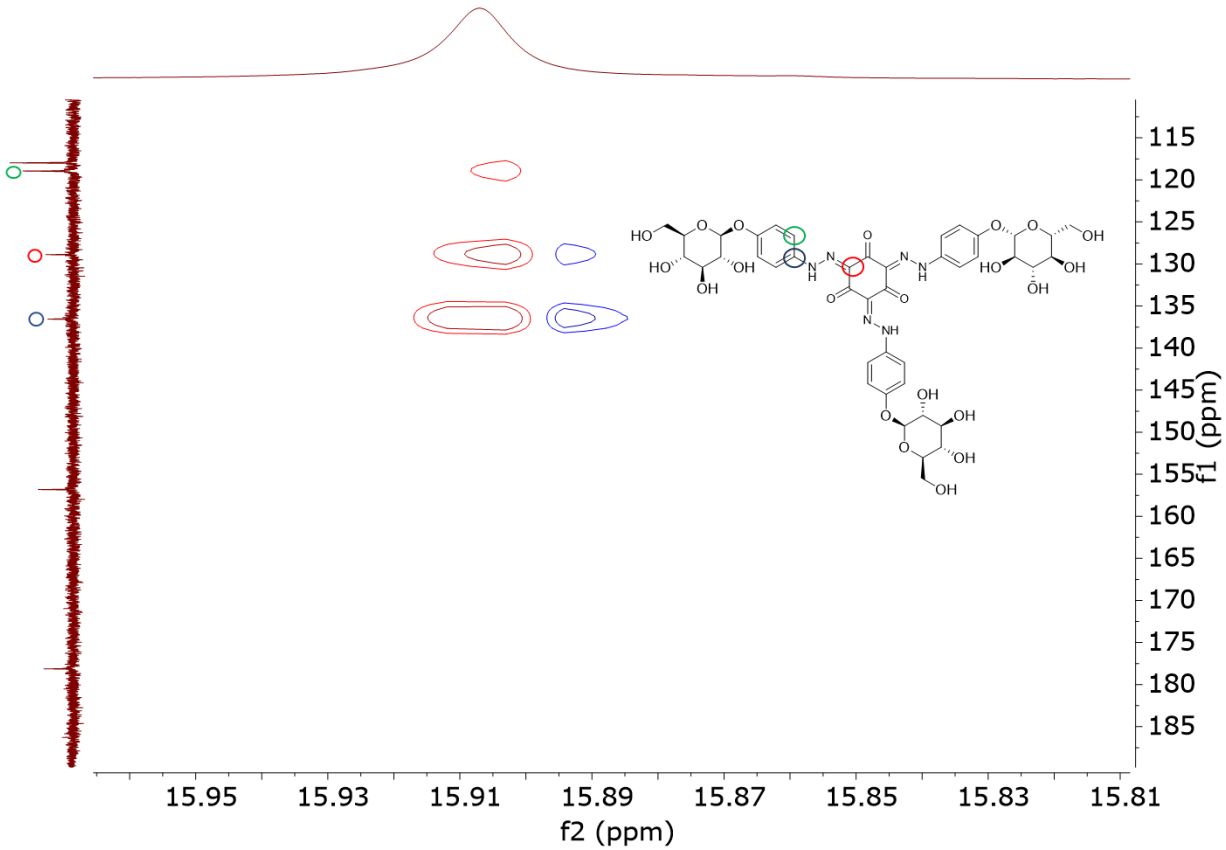

Figure 4.11 Partial HMBC NMR spectra of **1** in DMSO-d_6

Another method utilized to determine the tautomeric state of molecules relies on deuterium isotope effects on ^{13}C chemical shifts. Nuclear magnetic shielding is inversely dependent on bond length. Since the X-H bond lengths (where X is a heteroatom like O or N) are longer than X-D bond lengths due to lower zero-point energy of X-D bonds, substitution of a proton with a deuterium atom results in upfield chemical shifts of neighboring atoms or those next to the neighboring atoms. [22] Carbon atoms two bonds from the deuterium/hydrogen show upfield shifts of 100-115 ppb (β shift) and carbon atoms three bonds away show upfield shifts of 30-60 ppb (γ shift) upon substitution of hydrogen with deuterium. Further, in intramolecularly hydrogen bonded systems, upfield β shifts upto 1000 ppb can occur.[23] This phenomenon of deuterium isotope shifts (DIS) can be utilized to determine tautomeric shifts because the carbon atoms expected to show upfield chemical shifts would depend on which tautomeric state is present in solution. For example, the pure azo model **17** (Scheme 4.1) and pure hydrazone model **18**

(Scheme 4.1) utilized in the semi-quantitative NMR studies show expected results when studied with deuterium isotope shift (DIS) experiments.[24] Upfield shifts are seen in the *C*-O-H carbon C2 in the pure azo model **17** (370 ppb) and *C*-N-H carbon C1 in the pure hydrazone model **18** (140 ppb). A γ shift is also seen for **18** in C2 as expected for a hydrazone tautomer (60 ppb) and a downfield shift is seen in C1 for **17** (-100 ppb) consistent with lack of hydrazone in **17**. However, it is to be noted that in 1-azophenyl-2-napthol (**16**) (Scheme 4.1), upfield shifts were seen for the *C*-NH/*C*-N carbon C1 (130 ppb) but not for *C*=O/*C*-OH carbon C2 (-190 ppb) even though both NMR and UV/Vis deconvolution experiments indicate a significant (20-30%) presence of the azo tautomer. Finally, another hydroxyazo dye **20** (Scheme 4.1) using semi-quantitative methods was showed to contain a significant amount of both azo and hydrazone tautomer (60% Hydrazone and 40% Azo). **20** does show upfield shifts in both the *C*-OH/C=O carbon C1 (30 ppb) and C-NH/C-N carbon C2 (150 ppb). This indicates that the DIS experiment is not always sensitive to the presence of both tautomers but is extremely useful in determining which tautomer is the major tautomeric form.

To confirm the tautomeric state of **1** in DMSO, the DIS experiment was used. An upfield shift is observed in the ^{13}C NMR resonance for a carbon when a nearby heteroatom undergoes deuteration. Therefore, if nitrogen is deuterated as would be expected for the hydrazone tautomer, an upfield chemical shift would be observed in C9 and C10 (Scheme 4.3). However, if the oxygen is deuterated, as would be expected for the azo tautomer, an upfield chemical shift in C12 is expected. To prepare the deuterated NMR sample of **1**, it was dissolved in D_2O, subsequently lyophilized and then dissolved in DMSO-d_6. However, it must pointed out that a ^{1}H NMR for the deuterated sample was not obtained, therefore it cannot be confirmed if deuteration actually took place, however the ^{13}C NMR results are certainly consistent with presence of DIS effects. Upfield shifts were seen in C9 and C10 (Figure 4.12a and 4.14b) as expected for a hydrazone tautomer and no upfield shift was seen for C12 consistent with a hydrazone tautomer (Figure 4.12c).

However, C7 also shows an upfield shift and C11 does not (Table 4.1). C7 is not close to any heteroatom that is deuterated, therefore no shift was expected, whereas C11 is 2 bonds away from both the nitrogen and oxygen which would be deuterated regardless of which tautomer is present and therefore an upfield shift was expected here. The upfield shifts in C7 can be explained by long range DIS effects that are commonly seen in aromatic systems.[24] Downfield shifts are also commonly noticed upon deuteration, therefore lack of any shift in C11 could be due to two opposing effects.[24] Therefore, these results are consistent with the hydrazone tautomer being the dominant tautomer. Each of the carbons attached to sugar-OHs (C2,C3,C4,C6) show β shifts as expected. C1 and C5 also show small upfield shifts consistent with γ shifts. Finally, the aromatic carbon C8 shows a very slight upfield shift (9 ppb). The DIS results combined with other NMR methods suggest it is unlikely that the azo-hydrazone hypothesis could explain the identity of the chromophore(s) that give rise to the peaks we see in the UV/Vis spectra in DMSO because we see no evidence for the presence of the azo tautomer.

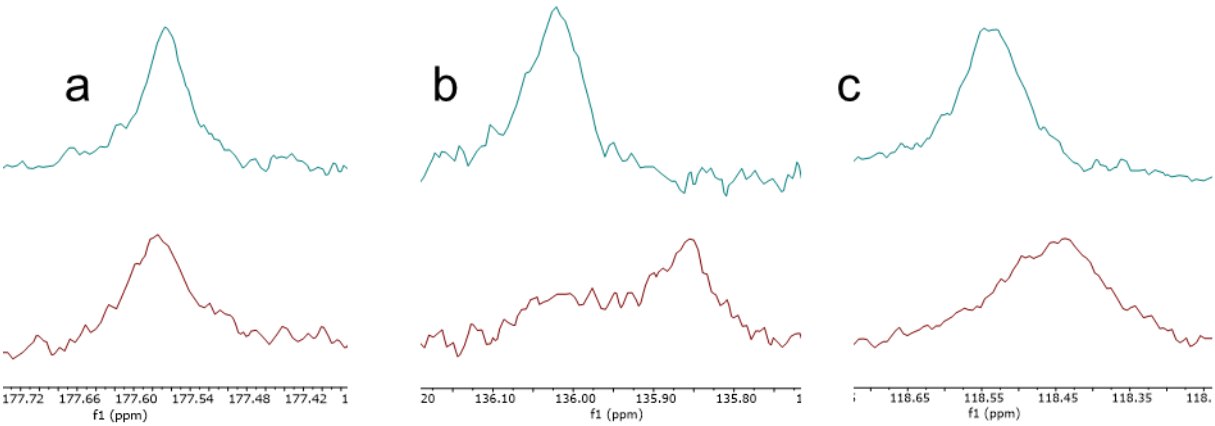

Figure 4.12 Partial ^{13}C NMR of the non-deuterated and deuterated samples of **1** a) C=O/C-OH (C12), b) C-N/C-NH (C10), and c) ArC next to C-NH/N (C9). Top: Regular, Bottom: Deuterated

Table 4.1. Comparison of ^{13}C chemical shift (ppm) in regular vs DIS sample of **1** (in DMSO-d_6)

Carbon	**C1**	**C2**	**C3**	**C4**	**C5**	**C6**	**Ar, C-O-Sugar**	**Ar, C−C−O −sugar**	**Ar, C−C −N**	**Ar C-N**	**core Ar C-N**	**core Ar, C−O**

Carbon Number/Sample	1	2	3	4	5	6	7	8	9	10	11	12
1	100.4976	73.3215	76.6468	69.7697	77.1532	60.7941	156.3748	117.47	118.5436	136.0205	128.2821	177.5662
1-DIS	100.4834	73.1856	76.4686	69.6288	77.1084	60.6638	156.3272	117.4613	118.4421	135.8549	128.3256	177.5744
DIS effect (ppb)	14.2	135.9	178.2	140.9	44.8	130.3	47.6	8.7	101.5	165.6	-43.5	-8.2

4.3 Analysis of tautomeric state of 8 and 11 in DMSO

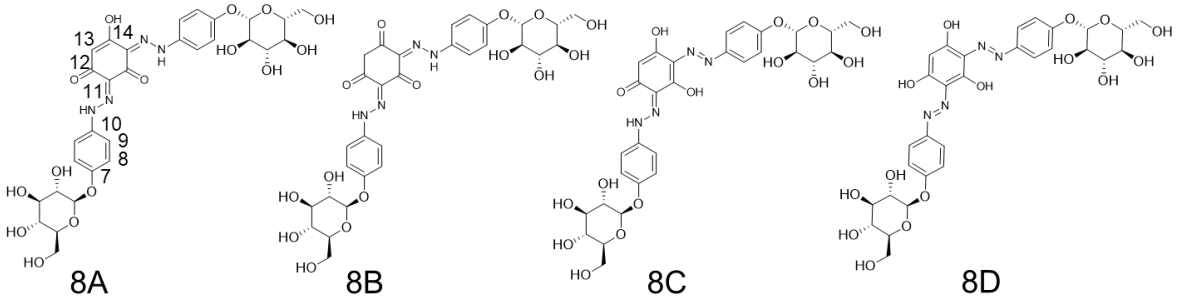

Scheme 4.4 Various tautomeric structures of the bis azo variant **8**

The correlation between tautomeric state and UV/vis spectra was further evaluated by studying Yariv reagent homologs such as the bis (**8**) and the mono azo variant (**11**) (scheme 4.4 and 4.5) of the Yariv reagent **1** in DMSO. Like the tris azo variant **1**, both the mono azo and bis azo homolog's UV/vis spectra in DMSO contain two peaks (Figure 4.13). However, the overlap between the two peaks increases in the order of tris < bis < mono. While in **1**, the two peaks appear at 383 and 530 nm, in **8** the two peaks appear as a shoulder peak at 380 nm and a peak at 450 nm, and finally in **11** the peaks appear at 390 and 420 nm. In the **8** the ratio of the intensity of the peaks are like what we see in **1**, as the peak at the longer wavelength is significantly stronger than the one at the shorter wavelength. However, in the mono azo variant **11** the shorter wavelength peak is slightly more intense than the longer wavelength peak. We decided to evaluate the tautomeric state of the bis and mono analog using the same techniques utilized for

the tris Yariv reagent **1**, if only one tautomer is dominant, it would suggest that the two peaks are unlikely to represent tautomeric states.

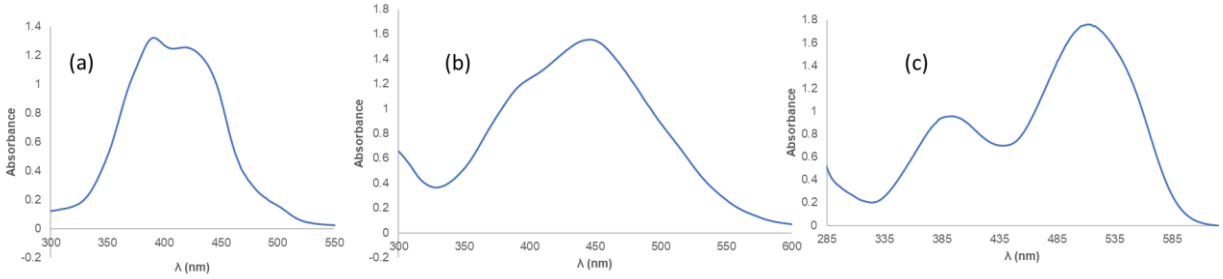

Figure 4.13 The UV/vis spectra in DMSO (all 300 μM) of a) mono azo variant **11** b) bis azo variant **10** c) tris azo variant **1**

The ^{1}H NMR spectrum of the bis azo variant contains a peak at 5.7 ppm corresponding to the hydrogen on the carbon C13. This peak integrates to 1, indicating that the tautomer **8B** is unlikely to a major contributor as this hydrogen in **8B** should integrate to 2 (Scheme 4.4). The ^{13}C NMR spectrum of **8** was also obtained. The ^{13}C NMR spectrum of **8** was very similar to the ^{13}C NMR spectrum of **1** and the assignments could be made via analogy to **1** (Figure 4.14).

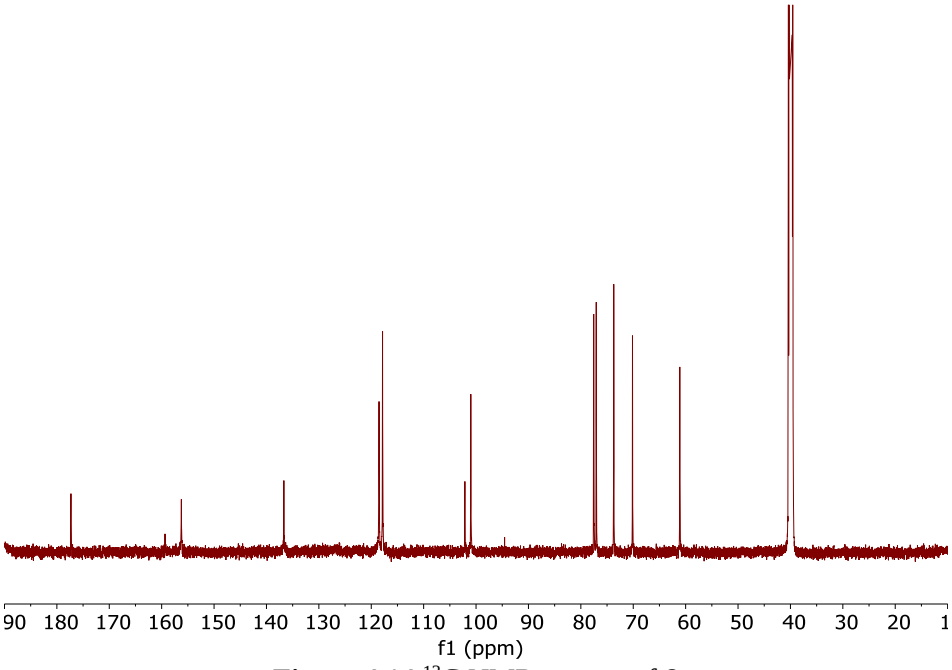

Figure 4.14 ^{13}C NMR spectra of **8**

A few important differences however were the presence of a peak corresponding to the unsubsituted core carbon (C13) in the ^{13}C NMR spectrum of **8** and the absence of the analogous peak at 128 ppm which corresponds to the C=N/C-N carbon (C11) in **1**. It was hypothesized that the absence of the C=N/C-N carbon (C11) was because of this carbon being invovled in some form of equilibrium and therefore the peak corresponding to it could be broadened in ^{13}C NMR spectrum of **8**. A closer look at the ^{13}C NMR spectrum shows the presece of a broad "peak" at 128 ppm which suggests that the broadening hypothesis is true (Figure 4.14). To test this hypothesis, the sample was heated to 80° C and the ^{13}C NMR spectrum was acquired. Upon heating, a sharp peak at 128 appeared, confirming the hypothesis that the peak corresponding to C11 was broadened (Figure 4.15). Further, another broad peak at 175 ppm appeared upon heating, which likely corresponds to another C=O/C-OH core carbon (C14). The fact that both sets of C=O/C-OH carbons (C12 and C14) resonate at a very downfield chemical shift (175 and 178 ppm) suggests that it is unlikely that the tautomer **8D** (Scheme 4.4) is a major contributor.

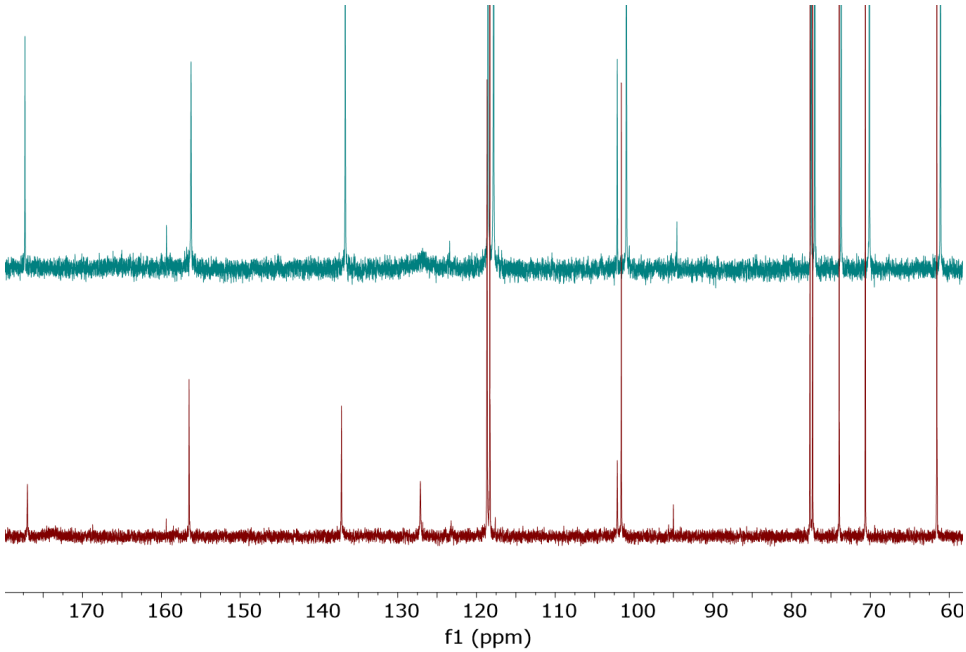

Figure 4.15 ^{13}C NMR spectra of **8** at room temperature (top) and 80° C in DMSO-d_6 (bottom)

Next, the DIS experiment was repeated with the **8**. A sample of **8** was dissolved in D_2O followed by lypohilisation and dissolution in DMSO-d_6. First the ^{1}H NMR of the "DIS sample" was

acquired and compared to the ^{1}H NMR of the regular sample of **8**. Only a 8% reduction in the integration of the NH/OH peak was seen suggesting not very much deutero incorporation (Figure 4.16). However when the ^{13}C NMR spectra of the "DIS sample" of 10 was acquired, upfield shifts in C9 (95 ppm) and C10 (155 ppm) (Figure 4.18a and b) and lack of upfield shifts in C12 were (Figure 4.18c) seen which are consistent with the presence of a hydrazone tautomer. As stated earlier, in other intramolecularly hydrogen bonded systems, sometime upfield shifts upto 1000 ppb can occur. Therefore, the upfields shifts seen in C9 and C10 could still be consistent with upfield shifts due to partial deutaration. An unexpected result is the presence of both an upfield and downfield shift for C13(Figure 4.18d). A summary of the DIS results of 8 is presented in Table 4.2. Overall, the DIS results allow us to determine that tautomers such as **8A** and/or **8C** (scheme 4.4) are likely to be major contributors as signficant presence of hydrazone is detected.

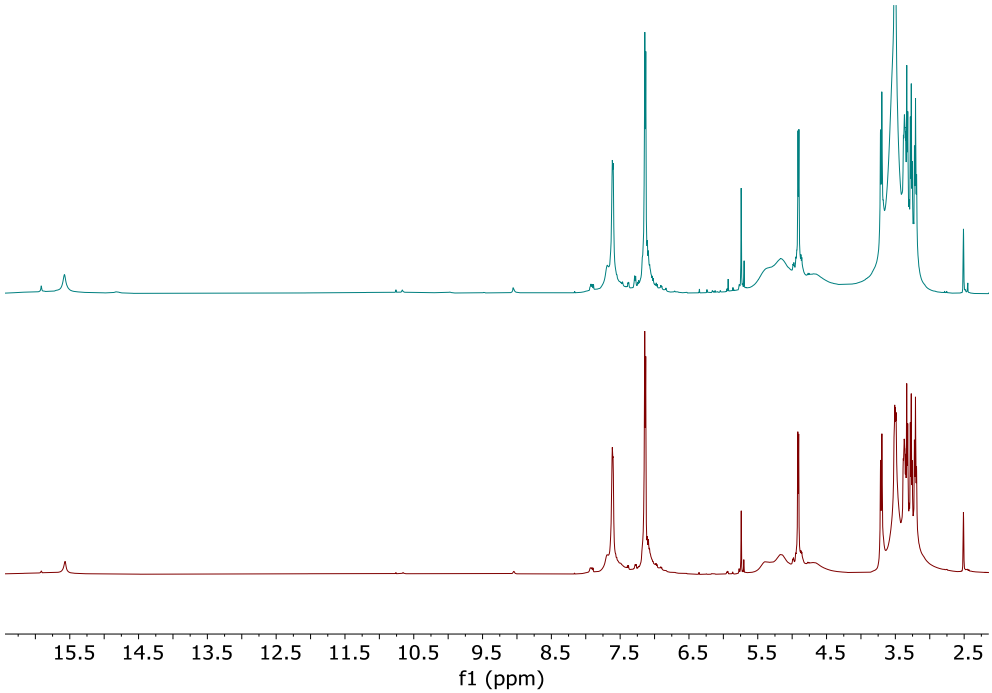

Figure 4.16 Comparison of ^{1}H spectrum of **8** regular (top) vs "DIS" sample (bottom) in DMSO-d_6

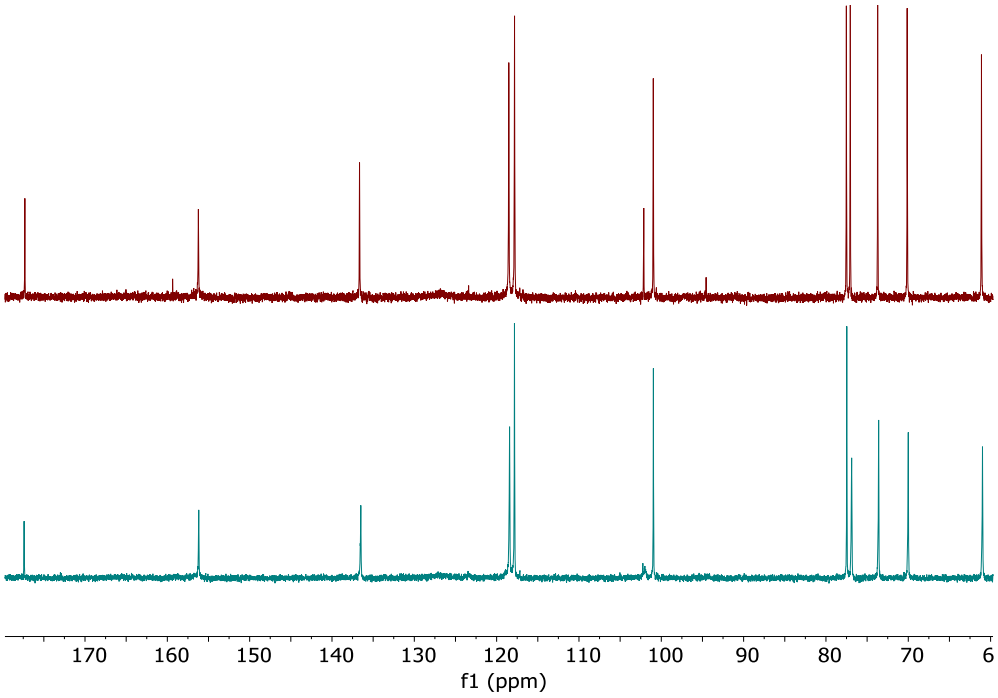

Figure 4.17 Comparison of ^{13}C spectrum of **8** regular (top) vs "DIS" sample (bottom) in DMSO-d_6

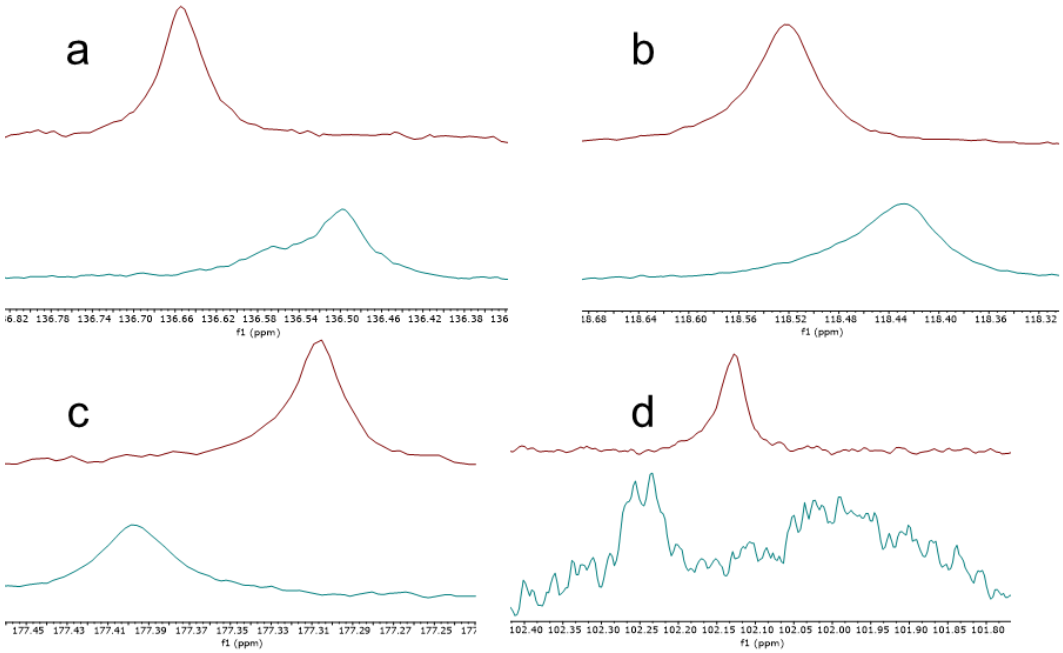

Figure 4.18 ^{13}C spectra of **8** in DMSO-d_6 zoomed in on a) <u>*C*</u>-N/<u>*C*</u>-NH (C10), b) Ar<u>*C*</u> next to <u>*C*</u>-NH/N (C9) c) C=O/C-OH (C12) and d) Core CH (C13) Top: Regular, Bottom: Deuterated

Table 4.2 Comparison of ^{13}C chemical shift (ppm) in regular vs DIS sample of **8** (DMSO-d_6)

Carbon	C1	C2	C3	C4	C5	C6	Ar, C-O-sugar	Ar, C–C–O–sugar	Ar, C–C–N	Ar C-N	Core Ar C-N	core Ar, C=O/C-OH	core Ar, C-H	Core Ar, C-OH/C=O

Carbon Number/ Sample	1	2	3	4	5	6	7	8	9	10	11	12	13	14
8	100.9711	73.7137	77.0471	70.1305	77.521	61.1079	156.233	117.8259	118.5219	136.6530	128 (heated)	177.3058	102.1276	175 (heated) (broad peak)
8-DIS	100.9595	73.5995	76.8735	69.9989	77.4676	60.9848	156.1852	117.8343	118.4278	136.4979	Cannot see	177.3975	102.2537 and 101.9926 (split)	Cannot see
DIS effect (ppb)	11.6	114.2	173.6	131.6	53.4	123.1	47.8	-8.4	94.1	155.1		-91.7	-126.1 and 135	

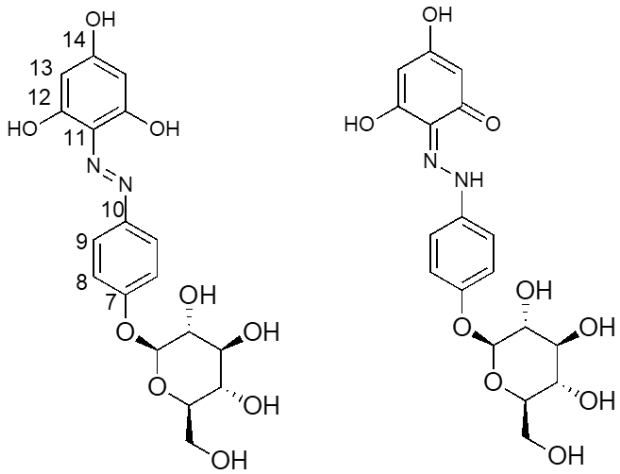

Scheme 4.5 Various tautomeric structures of the mono azo variant, **11**

The mono azo variant **11** is likely present in either the hydrazone or the azo form or as a mixture of the two (Scheme 4.5). The ^{13}C NMR spectrum was obtained in DMSO-d_6. While **8** could be assigned by analogy to **1**, the ^{13}C NMR spectrum of **11** looked significantly different and some peaks could not be assigned by analogy. Carbons such as the aromatic carbon ortho to the *C*-O-Sugar (C8), and core aromatic carbon (C14) could easily be assigned by analogy. C8 in the ^{13}C NMR spectrum of **1** appears at 117.4 ppm and in **8** at 117.8 ppm. Therefore the peak at 116.7 ppm in the ^{13}C NMR of **11** could be assigned to C8. C14 was assigned to the 95.5 ppm peak by analogy to phloroglucinol, where this peak appears at 94 ppm. However, to assign other carbons HMBC and HSQC NMR data was required. The outside C-N (C10) appears at 135 ppm for **8** and **1**. This carbon is likely the one that resonates at 144 ppm in mono azo. This is supported by the

HMBC NMR where the peak at 144 ppm shows correlations to the two aromatic hydrogens on the peripheral aromatic moeity (Figure 4.19).

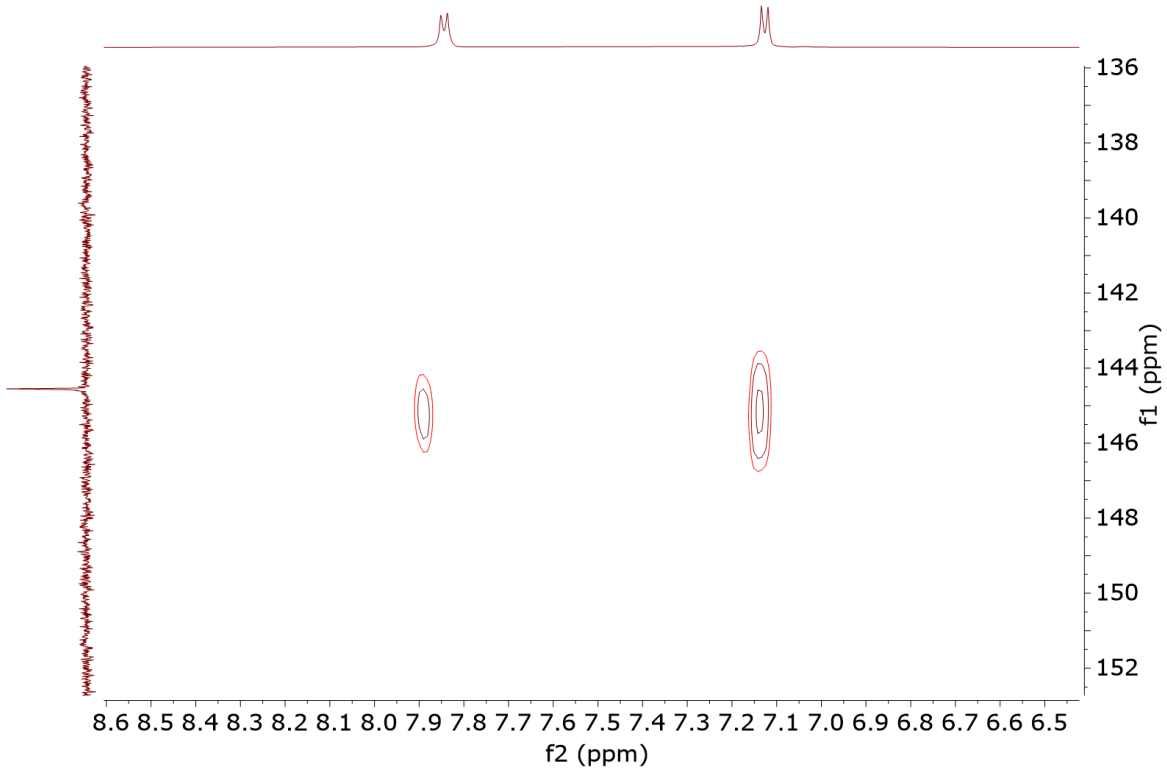

Figure 4.19 Partial HMBC NMR of **11** in DMSO-d_6

It is to be noted that the center of the HMBC cross peaks do not align with the ^{13}C NMR peaks, but rather the top of cross peaks align with the ^{13}C NMR peaks, it is unclear why this is the case. The aromatic carbon C9 resonates at 122.5 ppm, as the HSQC NMR shows correlation to the aromatic proton at 7.84 ppm (Figure 4.20). The carbon at 122.2 ppm is therefore the core C-N (C11) which in **1** and **8** resonante at 128 ppm. The carbon resonating at 158 ppm is likely the C-O-Sugar (C7), as it shows HMBC correlations to the two peripheral aromatic protons (7.86 and 7.13 ppm) and the sugar anomeric proton (4.97 ppm) (Figure 4.21). The carbon resonating at 158.5 ppm is correlated to the core aromatic proton at 5.75 ppm and is therefore likely the phenol carbon (C13) (Figure 4.22). Finally, the resonance at 167 ppm likely corresponds to the C=O/C-

OH carbon (C12) by virtue of its chemical shift. No HMBC correlation was seen to the broad OH/NH proton resonance at 12 ppm.

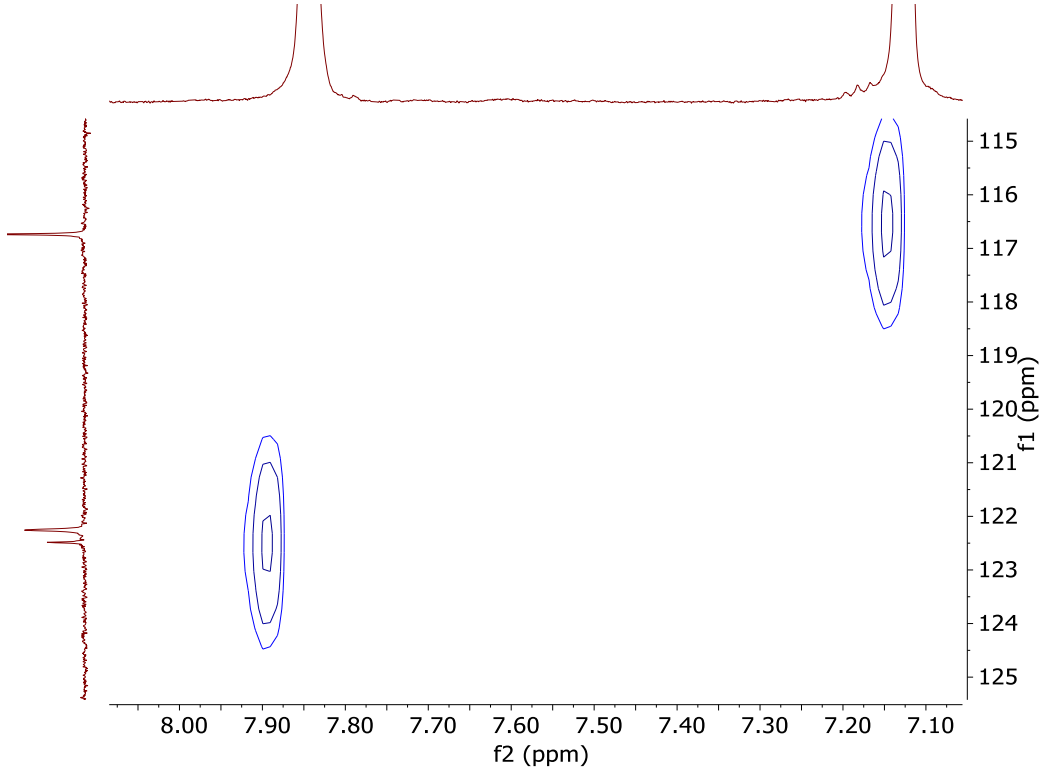

Figure 4.20 Partial HSQC NMR of **11** in DMSO-d_6

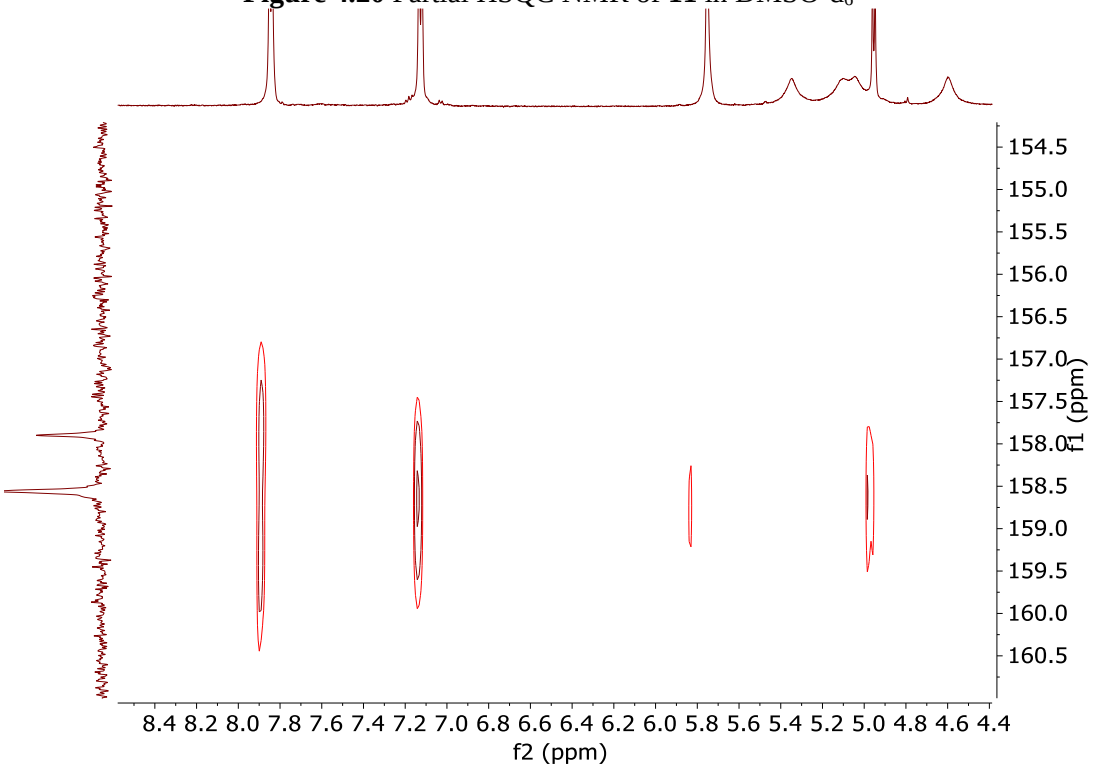

Figure 4.21 Partial HMBC NMR of **11** in DMSO-d_6

To study the tautomeric state, DIS experiment was repeated with **11**. Comparison of ^{1}H spectra of the "DIS sample" vs the regular sample again indicates lack of strong deutero incorporation as the integration of the NH/OH proton does not decrease. However, significant broadening of the NH/OH peak does occur (Figure 4.22). A upfield shift in C9 (Figure 4.24a) but an downfield shift in C10 (Figure 4.24b) makes it unclear whether a hydrazone tautomer is present. Upon deutaration, the C12 peak broadened to the point where it is not visible. A small upfield shift in C11 (Figure 4.24c) could be consistent with either an azo or hydrazone tautomer. ^{13}C the spectrum of the "DIS sample" indicates the presence of one phenolic carbon as strong upfield shift is seen in C13 (Figure 4.24d). Therefore, it was unclear from the DIS experiments which tautomeric state is likely, azo, hydrazone or a mixture of both. However, if the semi-quantitative approach is chosen, with 180 ppm as the "pure hydrazone" chemical shift and 147 ppm as the "pure azo" chemical shift of the C=O/C-OH carbon (C12), then a mixture between the tautomers is suggested. This result would be consistent with the tautomeric hypothesis for the chromophores as we see two peaks in the UV/vis and a mixture of tautomers.

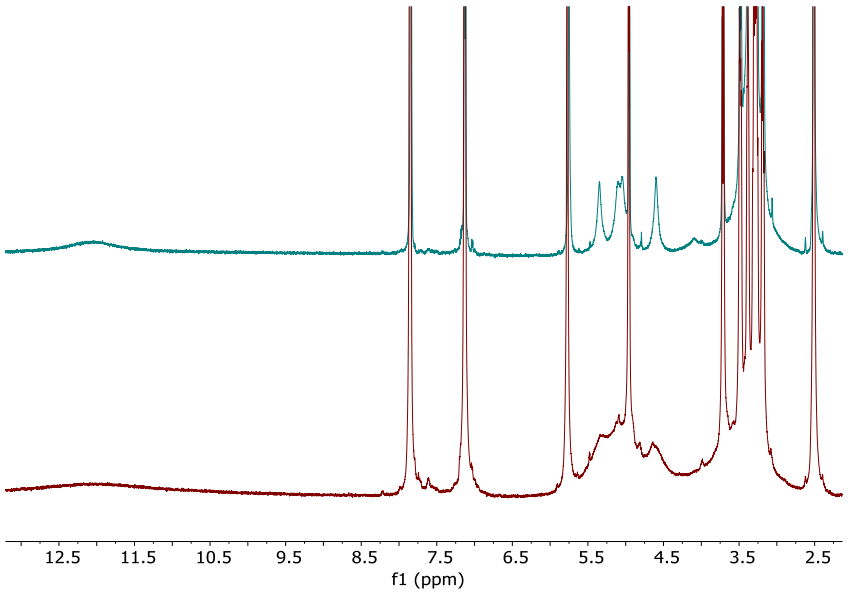

Figure 4.22 Comparison of ^{1}H spectrum of **11** regular (top) vs "DIS" sample (bottom) in DMSO-d_6

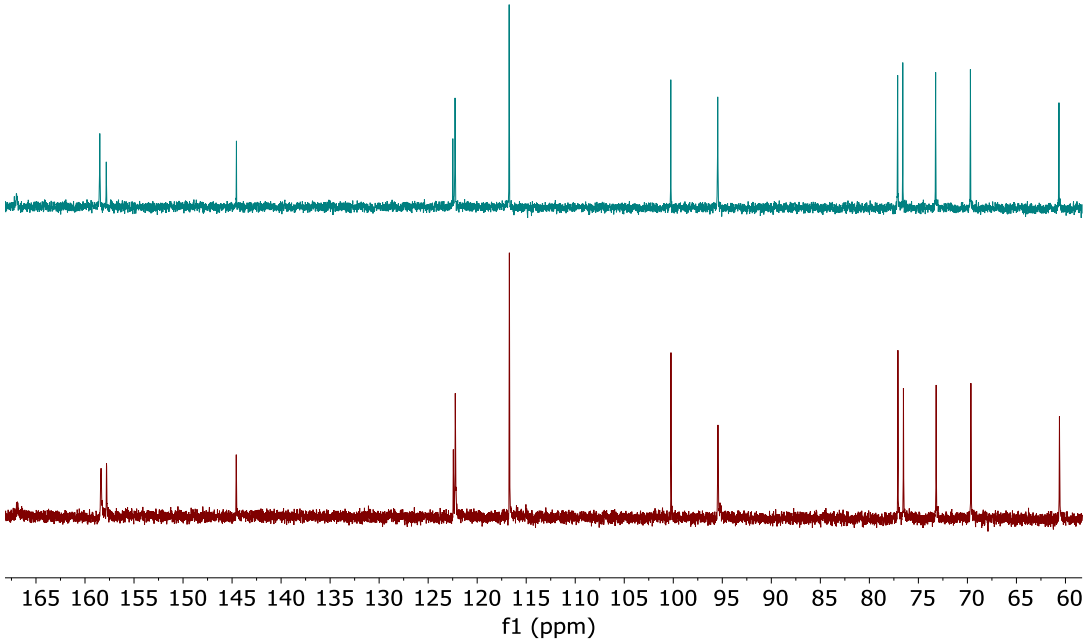

Figure 4.23 Comparison of ^{13}C spectrum of **11** regular (top) vs "DIS" sample (bottom) in DMSO-d_6

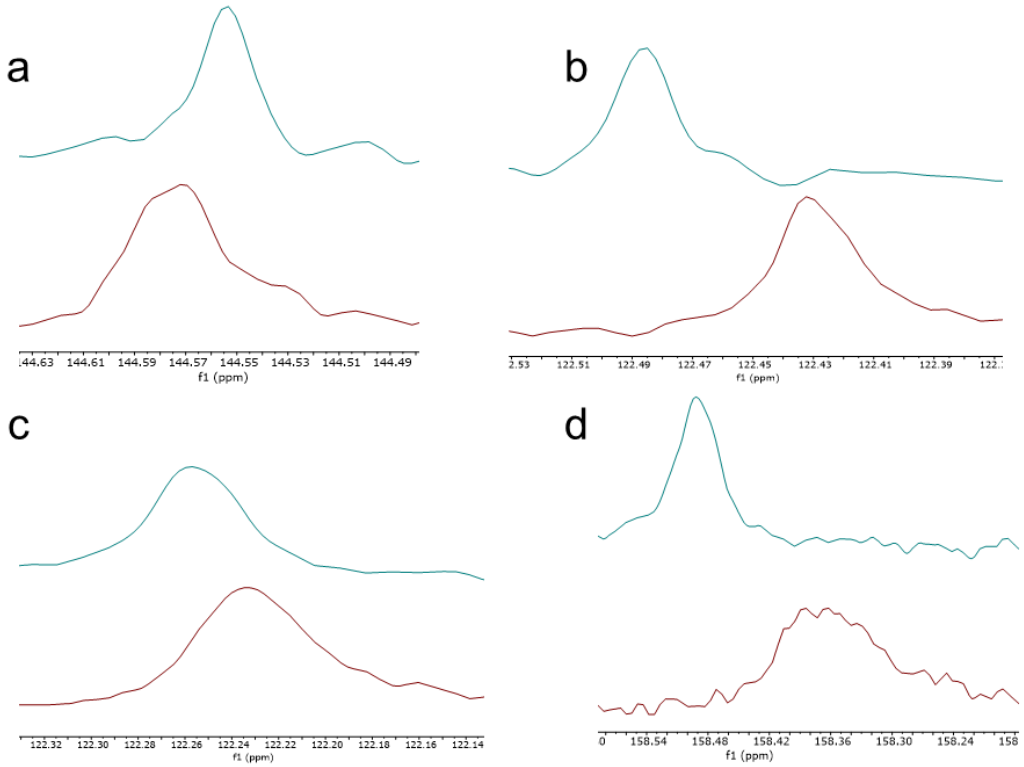

Figure 4.24 ^{13}C spectra of **11** in DMSO-d_6 zoomed in on a) <u>C</u>-N/<u>C</u>-NH (C10) b) Ar<u>C</u> next to <u>C</u>-NH/N (C9) c) Core Ar <u>C</u>-N (C11) and d) <u>C</u>=O/<u>C</u>-OH (C13) Top: Regular, Bottom: Deuterated

Table 4.3 Comparison of ^{13}C chemical shift (ppm) in regular vs DIS sample of **11** (in DMSO-d_6)

Carbon	**C1**	**C2**	**C3**	**C4**	**C5**	**C6**	**Ar, C-O-Sugar**	**Ar, C−C−O −sugar**	**Ar, C−C−N**	**Ar C-N**	**Core Ar C-N**	**core Ar, C−OH/ C=O**	**core Ar, C−OH**	**core Ar, C-H**
Carbon Number	**1**	**2**	**3**	**4**	**5**	**6**	**7**	**8**	**9**	**10**	**11**	**12**	**13**	**14**
11	100.2518	73.2417	76.5923	69.6939	77.1157	60.6613	157.8304	116.7366	122.4857	144.5537	122.257	166.8877-167.0004	158.4905	95.4642
11-DIS	100.2331	73.1874	76.5229	69.6421	77.0866	60.6119	157.8019	116.7171	122.4322	144.5702	122.2315	166.8387-167.0196	158.3807	95.4404
DIS effect (ppb)	18.7	54.3	69.4	51.8	29.1	49.4	28.5	19.5	53.5	-16.5	25.5	49-(-19.2)	109.8	23.8

4.4 Analysis of Yariv reagent UV/vis spectra in other solvents

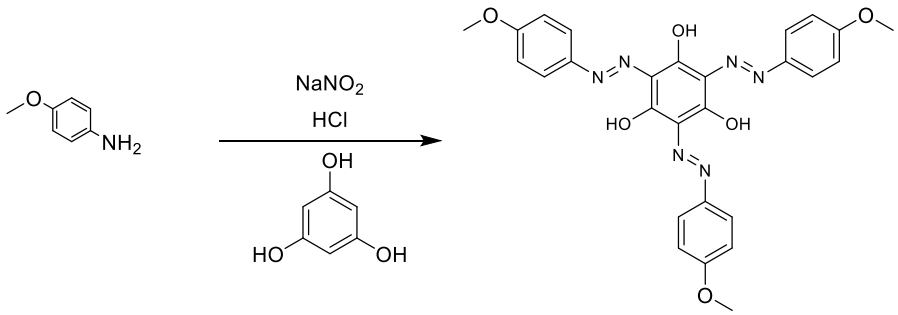

Scheme 4.6 Synthesis of the anisidine Yariv reagent **23**

An “anisidine Yariv Reagent” **23** was synthesized. It was found that **23** is soluble in chloroform. The UV/vis spectrum of **23** was acquired in chloroform. It was seen that besides the two peaks that are seen for other Yariv reagents in DMSO and water, there is also a shoulder peak next to the long wavelength peak (Figure 4.25). The UV/vis spectrum was also acquired in DMSO. The UV/vis spectrum of **23** in DMSO looked qualitatively similar to the UV/vis spectra of all other Yariv reagents in DMSO with two peaks. However, when the UV/vis spectrum of **23** in DMSO is compared to the UV/vis spectrum in chloroform, it is seen that UV/vis spectrum in chloroform is significantly weaker (Figure 4.25). The comparison of the normalized spectra in chloroform and regular spectrum in DMSO shows that the short wavelength peak is slightly red shifted in

chloroform and that a shoulder next to the long wavelength peak has appeared in chloroform. The ^{13}C NMR spectrum in $CDCl_3$ was also acquired for **23 (**Figure 4.26**)**. The C=O/C-OH carbon resonates at 178.3 ppm suggesting high hydrazone content in **23**. Therefore, while the ^{13}C NMR chemical shifts of **23** is similar to the ^{13}C NMR chemical shifts of other Yariv reagents in DMSO-d_6, the UV/vis spectrum in the two solvents is somewhat different.

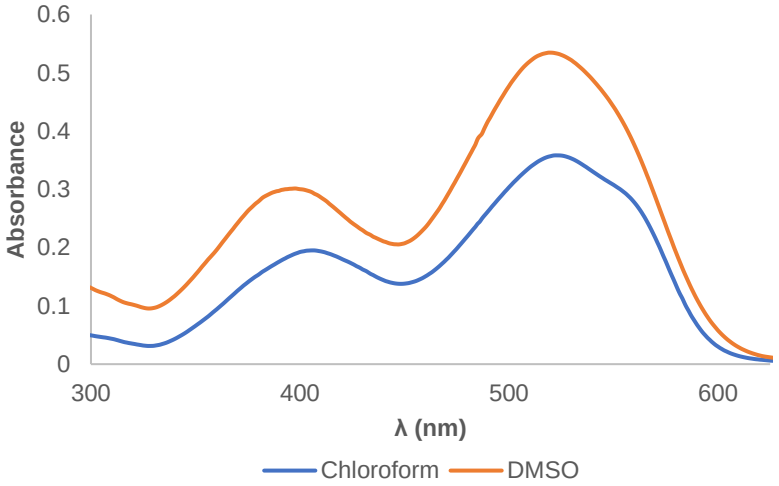

Figure 4.25 UV/vis spectra of **23** (30 μM)

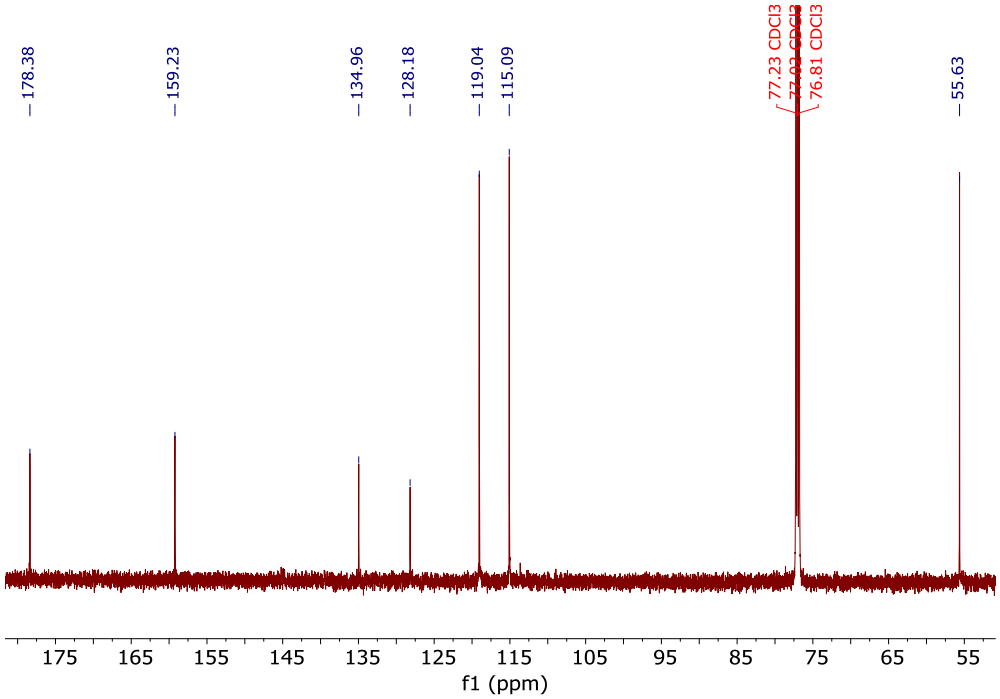

Figure 4.26 ^{13}C spectrum of **23** in $CDCl_3$

4.5 Analysis of presence of aggregates in DMSO

Next, we shifted our focus to the tris azo Yariv **1** again. While the tautomeric hypothesis is unlikely to be true for **1**, the "aggregate vs monomer" hypothesis still needed to be evaluated. Due to exciton coupling upon formation of H-aggregates the long wavelength transition could blue shift giving rise to the two peaks we see in the UV/vis spectra. This hypothesis is unlikely to be true in water because the CD spectra in water shows two overlapping bisignate cotton effects. The presence of two bisignate cotton effects suggests that the long wavelength transtion is also associated with the aggregate rather than a monomer. However, since the CD spectra with two bisignate cotton effects are seen in water, it cannot ruled out that the long wavelength peak is associated with the monomer and short wavelength peak is associated with aggregates in DMSO. Finally, it must be pointed out that when the UV/vis spectra for **1** in water is acquired at various temperatures, a change in the ratio of the two peaks along with an isosbestic point is seen, consistent with exchange between two species in water (Figure 4.27). Therefore, while in the water both the transitions are associated with aggregated species, they maybe two different species in equilibrium with one another. However, they may also be one chromophore, whose two transitions vary in intensity with temperature.

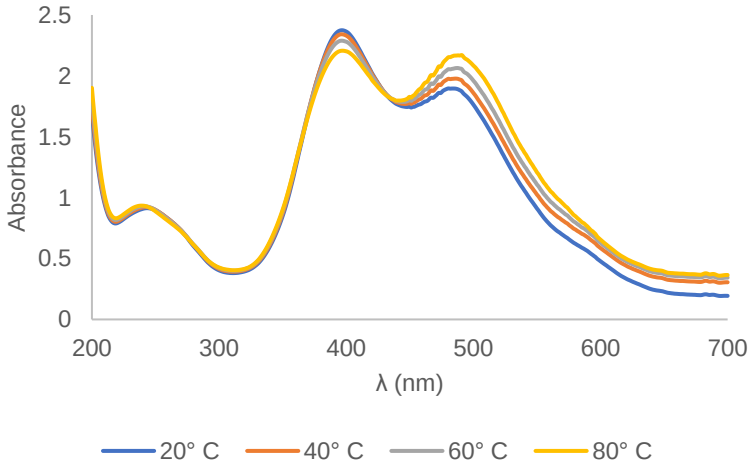

Figure 4.27 UV/vis spectra of **1** in water (300 μM) at various temperatures

We see no CD signal in DMSO even at remarkably high concentrations like 50 mM (Figure 1.13). Lack of CD signal in DMSO suggests that the short wavelength peak in DMSO is not

associated with the aggregate. However, as previously mentioned this could be because in DMSO equal left- and right-handed aggregates are formed. For the "aggregate vs monomer" hypothesis to be true, a significant amount of aggregates should be present in DMSO since we see two peaks in the UV/vis in DMSO. To determine if aggregates are present in DMSO, DOSY NMR was utilized. The diffusion constants obtained from DOSY NMR can be used to calculate the molecular weight of the species using an internal reference.[25-26] The relationship between molecular weight and the diffusion constant obtained from the DOSY experiment is described in equation 3.

$$\log D_{x,norm} = \log K + \alpha^* \log MW \quad \textbf{Equation 3}$$

where MW is the molecular weight of the aggregate of interest, K and α are constants that depend on the choice of shape of molecule, internal reference and solvent, and $D_{x,norm}$ is the normalized diffusion constant obtained from equation 3. The constants K and α were obtained from *Chemistry* **2016,** *22* (25), 8462-5

$$\log D_{x,norm} = \log D_{ref,\ fix} - \log D_{ref} + \log D \quad \textbf{Equation 4}$$

where $D_{ref,\ fix}$is the "fixed value" for an internal reference of your choice, in this case DMSO, obtained from *Chemistry* **2016,** *22* (25), 8462-5, D_{ref} is the experimental diffusion constant of the internal reference, and D is the experimental diffusion constant of the molecule of interest.

The molecular weight of the Yariv reagent **1** was obtained in DMSO, using DMSO as the internal reference and the "dissipated spheres and ellipsoids" as the chosen shape at various different concentrations ranging from 19 mM to 175 mM (Table 4.4). At the lowest concentration examined (19 mM) we see that N = 1.5 suggesting very little if any aggregation. Therefore, at a concentration of 30 μM where two peaks are observed in the UV/vis, there is unlikely to be any aggregate present. Examination of DOSY NMR at such low concentrations were not possible

because of the low intensity of the NMR peaks. This data suggests that the aggregate vs monomer" hypothesis is unlikely to be true due to lack of aggregates in DMSO.

Table 4.4 Molecular Weight (MW) calculation of **1** via DOSY NMR in DMSO

Conc (mM)	Yariv D (m^2/s)	DMSO D (m^2/s)	MW	N
19	8.00E-11	5.65E-10	1479.73	**1.52**
41	6.50E-11	5.14E-10	1735.49	**1.78**
83	4.50E-11	4.00E-10	2046.77	**2.10**
126	3.10E-11	3.26E-10	2594.43	**2.67**
175	2.00E-11	2.66E-10	3613.27	**3.71**

4.6 Conclusion

In this section it has been shown that the C_3 symmetric hydroxyazo dyes such as the Yariv reagent, are unlikely to exist in the azo tautomeric state. This suggests that the "tautomeric hypothesis" for identity of the chromophore(s) is not true. A hypothesis presented by Paulsen et al, which states that the two peaks in the UV/vis spectra arise from the aggregated and monomeric forms of the Yariv reagent is also unlikely to be true, as we see minimal aggregation in DMSO. The tautomeric state of the other Yariv reagent analogs such as **8** and **11** was also analyzed but no clear evidence for the presence of any one or more particular tautomer(s) was found. Although, in the case of **8** it was shown that some tautomers such as **8B** or **8D** are unlikely to be major contributors. Therefore, we have not ruled out the tautomeric hypothesis for the identity of the chromophores for the Yariv reagent analogs **8** and **11**. It has been suggested in the past that the two peaks in UV/vis spectra of C_3 symmetric hydroxyazo dyes may arise from two different transitions from the same chromophore, such as π to π^* (short wavelength) and n to π^*

(long wavelength). Evidence put forth in favor of this hypothesis is the fact that a decrease in the intensity of the long wavelength transition was seen along with planarization of the peripheral aromatic rings upon aggregation of a C_3 symmetric hydroxyazo dye. Since it had previously been shown that n to π* transtions in azobenzenes increase in intensity with de-planarization and decrease in intensity with planarization, it was claimed that the long wavelength peak in the UV/vis of C_3 symmetric hydroxyazo dyes also arises from the n to π* transition. However, others have argued that n to π* transition assignment even in the case azobenzenes is incorrect, calling into question this assignment for C_3 symmetric hydroxyazo dyes. In the future, the synthesis of either the "O-methylated" or "N-methylated" analog of the Yariv reagent similar to **14** and **15** may be useful to help examine the effect of locking the Yariv reagent in one tautomeric state on the UV/Vis spectrum. If the N-methylated analog shows the same UV/Vis spectra as the regular Yariv reagents, it would strongly support the idea that the two peaks arise from different transitions of the hydrazone tautomer.

Supplemental Information

General Protocols, CD and UV/vis spectroscopy: Refer to chapter 2 SI for general, CD, UV/vis spectroscopy protocols. Variable temperature UV data was collected concurrently with the CD data using the Jasco J-815 spectropolarimeter instrument.

DIS protocols:

1: 95 mg of **1** was weighed out into a scintillation vial, 2 mL of D_2O was added to deuterate the sample and then lyophilised overnight, 750 uL of DMSO-d_6 was added. ^{13}C NMR spectra was obtained and compared to previously obtained ^{13}C NMR of 95 mg in 750 uL DMSO-d_6 non-deuterated sample.

8: 103 mg of **8** was weighed out into a scintillation vial, 2 mL of D_2O was added to deuterate the sample and then lyophilised overnight, 750 uL of DMSO-d_6 was added. ^{13}C and ^{1}H NMR spectra was obtained and compared to previously obtained ^{13}C NMR and ^{1}H NMR spectra of 100 mg in 750 uL DMSO-d_6 non-deuterated sample.

11: 12.5 mg of **11** was weighed out into a scintillation vial, 2 mL of D_2O was added to deuterate the sample and then lyophilised overnight, 750 uL of DMSO-d_6 was added. ^{13}C and ^{1}H NMR spectra was obtained and compared to previously obtained ^{13}C NMR and ^{1}H NMR spectra of 17 mg in 750 uL DMSO-d_6 non-deuterated sample.

DOSY protocol and sample calculation for molecular weight:

DOSY experiments were performed using the ledbpg2s pulse sequence. The experiments were conducted with an exponential gradient stepped between 20% and 95%. 16 1D ^{1}H spectra were collected with a gradient duration of 1.5 ms and an echo delay of 200 ms.

Sample MW calculation for the 19 mM sample:

Using equation 4-

$\log D_{x,norm} = \log D_{ref,\ fix} - \log D_{ref} + \log D = -9.1787 - (\log (5.65E\text{-}10)) + (\log(8E\text{-}11)) = -10.02$

Using Equation 3:

$\log D_{x,norm} = \log K + \alpha * \log MW$, therefore $-10.02 = -7.78 + (-0.709 * \log MW)$

$\log D_{ref,\ fix}$ obtained from table 4 and log K and α obtained from table 3 in reference 25.

References

1. Chen, X. C.; Tao, T.; Wang, Y. G.; Peng, Y. X.; Huang, W.; Qian, H. F., Azo-hydrazone tautomerism observed from UV-vis spectra by pH control and metal-ion complexation for two heterocyclic disperse yellow dyes. *Dalton Trans* **2012,** *41* (36), 11107-15.

2. Joshi, H.; Kamounah, F. S.; van der Zwan, G.; Gooijer, C.; Antonov, L., Temperature dependent absorption spectroscopy of some tautomeric azo dyes and Schiff bases. *Journal of the Chemical Society, Perkin Transactions 2* **2001,** (12), 2303-2308.

3. O'Shea, K. E.; Kirmse, K. M.; Fox, M. A.; Johnston, K. P., Polar and hydrogen-bonding interactions in supercritical fluids: effects on the tautomeric equilibrium of 4-(phenylazo)-1-naphthol. *The Journal of Physical Chemistry* **2002,** *95* (20), 7863-7867.
4. Stoyanov, S.; Antonov, L., Quantitative analysis of azo-quinonehydrazone tautomeric equilibrium. *Dyes and Pigments* **1989,** *10* (1), 33-45.
5. Paulsen, B. S.; Craik, D. J.; Dunstan, D. E.; Stone, B. A.; Bacic, A., The Yariv reagent: behaviour in different solvents and interaction with a gum arabic arabinogalactan-protein. *Carbohydr Polym* **2014,** *106*, 460-8.
6. Kuhn, R.; Bär, F., Über die Konstitution der Oxy-azo-verbindungen. *Justus Liebig's Annalen der Chemie* **1935,** *516* (1), 143-155.
7. Fedorov, L. A.; Sokolovskii, S. A., MR spectra and azo-quinonehydrazone tautomerism in 4-arylazo-1-naphthol derivatives, without intramolecular proton transfer. *Bulletin of the Academy of Sciences of the USSR, Division of chemical science* **1988,** *37* (6), 1136-1141.
8. Antonov, L.; Nedeltcheva, D., Resolution of overlapping UV–Vis absorption bands and quantitative analysis. *Chemical Society Reviews* **2000,** *29* (3), 217-227.
9. Nedeltcheva, D.; Antonov, L.; Lycka, A.; Damyanova, B.; Popov, S., Chemometric Models For Quantitative Analysis of Tautomeric Schiff Bases and Azo Dyes. *Current Organic Chemistry* **2009,** *13* (3), 217-240.
10. Bekárek, Y.; Rothschein, K.; Vetešník, P.; Večeřa, M., Estimation of azo - hydrazo tautomeric equilibrium in ortho-hydroxy-azocompounds by N.M.R. *Tetrahedron Letters* **1968,** *9* (34), 3711-3713.
11. Lyčka, A.; Šnobl, D., Coupling constants nitrogen-15-nitrogen-15 and nitrogen-15-hydrogen in phenylhydrazones forming hydrogen bond. *Collection of Czechoslovak Chemical Communications* **1981,** *46* (4), 892-897.
12. Lee, H. Y.; Song, X.; Park, H.; Baik, M. H.; Lee, D., Torsionally responsive C3-symmetric azo dyes: azo-hydrazone tautomerism, conformational switching, and application for chemical sensing. *J Am Chem Soc* **2010,** *132* (34), 12133-44.
13. Luo, X. S.; Deng, H. L.; Chi, S.; Liu, Y.; Huang, M. H., (15)N Solid-State NMR as Bright Eyes to See the Isomerization of the Azo Bond: Revision of Tris(beta-hydroxyl-azo)-benzene to Tris(beta-keto-hydrazo)-cyclohexane in Porous Organic Polymers. *J Phys Chem Lett* **2021,** *12* (29), 6767-6772.
14. Liu, X.; Luo, X. S.; Fu, H. X.; Fan, W.; Chen, S. L.; Huang, M. H., Irreversible tautomerization as a powerful tool to access unprecedented functional porous organic polymers with a tris(beta-keto-hydrazo)cyclohexane subunit (TKH-POPs). *Chem Commun (Camb)* **2020,** *56* (14), 2103-2106.
15. Han, M.; Cho, S. J.; Norikane, Y.; Shimizu, M.; Kimura, A.; Tamagawa, T.; Seki, T., Multistimuli-responsive azobenzene nanofibers with aggregation-induced emission enhancement characteristics. *Chem Commun (Camb)* **2014,** *50* (99), 15815-8.
16. Buendia, J.; Calbo, J.; Garcia, F.; Arago, J.; Viruela, P. M.; Orti, E.; Sanchez, L., Helical supramolecular polymerization of C3-symmetric amides and retroamides: on the origin of cooperativity and handedness. *Chem Commun (Camb)* **2016,** *52* (42), 6907-10.
17. Hendrikse, S. I. S.; Su, L.; Hogervorst, T. P.; Lafleur, R. P. M.; Lou, X.; van der Marel, G. A.; Codee, J. D. C.; Meijer, E. W., Elucidating the Ordering in Self-Assembled Glycocalyx Mimicking Supramolecular Copolymers in Water. *J Am Chem Soc* **2019,** *141* (35), 13877-13886.

18. Van Gorp, J. J.; Vekemans, J. A.; Meijer, E. W., C3-symmetrical supramolecular architectures: fibers and organic gels from discotic trisamides and trisureas. *J Am Chem Soc* **2002,** *124* (49), 14759-69.
19. Kobayashi, N.; Muranaka, A., Chapter 1. Theory of Optical Spectroscopy. **2011**, 1-41.
20. Nakashima, H.; Fujiki, M.; Koe, J. R.; Motonaga, M., Solvent and temperature effects on the chiral aggregation of poly(alkylarylsilane)s bearing remote chiral groups. *J Am Chem Soc* **2001,** *123* (9), 1963-9.
21. Landge, S. M.; Tkatchouk, E.; Benitez, D.; Lanfranchi, D. A.; Elhabiri, M.; Goddard, W. A., 3rd; Aprahamian, I., Isomerization mechanism in hydrazone-based rotary switches: lateral shift, rotation, or tautomerization? *J Am Chem Soc* **2011,** *133* (25), 9812-23.
22. Dziembowska, T., Studies based on deuterium isotope effect on 13C chemical shifts. *Progress in Nuclear Magnetic Resonance Spectroscopy* **2004,** *45* (1-2), 1-29.
23. Reuben, J., Intramolecular hydrogen bonding as reflected in the deuterium isotope effects on carbon-13 chemical shifts. Correlation with hydrogen bond energies. *Journal of the American Chemical Society* **2002,** *108* (8), 1735-1738.
24. Lyčka, A.; Hansen, P. E., Deuterium isotope effects on13C and15N nuclear shielding ino-hydroxyazo dyes. *Organic Magnetic Resonance* **1984,** *22* (9), 569-572.
25. Bachmann, S.; Neufeld, R.; Dzemski, M.; Stalke, D., New External Calibration Curves (ECCs) for the Estimation of Molecular Weights in Various Common NMR Solvents. *Chemistry* **2016,** *22* (25), 8462-5.
26. Li, D.; Kagan, G.; Hopson, R.; Williard, P. G., Formula weight prediction by internal reference diffusion-ordered NMR spectroscopy (DOSY). *J Am Chem Soc* **2009,** *131* (15), 5627-34

Appendix

4-aminophenyl β-D-glucopyranoside [^{1}H NMR (600 MHz, DMSO-d_6)]

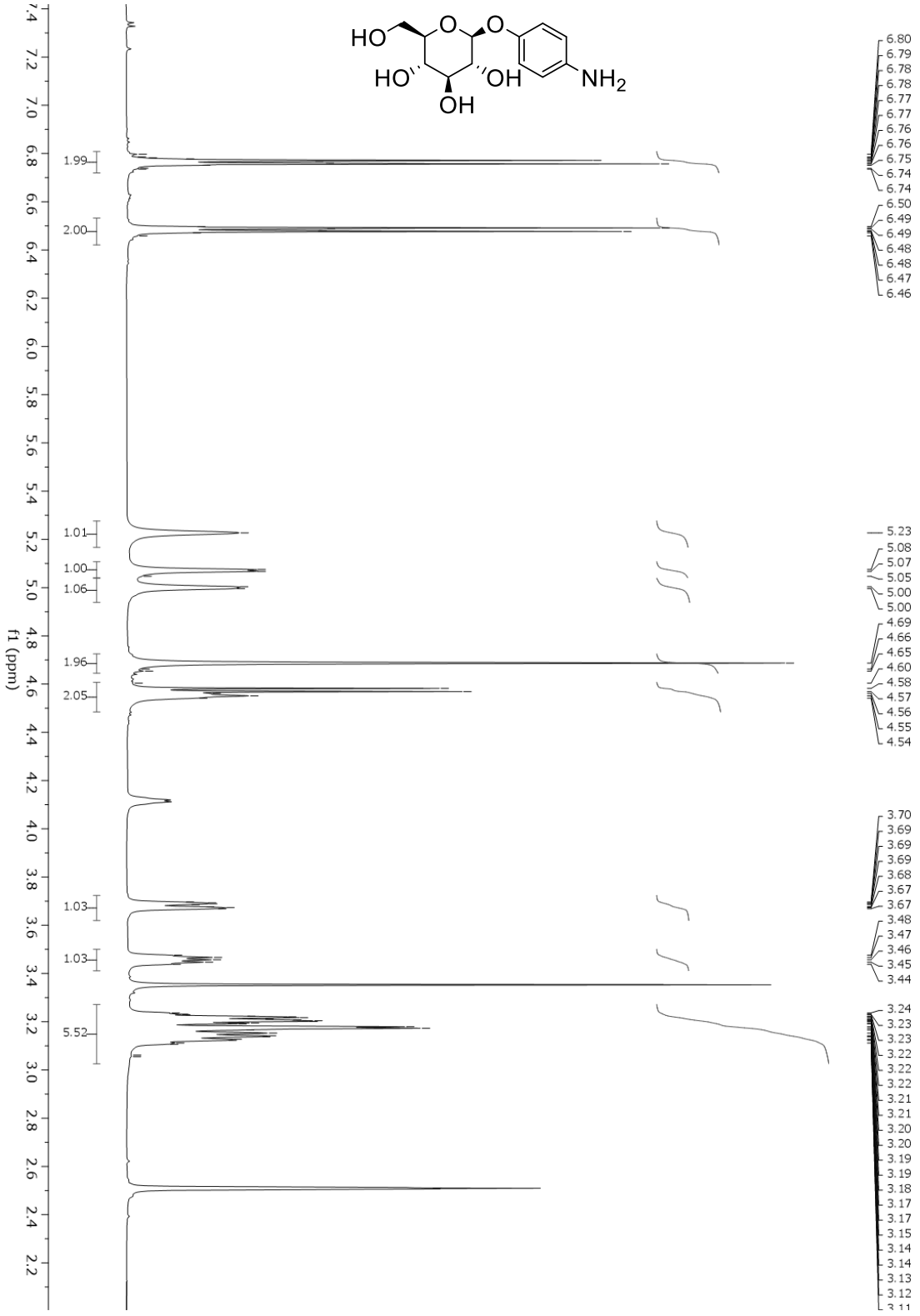

(1) β-D-glc Yariv Reagent, batch 4 R2XM [^{1}H NMR (600 MHz, DMSO-d_6)]

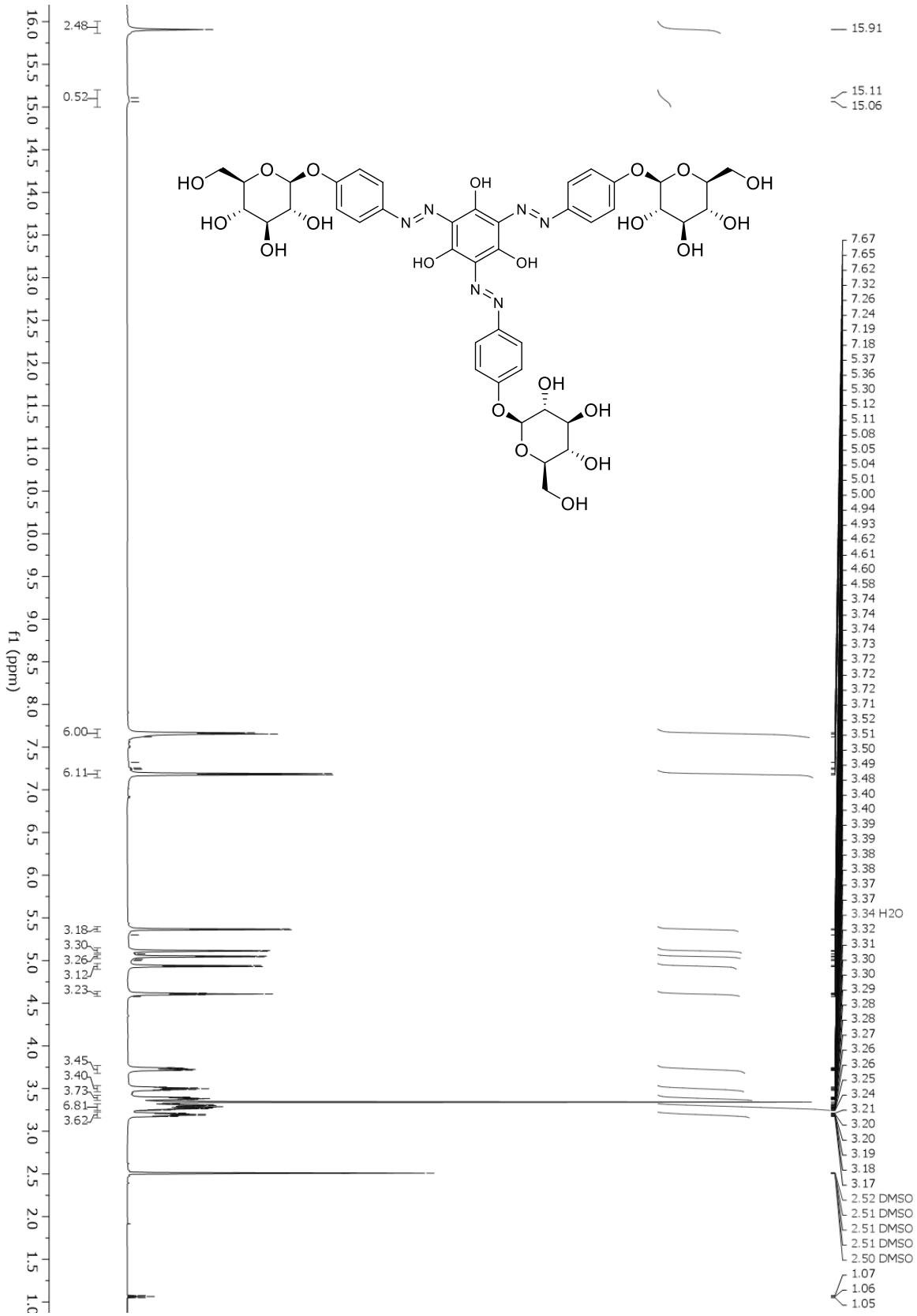

(1) β-D-glc Yariv Reagent, batch 4 R2XM [^{13}C NMR (151 MHz, DMSO-d_6)]

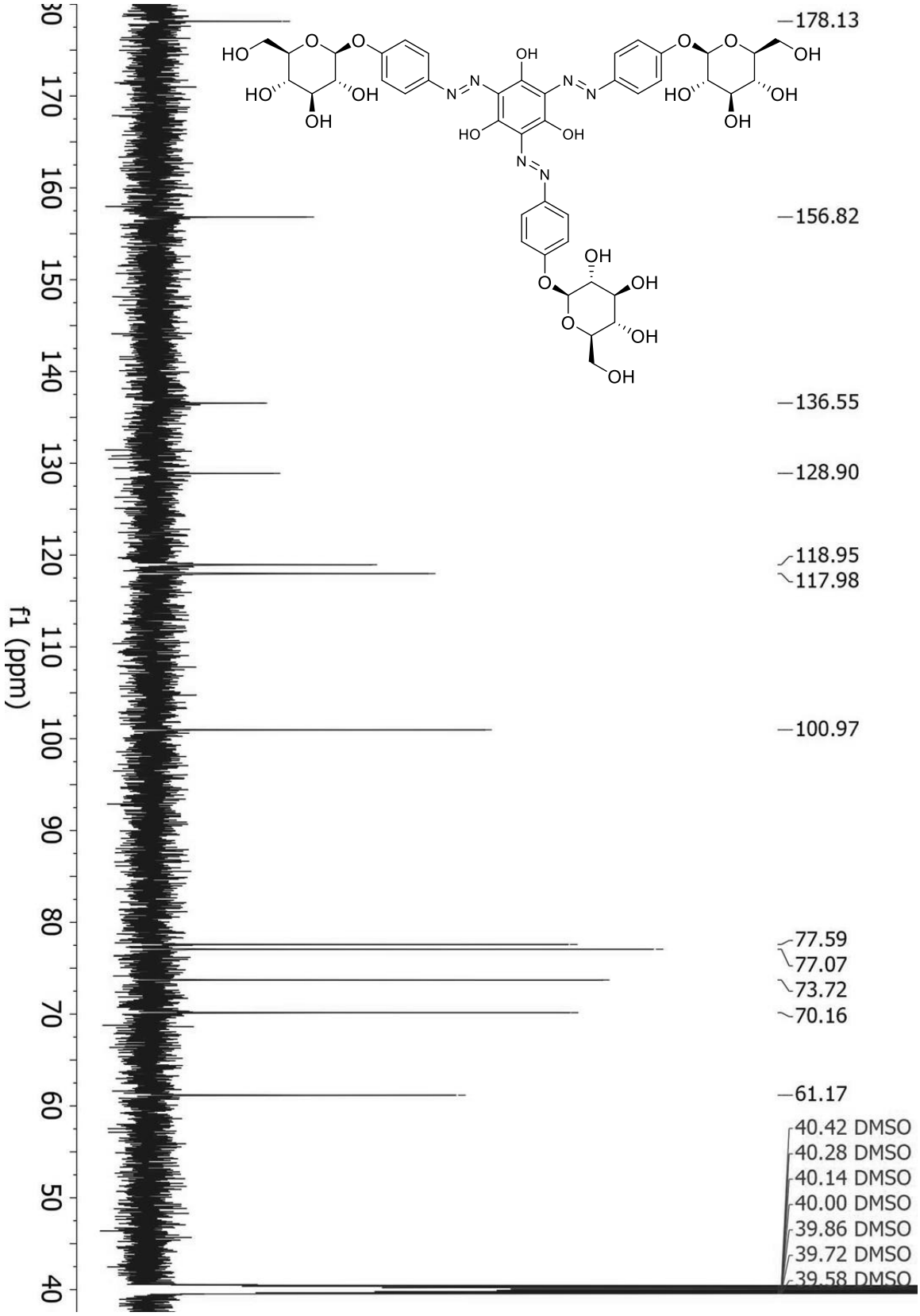

(1) β-D-glc Yariv Reagent, batch 4 R2XM [COSY (600 MHz for ^{1}H, DMSO-d_6)]

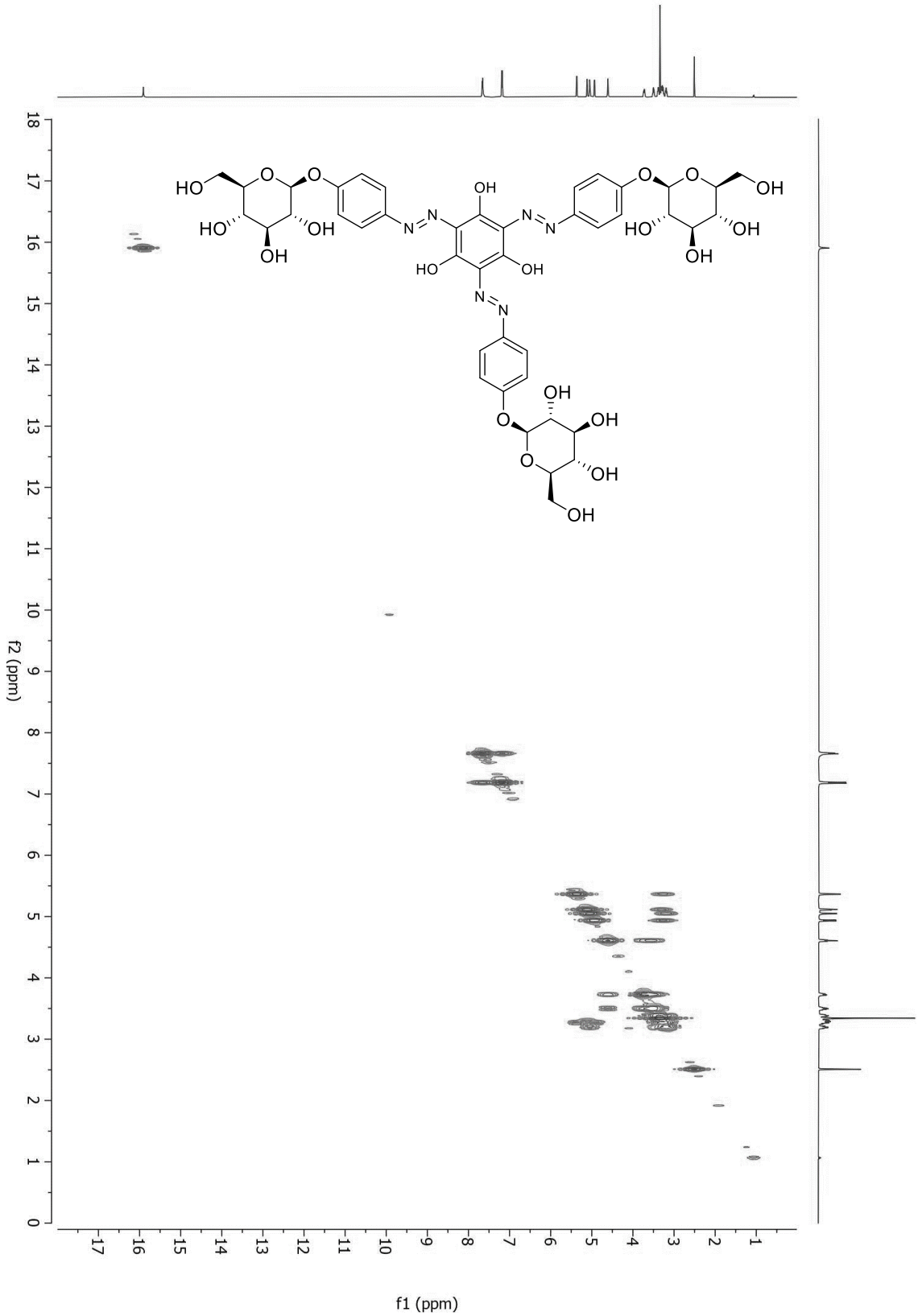

(1) β-D-glc Yariv Reagent, batch 4 R2XM [COSY (600 MHz for ^{1}H, DMSO-d_6)]

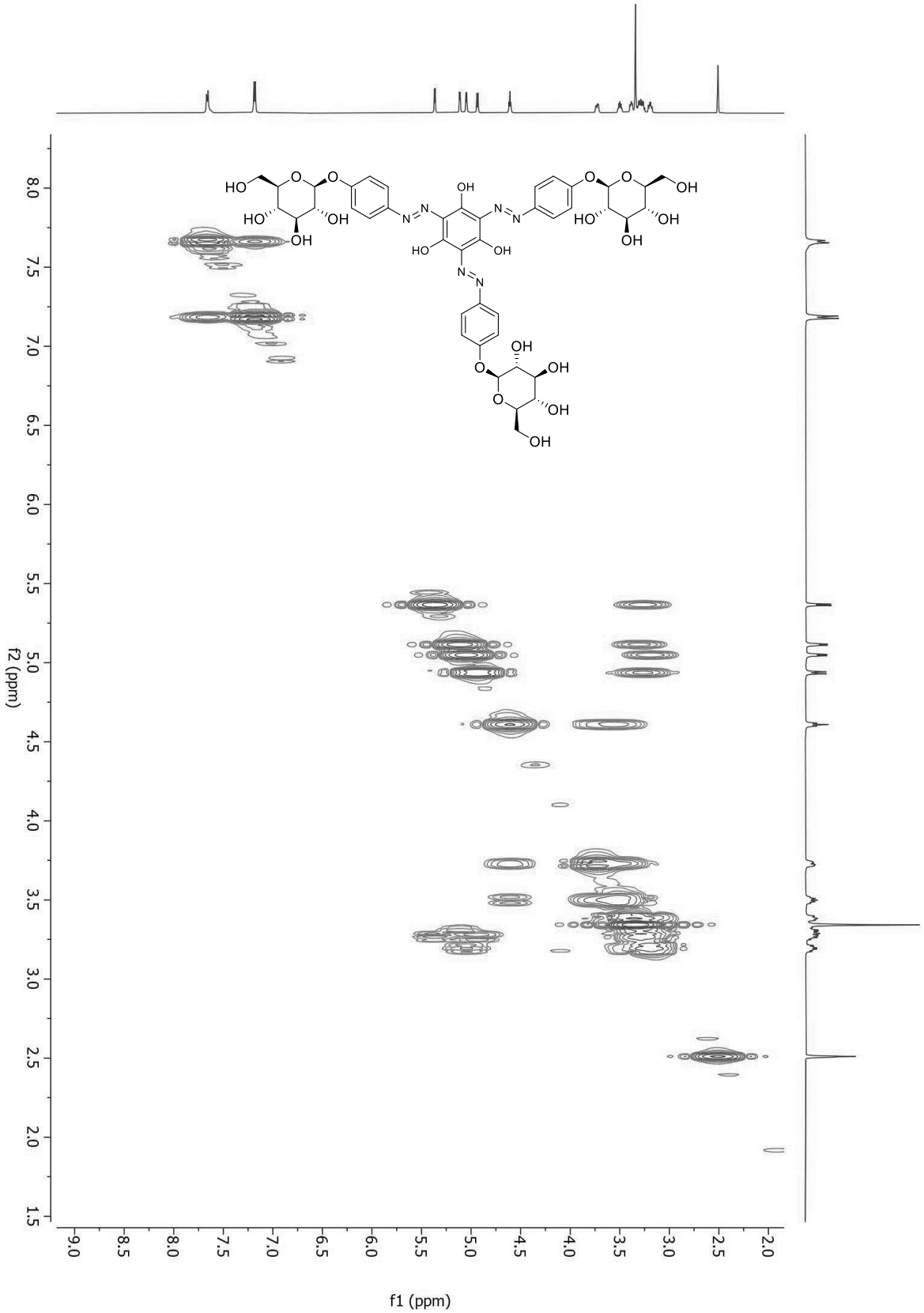

(1) β-D-glc Yariv Reagent, batch 4 R2XM [HSQC (600 MHz for ^{1}H, DMSO-d_6)]

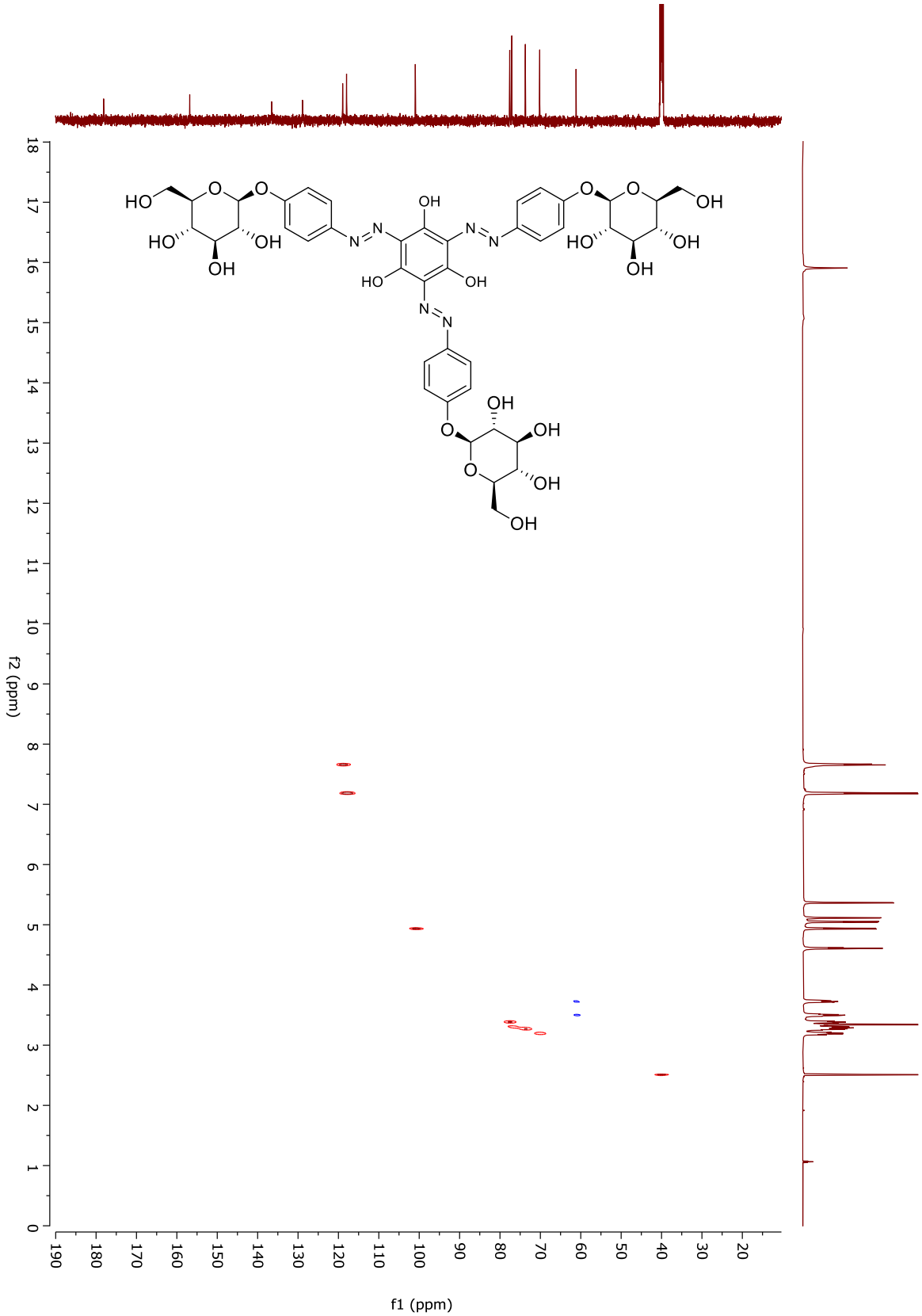

(1) β-D-glc Yariv Reagent, batch 4 R2XM [HSQC (600 MHz for ^{1}H, DMSO-d_6)]

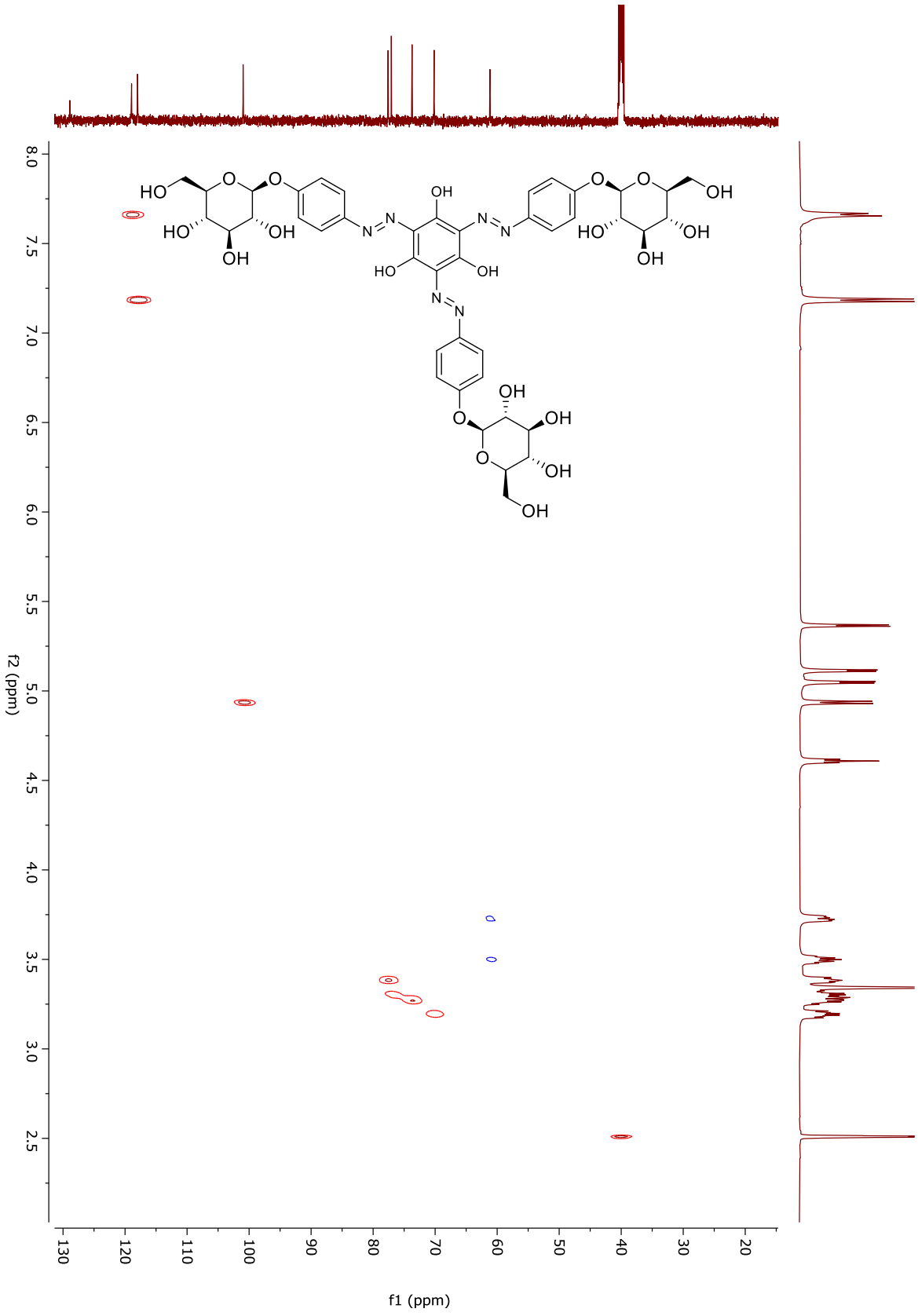
f2 (ppm)
f1 (ppm)
8.0
7.5
7.0
6.5
6.0
5.5
5.0
4.5
4.0
3.5
3.0
2.5
130
120
110
100
90
80
70
60
50
40
30
20
HO
OH
O
N
N

(1) β-D-glc Yariv Reagent, batch 4 R2XM [HMBC (600 MHz for ^{1}H, DMSO-d_6)]

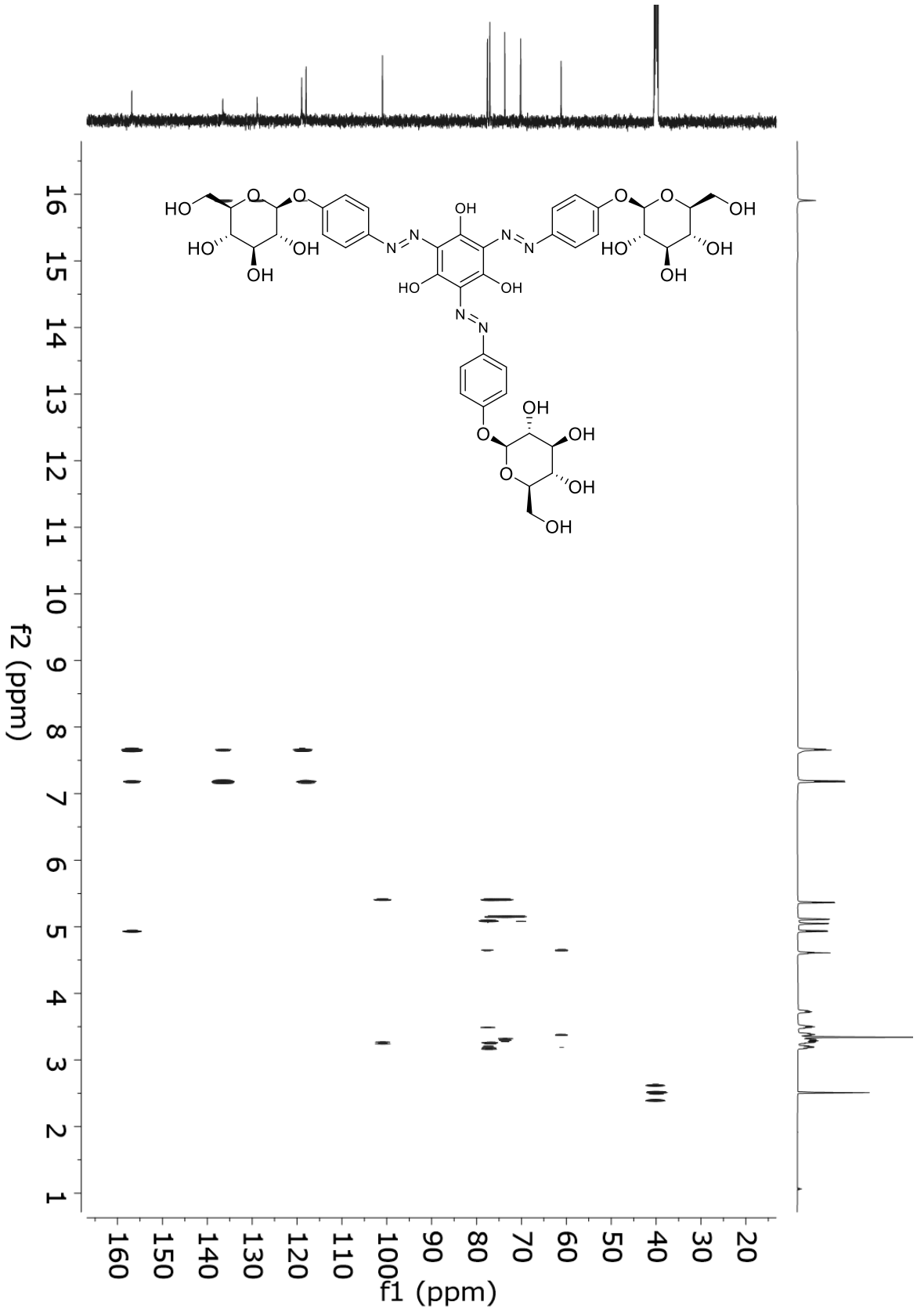
f2 (ppm)
f1 (ppm)
HO
OH
O
N=N

4-aminophenyl β-D-galactopyranoside [^{1}H NMR (600 MHz, DMSO-d_6)]

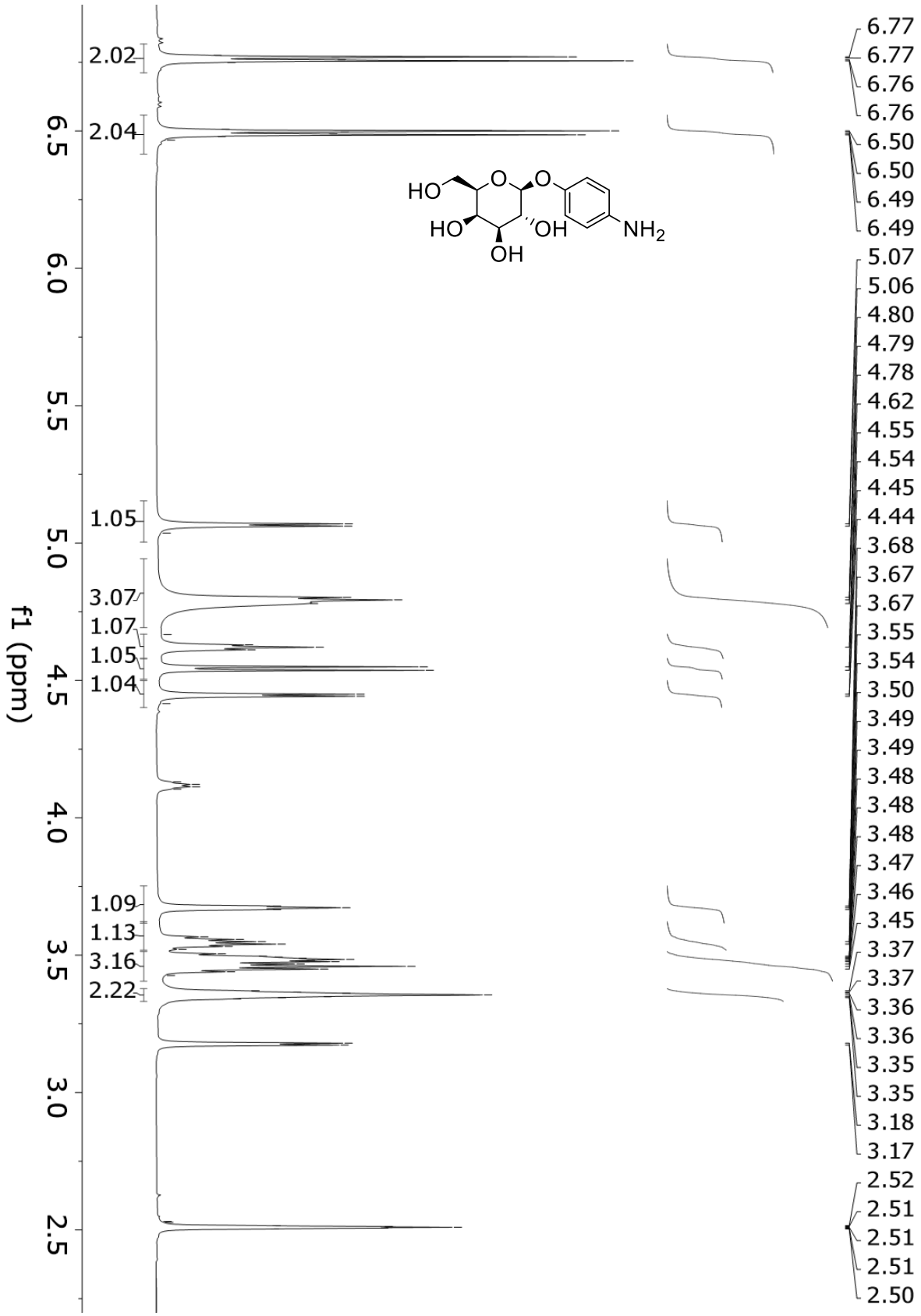
f1 (ppm)
6.5
6.0
5.5
5.0
4.5
4.0
3.5
3.0
2.5
2.02
2.04
1.05
3.07
1.07
1.05
1.04
1.09
1.13
3.16
2.22
HO
O
O
HO
OH
OH
NH2
6.77
6.77
6.76
6.76
6.50
6.50
6.49
6.49
5.07
5.06
4.80
4.79
4.78
4.62
4.55
4.54
4.45
4.44
3.68
3.67
3.67
3.55
3.54
3.50
3.49
3.49
3.48
3.48
3.48
3.47
3.46
3.45
3.37
3.37
3.36
3.36
3.35
3.35
3.18
3.17
2.52
2.51
2.51
2.51
2.50

(2) β-D-gal Yariv Reagent, R2XM [^{1}H NMR (600 MHz, DMSO-d_6)]

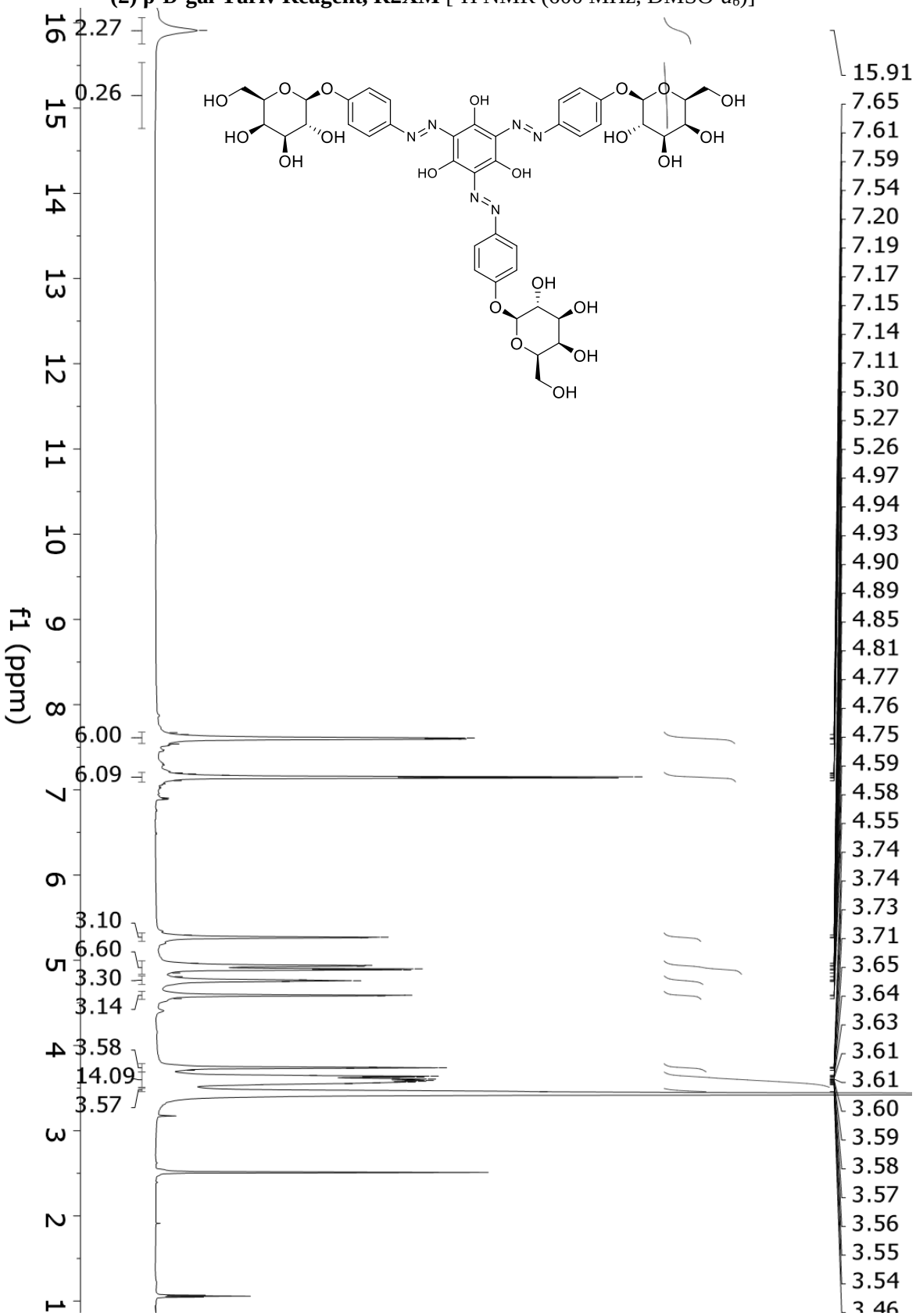

(2) β-D-gal Yariv Reagent, R2XM [^{13}C NMR (151 MHz, DMSO-d_6)]

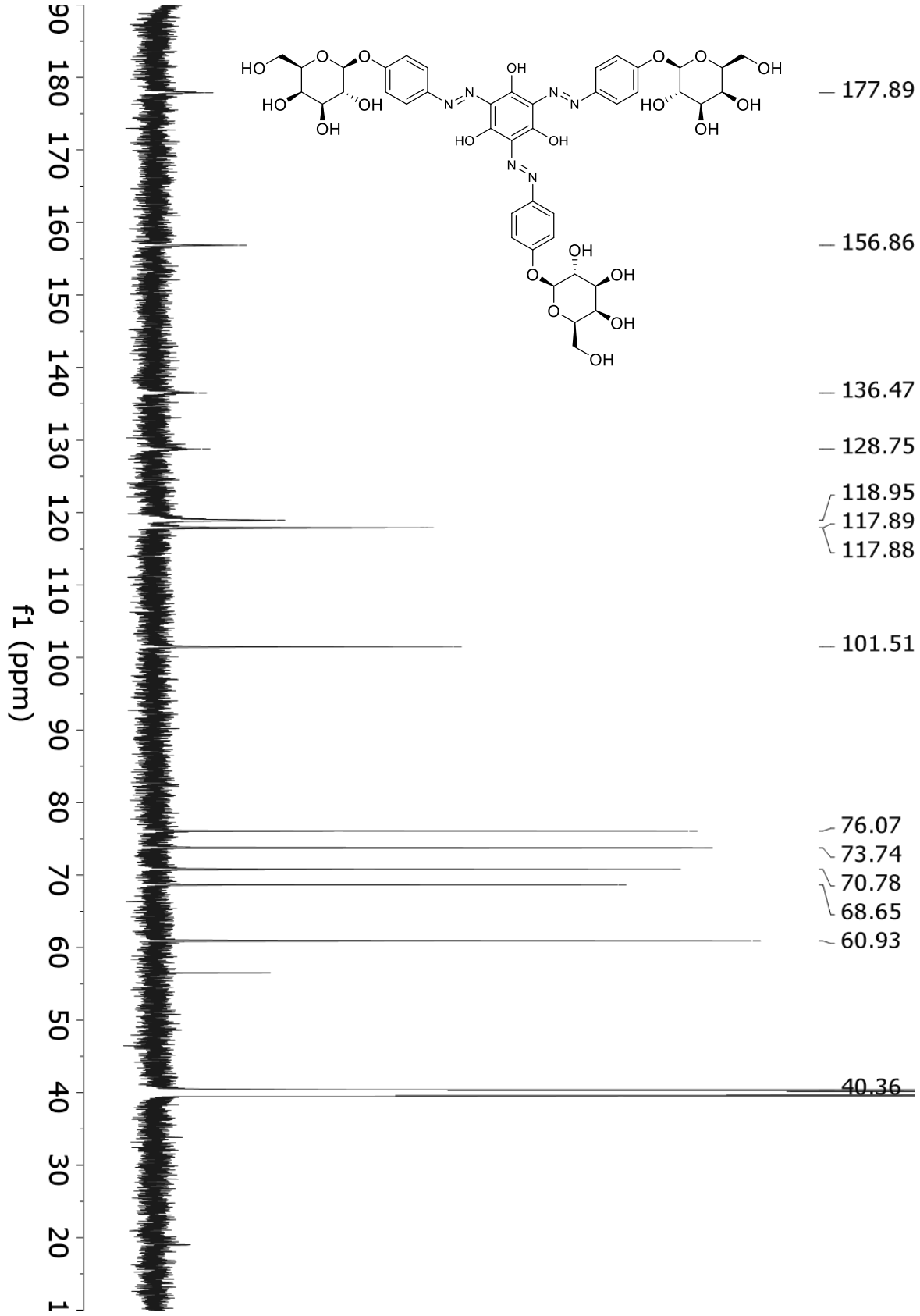
177.89
156.86
136.47
128.75
118.95
117.89
117.88
101.51
76.07
73.74
70.78
68.65
60.93
40.36
f1 (ppm)

(2) β-D-gal Yariv Reagent, R2XM [COSY (600 MHz for ^{1}H, DMSO-d_6)]

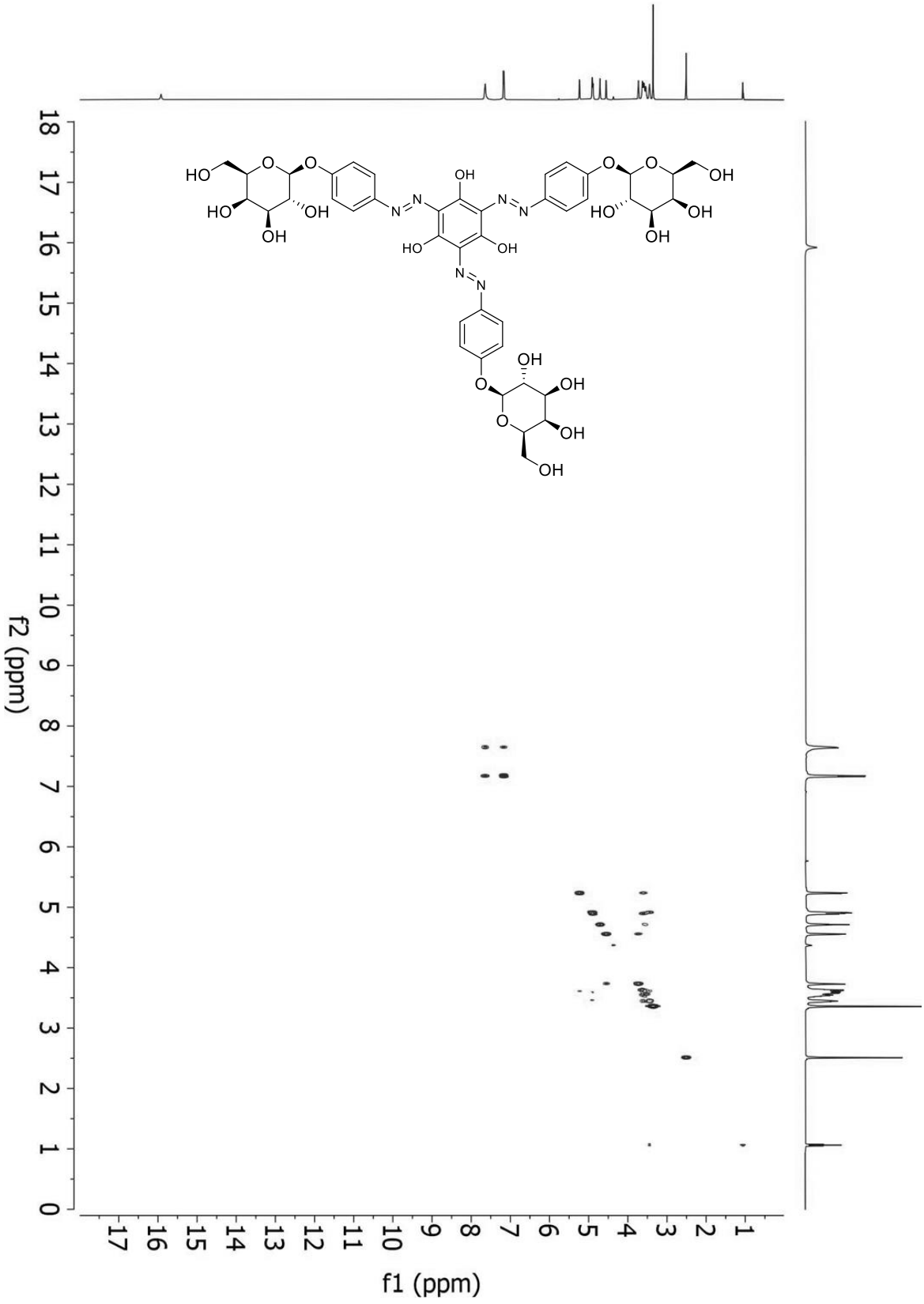

(2) β-D-gal Yariv Reagent, R2XM [COSY (600 MHz for ^{1}H, DMSO-d_6)]

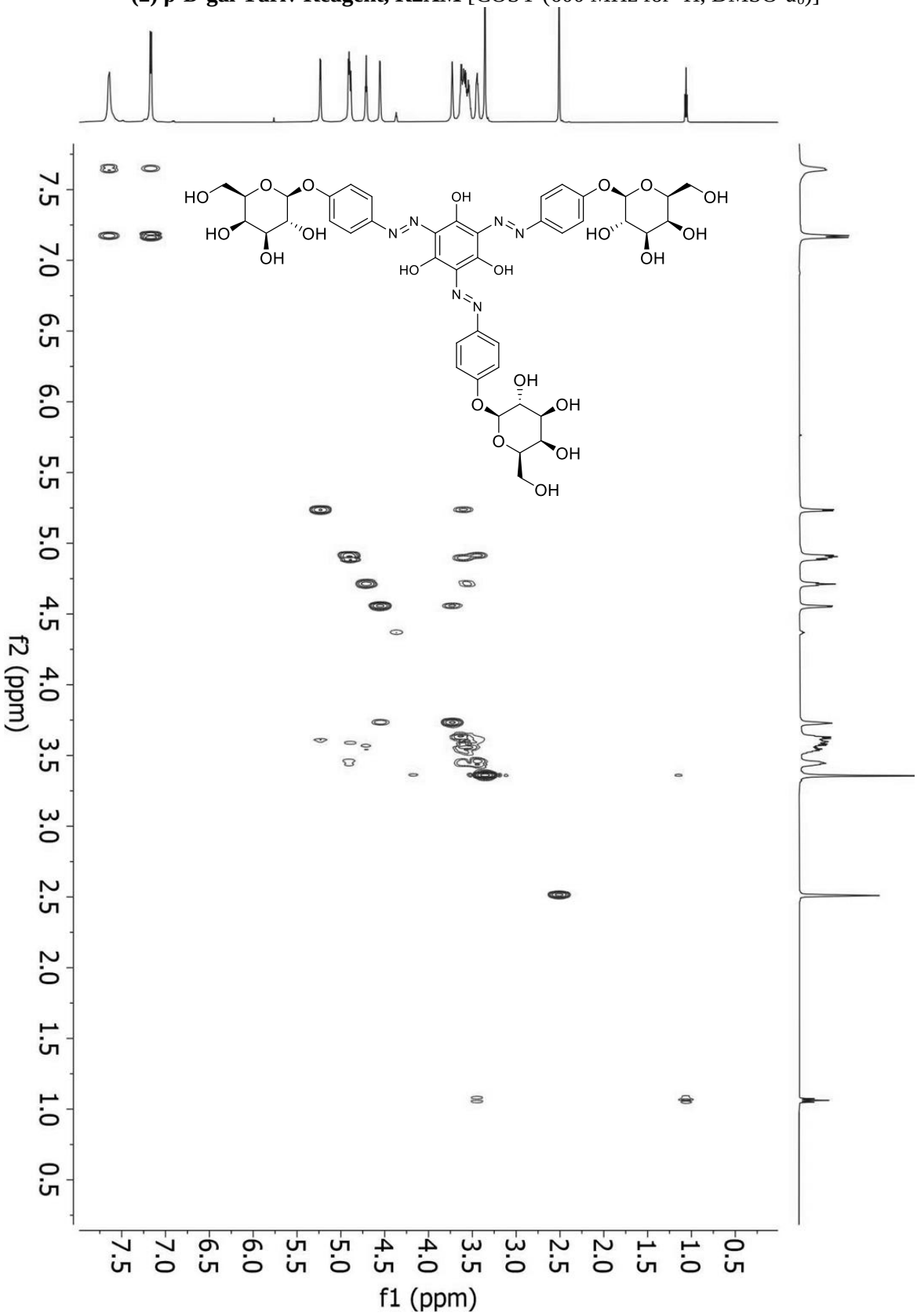

(2) β-D-gal Yariv Reagent, R2XM [HSQC (600 MHz for ^{1}H, DMSO-d_6)]

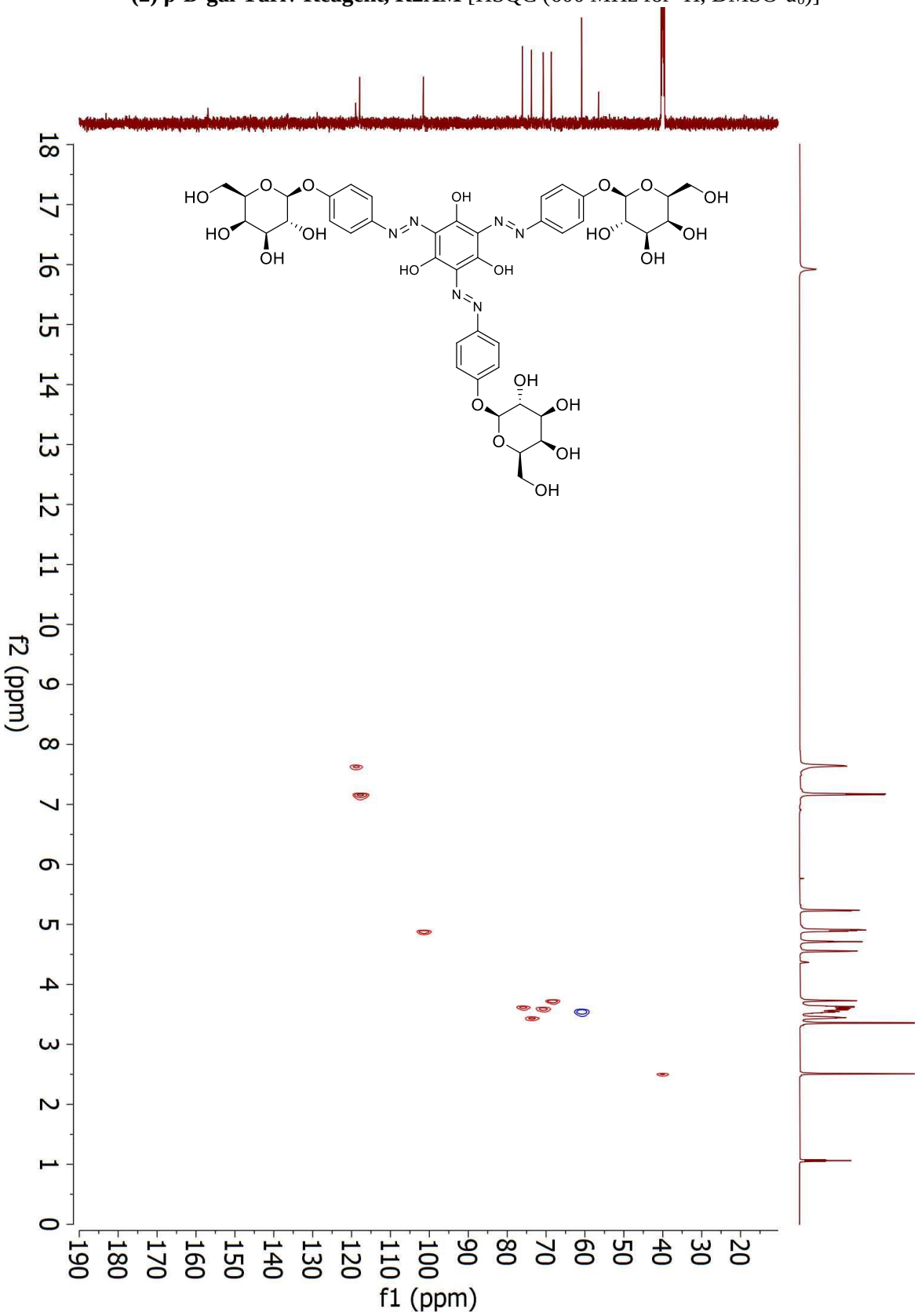

(2) β-D-gal Yariv Reagent, R2XM [HSQC (600 MHz for ^{1}H, DMSO-d_6)]

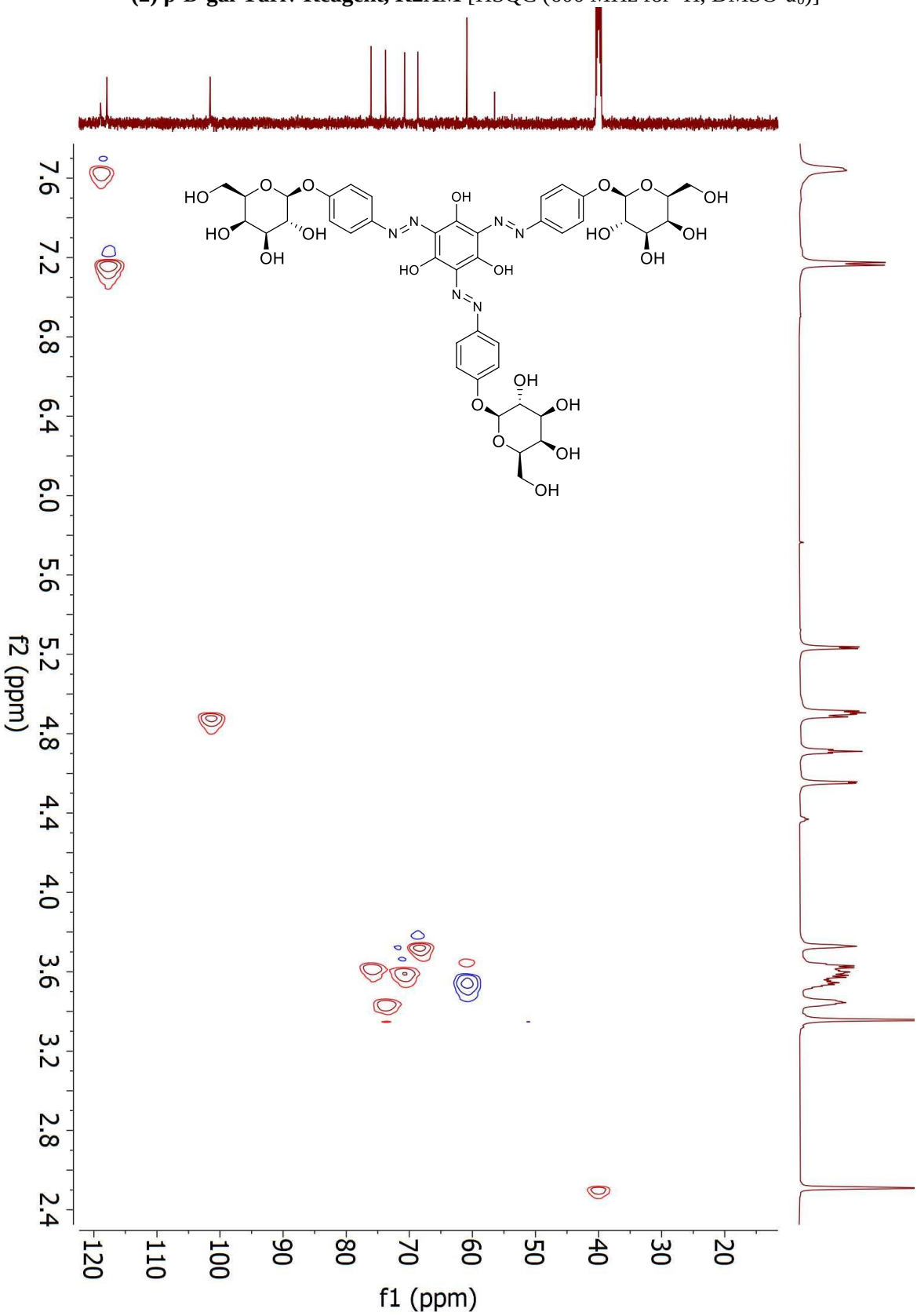

4-aminophenyl β-D-xylopyranoside [^{1}H NMR (600 MHz, DMSO-d_6)]

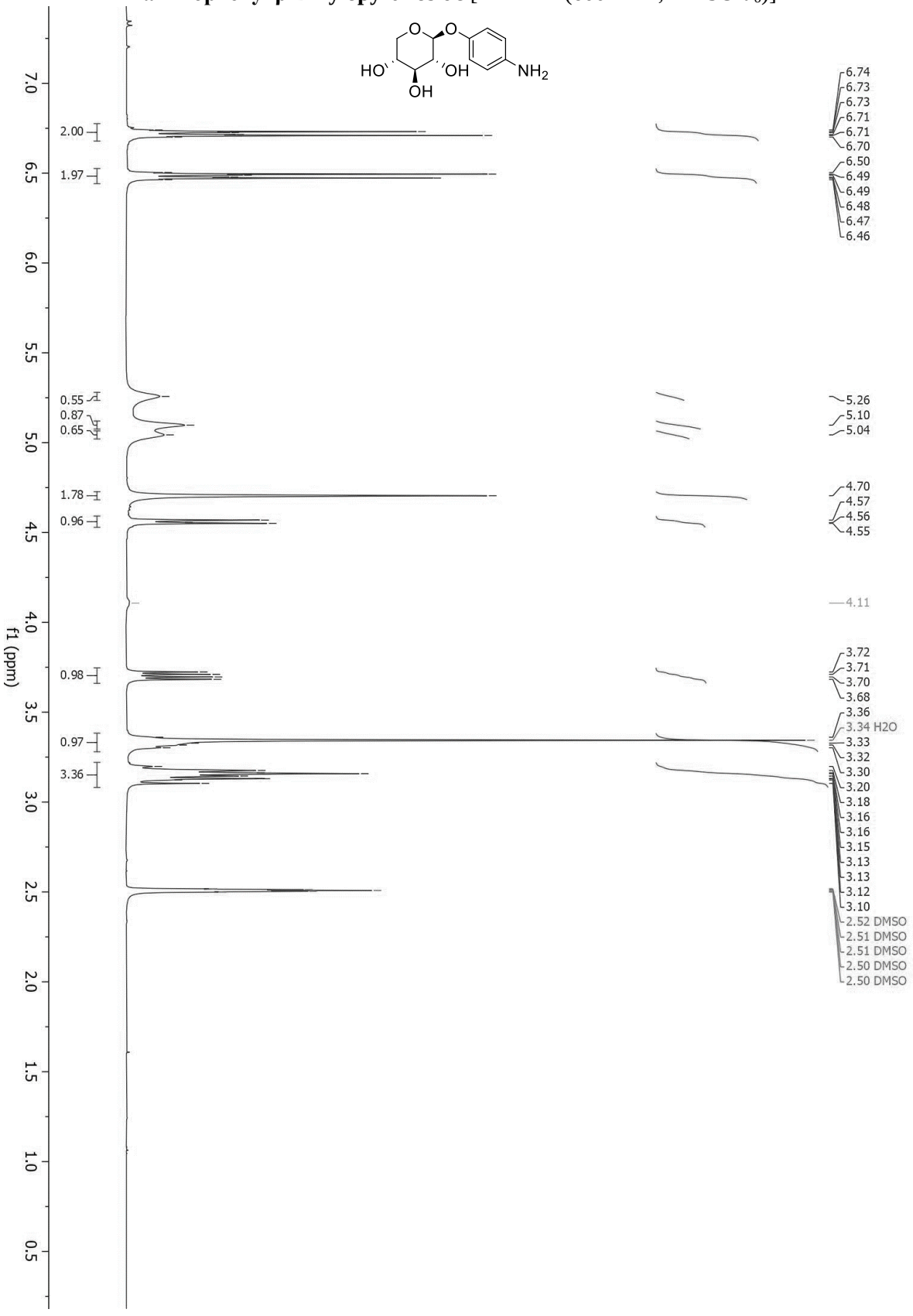

(3) β-D-xyl Yariv Reagent, R2XM2 [^{1}H NMR (600 MHz, DMSO-d_6)]

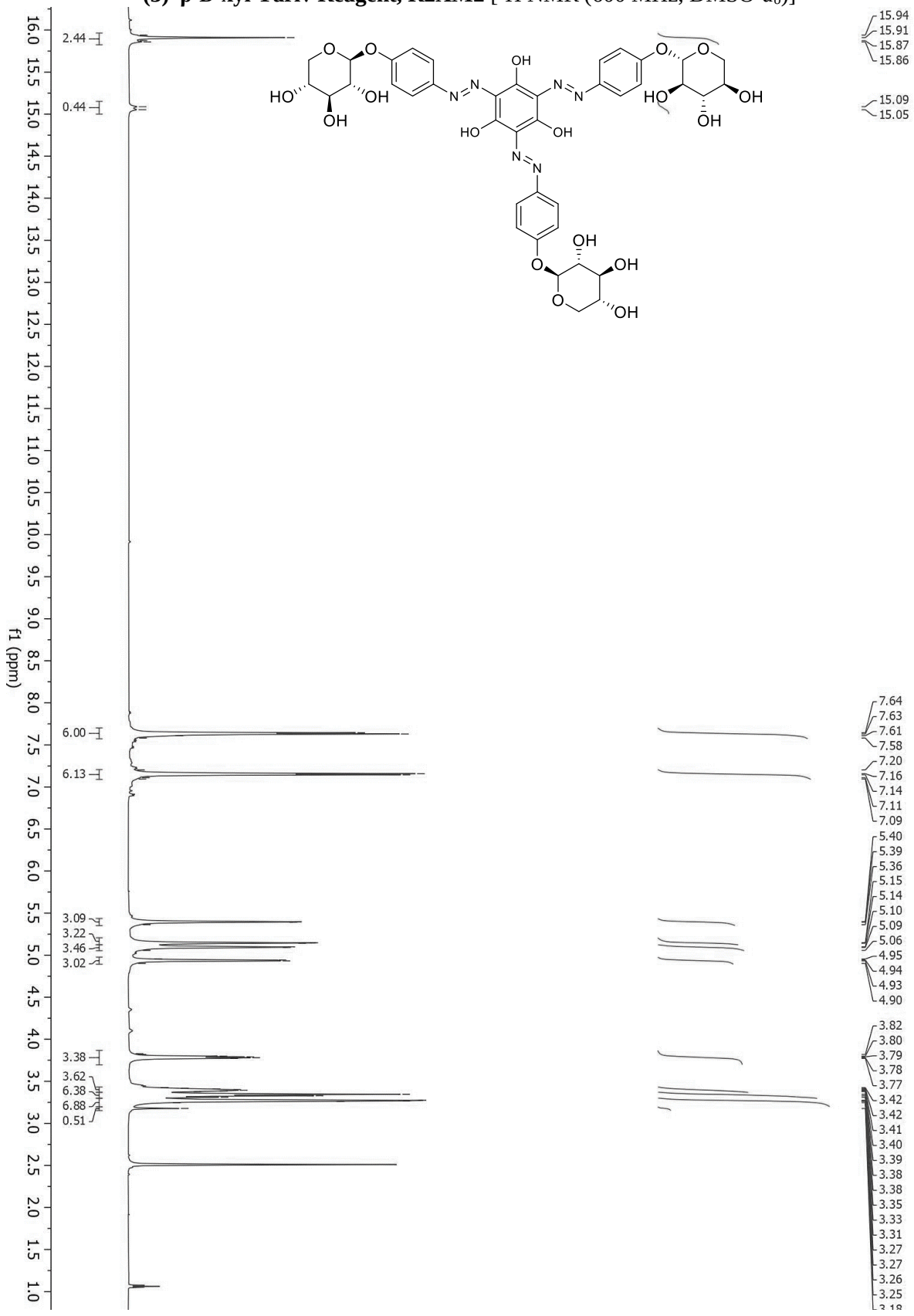

(3) β-D-xyl Yariv Reagent, R2XM2 [^{13}C NMR (151 MHz, DMSO-d_6)]

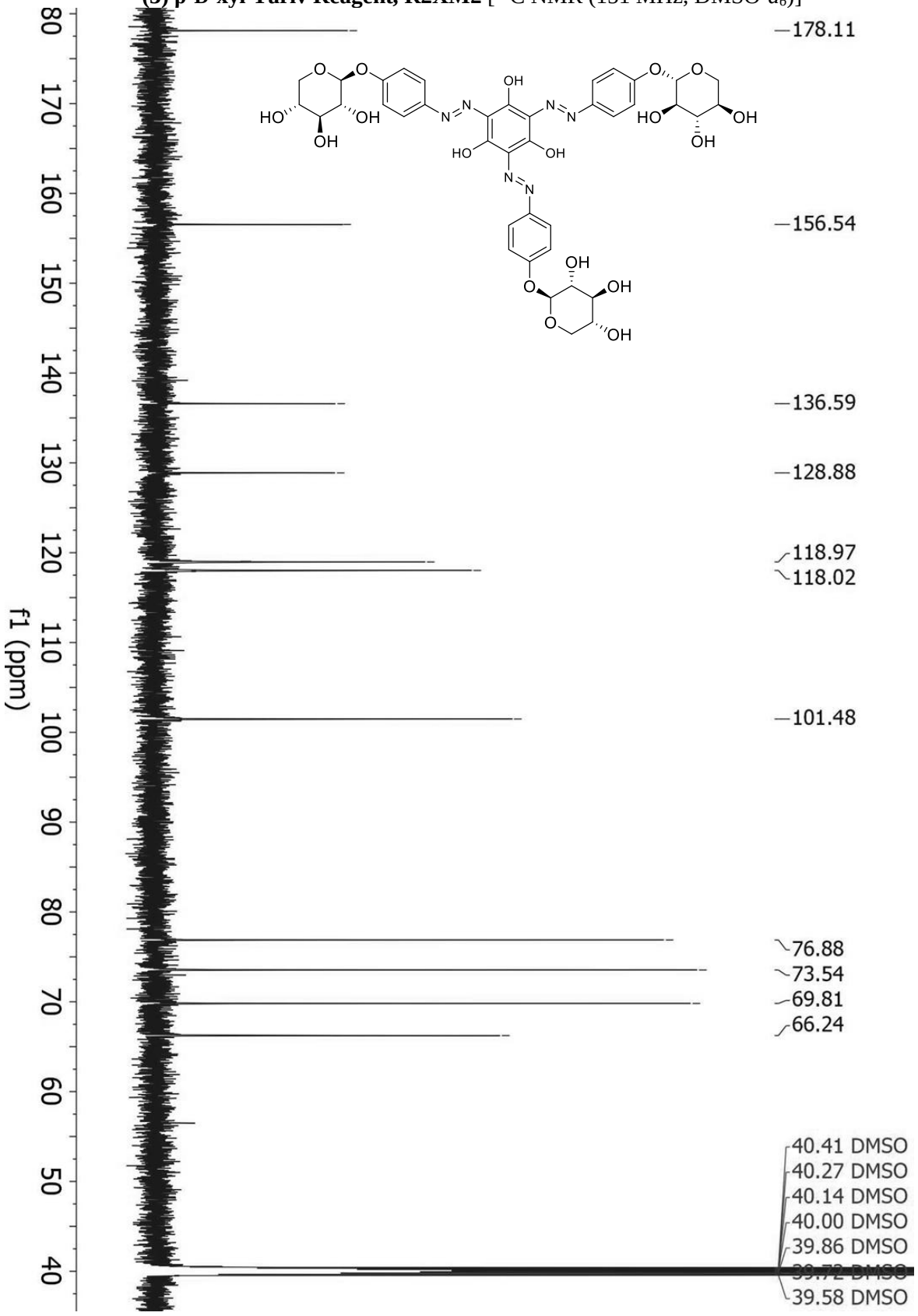

(3) β-D-xyl Yariv Reagent, R2XM2 [COSY (600 MHz for ^{1}H, DMSO-d_6)]

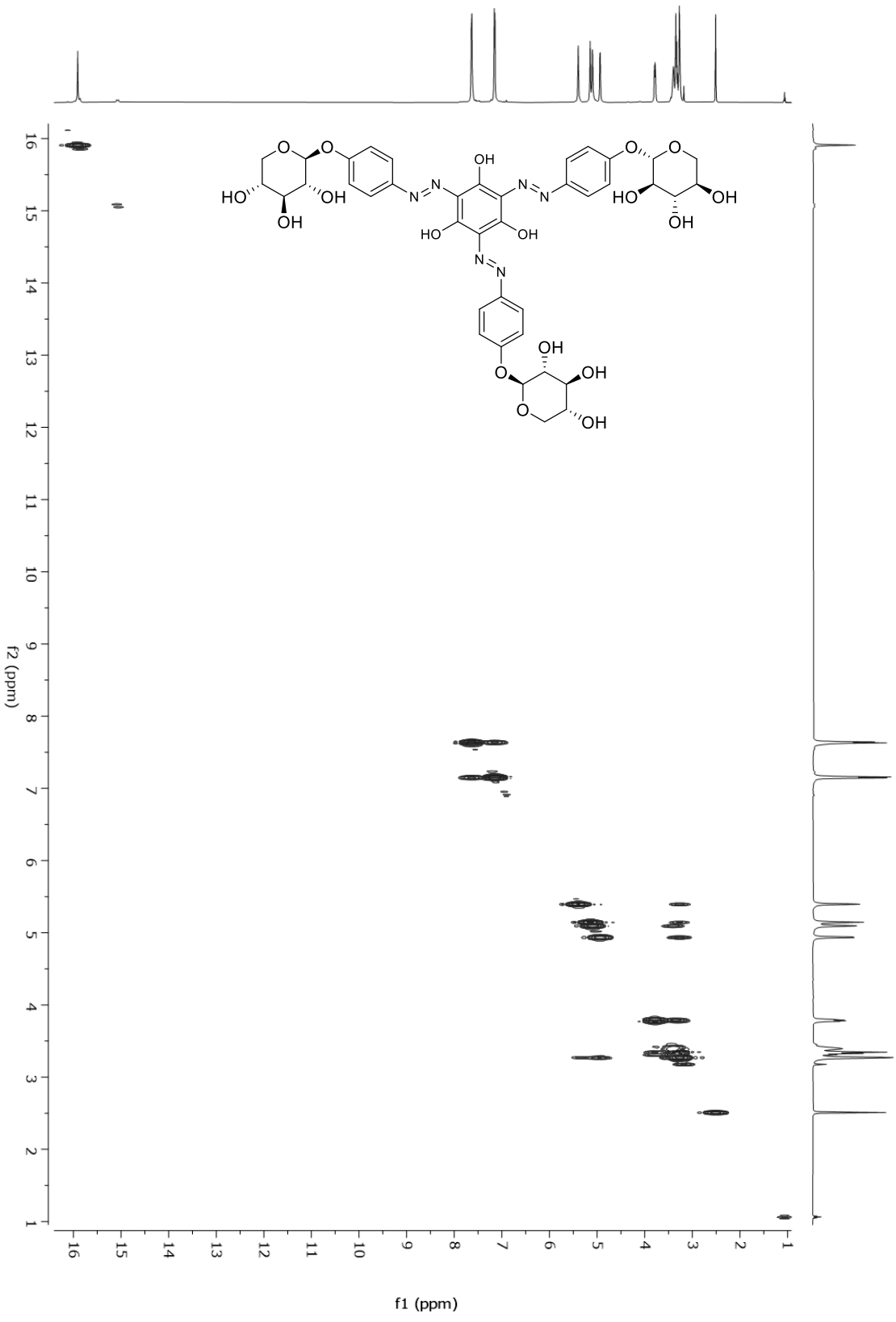

(3) β-D-xyl Yariv Reagent, R2XM2 [COSY (600 MHz for ^{1}H, DMSO-d_6)]

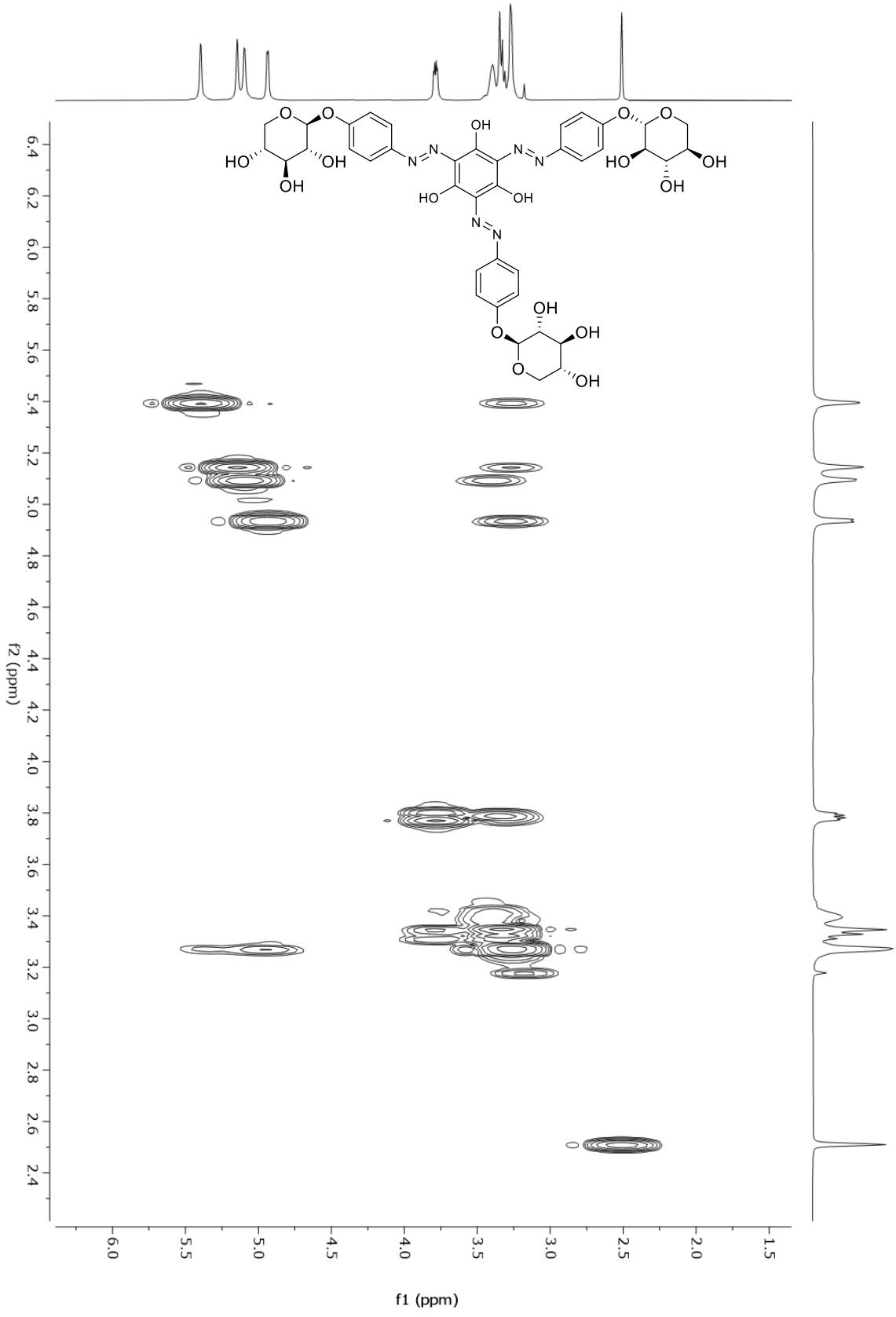

(3) β-D-xyl Yariv Reagent, R2XM2 [HSQC (600 MHz for ^{1}H, DMSO-d_6)]

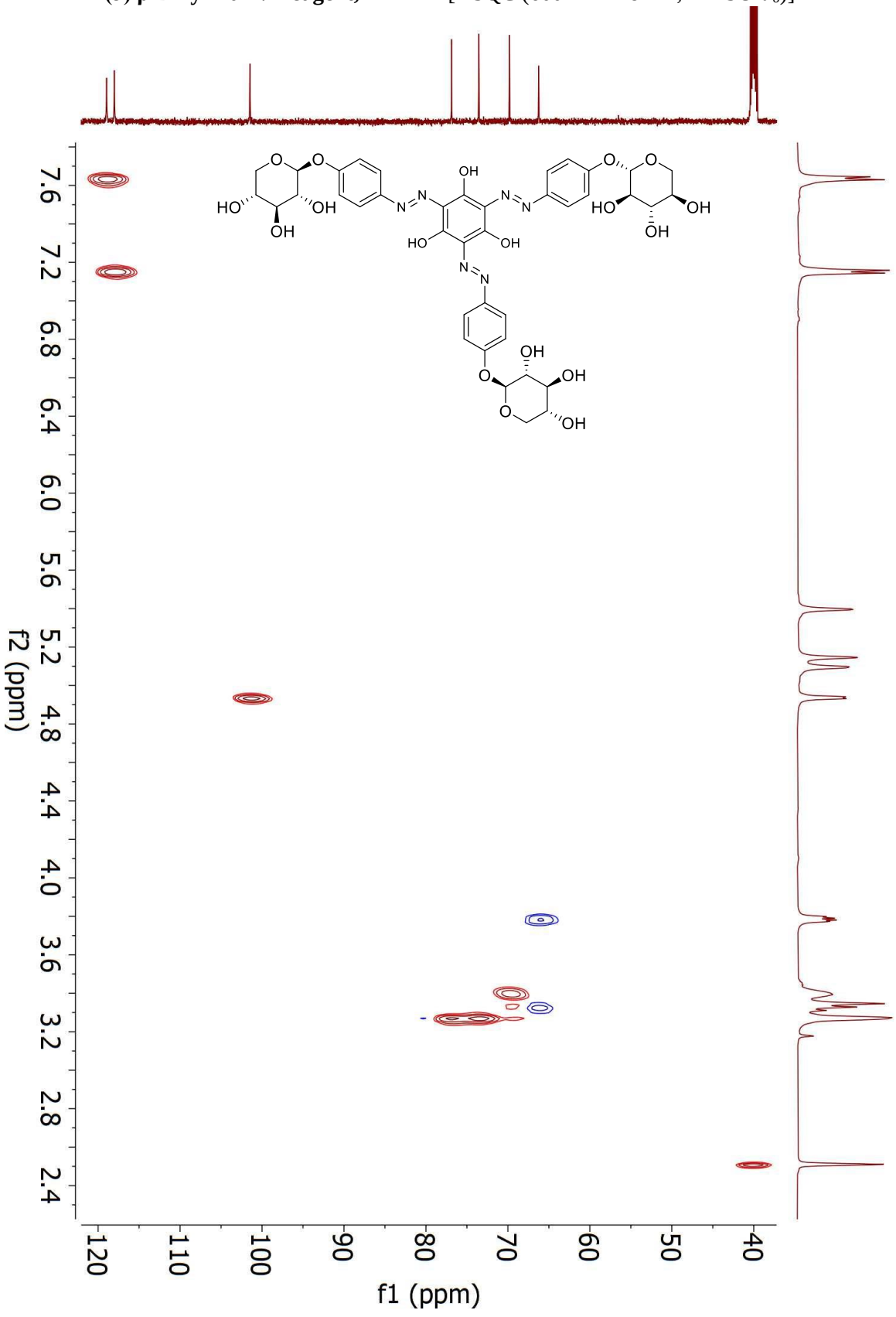

(3) β-D-xyl Yariv Reagent [HSQC (600 MHz for ^{1}H, DMSO-d_6)]

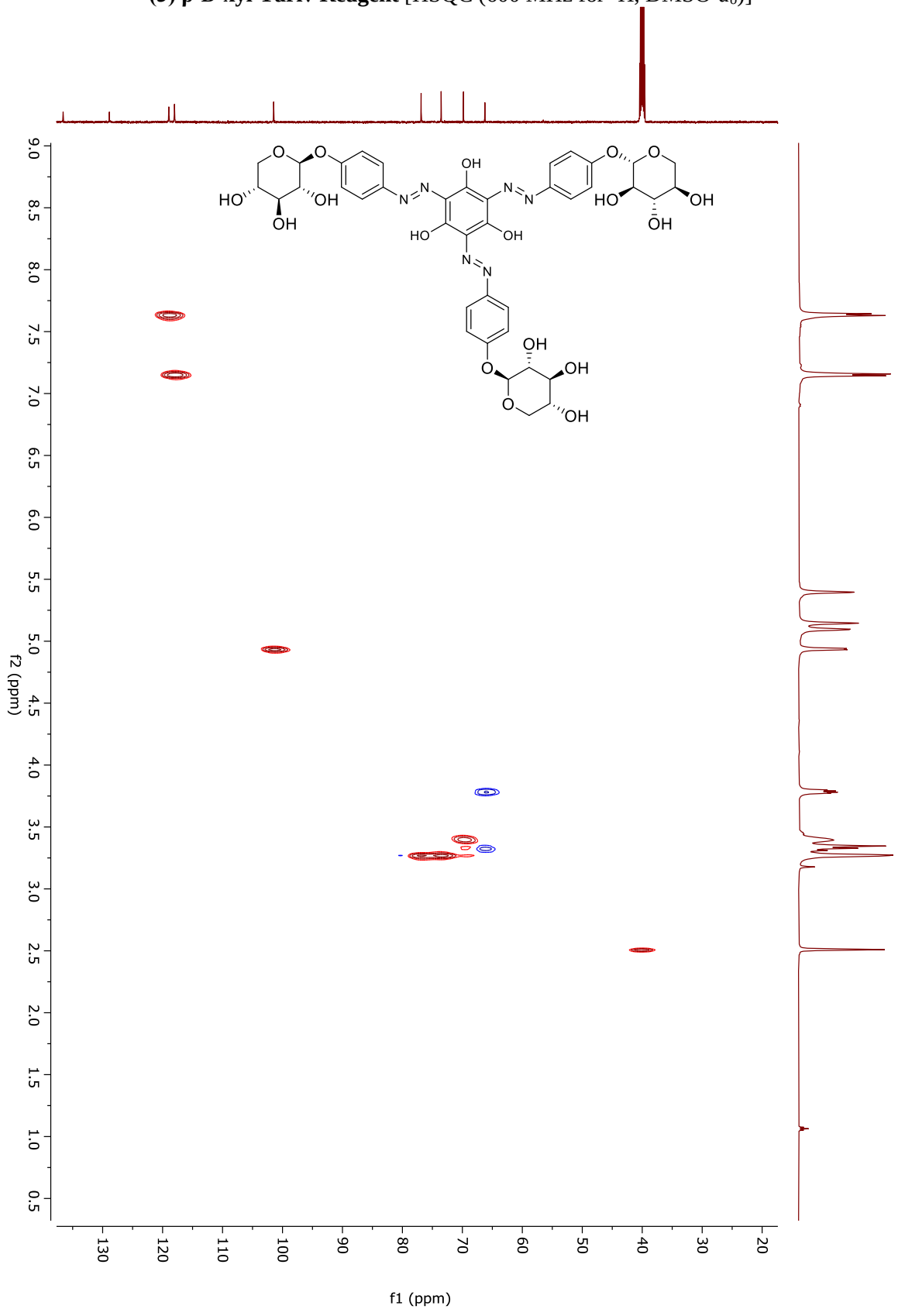

4-aminophenyl β-D-fucopyranoside [^{1}H NMR (600 MHz, DMSO-d_6)]

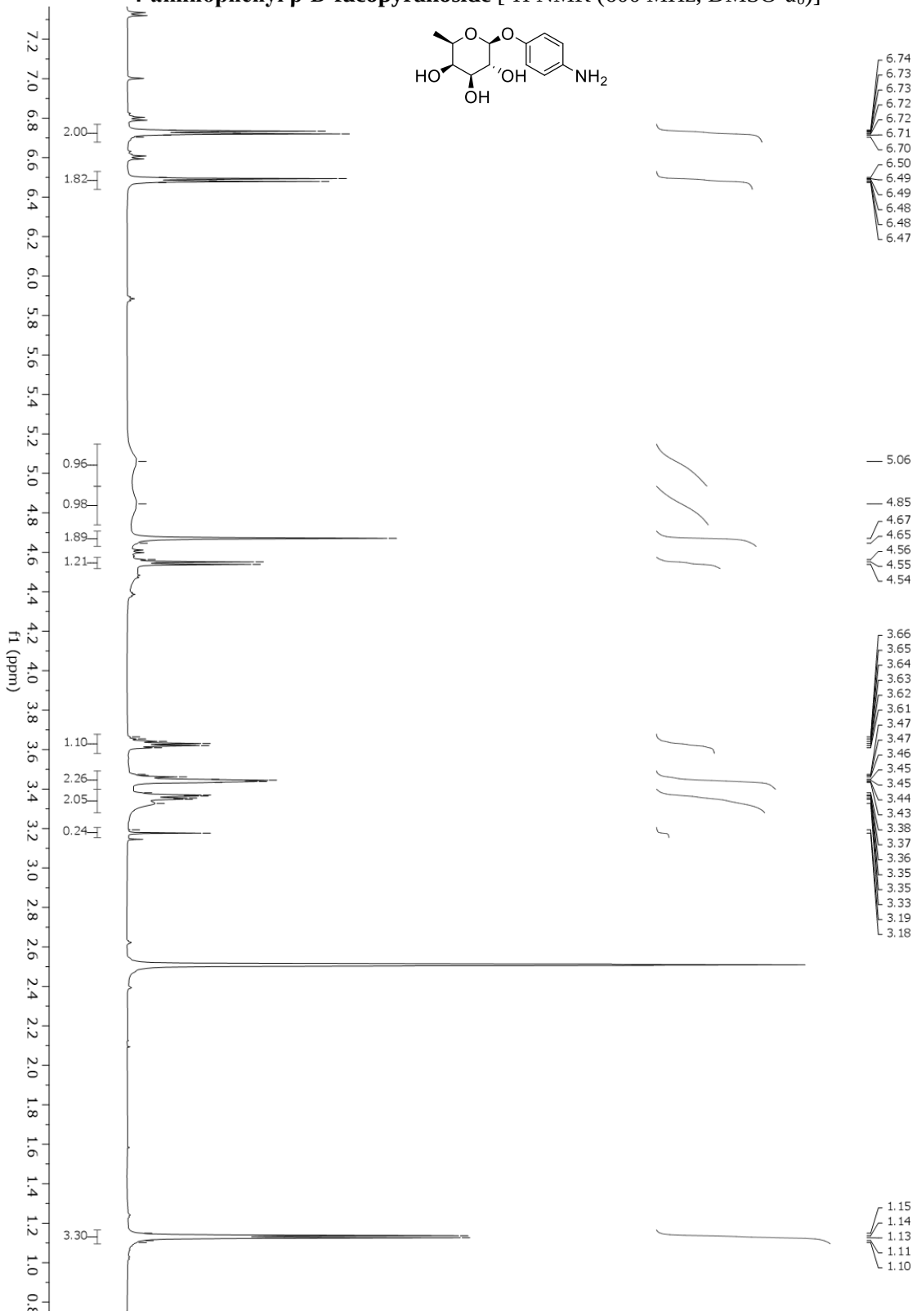

(10) β-D-fuc Yariv Reagent, R2X [^{1}H NMR (600 MHz, DMSO-d_6)]

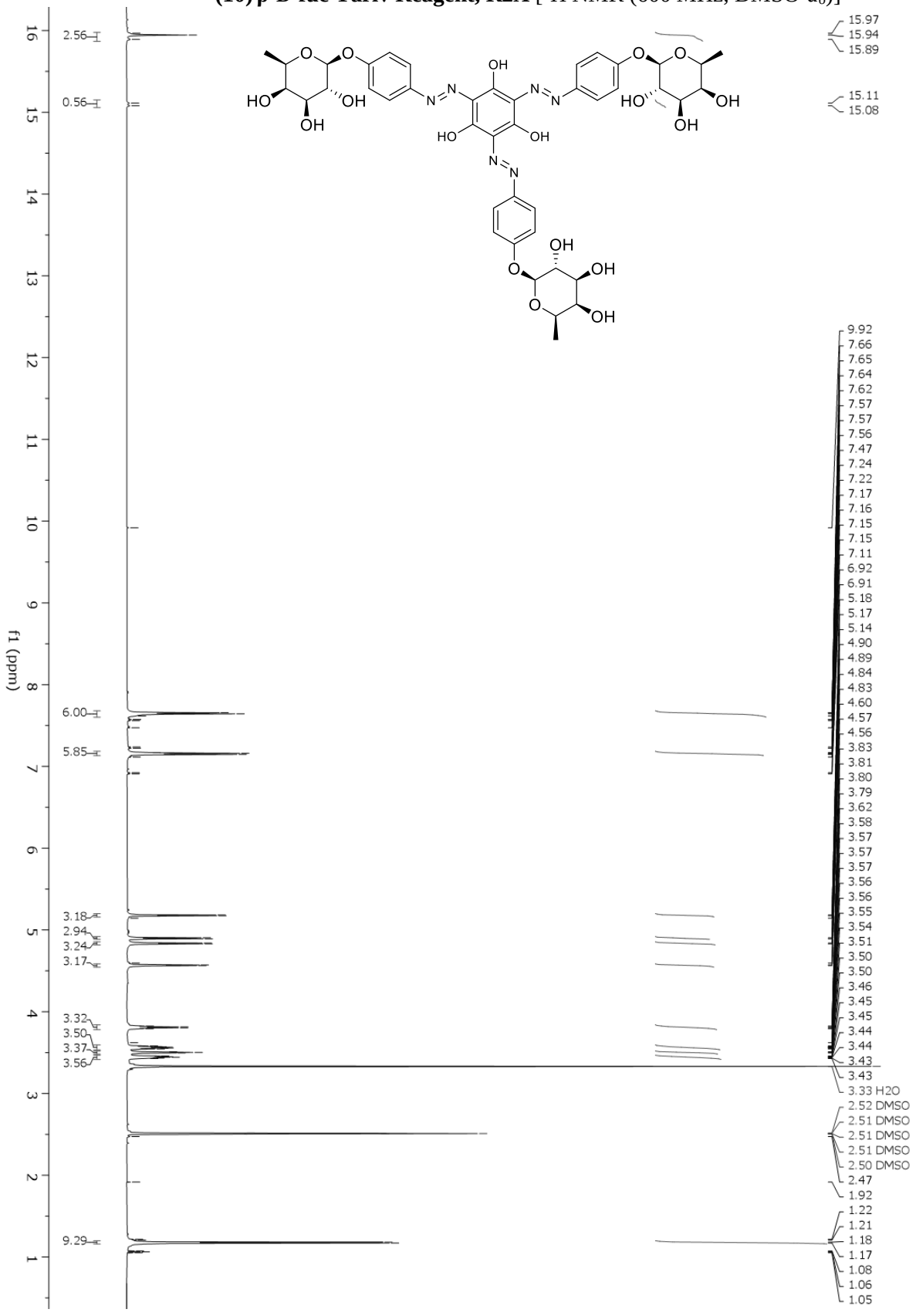

(10) β-D-fuc Yariv Reagent, R2X [^{13}C NMR (151 MHz, DMSO-d_6)]

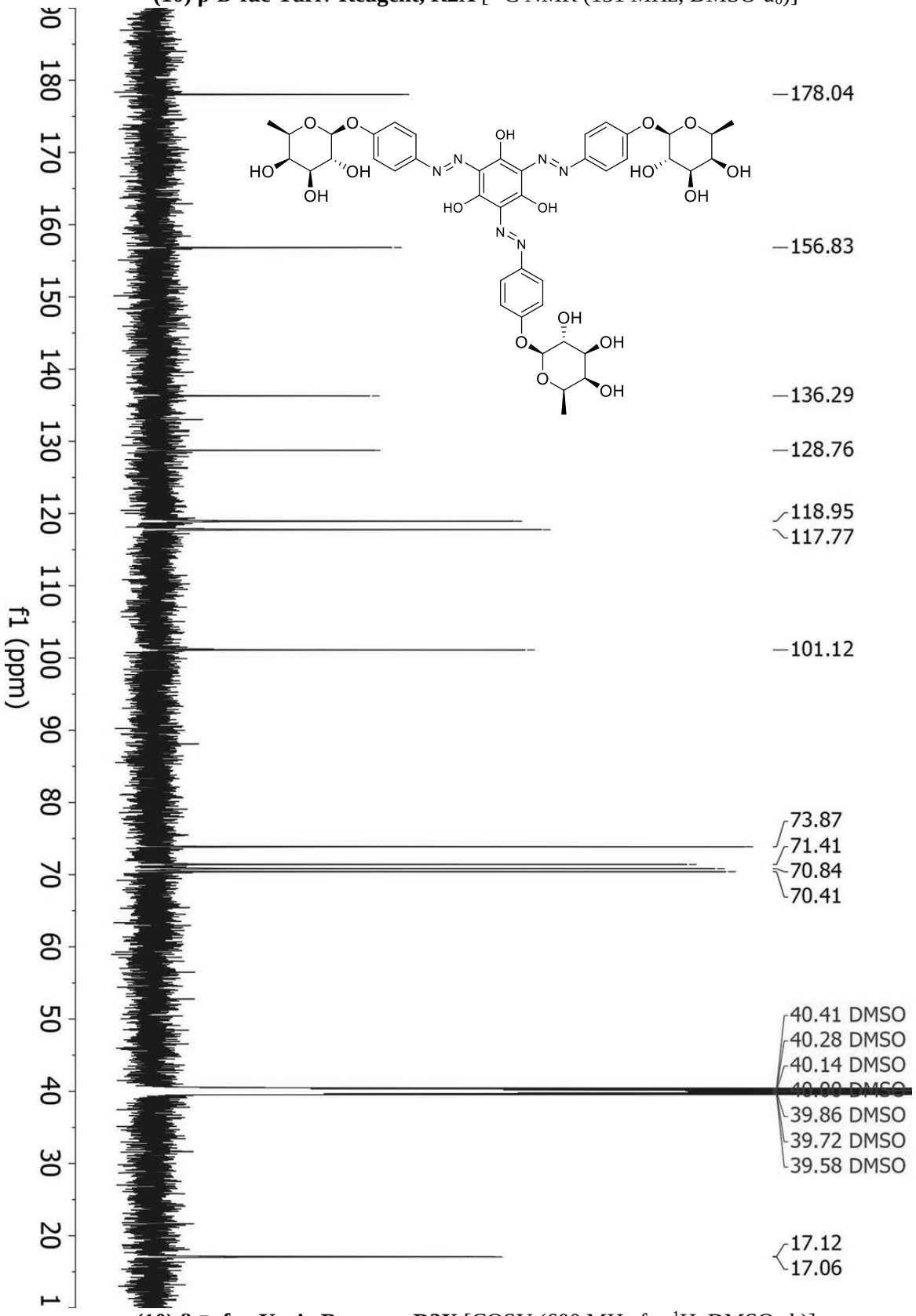

(10) β-D-fuc Yariv Reagent, R2X [COSY (600 MHz for ^{1}H, DMSO-d_6)]

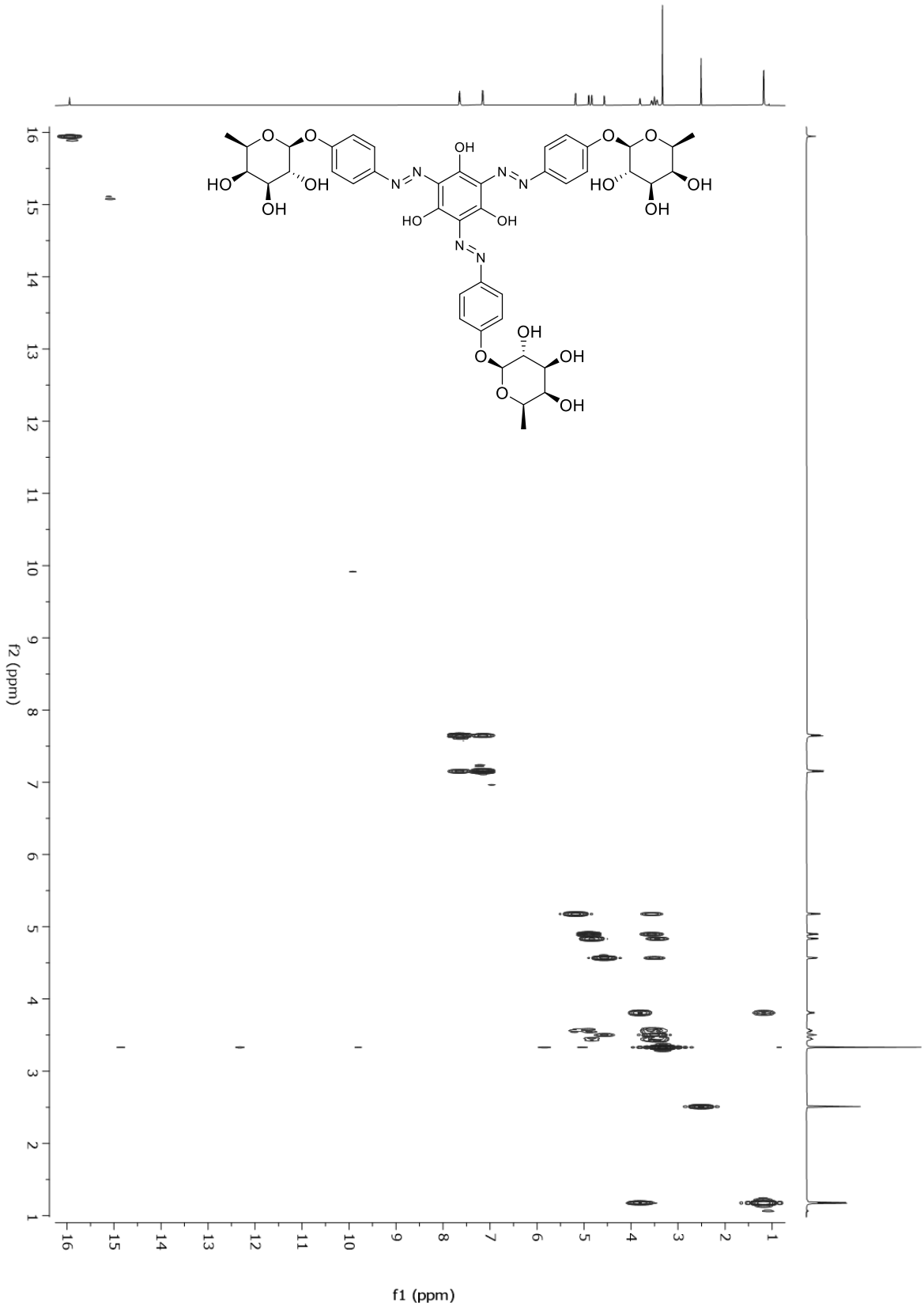
f2 (ppm)
f1 (ppm)
HO
OH
O
N=N

(10) β-D-fuc Yariv Reagent, R2X [COSY (600 MHz for ^{1}H, DMSO-d_6)]

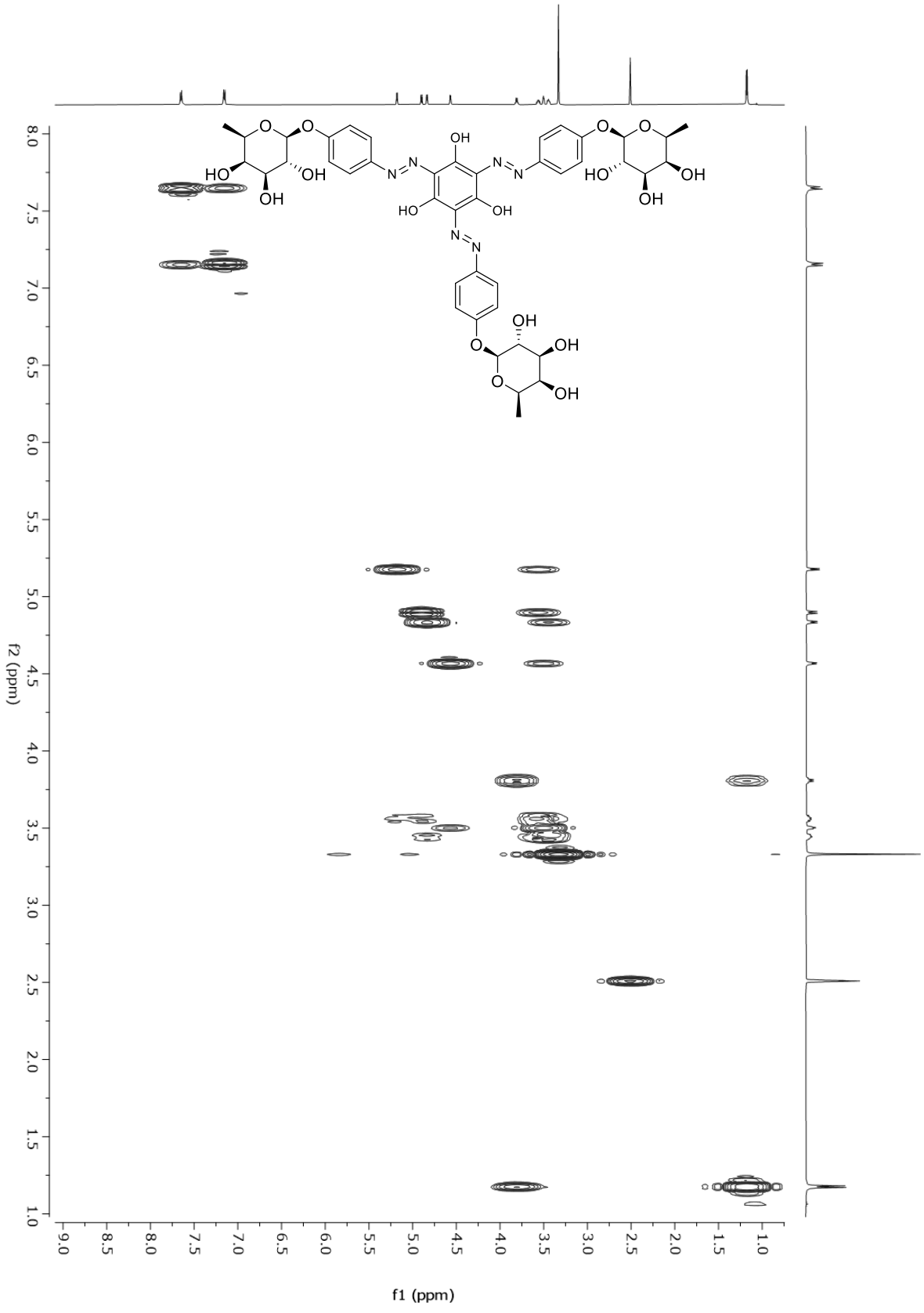

(10) β-D-fuc Yariv Reagent, R2X [HSQC (600 MHz for ^{1}H, DMSO-d_6)]

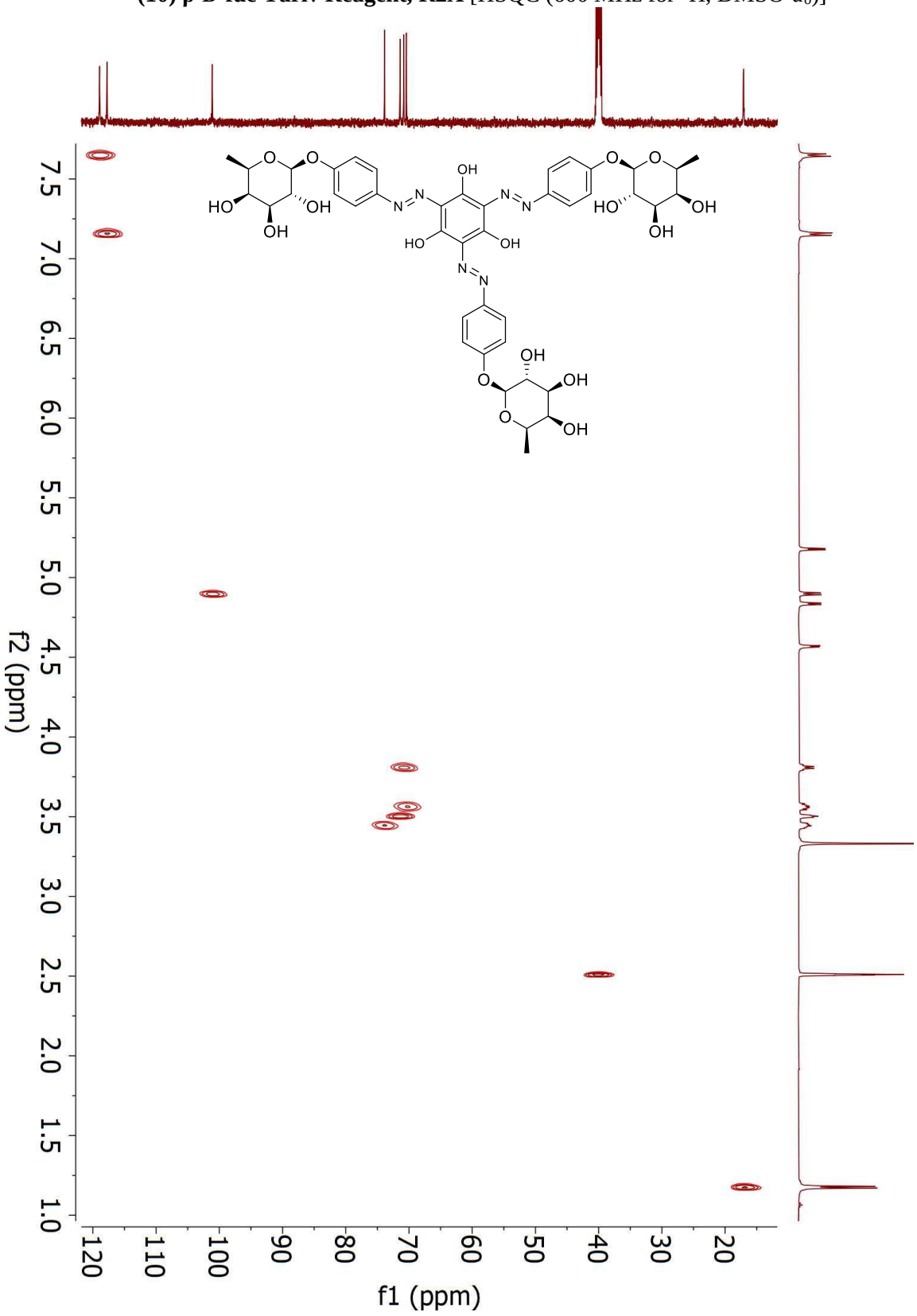

(10) β-D-fuc Yariv Reagent, R2X [HSQC (600 MHz for ^{1}H, DMSO-d_6)]

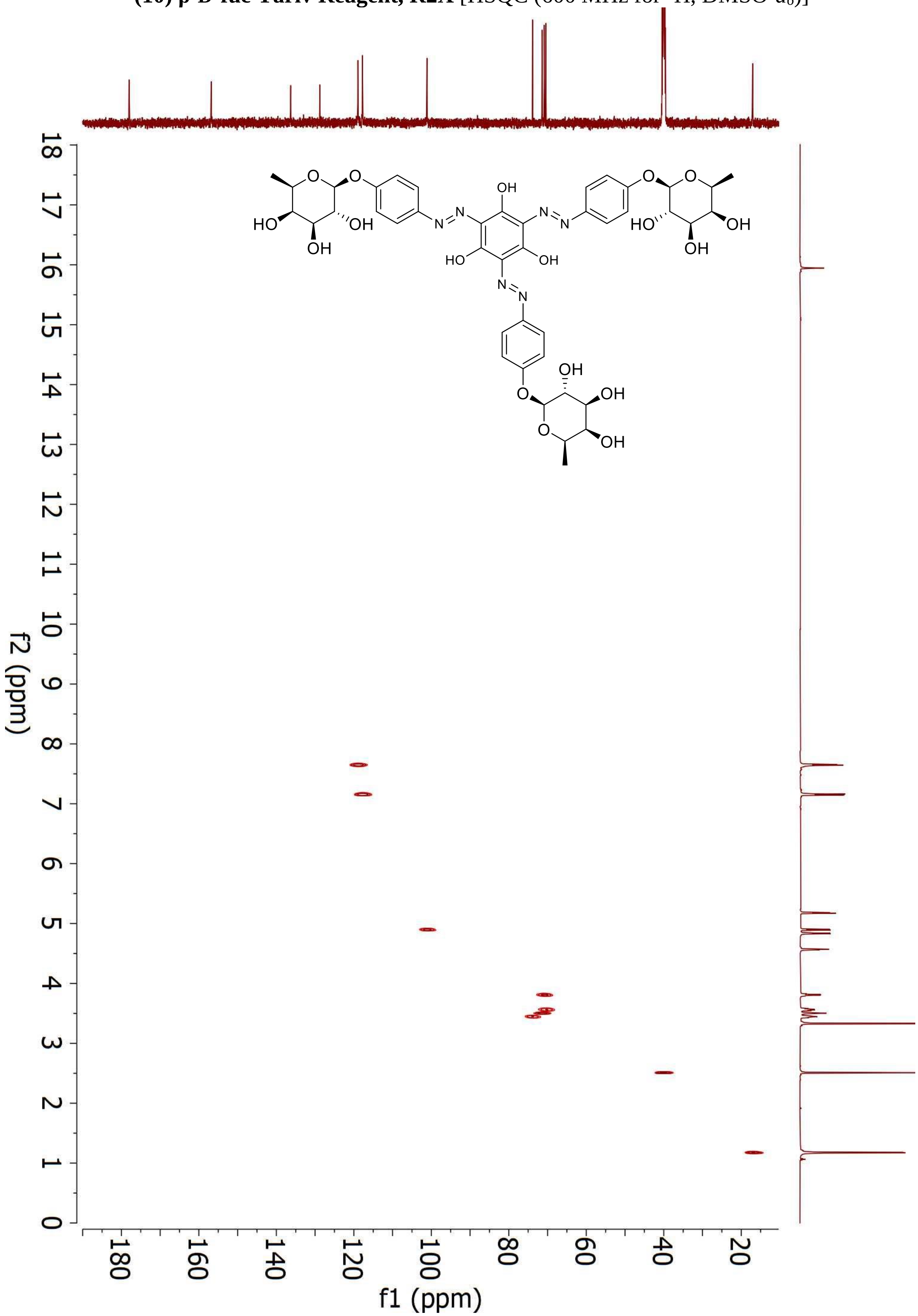

4-aminophenyl α-L-fucopyranoside [^{1}H NMR (400 MHz, DMSO-d_6)]

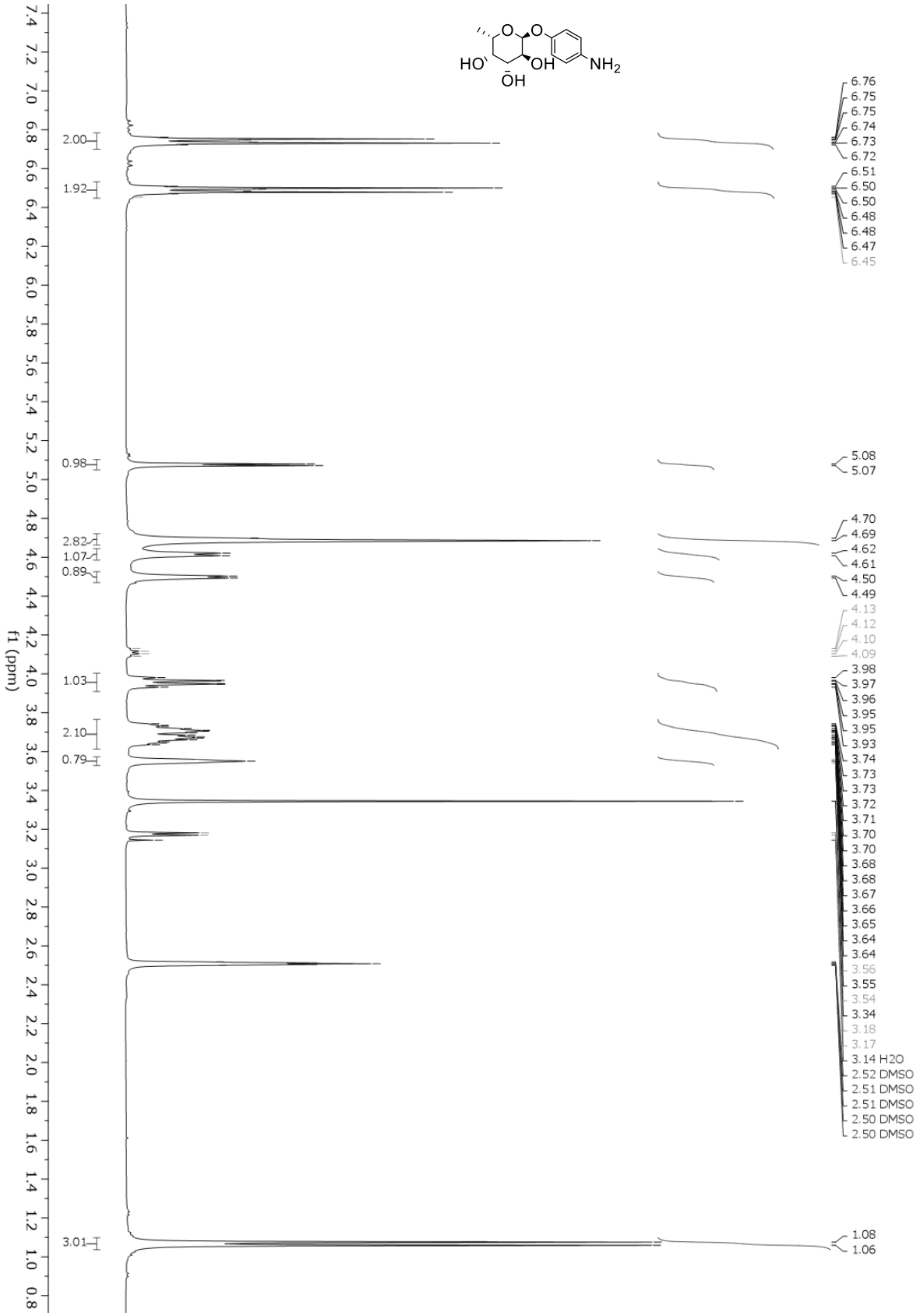
f1 (ppm)
2.00
1.92
0.98
2.82
1.07
0.89
1.03
2.10
0.79
3.01
6.76
6.75
6.75
6.74
6.73
6.72
6.51
6.50
6.50
6.48
6.48
6.47
6.45
5.08
5.07
4.70
4.69
4.62
4.61
4.50
4.49
4.13
4.12
4.10
4.09
3.98
3.97
3.96
3.95
3.95
3.93
3.74
3.73
3.73
3.72
3.71
3.70
3.70
3.68
3.68
3.67
3.66
3.65
3.64
3.64
3.56
3.55
3.54
3.34
3.18
3.17
3.14 H2O
2.52 DMSO
2.51 DMSO
2.51 DMSO
2.50 DMSO
2.50 DMSO
1.08
1.06

(7) α-L-fuc Yariv Reagent, R2XM [^{1}H NMR (600 MHz, DMSO-d_6)]

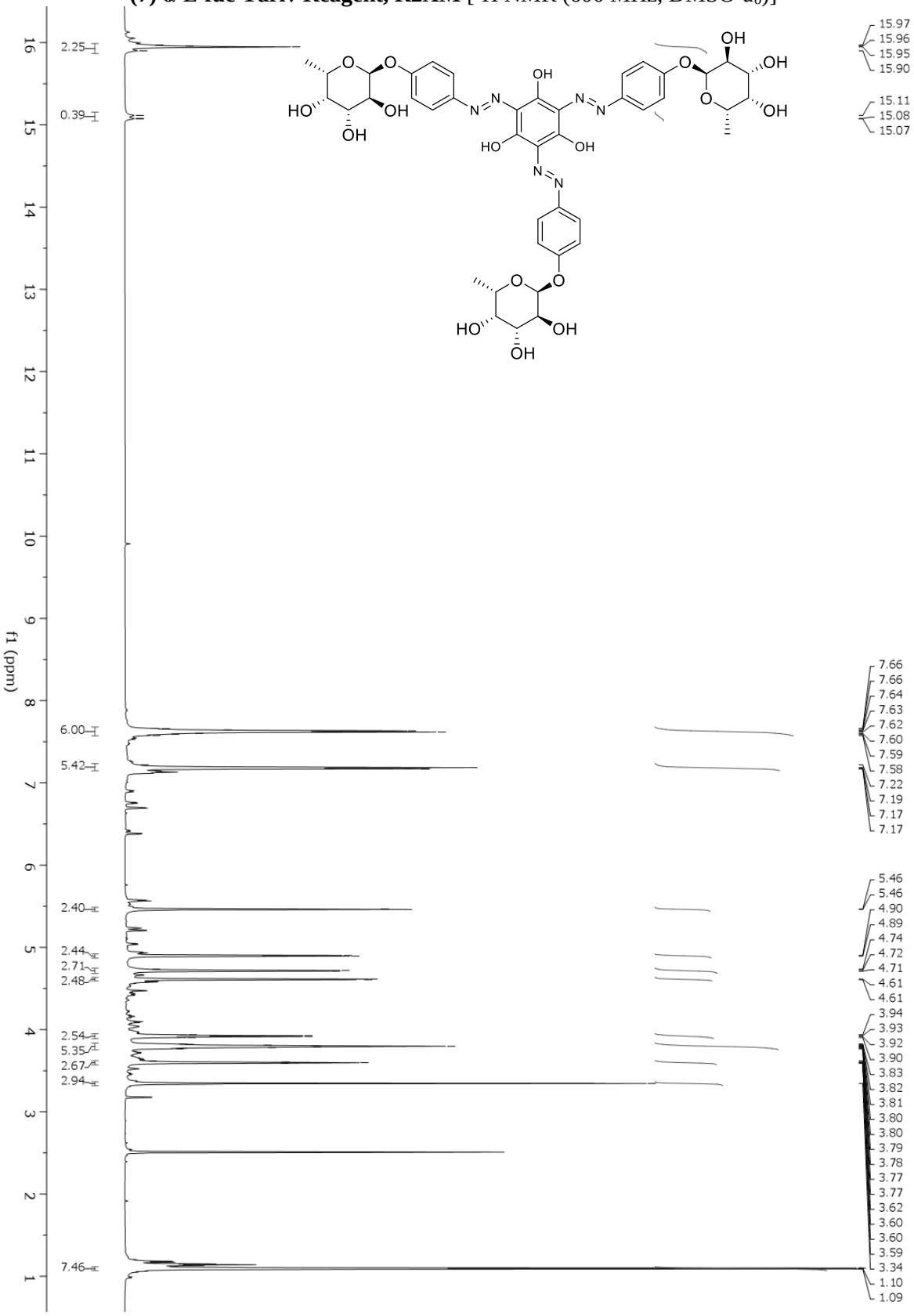

(7) α-L-fuc Yariv Reagent, R2XM [^{13}C NMR (151 MHz, DMSO-d_6)]

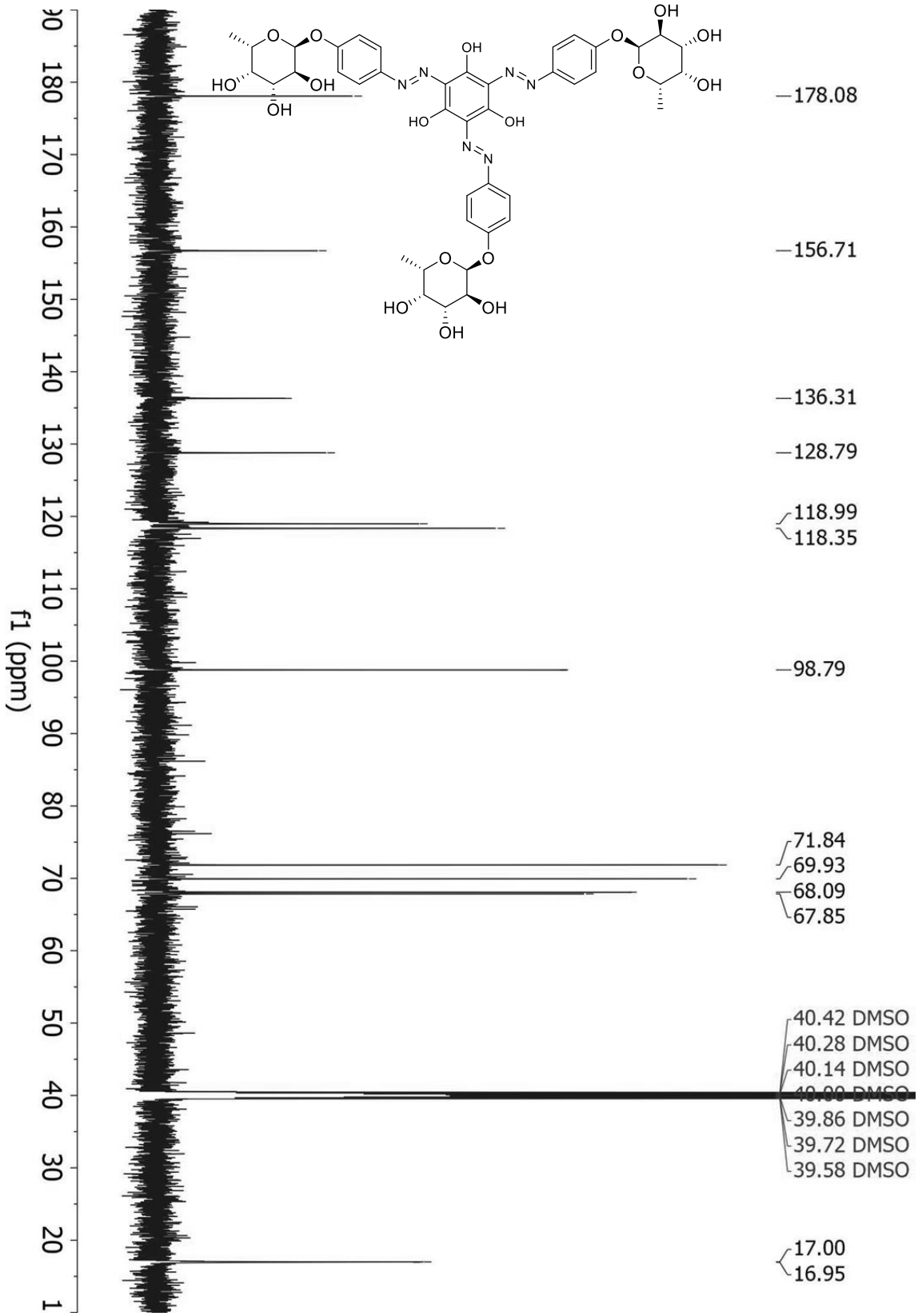

(7) α-L-fuc Yariv Reagent, R2XM [COSY (600 MHz for ^{1}H, DMSO-d_6)]

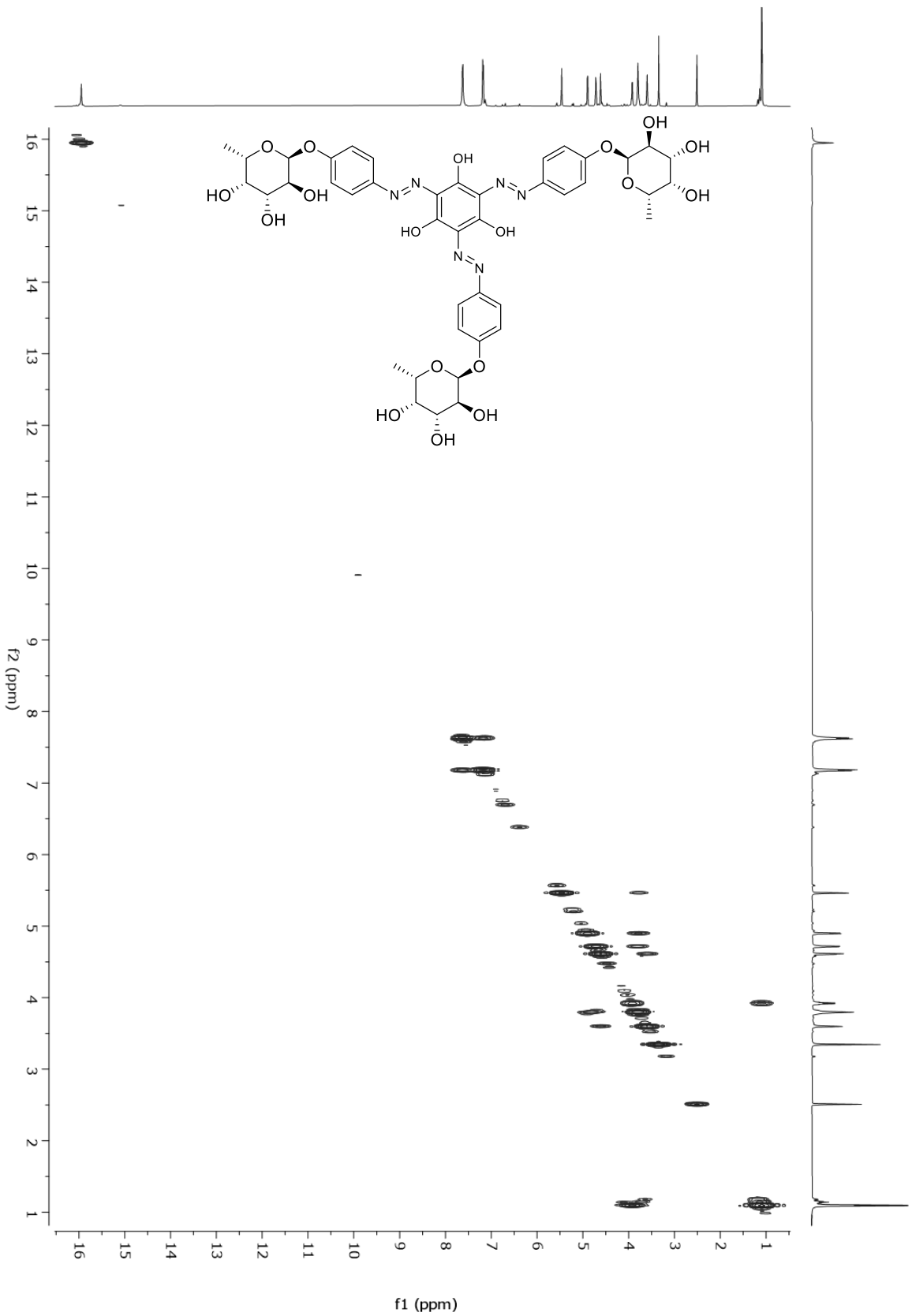

(5) α-L-fuc Yariv Reagent, R2XM [COSY (600 MHz for ^{1}H, DMSO-d_6)]

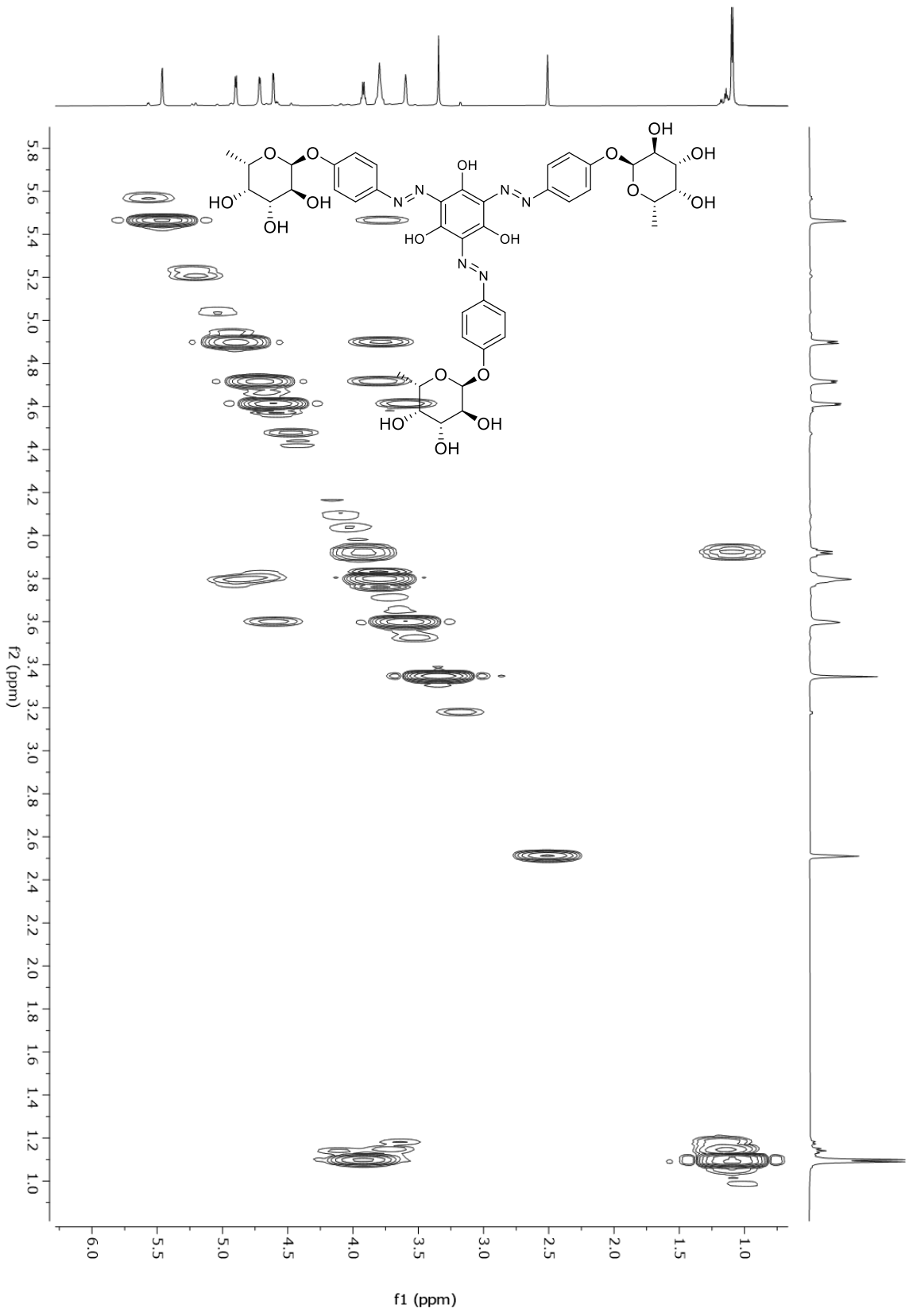
f2 (ppm)
f1 (ppm)

(7) α-L-fuc Yariv Reagent, R2XM [HSQC (600 MHz for ^{1}H, DMSO-d_6)]

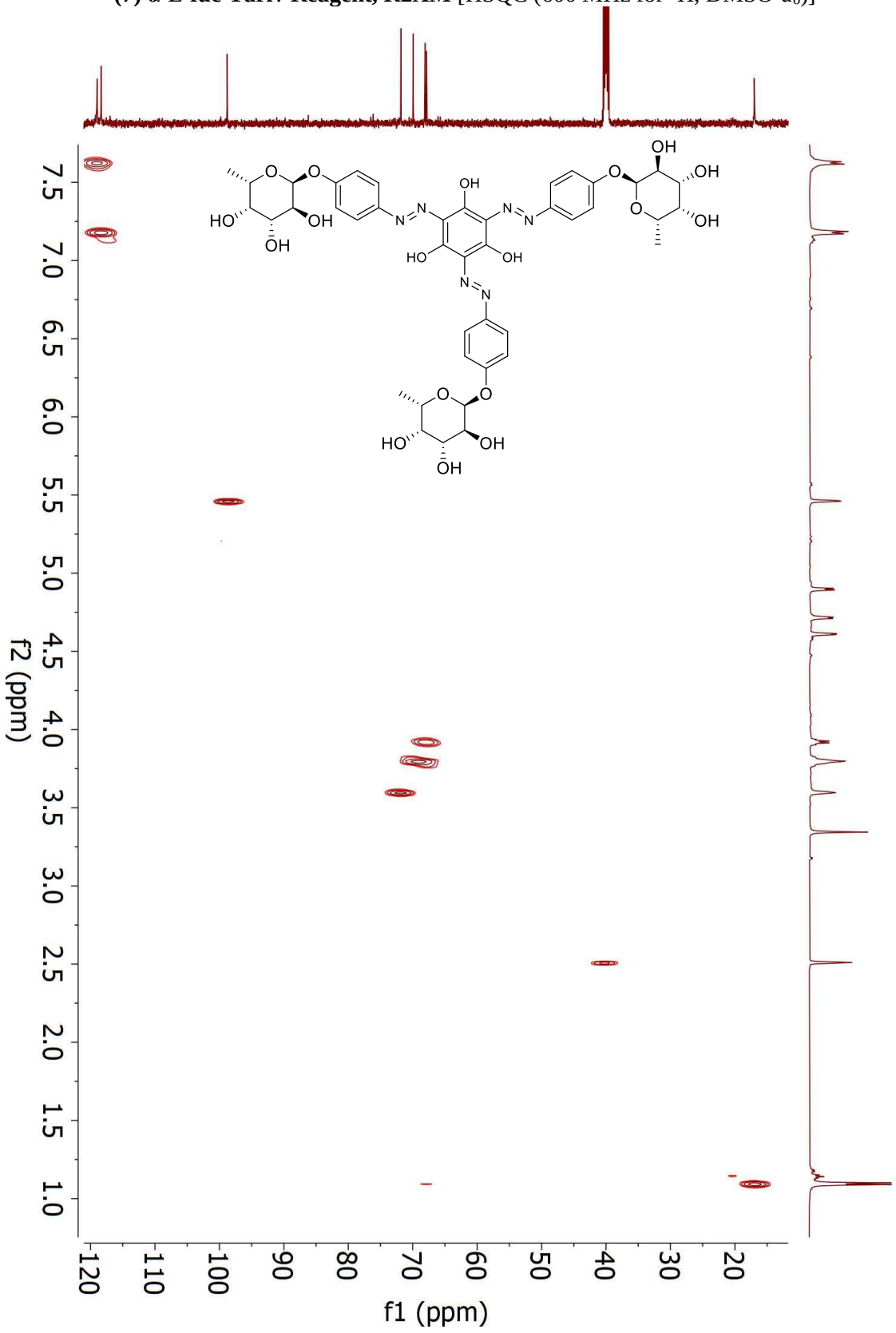

(7) α-L-fuc Yariv Reagent, R2XM [HSQC (600 MHz for ^{1}H, DMSO-d_6)]

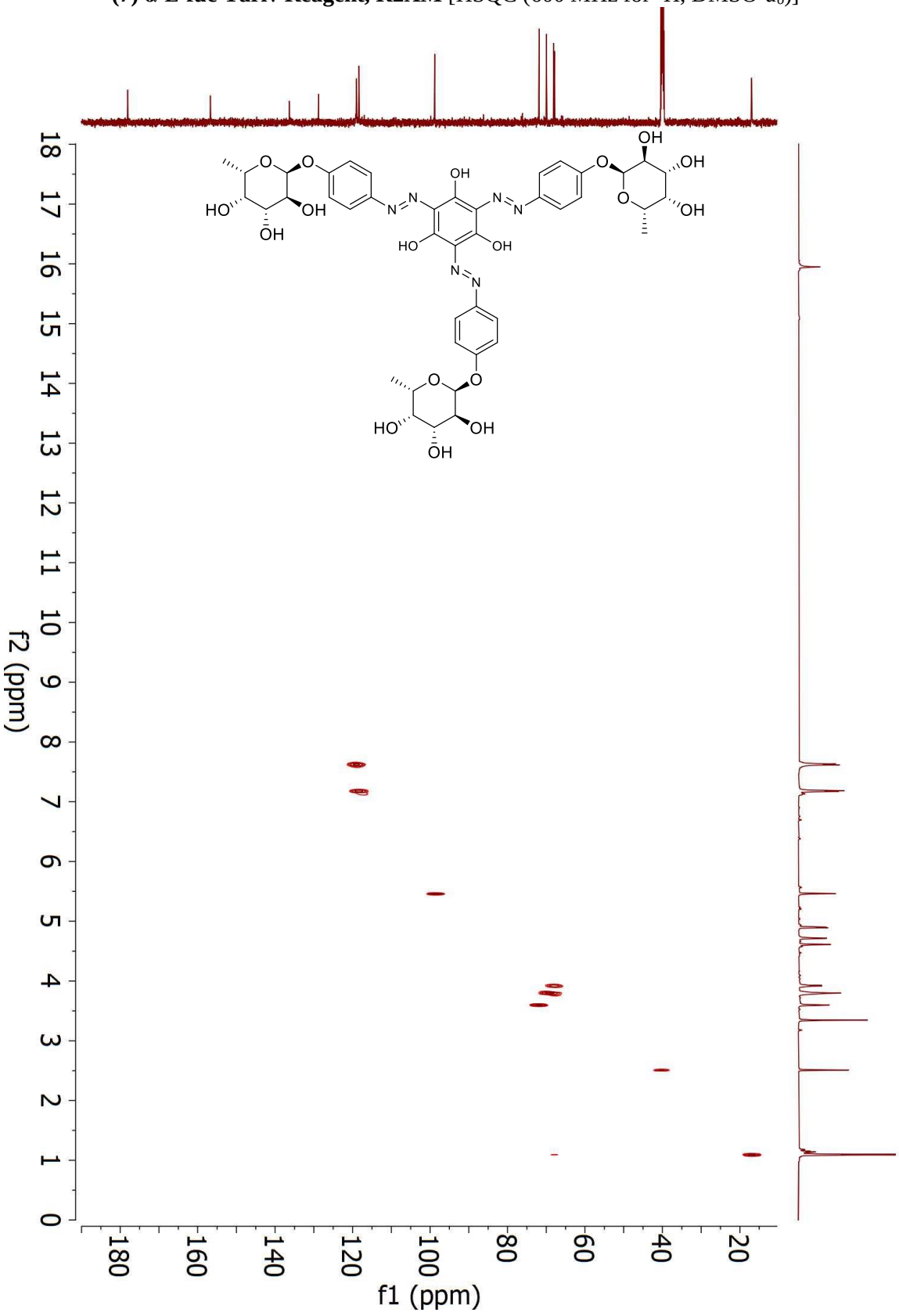

4-aminophenyl β-L-fucopyranoside [^{1}H NMR (600 MHz, DMSO-d_6)]

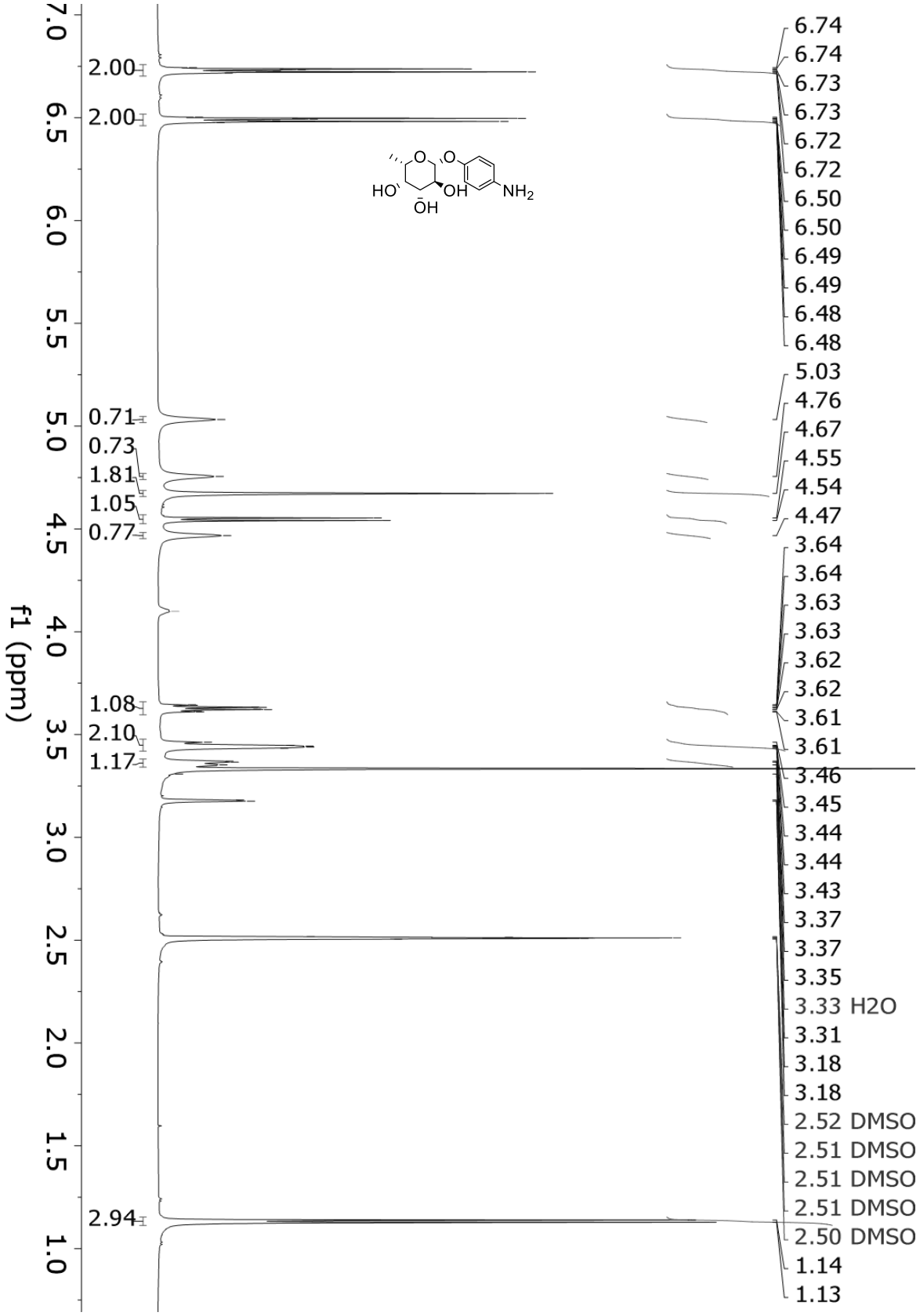

(6) β-L-fuc Yariv Reagent, R2XM [^{1}H NMR (600 MHz, DMSO-d_6)]

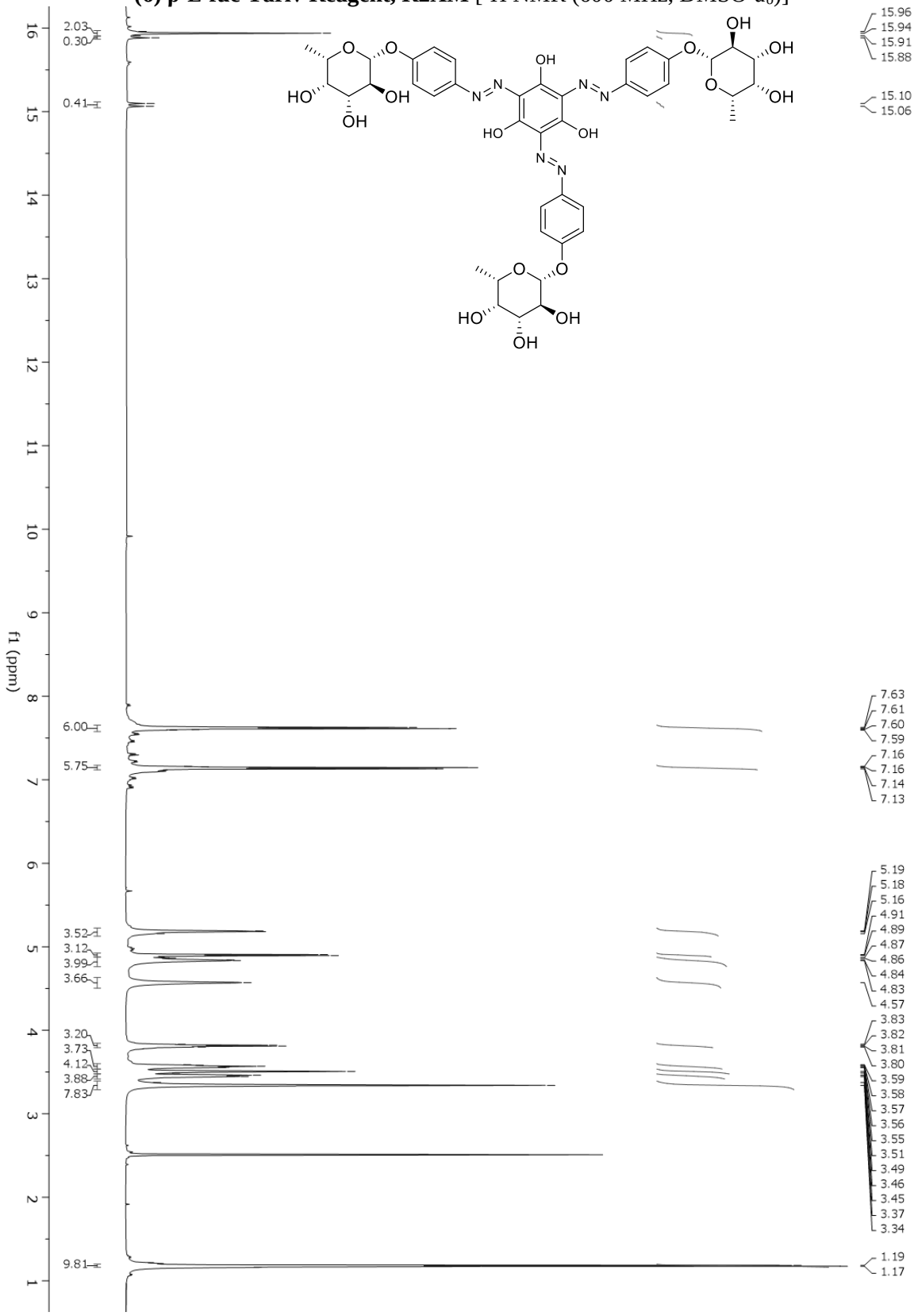

(6) β-L-fuc Yariv Reagent, R2XM [^{13}C NMR (151 MHz, DMSO-d_6)]

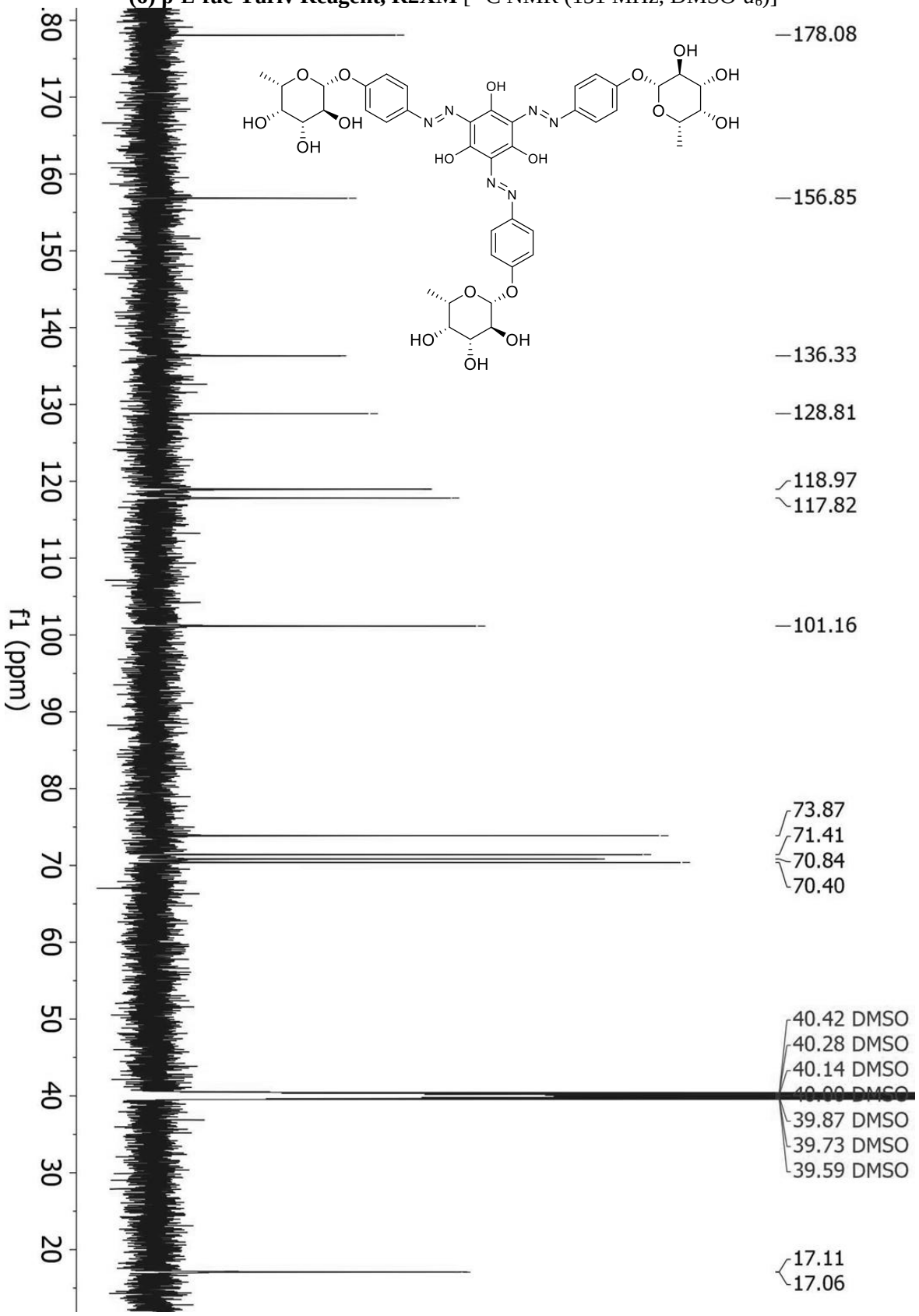

(6) β-L-fuc Yariv Reagent, R2XM [COSY (600 MHz for ^{1}H, DMSO-d_6)]

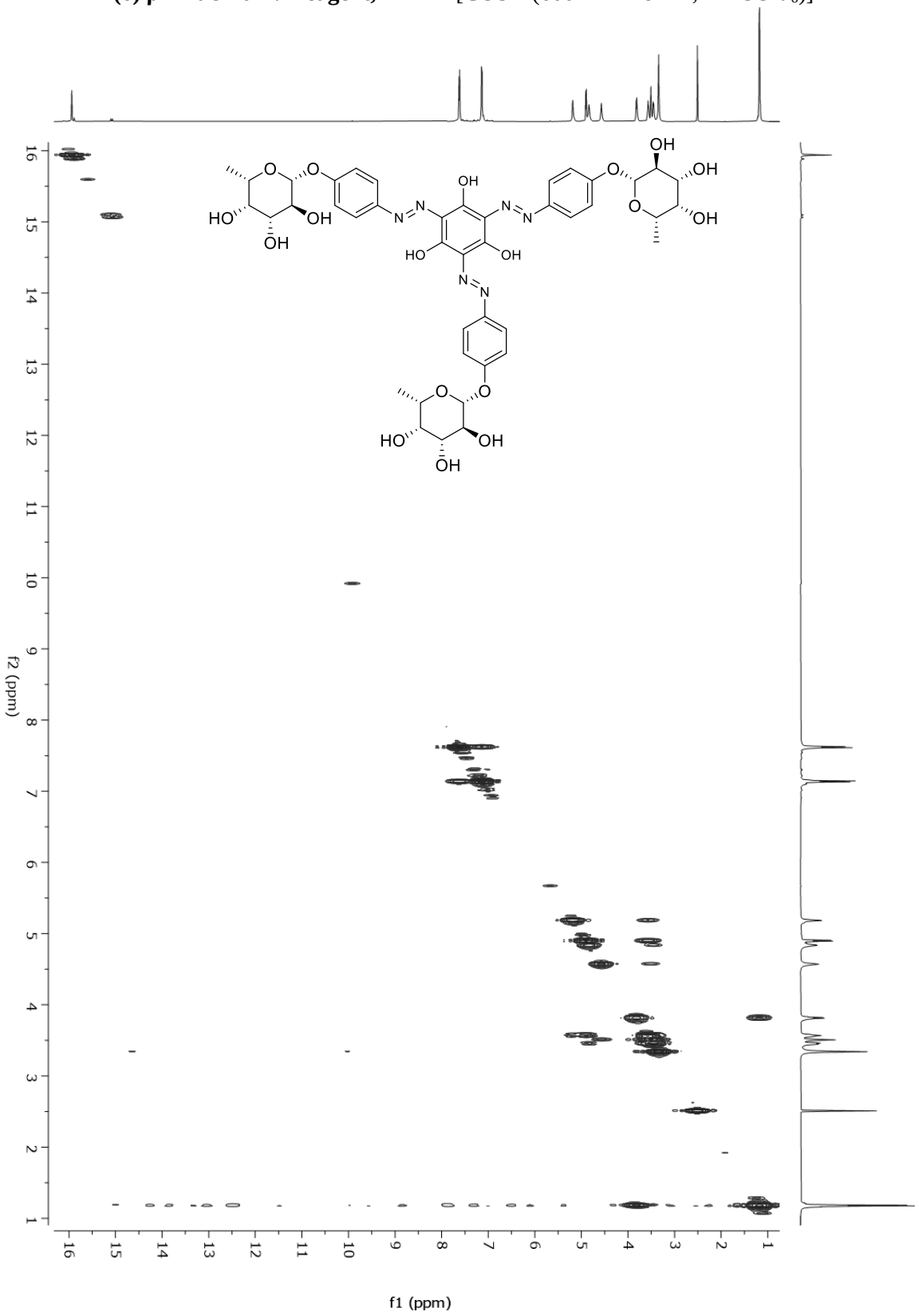

(6) β-L-fuc Yariv Reagent, R2XM [COSY (600 MHz for ^{1}H, DMSO-d_6)]

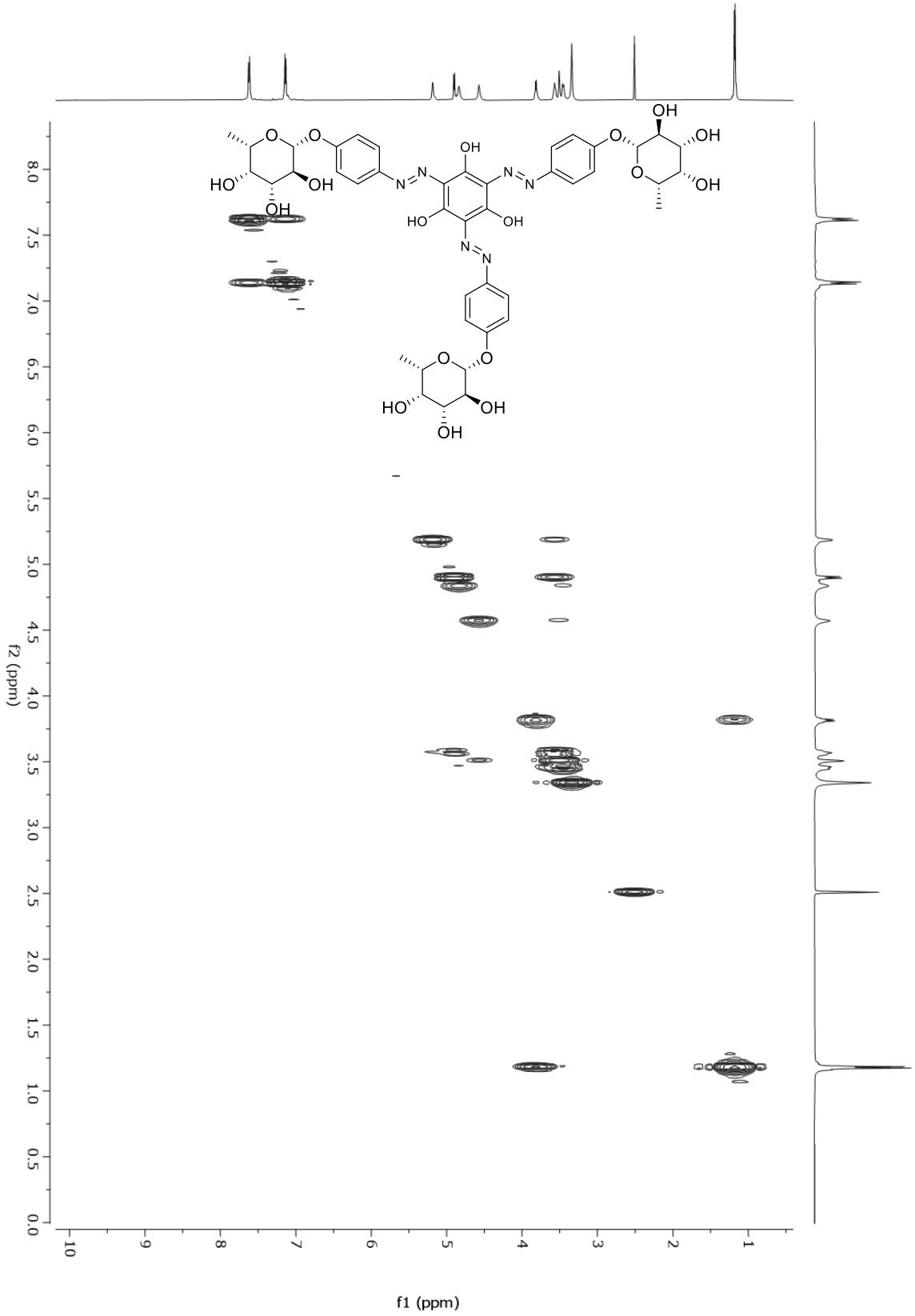

(6) β-L-fuc Yariv Reagent, R2XM [HSQC (600 MHz for ^{1}H, DMSO-d_6)]

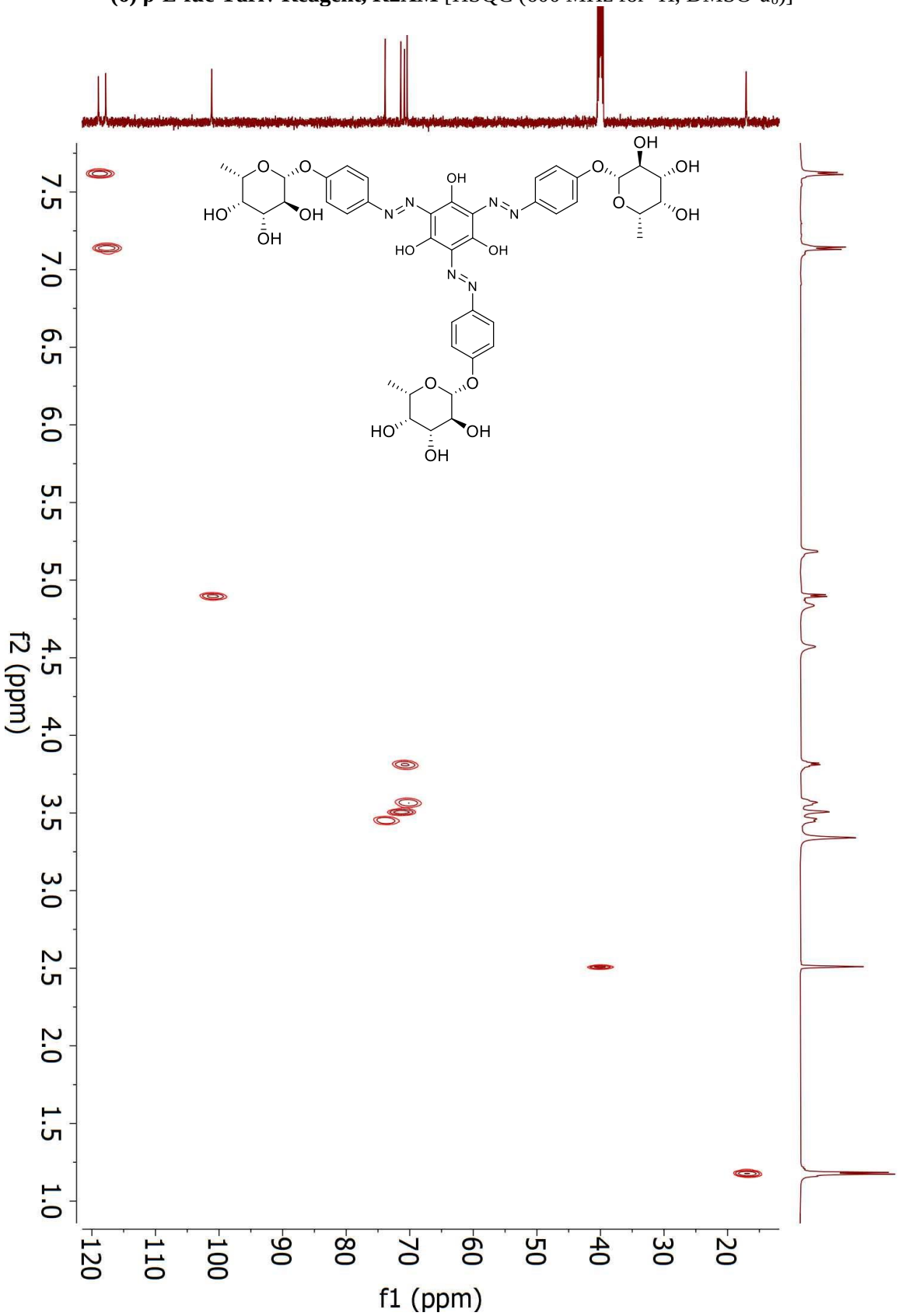

(6) β-L-fuc Yariv Reagent, R2XM [HSQC (600 MHz for ^{1}H, DMSO-d_6)]

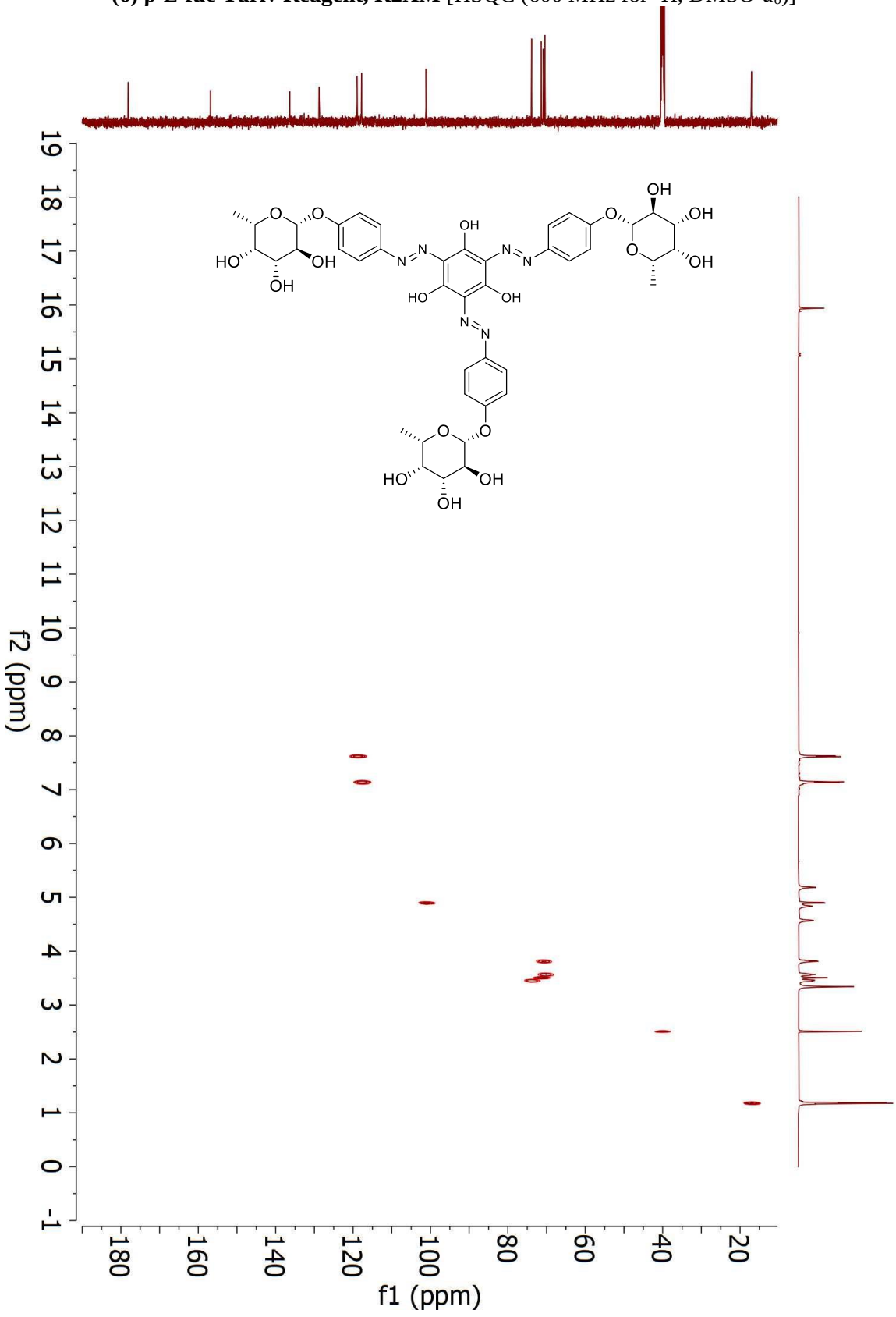

(**5**) **α-D-Gal Yariv Reagent, R2XM** [^{1}H NMR (600 MHz, DMSO-d_6)]

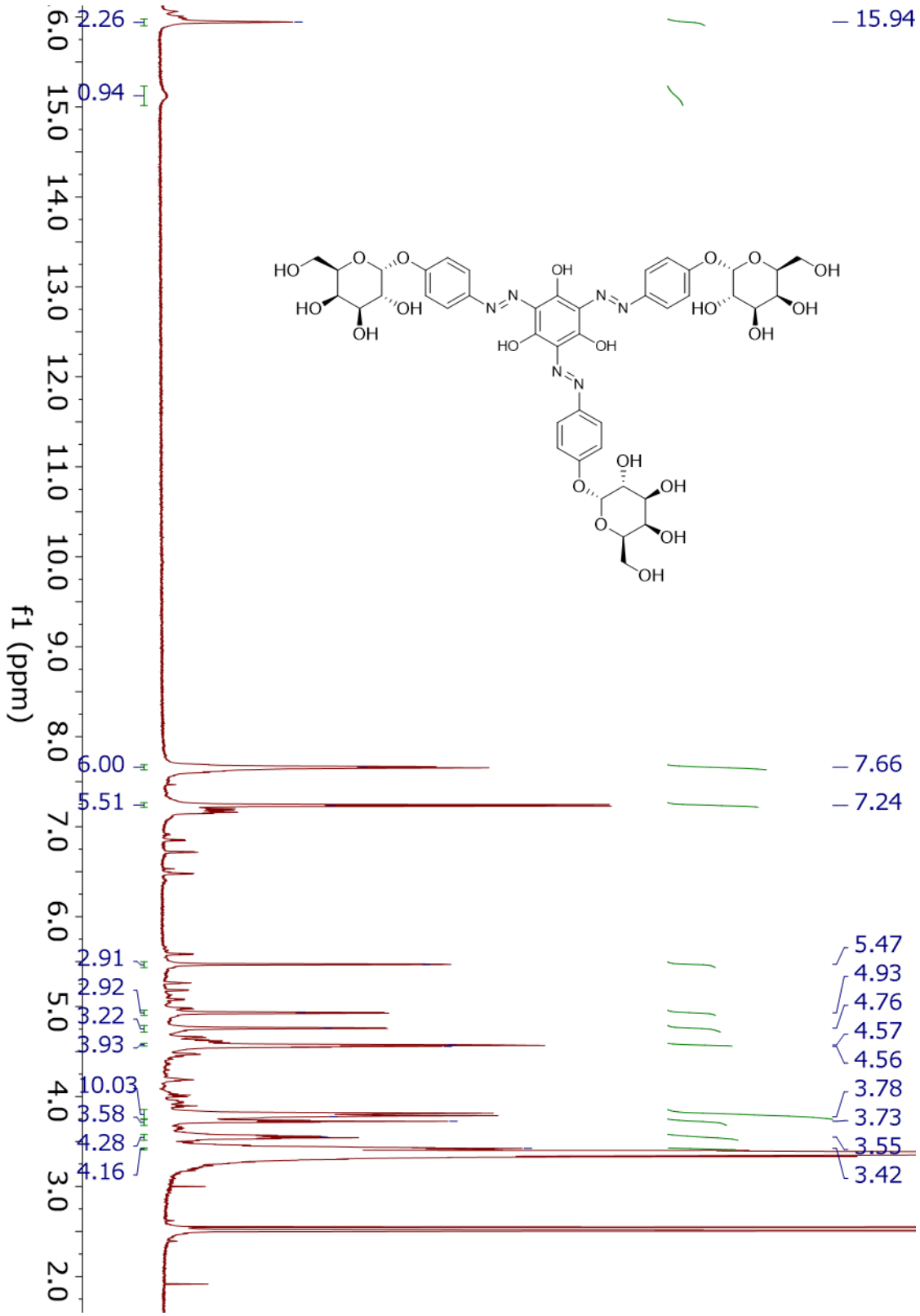

(**5**) **α-D-Gal Yariv Reagent, R2XM** [^{13}C NMR (151 MHz, DMSO-d_6)]

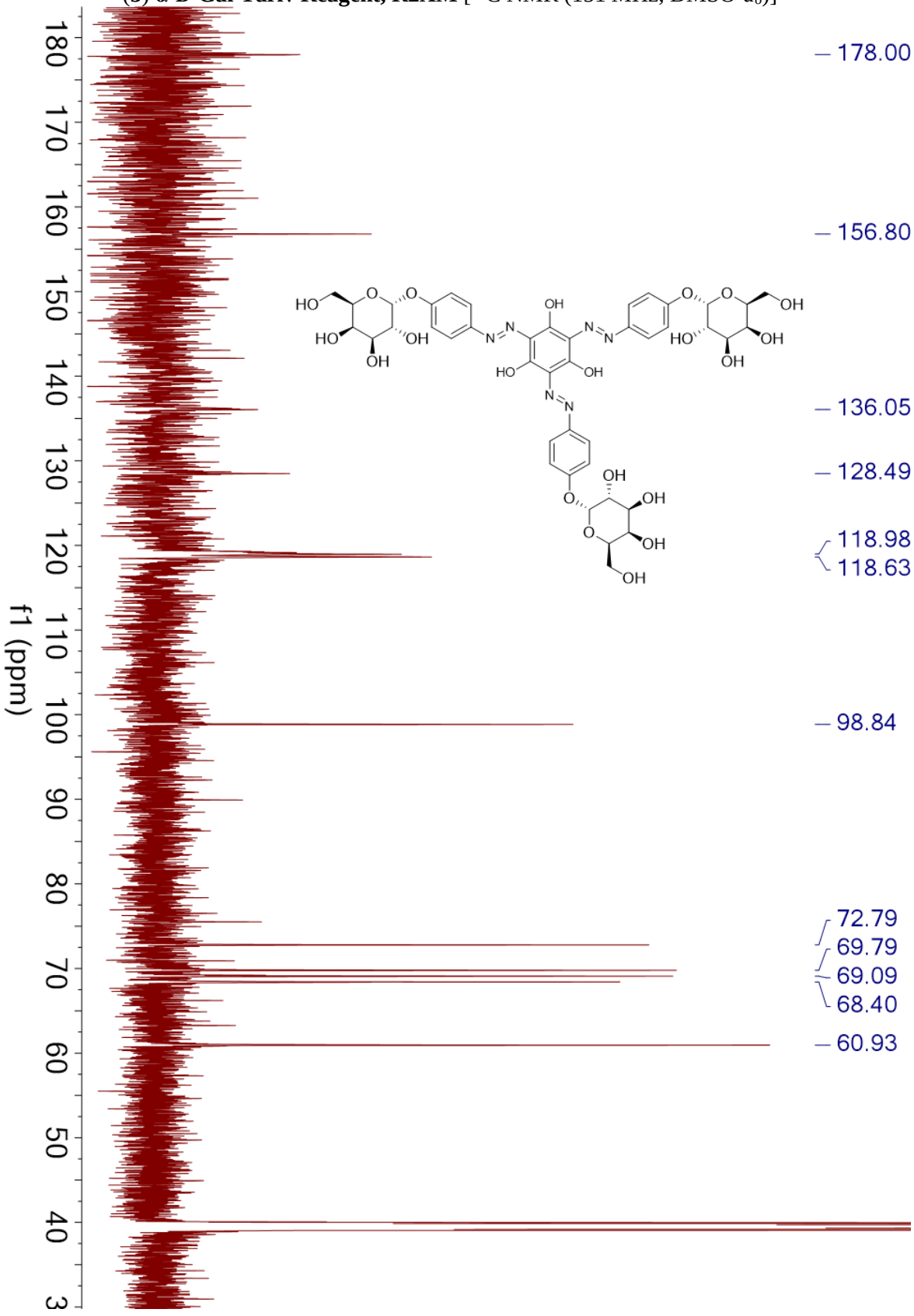

(**5**) **α-D-Gal Yariv Reagent, R2XM** [COSY NMR (600 MHz, DMSO-d_6)]

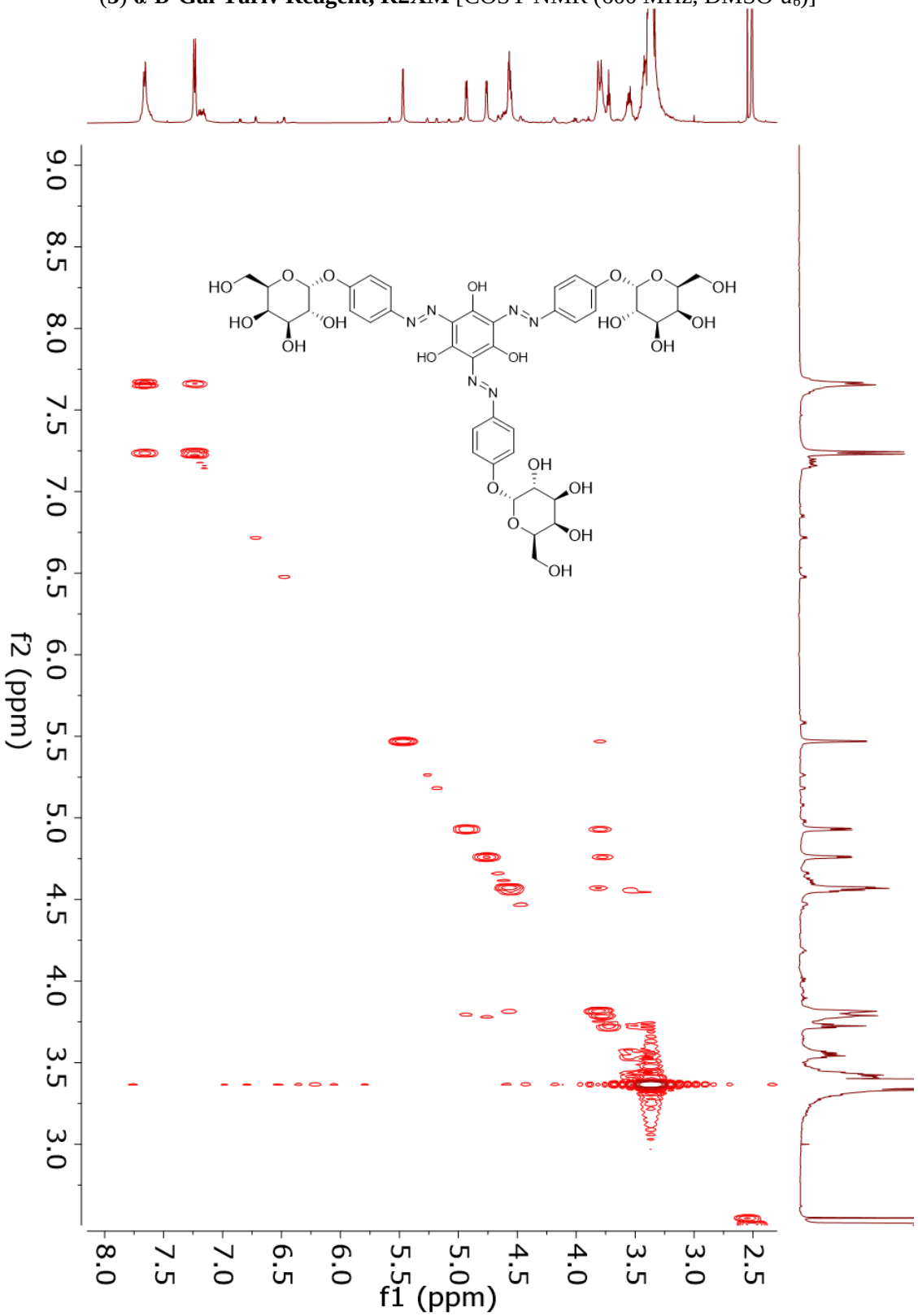

(**5**) **α-D-Gal Yariv Reagent, R2XM** [HSQC NMR (600 MHz, DMSO-d_6)]

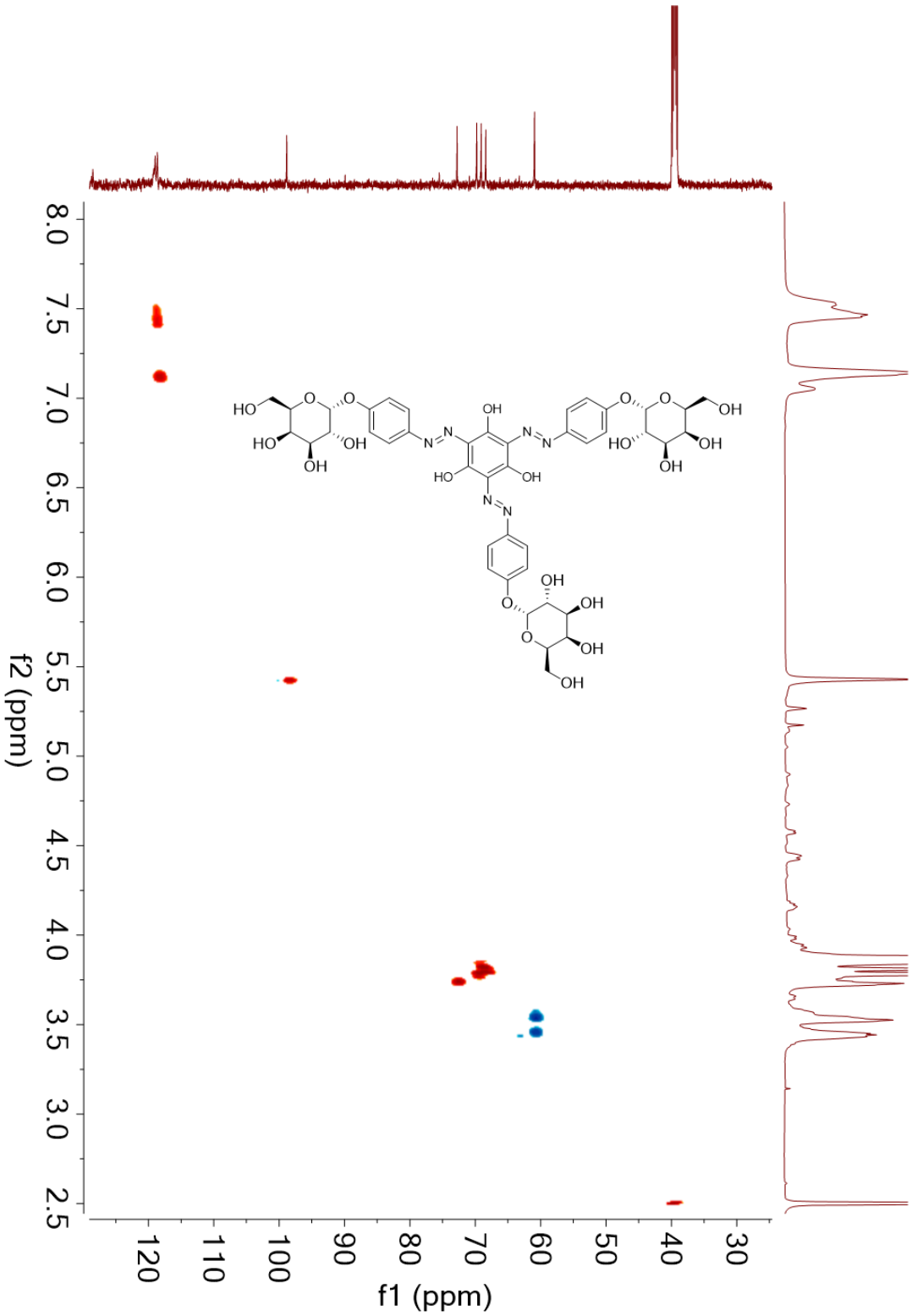

(4) β-D-Man Yariv Reagent, R1X [^{1}H NMR (600 MHz, DMSO-d_6)]

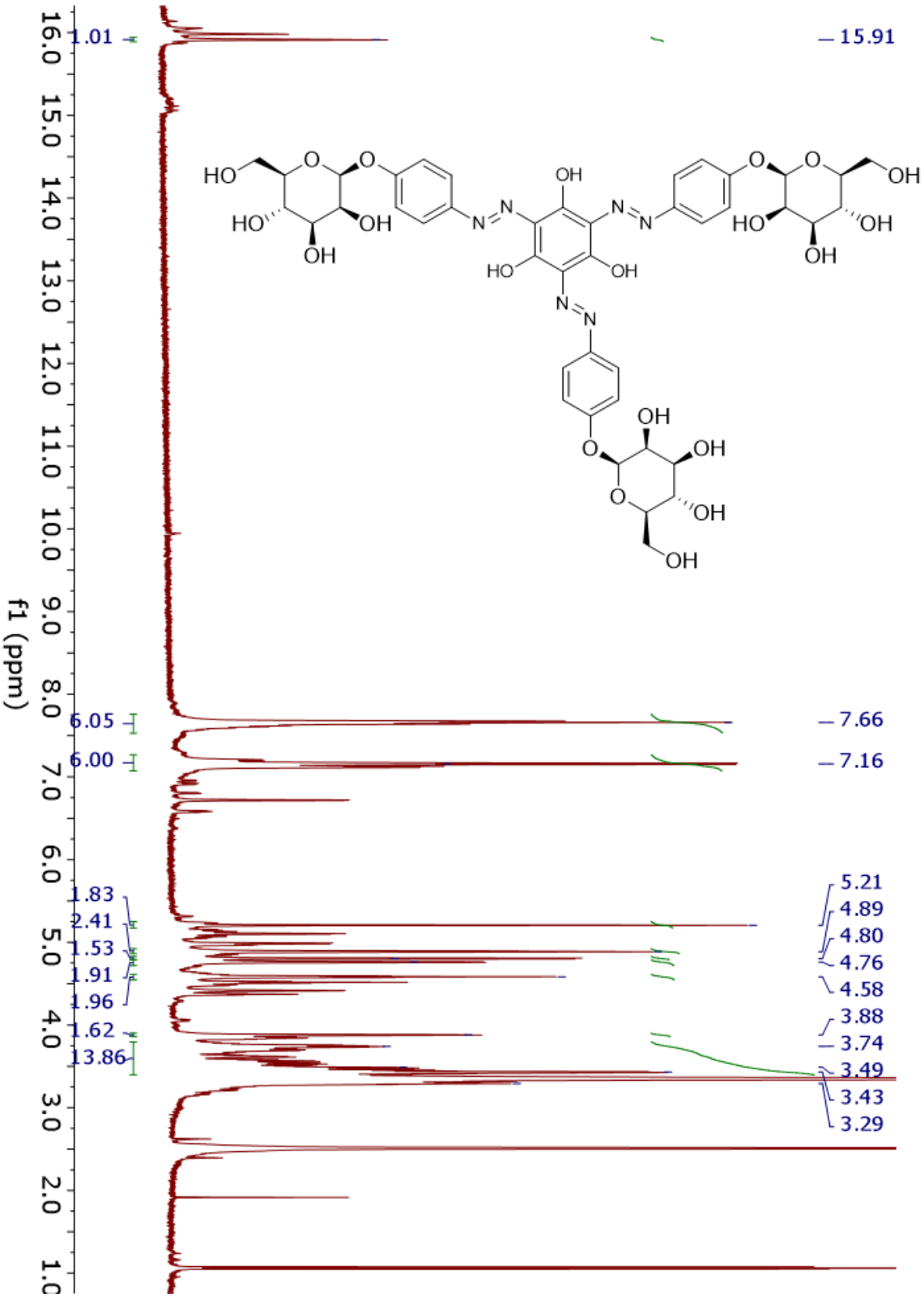

(4) β-D-Man Yariv Reagent, R1X [^{13}C NMR (151 MHz, DMSO-d_6)]

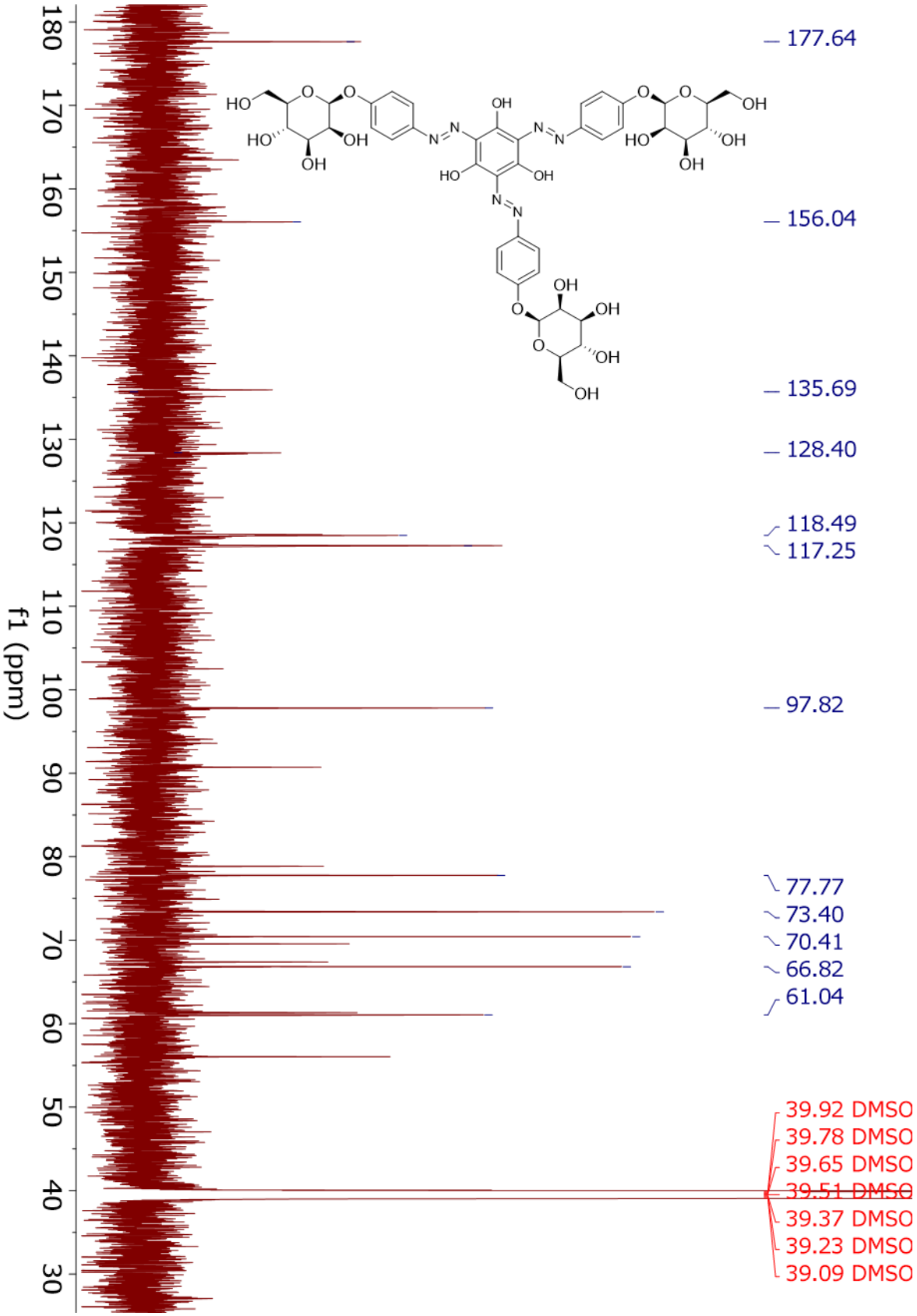
f1 (ppm)
180
170
160
150
140
130
120
110
100
90
80
70
60
50
40
30
177.64
156.04
135.69
128.40
118.49
117.25
97.82
77.77
73.40
70.41
66.82
61.04
39.92 DMSO
39.78 DMSO
39.65 DMSO
39.51 DMSO
39.37 DMSO
39.23 DMSO
39.09 DMSO

(4) β-D-Man Yariv Reagent, R1X [HSQC NMR (600 MHz, DMSO-d_6)]

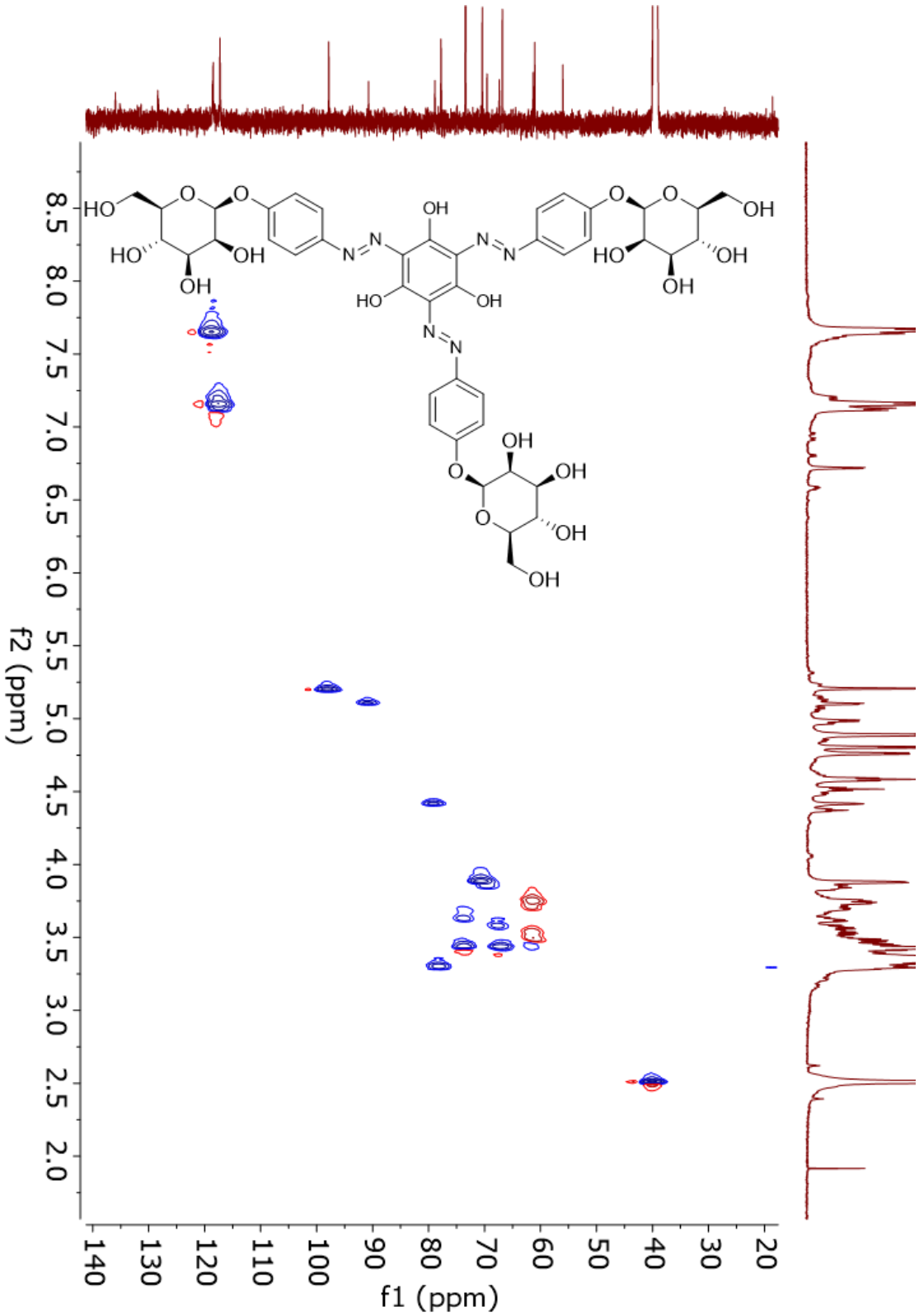

(4) β-D-Man Yariv Reagent, R1X [COSY NMR (600 MHz, DMSO-d_6)]

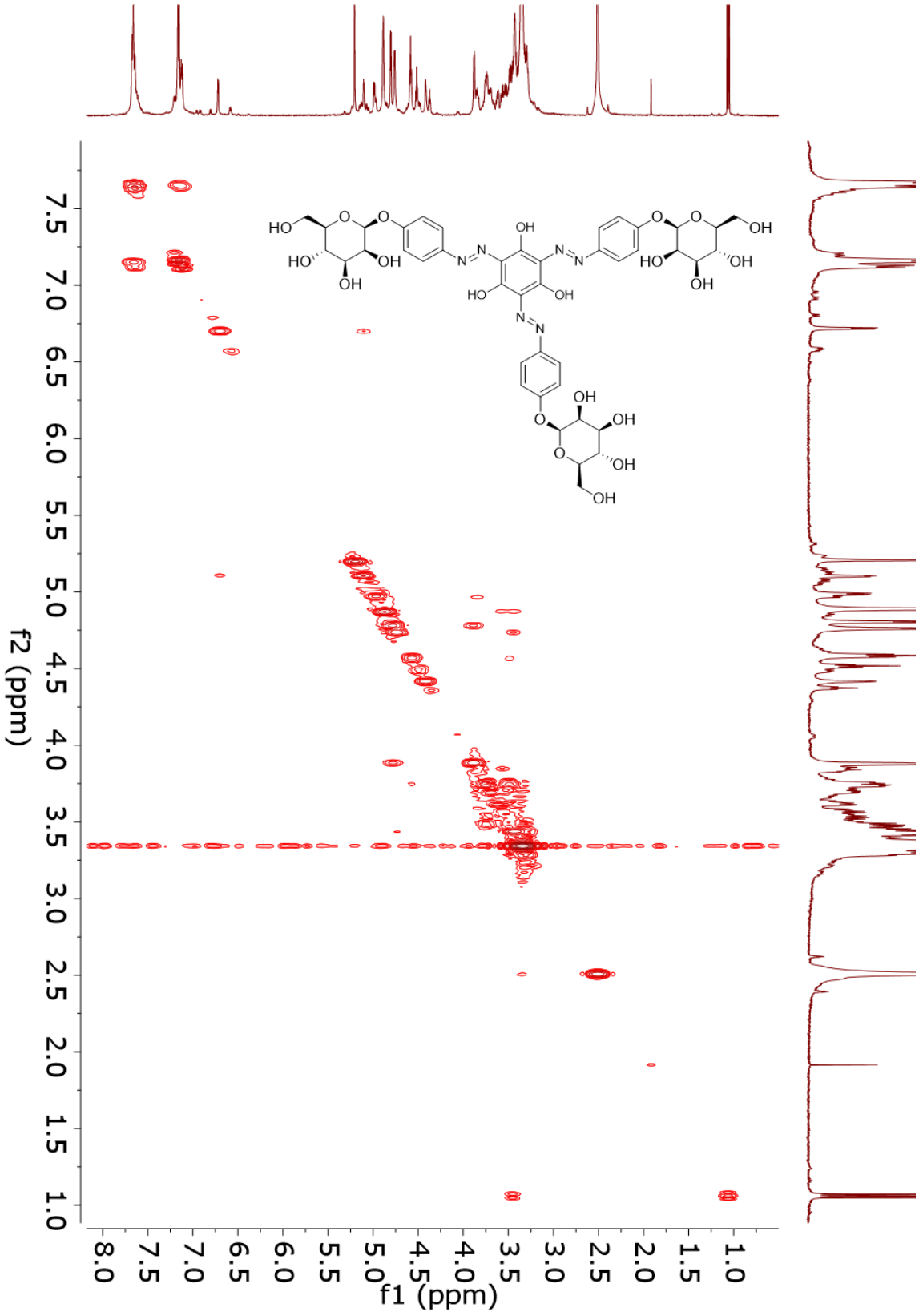

(4) β-D-Man Yariv Reagent, R1X [HMBC NMR (600 MHz, DMSO-d_6)]

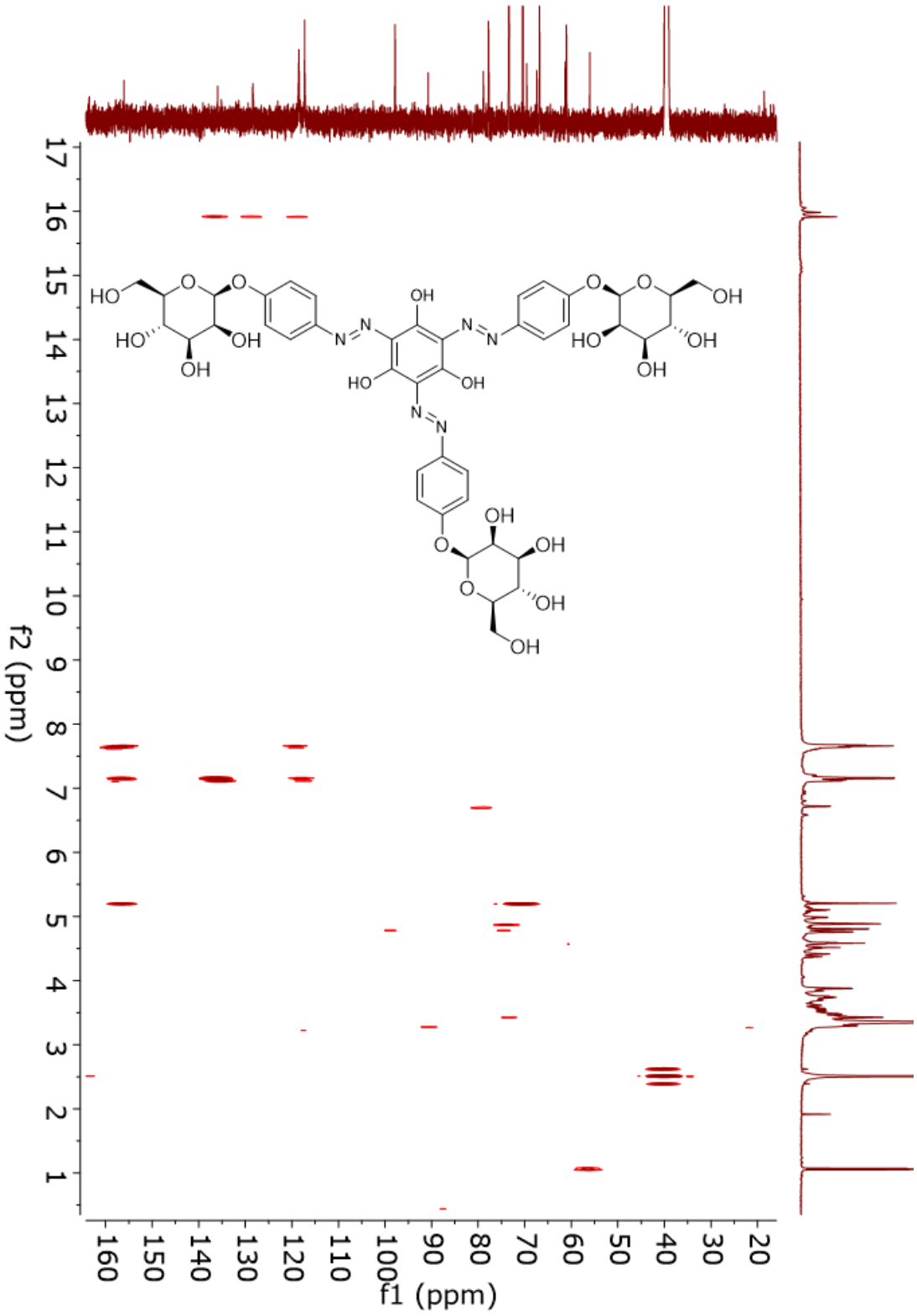

(**9**) ***α*-D-Man Yariv Reagent, R1X** [^{1}H NMR (600 MHz, DMSO-d_6)]

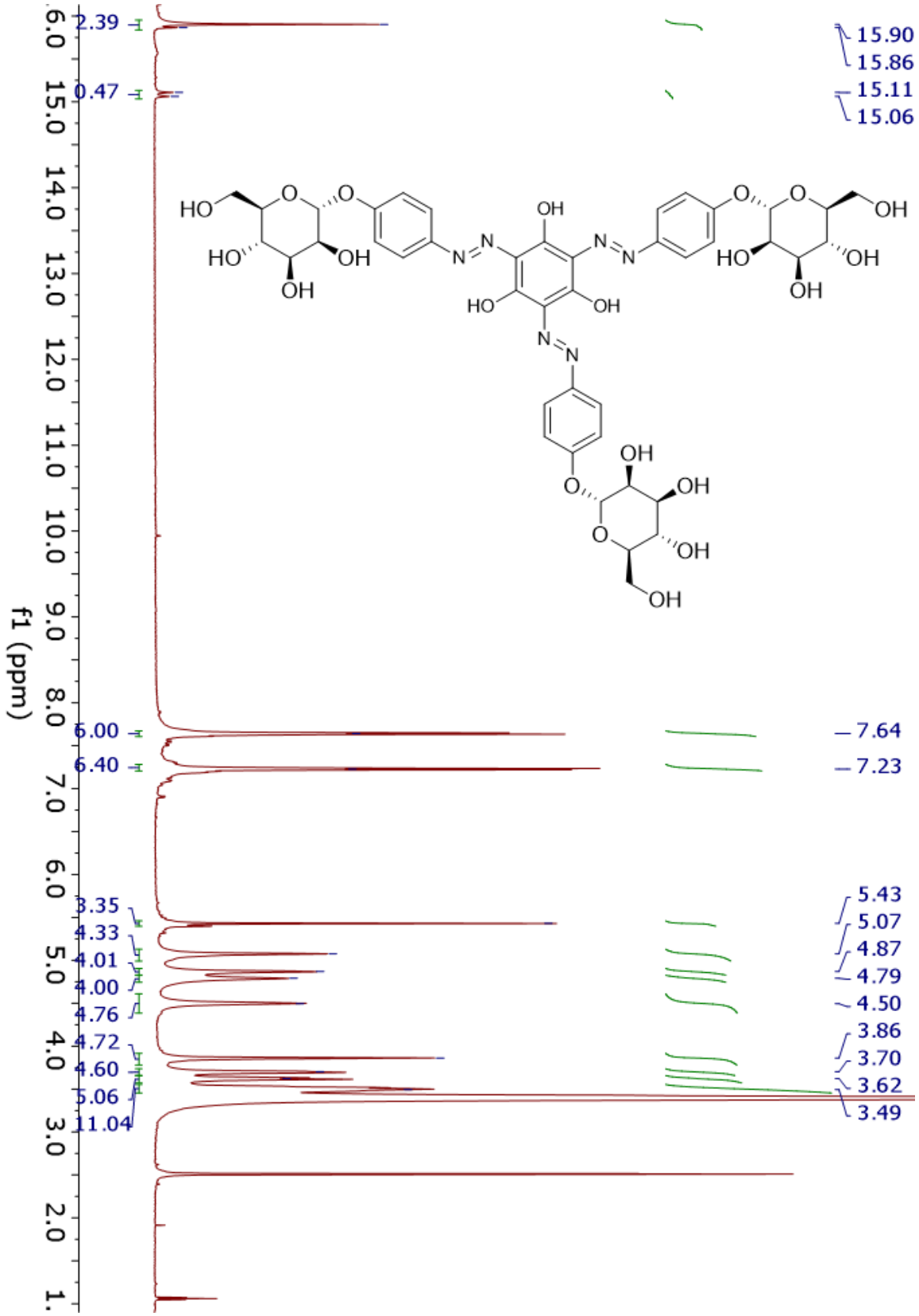

(**9**) **α-D-Man Yariv Reagent, R1X** [^{13}C NMR (151 MHz, DMSO-d_6)]

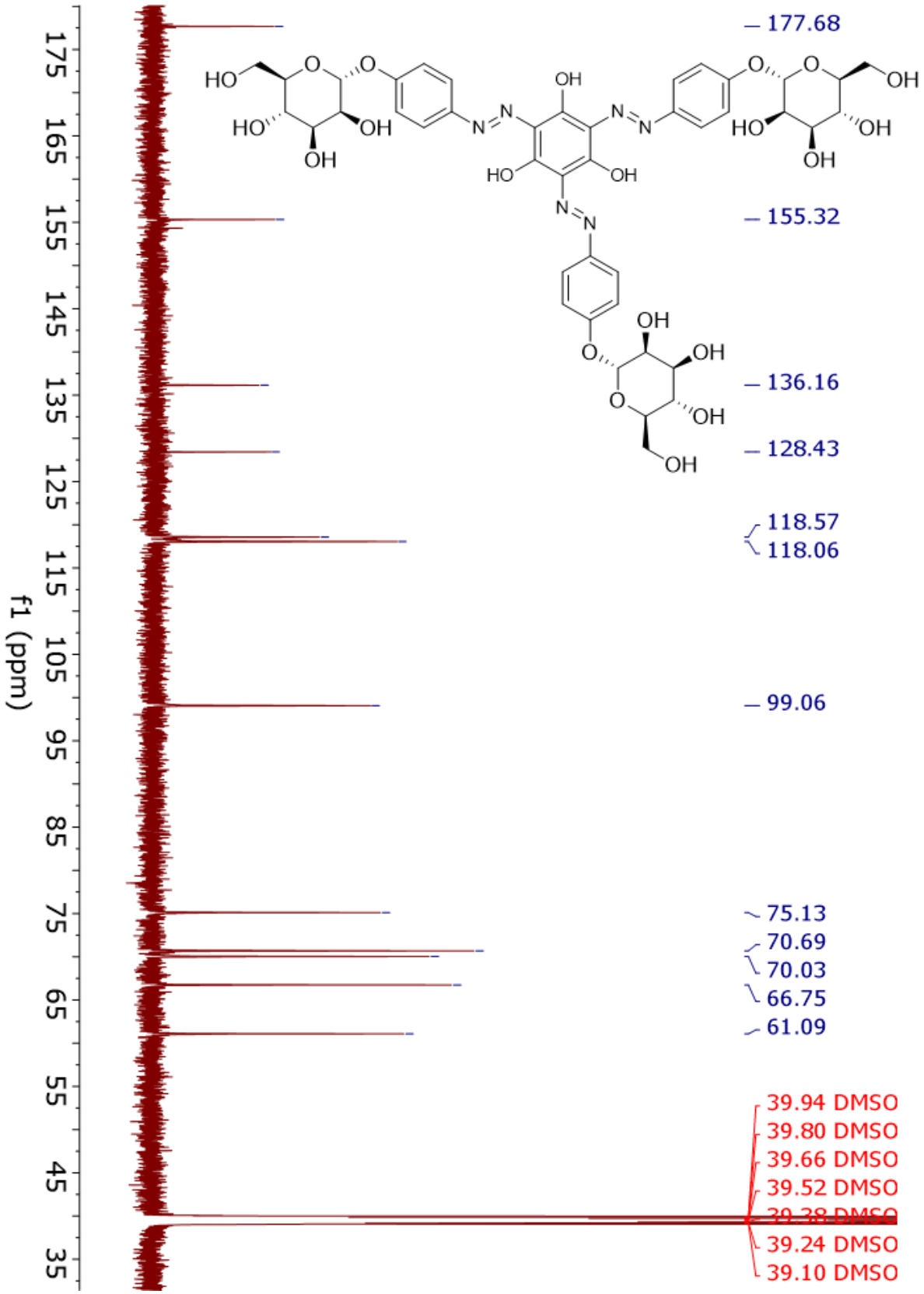

(**9**) **α-D-Man Yariv Reagent, R1X** [COSY NMR (600 MHz, DMSO-d_6)]

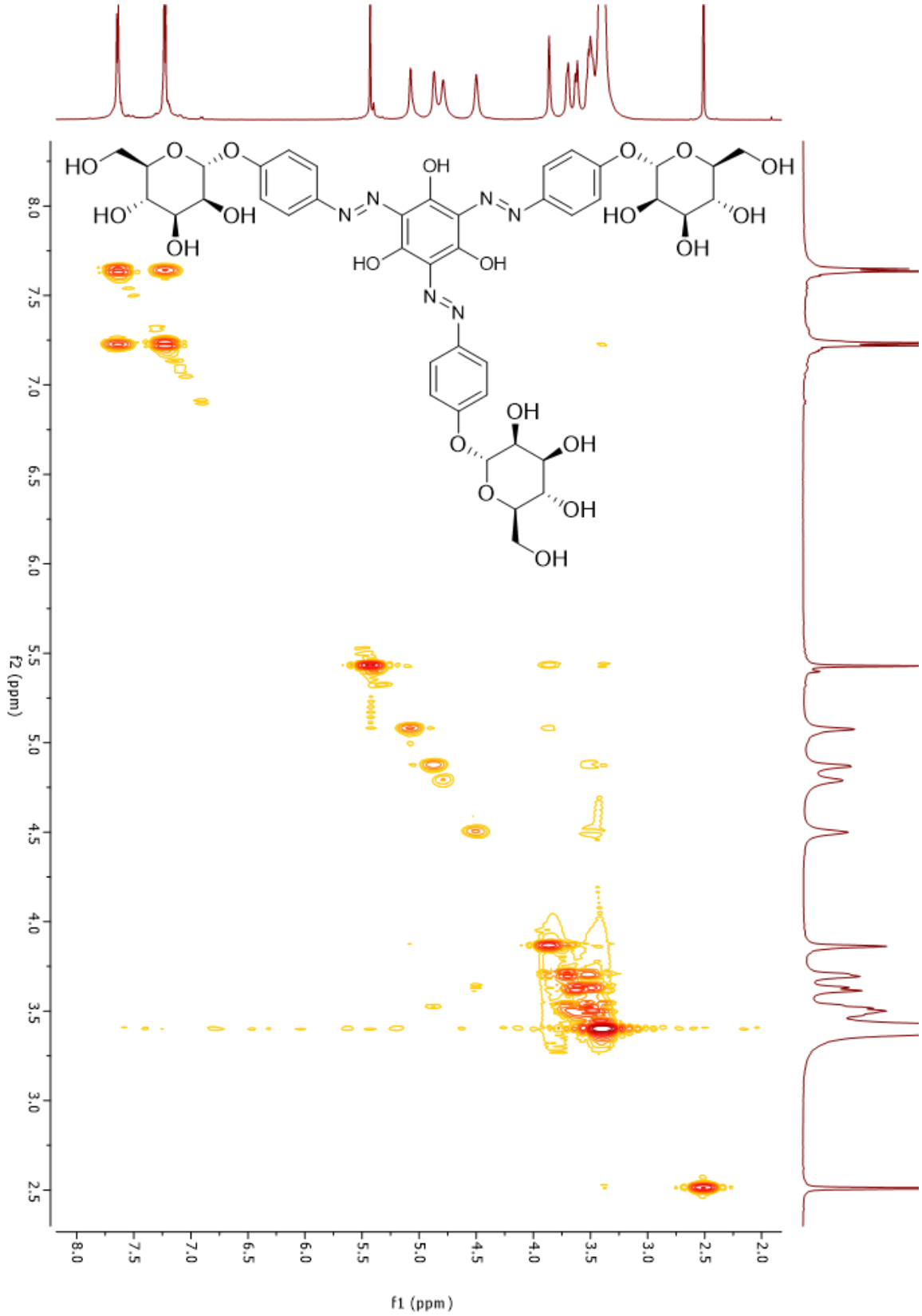
HO
OH
N=N
O
f2 (ppm)
f1 (ppm)
8.0
7.5
7.0
6.5
6.0
5.5
5.0
4.5
4.0
3.5
3.0
2.5
2.0

(9) α-D-Man Yariv Reagent, R1X [HSQC NMR (600 MHz, DMSO-d_6)]

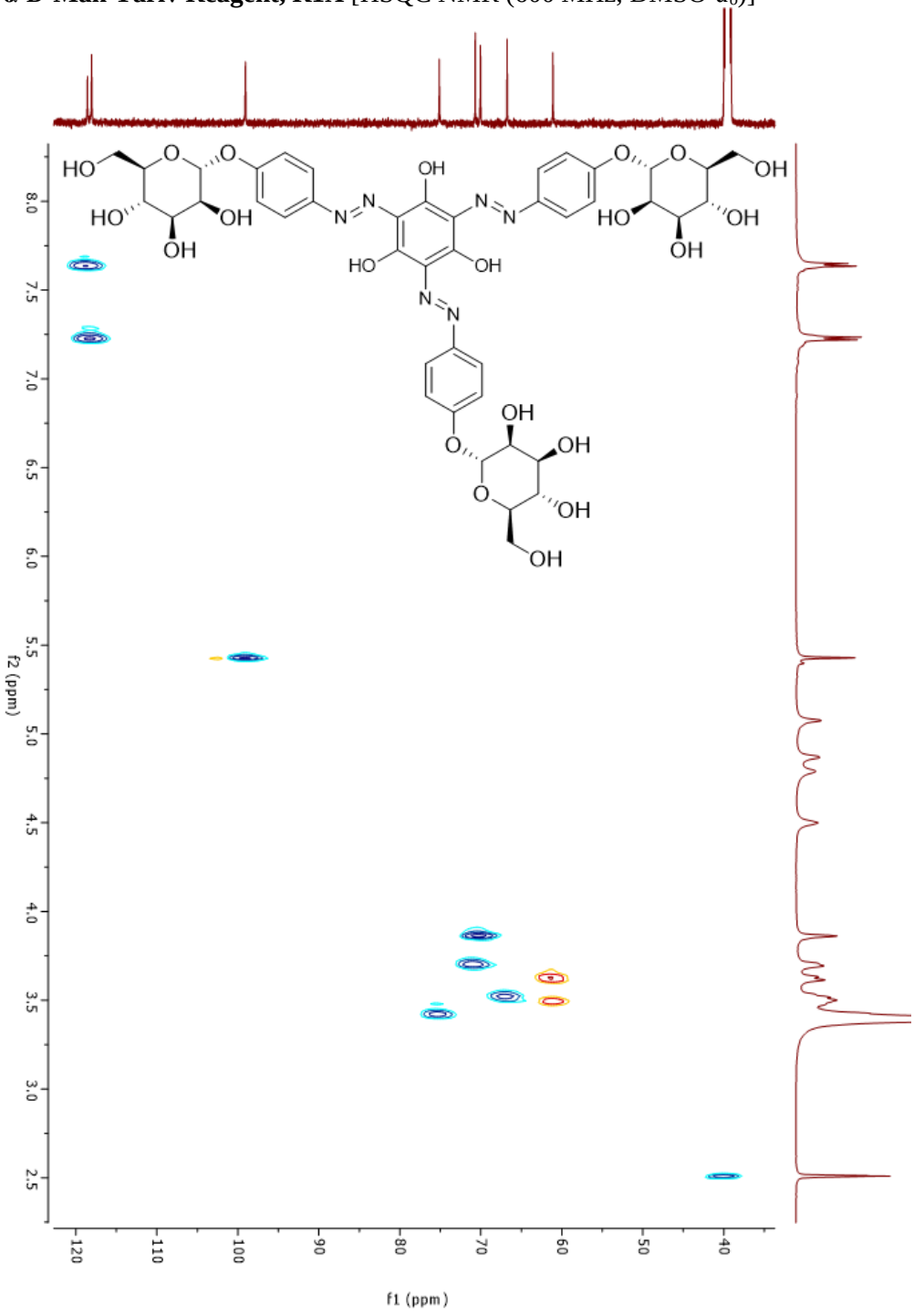

(8) Bis β-D-Glc Yariv Reagent [^{1}H NMR (600 MHz, DMSO-d_6)]

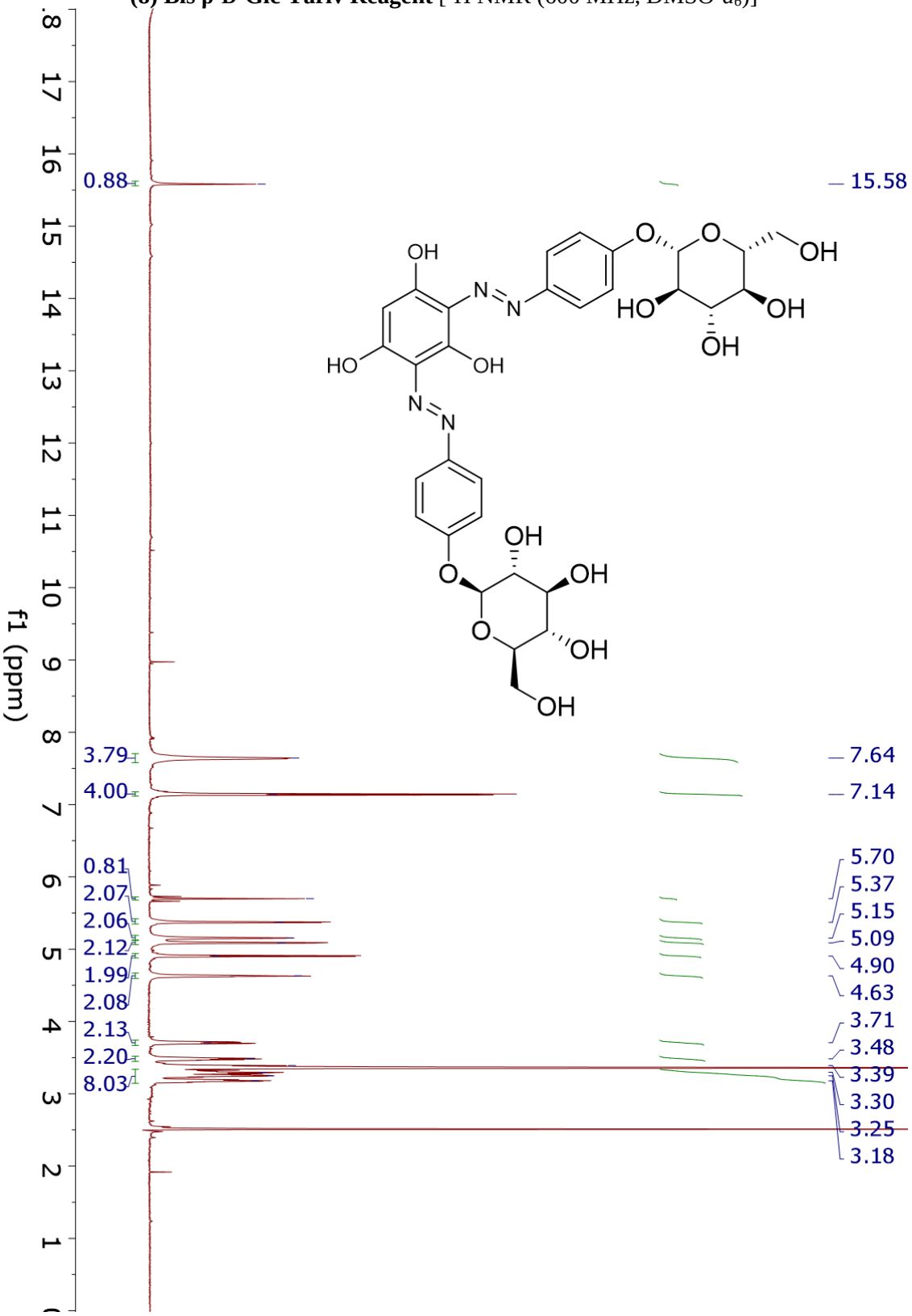

(8) Bis β-D-Glc Yariv Reagent [^{13}C NMR (600 MHz, DMSO-d_6)]

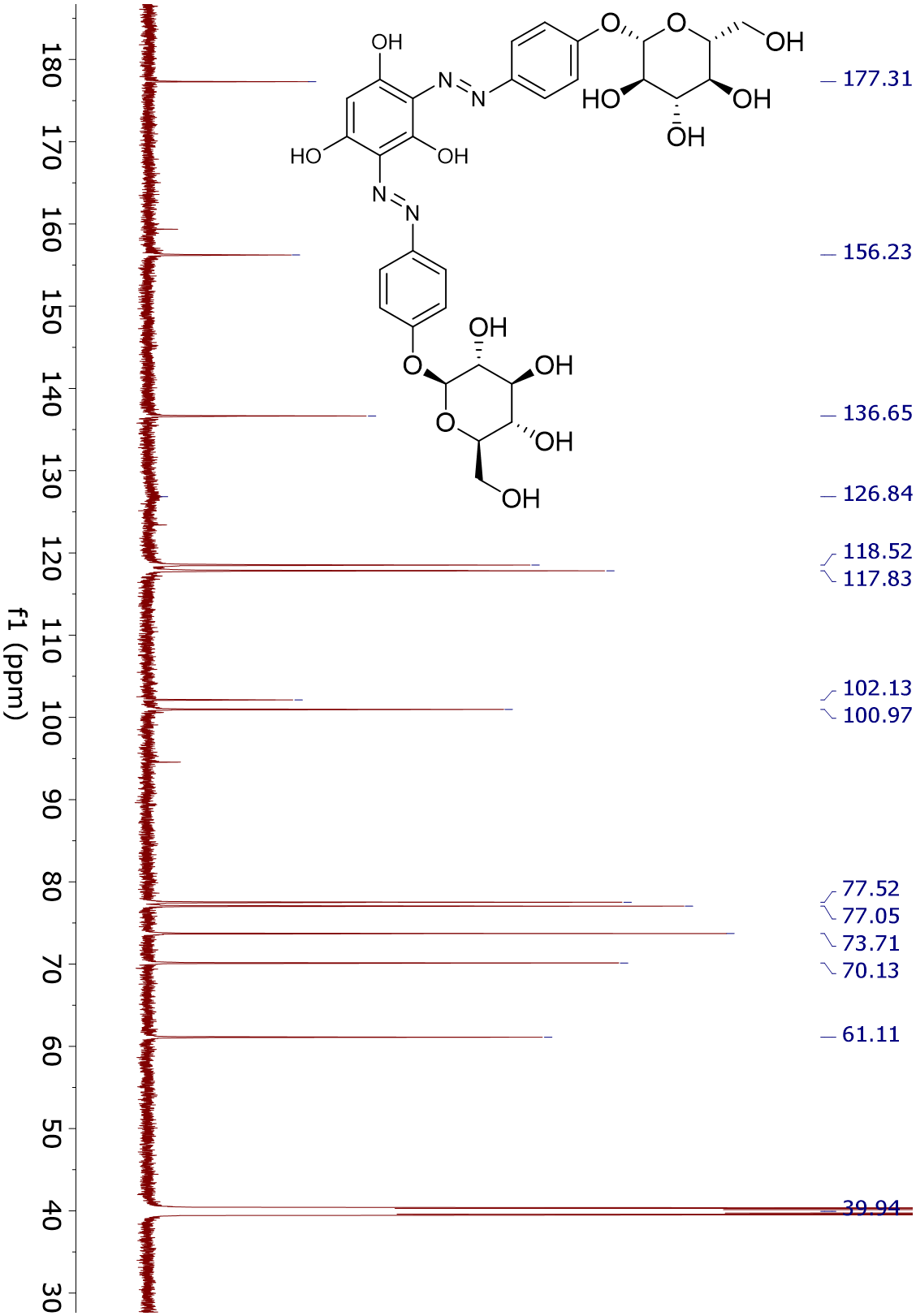

(8) Bis β-D-Glc Yariv Reagent [HSQC NMR (600 MHz, DMSO-d_6)]

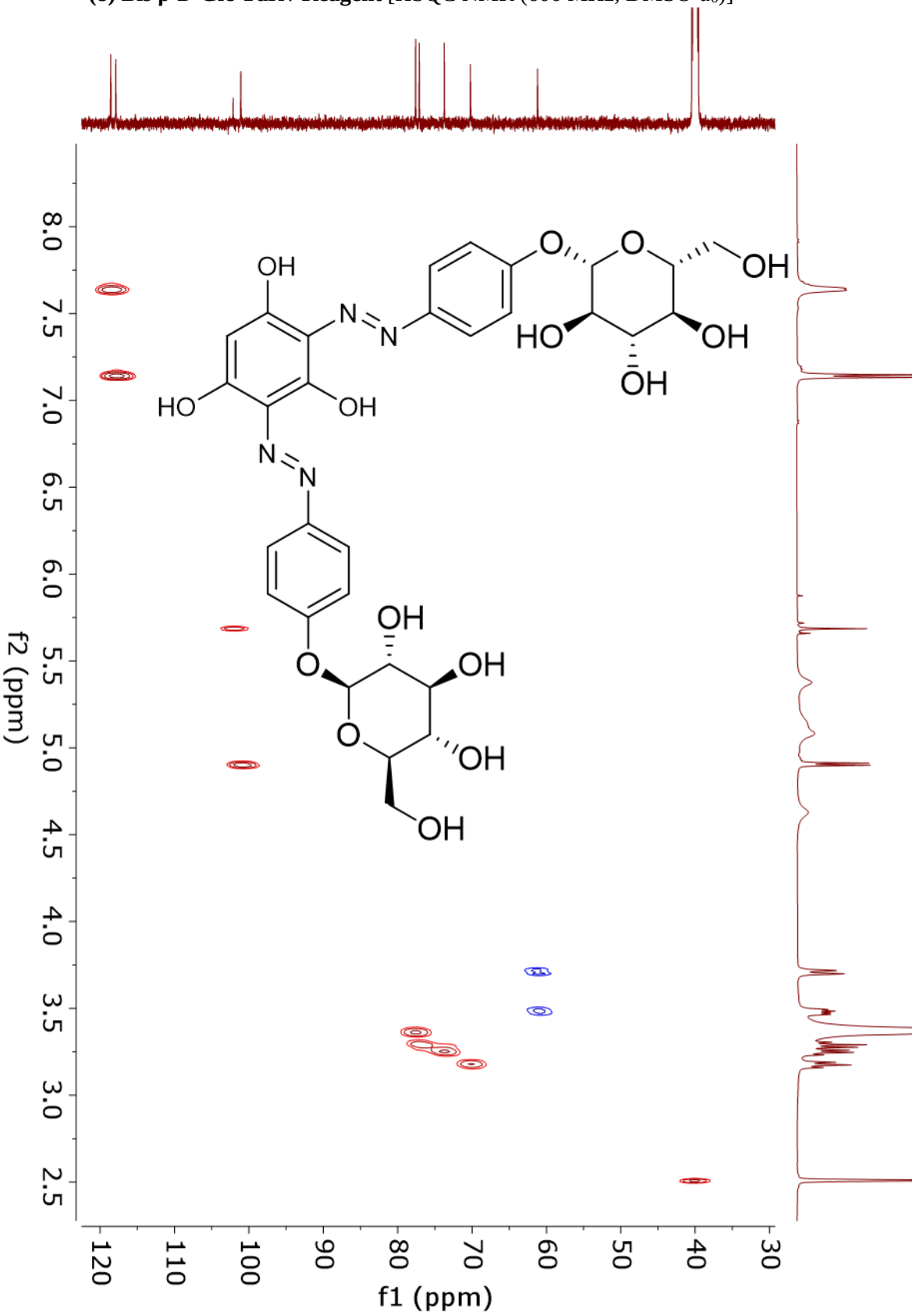

(8) Bis β-D-Glc Yariv Reagent [COSY NMR (600 MHz, DMSO-d_6)]

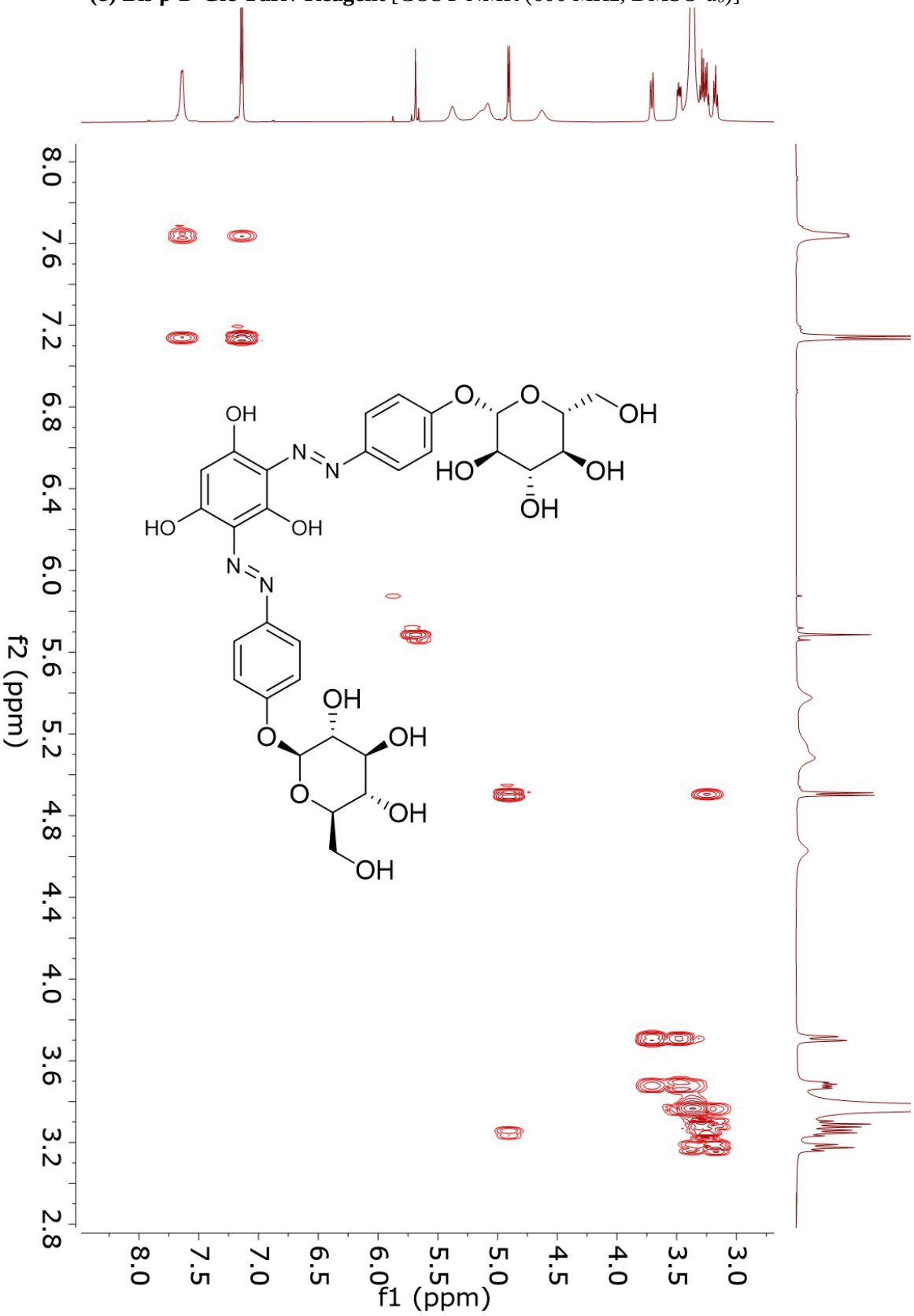

(8) Bis β-D-Glc Yariv Reagent [HMBC NMR (600 MHz, DMSO-d_6)]

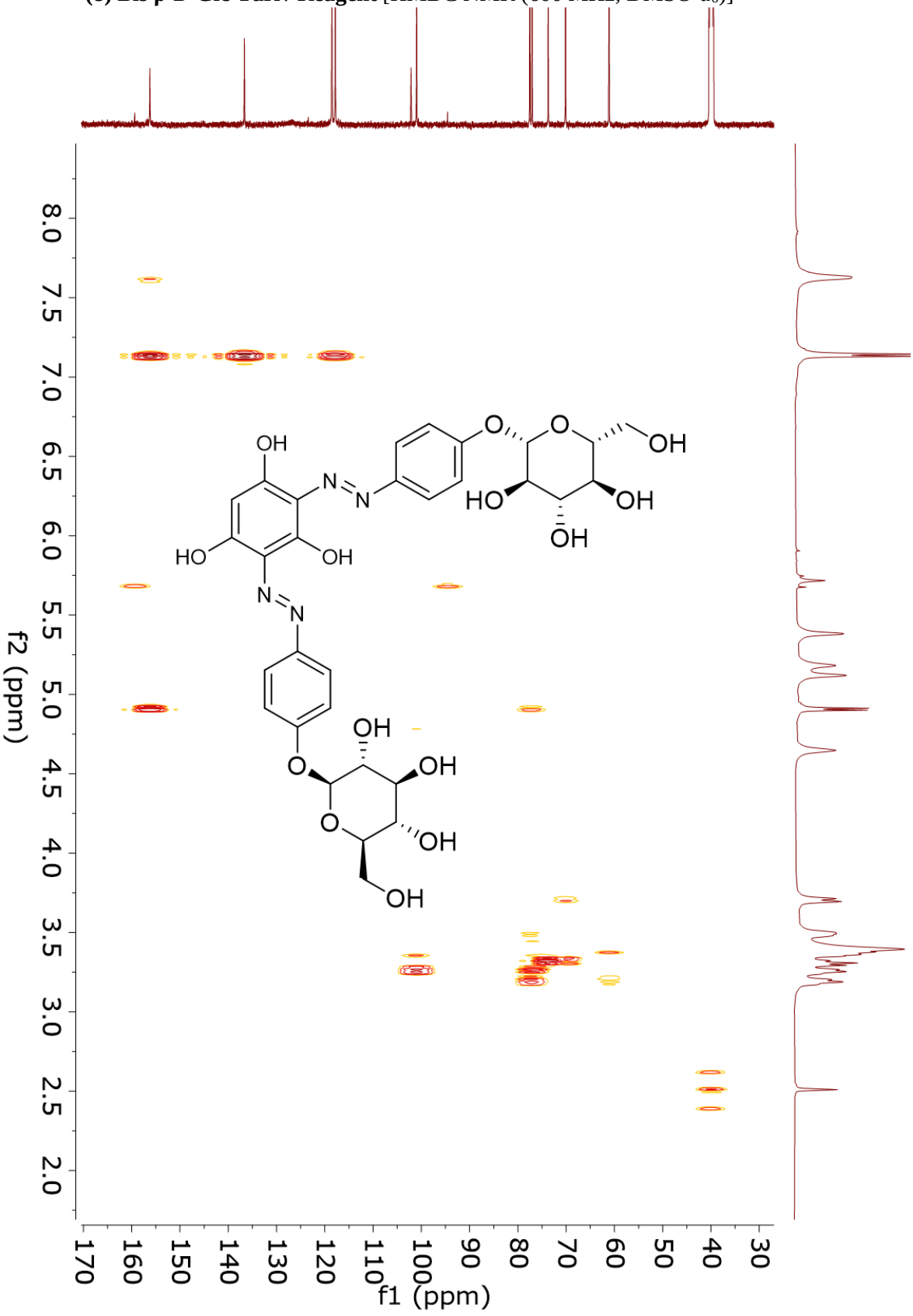

(11) Mono β-D-Glc Yariv Reagent [^{1}H NMR (600 MHz, DMSO-d_6)]

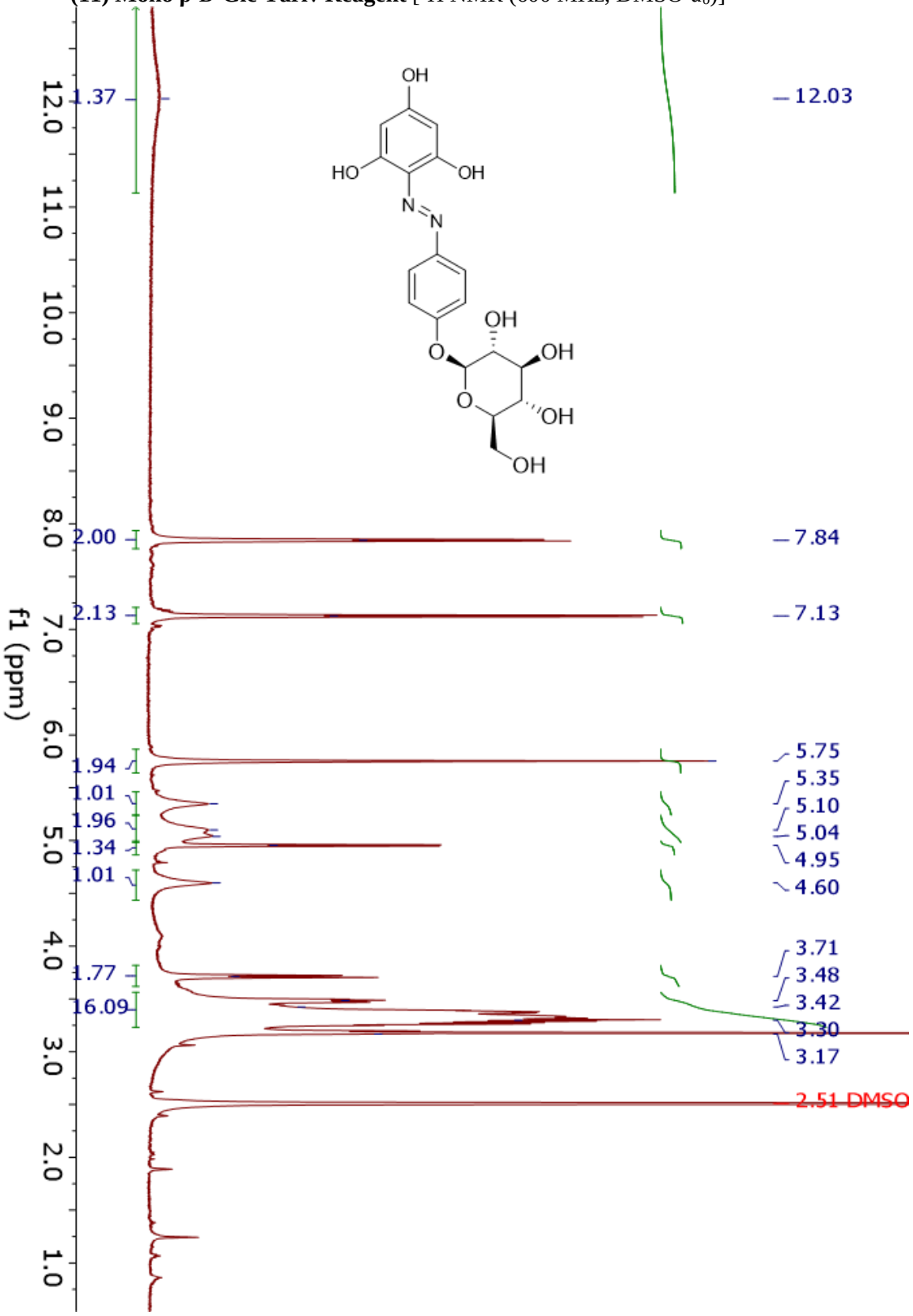

(11) Mono β-D-Glc Yariv Reagent [^{13}C NMR (151 MHz, DMSO-d_6)]

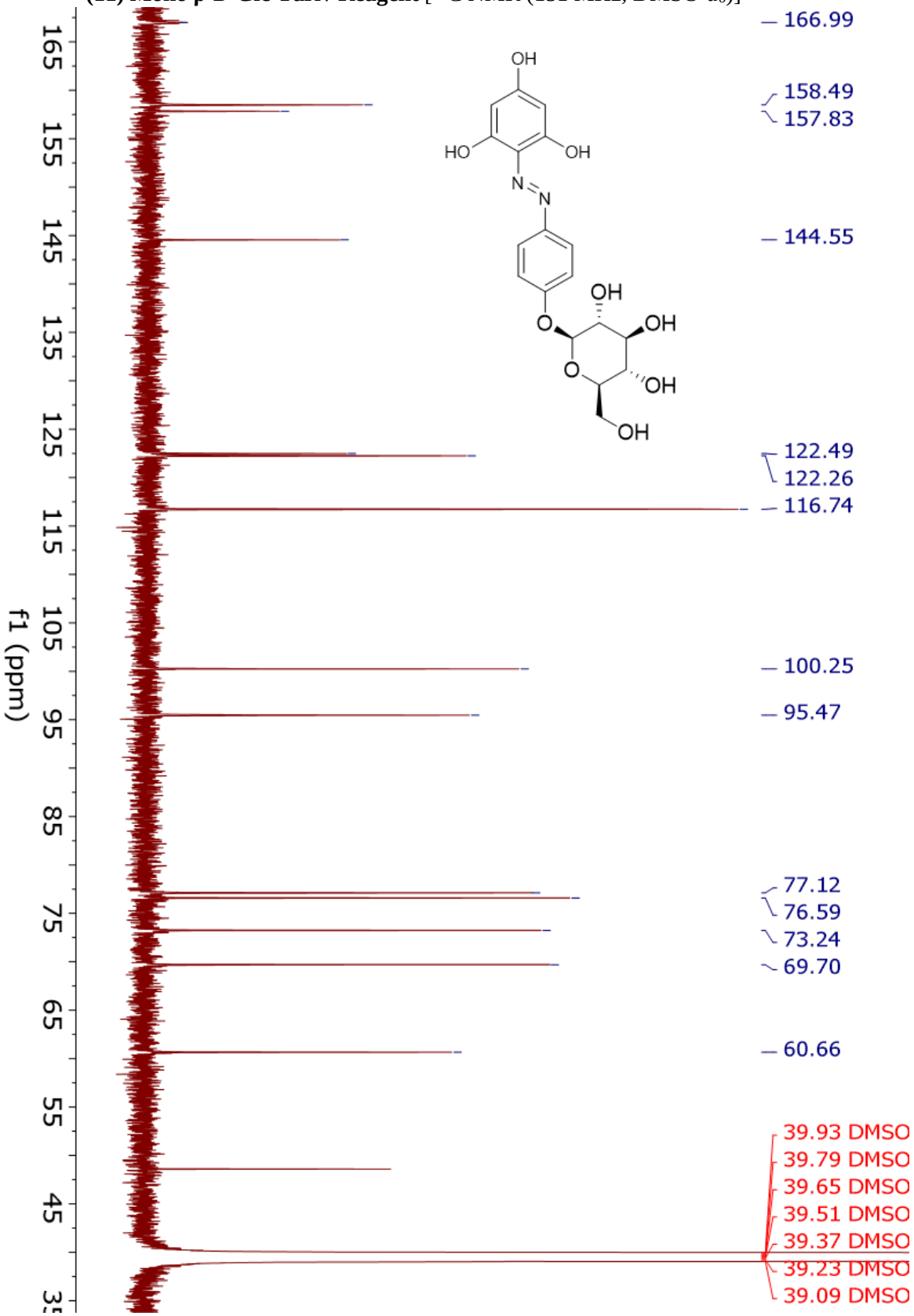

(11) Mono β-D-Glc Yariv Reagent [HSQC NMR (600 MHz, DMSO-d_6)]

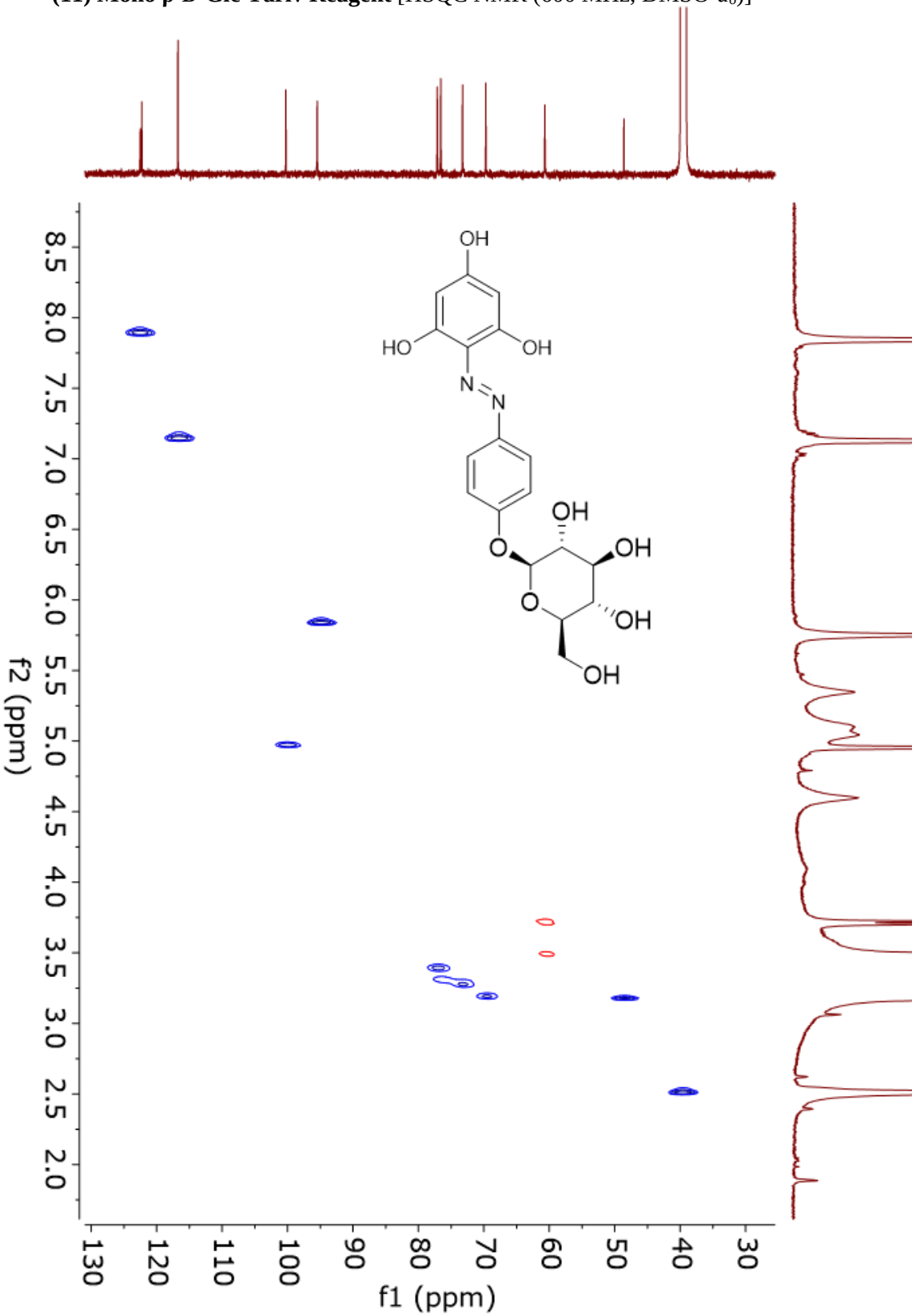

(11) Mono β-D-Glc Yariv Reagent [HMBC NMR (600 MHz, DMSO-d_6)]

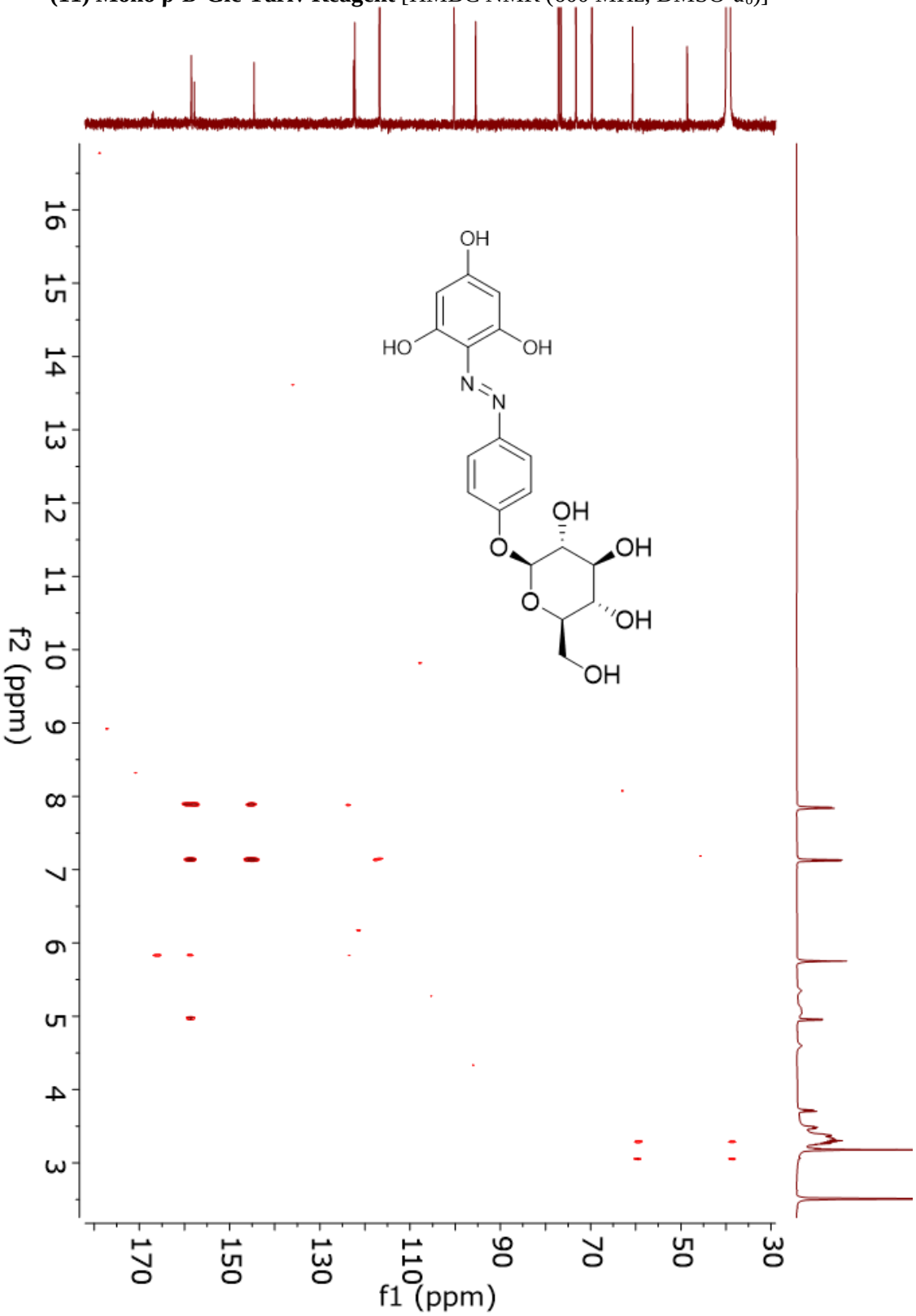

(11) Mono β-D-Glc Yariv Reagent [COSY NMR (600 MHz, DMSO-d_6)]

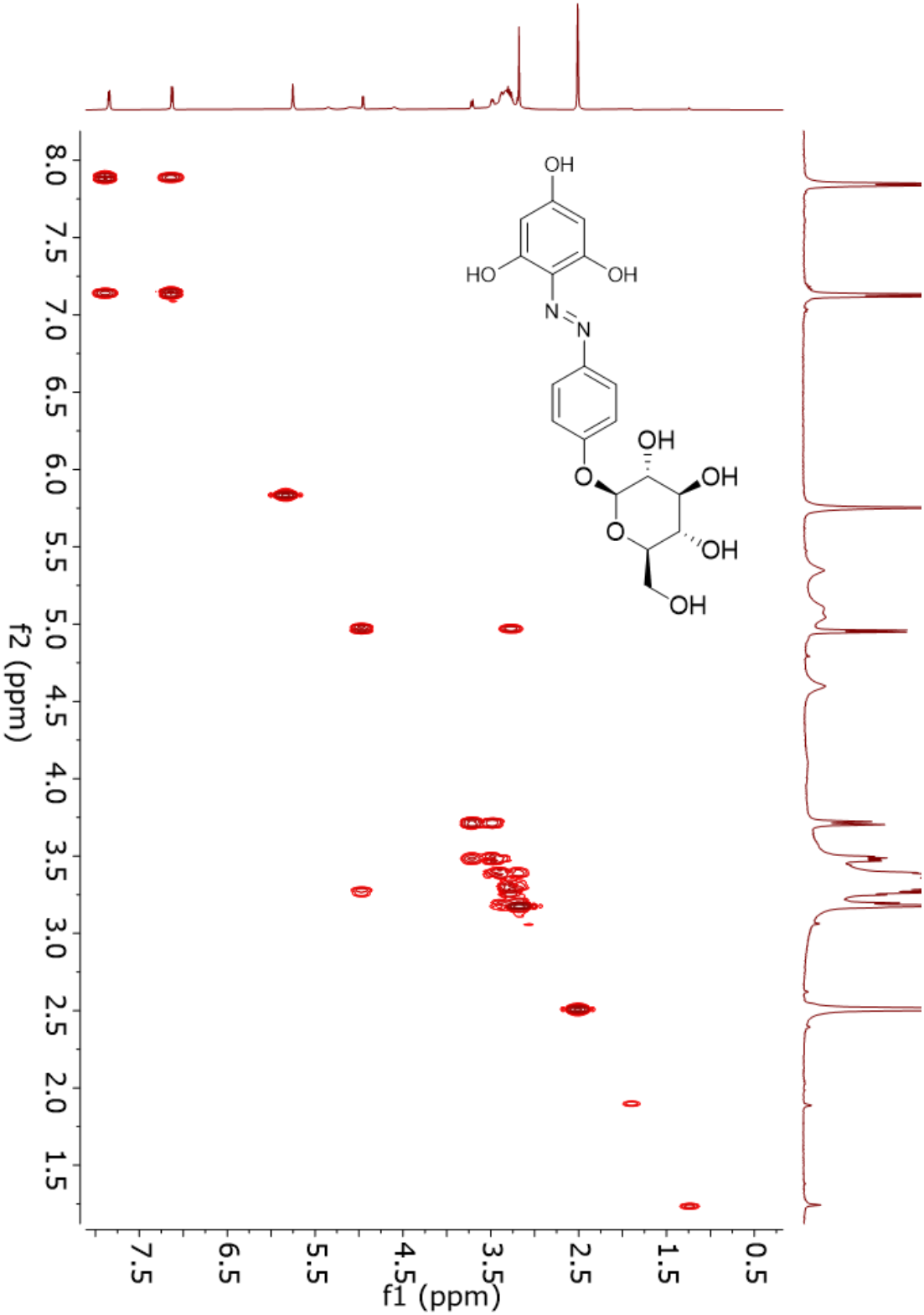

(12) Phenol Yariv Reagent [^{1}H NMR (600 MHz, DMSO-d_6)]

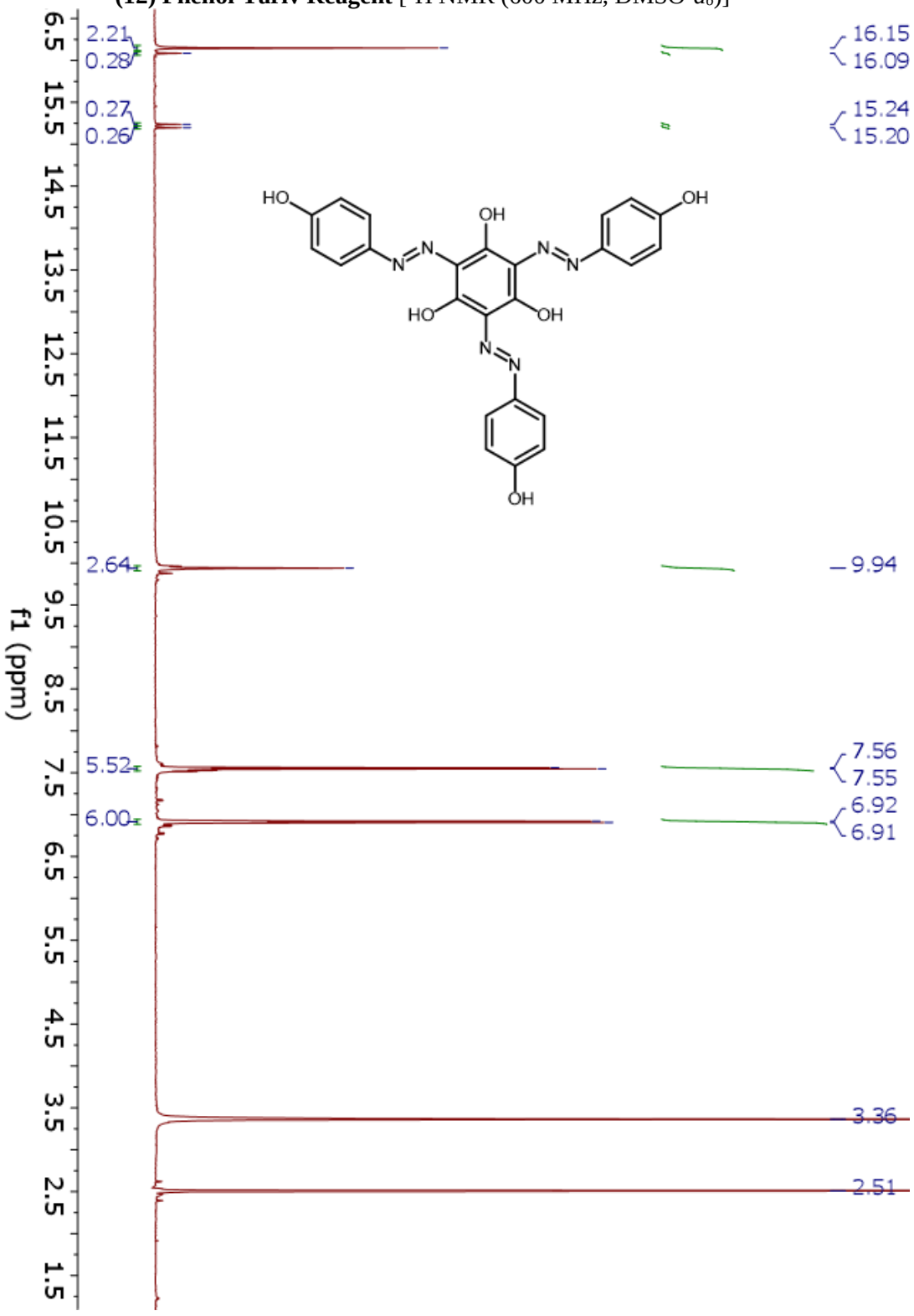

(12) Phenol Yariv Reagent [^{13}C NMR (151 MHz, DMSO-d_6)]

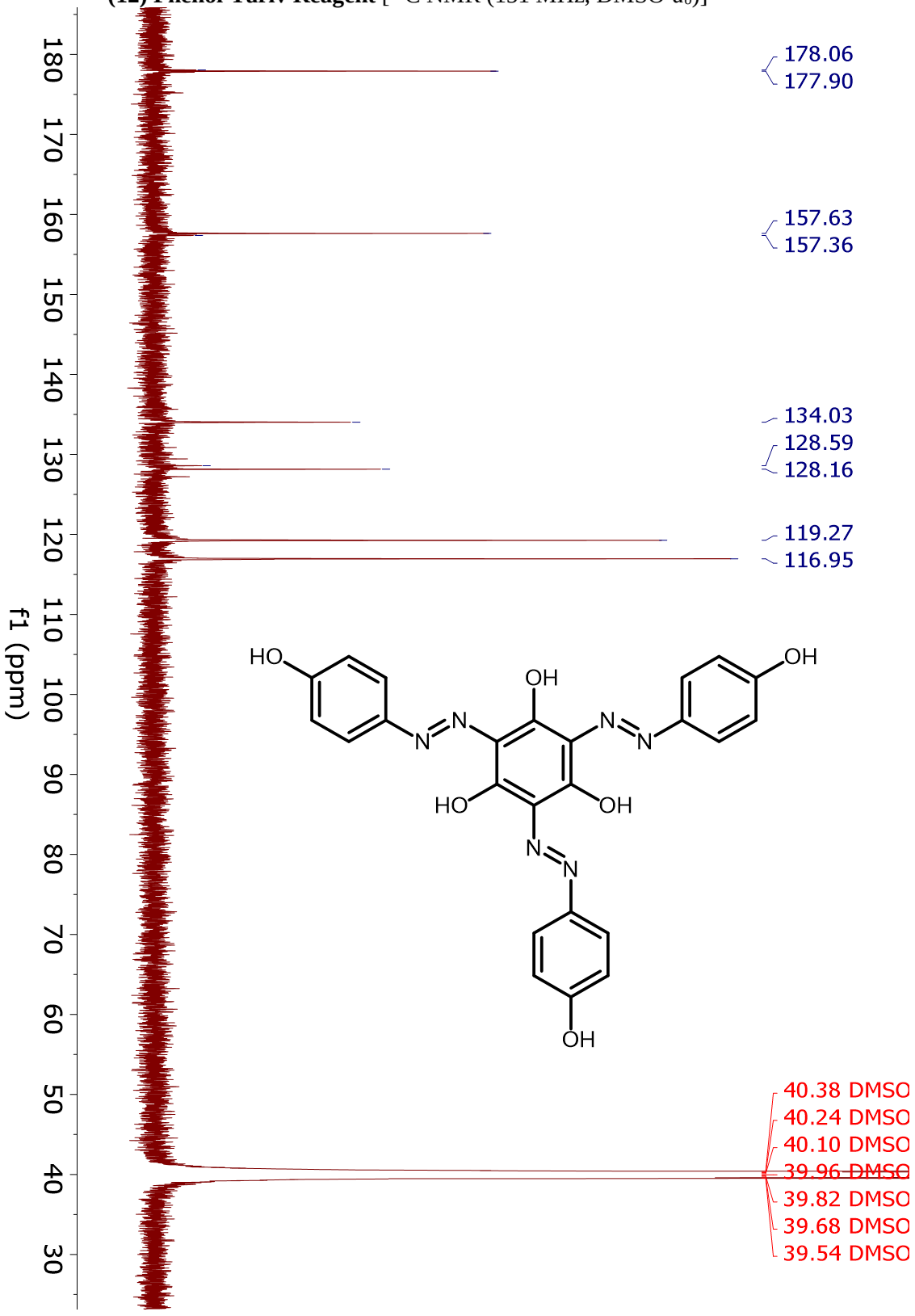

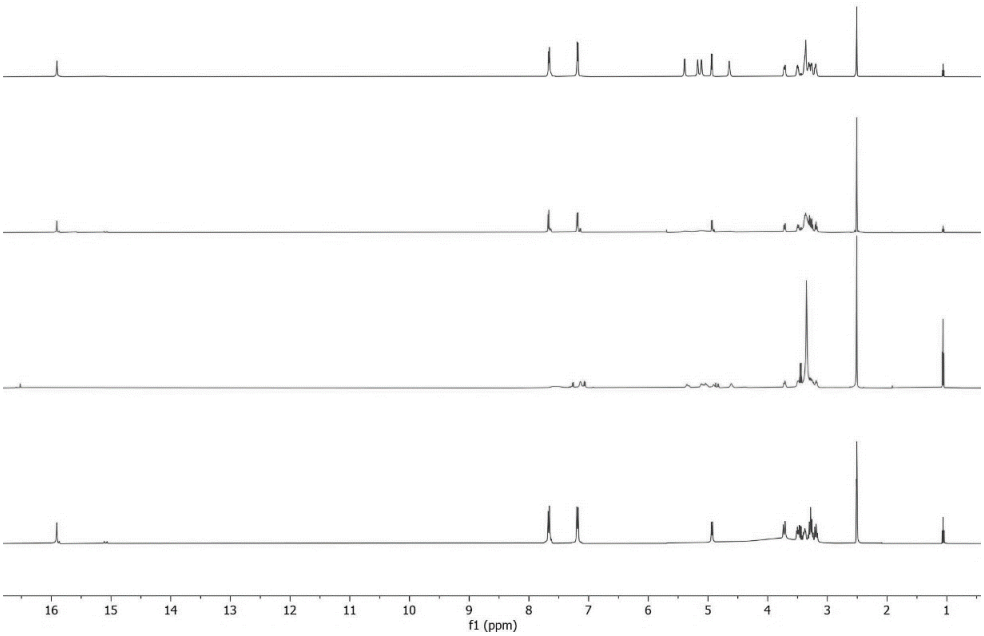

NMR spectra of the crude product from multiple batches of β-D-glucosyl Yariv reagent (**1**) syntheses (Bottom to top: Batch 1-4)

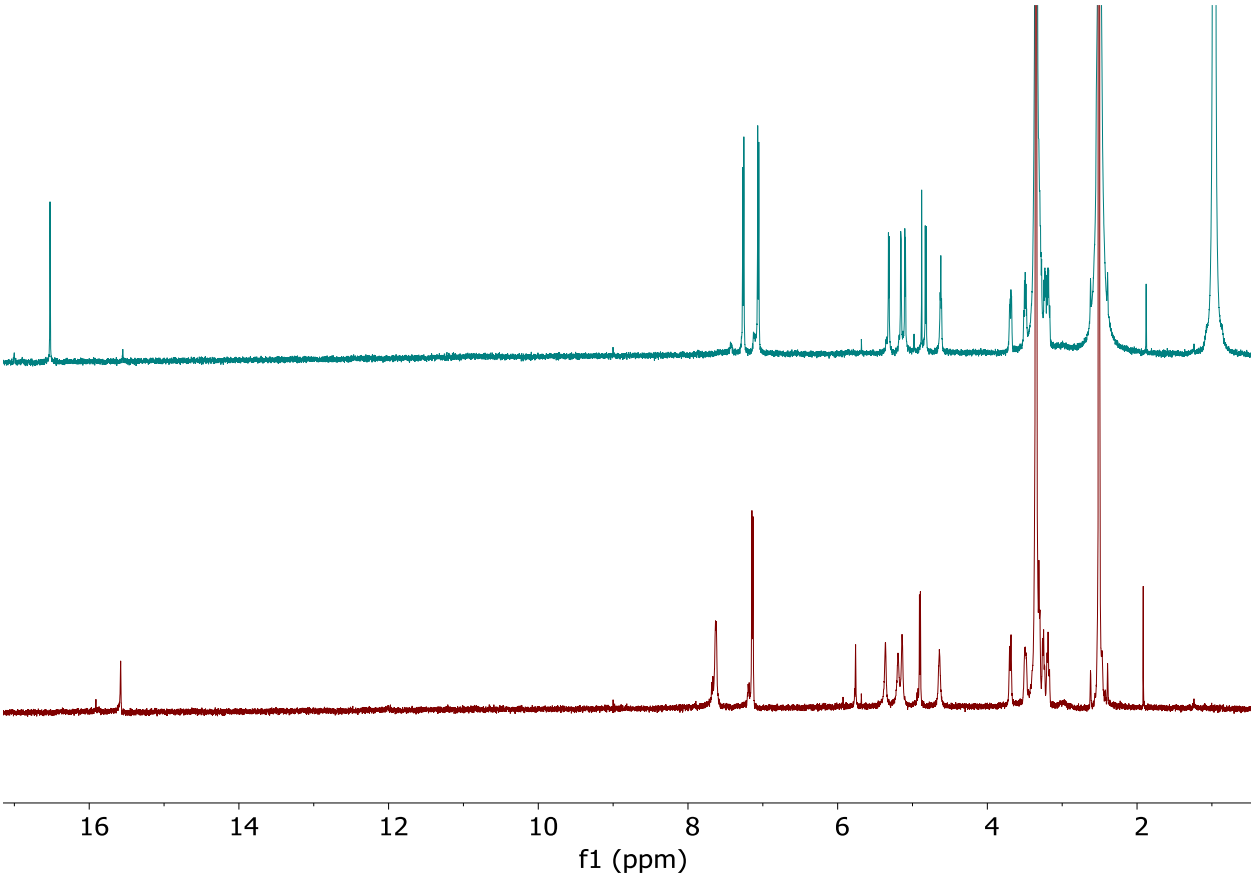

Comparison of ^{1}H NMR of Bis Azo Yariv reagent **8** before (bottom) and after (top) addition of 1 equivalent of TEA. Spectra were obtained in DMSO-d^{6}

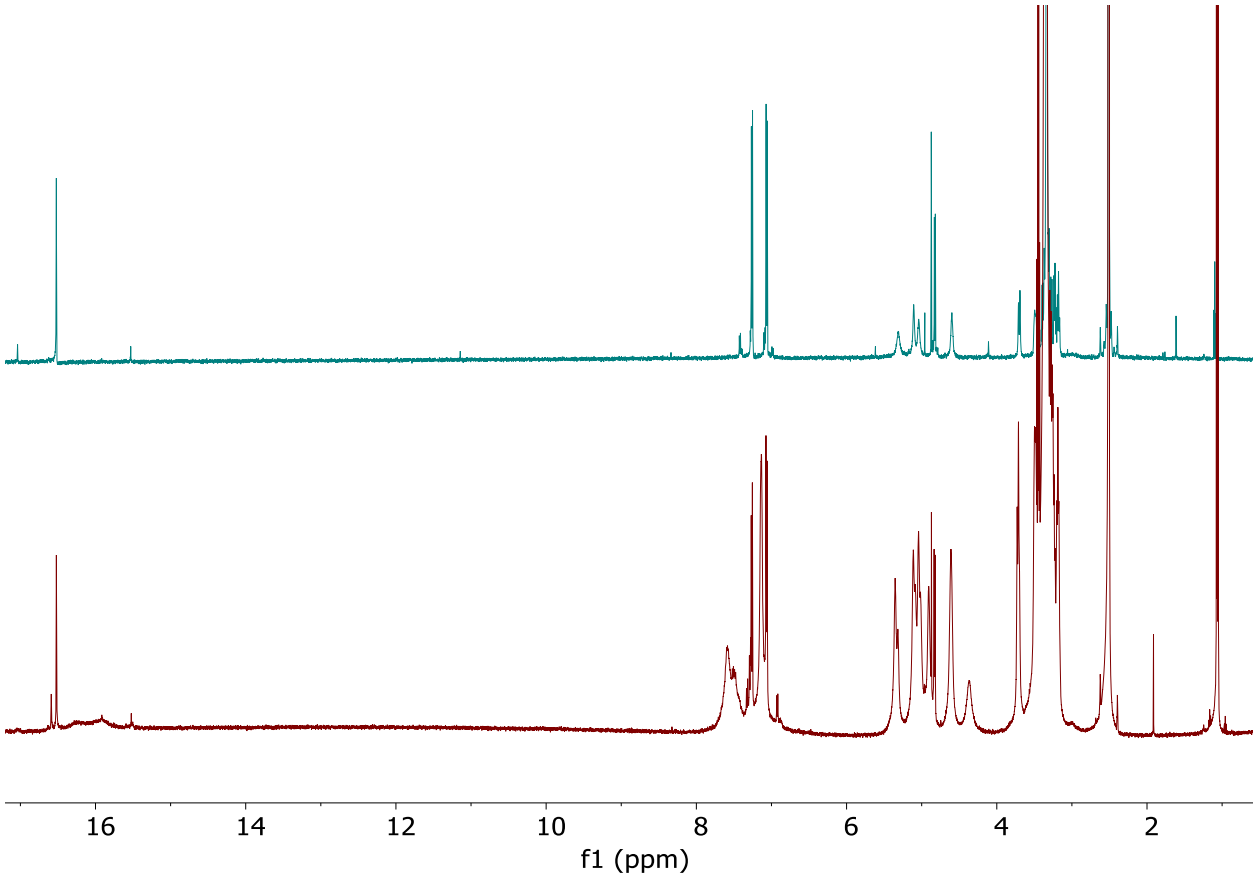

Comparison of ^{1}H NMR of Bis Azo Yariv reagent **8** after addition of 1 equivalent of TEA (top) and Tris Yariv **1** crude batch 2 (bottom). Spectra were obtained in DMSO-d^{6}

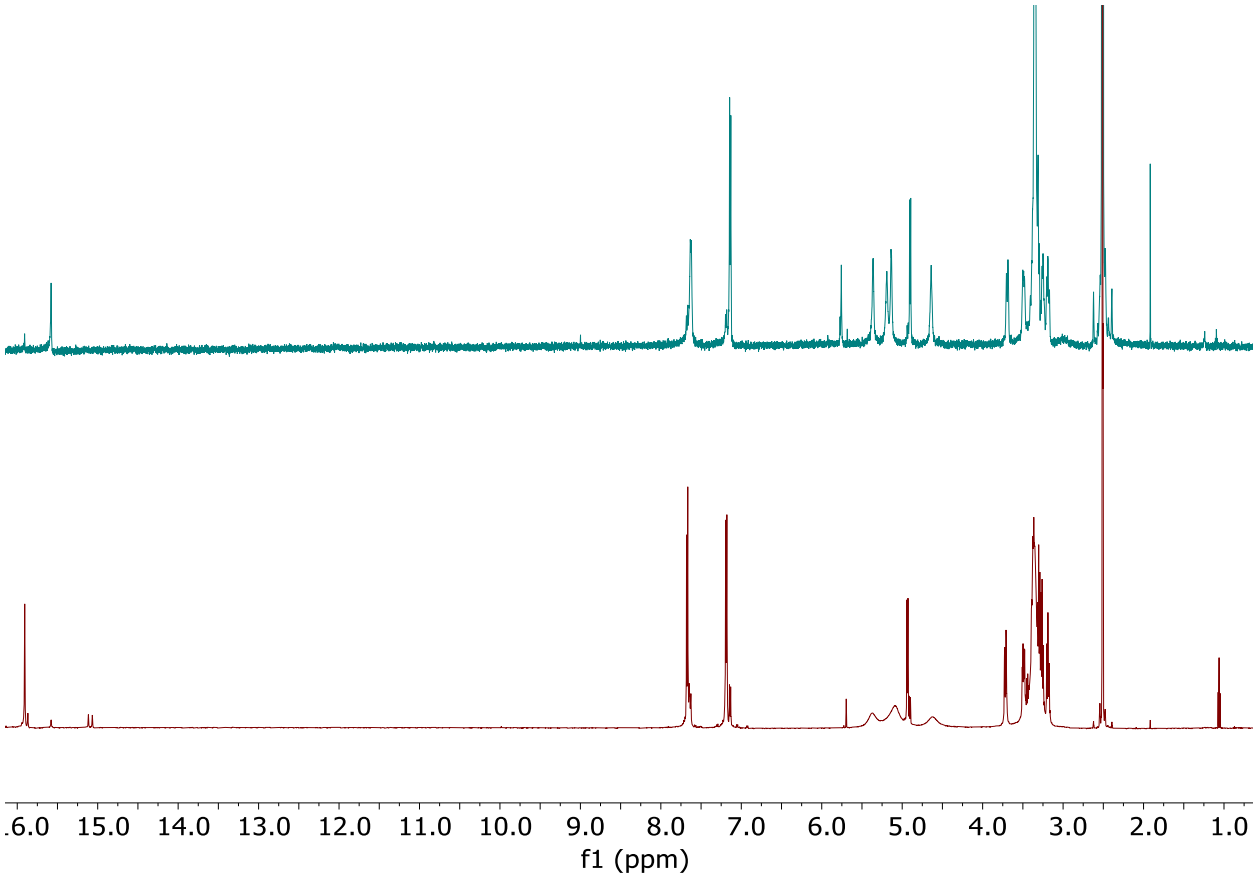

Comparison of ^{1}H NMR of Bis Azo Yariv reagent **8** (top) and Tris Yariv **1** crude batch 3. Spectra were obtained in DMSO-d^{6}

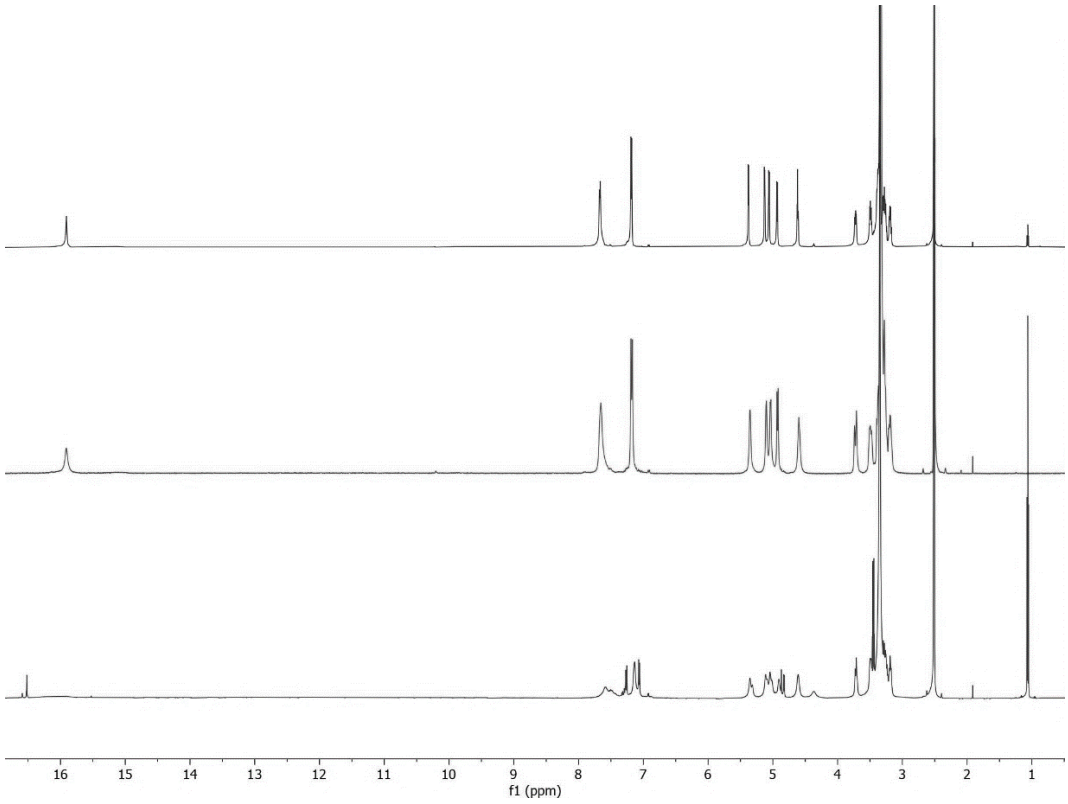

Purification of β-D-glucosyl Yariv reagent (**1**) batch 2 crude;
Bottom to top: crude, R1X, R2X

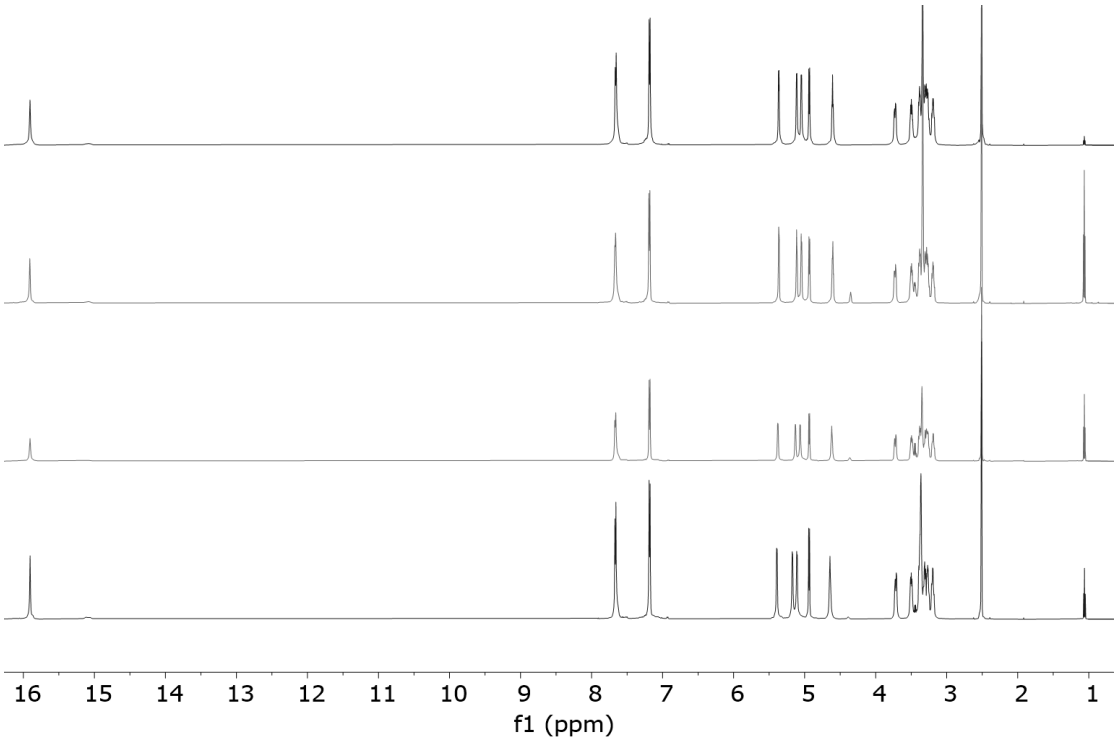

^{1}H NMR of β-D-glucosyl Yariv reagent (**1**) batch 4
From top to bottom: R2XM, R2X, R1X, crude

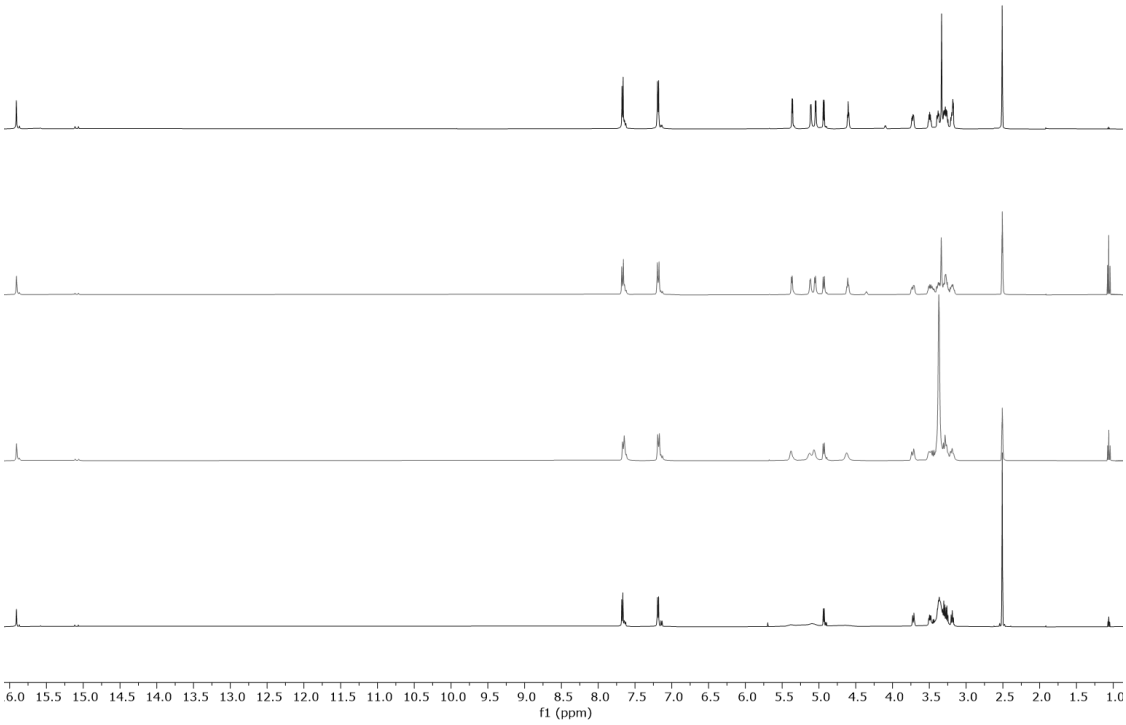

^{1}H NMR of β-D-glucosyl Yariv reagent (**1**) batch 3.
From bottom to top: crude, R1X, R2X, R2XM

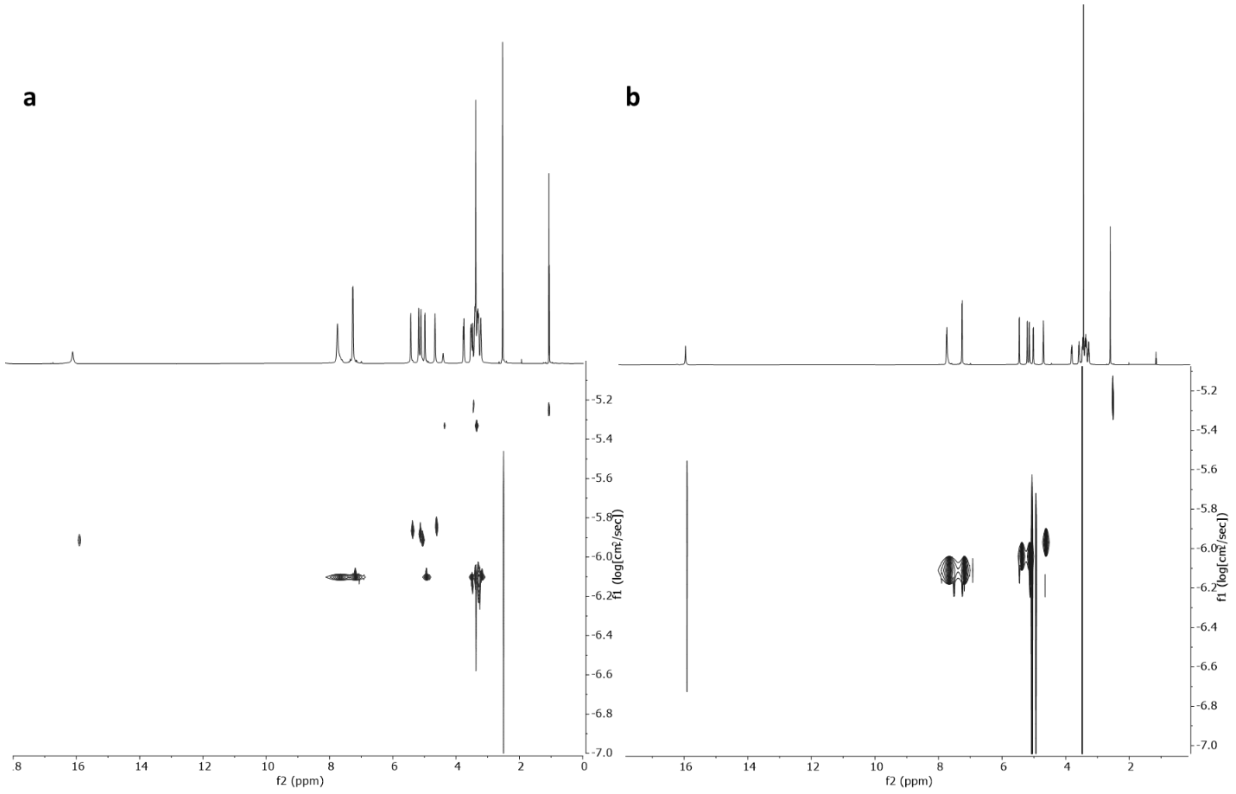

Comparison of ^{1}H NMR and DOSY NMR spectra and of a β-D-glucosyl Yariv reagent (**1**) batch 2 sample containing (a) broad -OH peaks vs sample containing (b) sharp -OH peaks

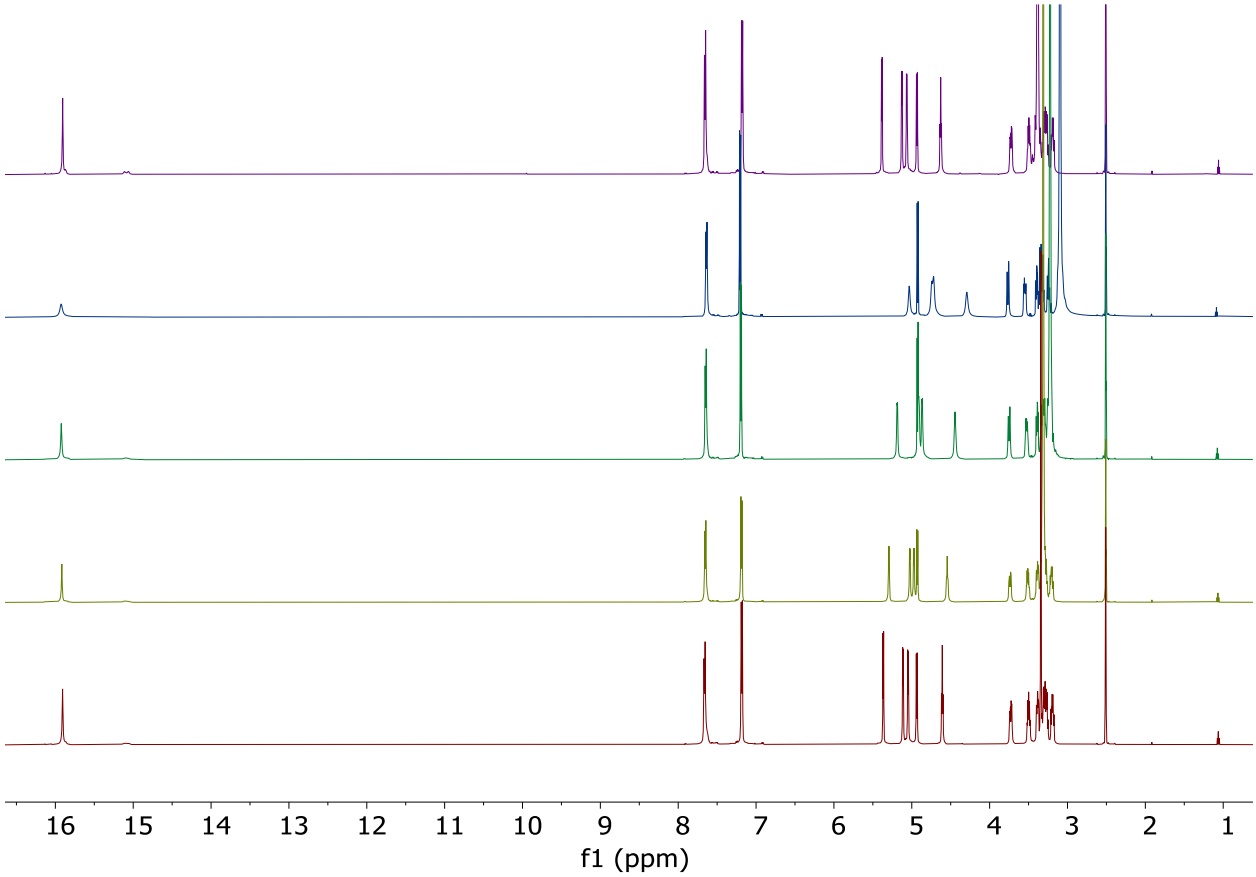

^{1}H NMR spectra of **1** at various temperatures. Bottom to top: 20, 40, 60 ,80, 20 (after cooling down)

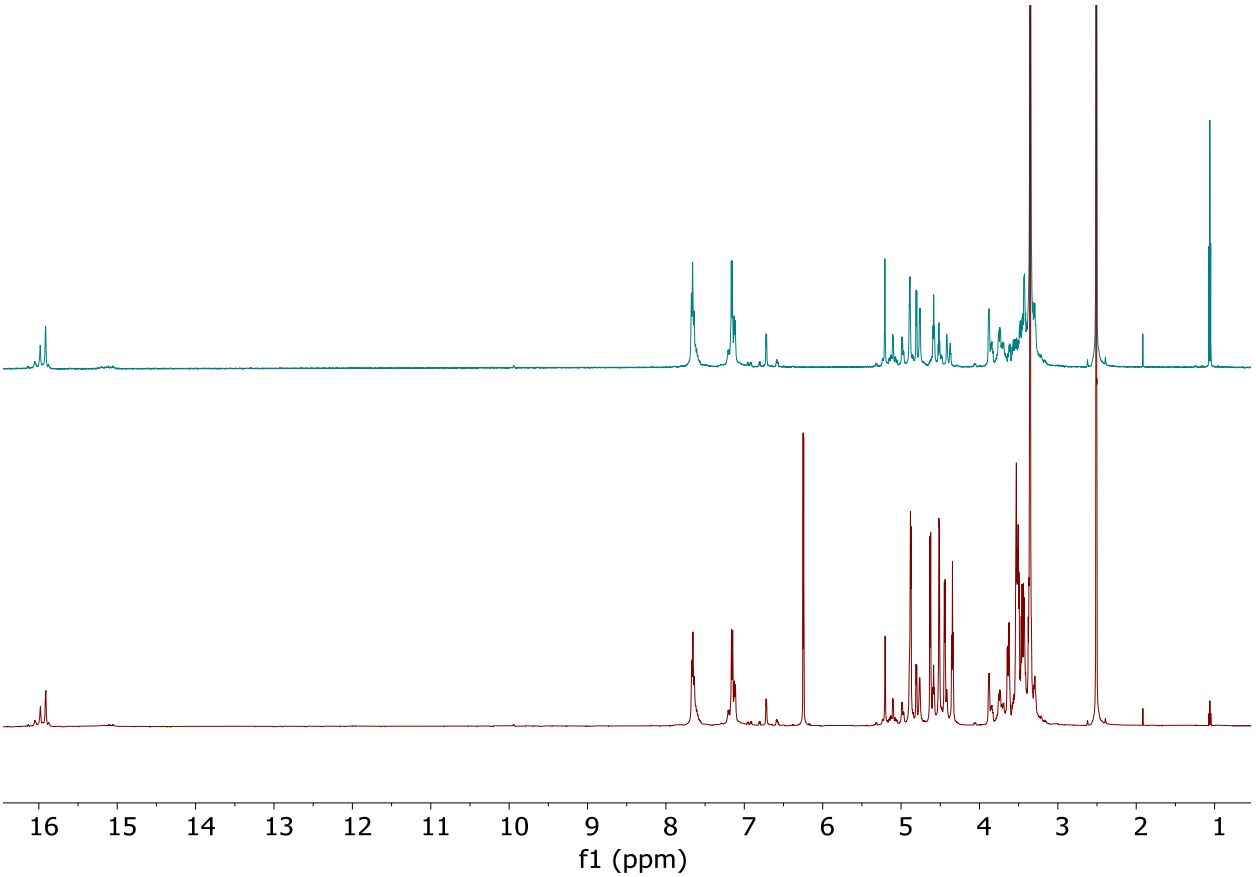

^{1}H NMR spectra of **4** before (top) and after addition of D-Mannose (bottom)

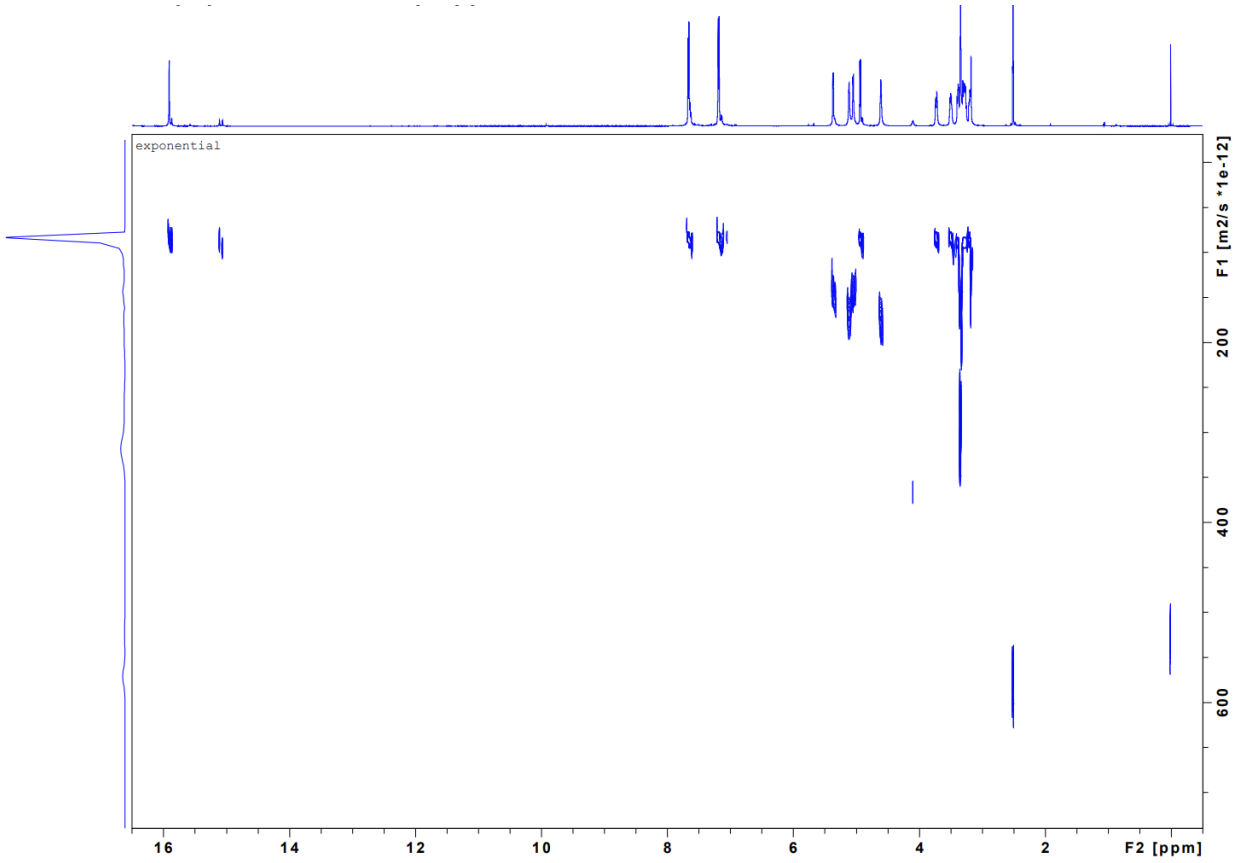

DOSY NMR of **1** (19 mM in DMSO-d_6)

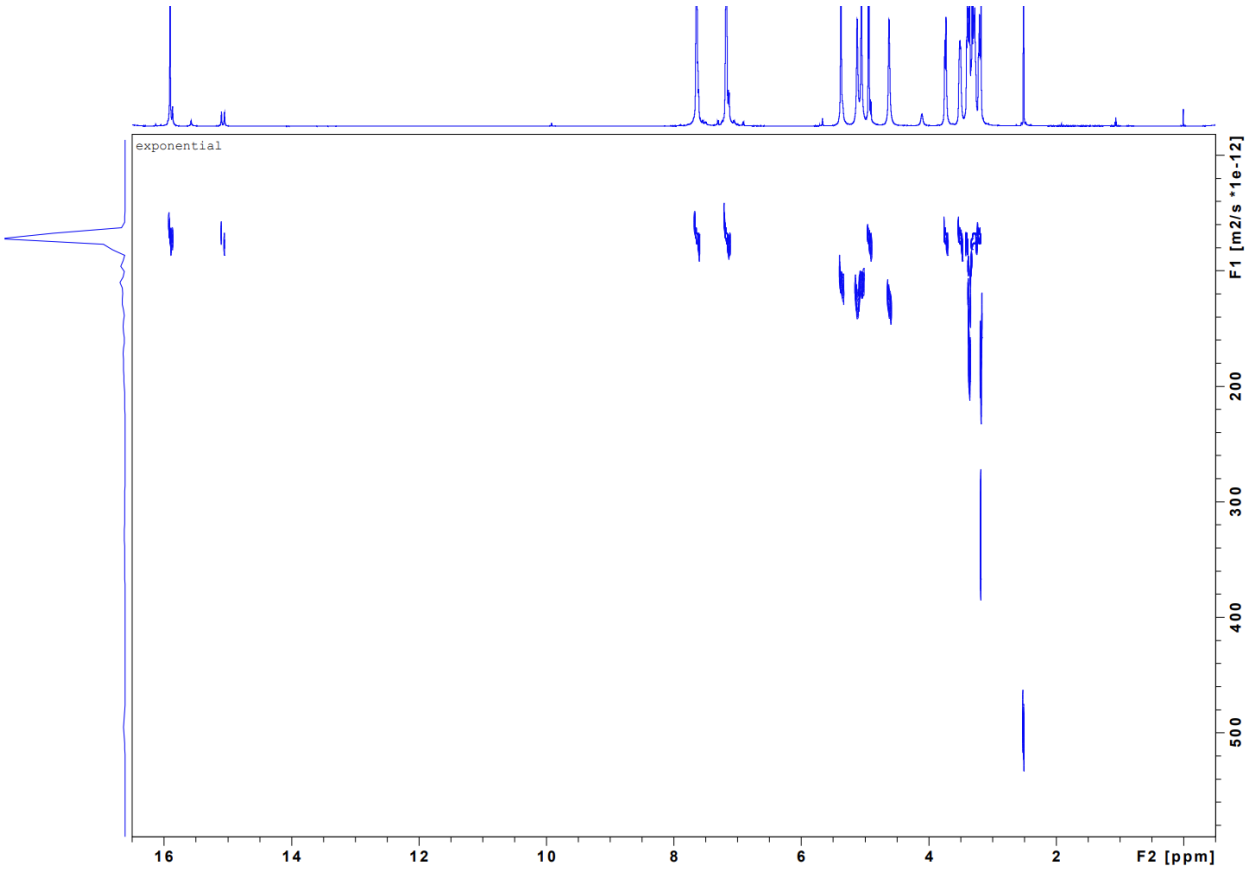

DOSY NMR of **1** (41 mM in DMSO-d_6)

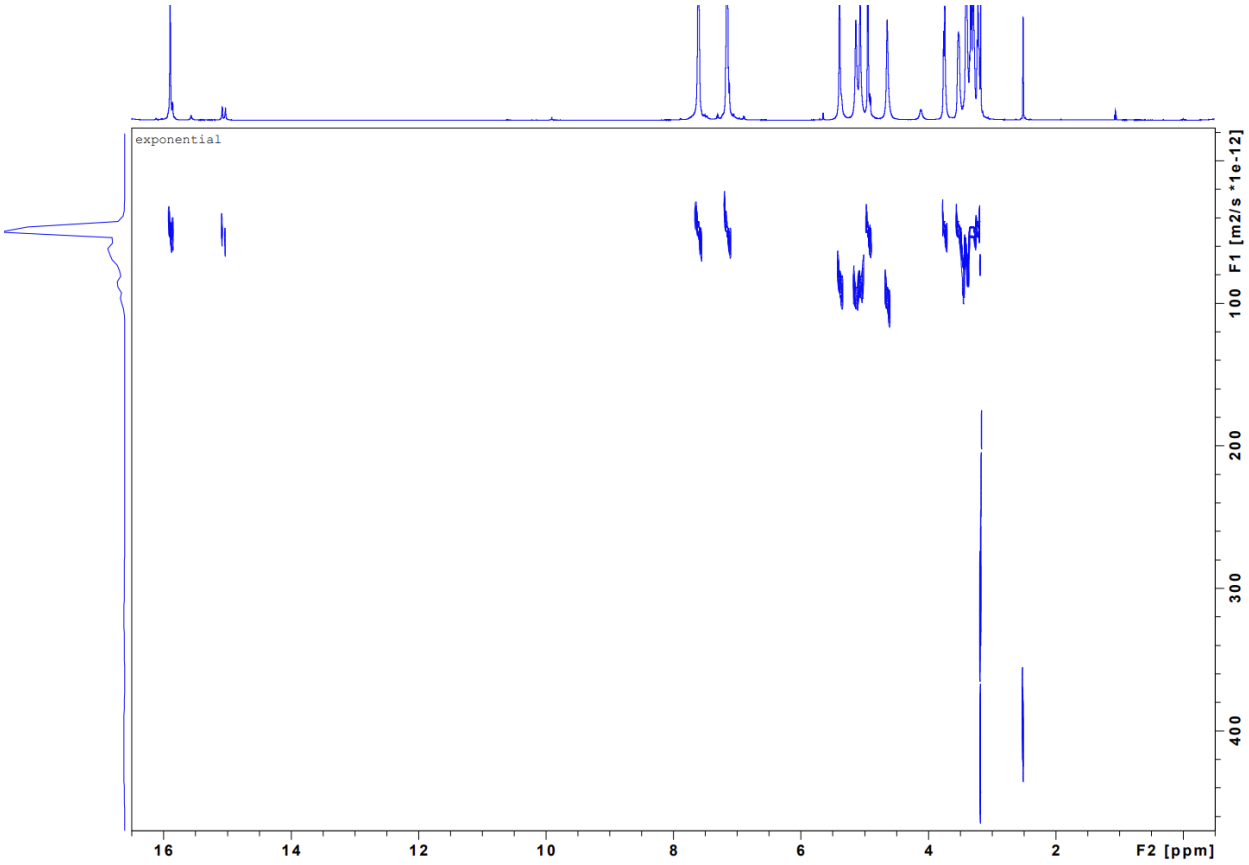

DOSY NMR of **1** (83 mM in DMSO-d_6)

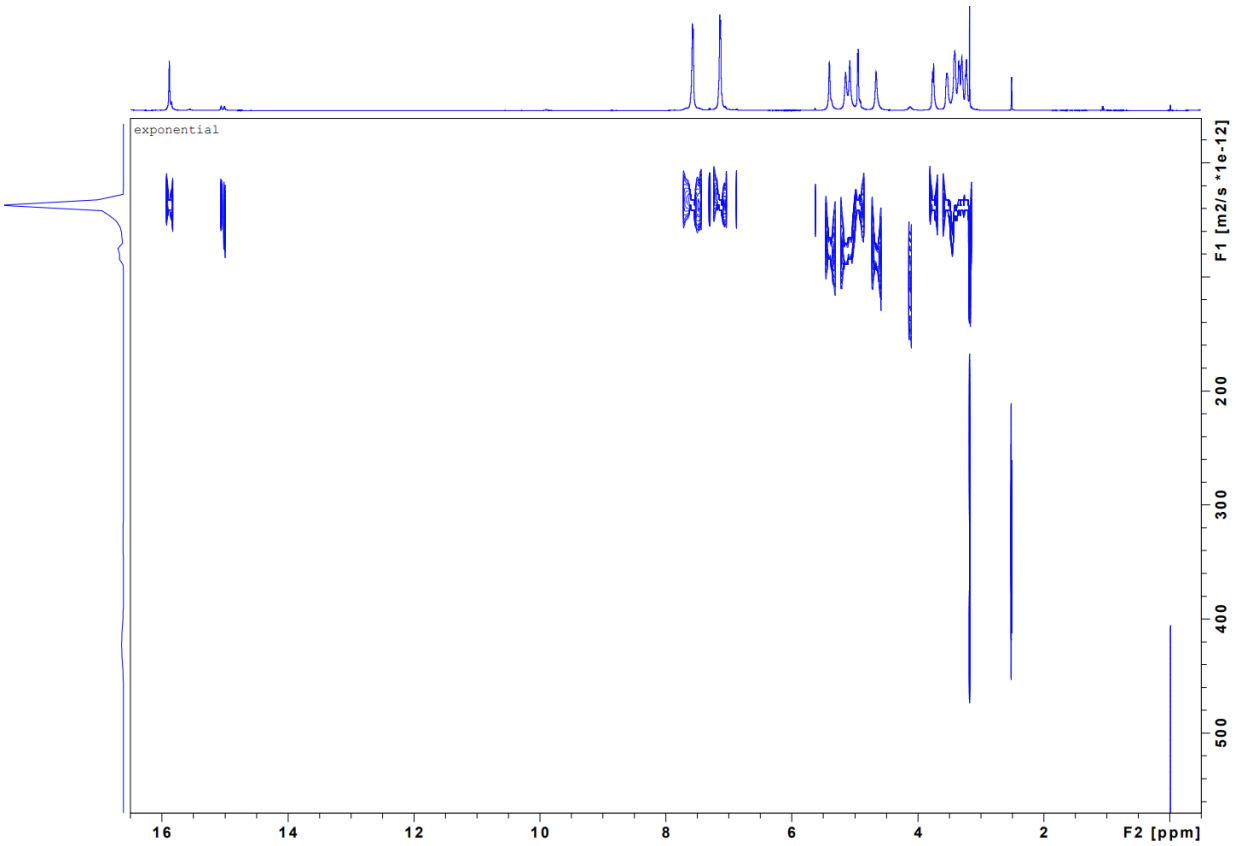

DOSY NMR of **1** (126 mM in DMSO-d_6)

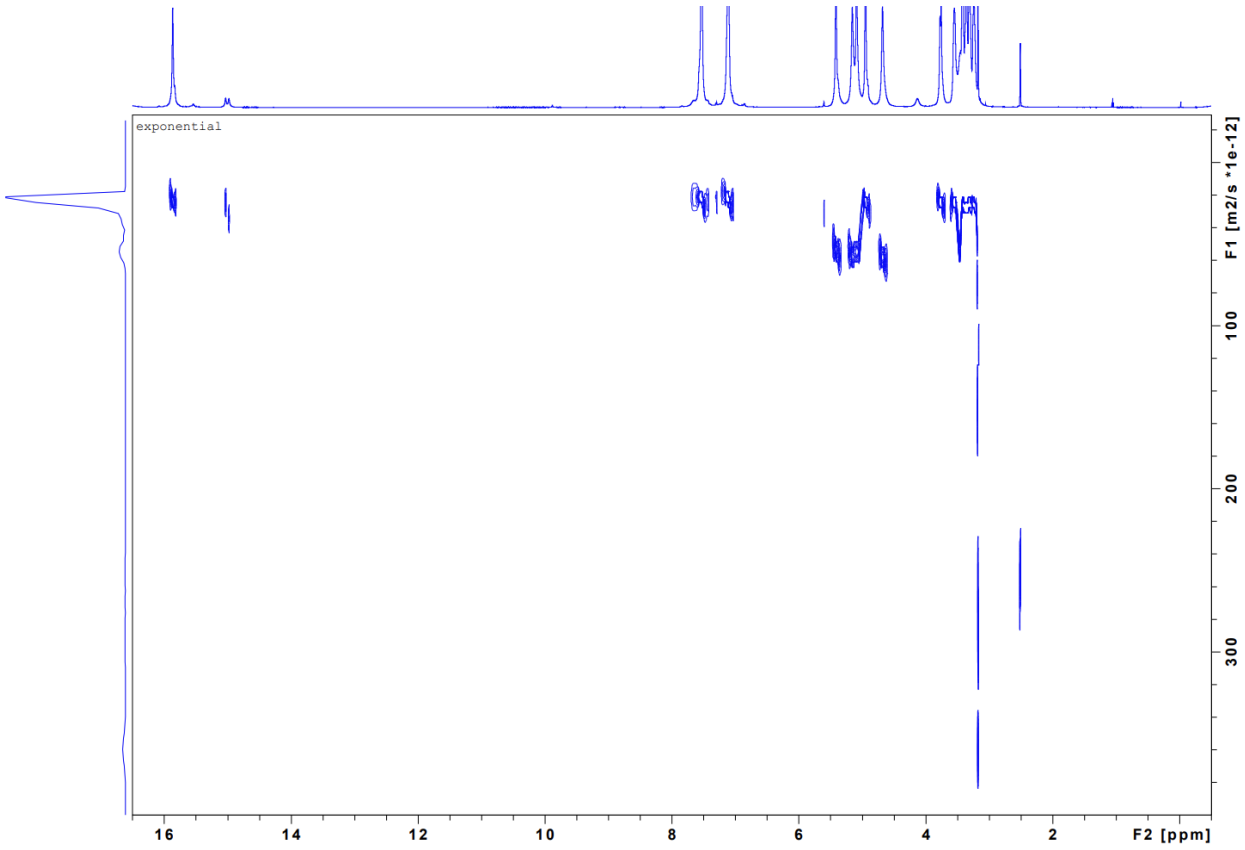

DOSY NMR of **1** (175 mM in DMSO-d_6)

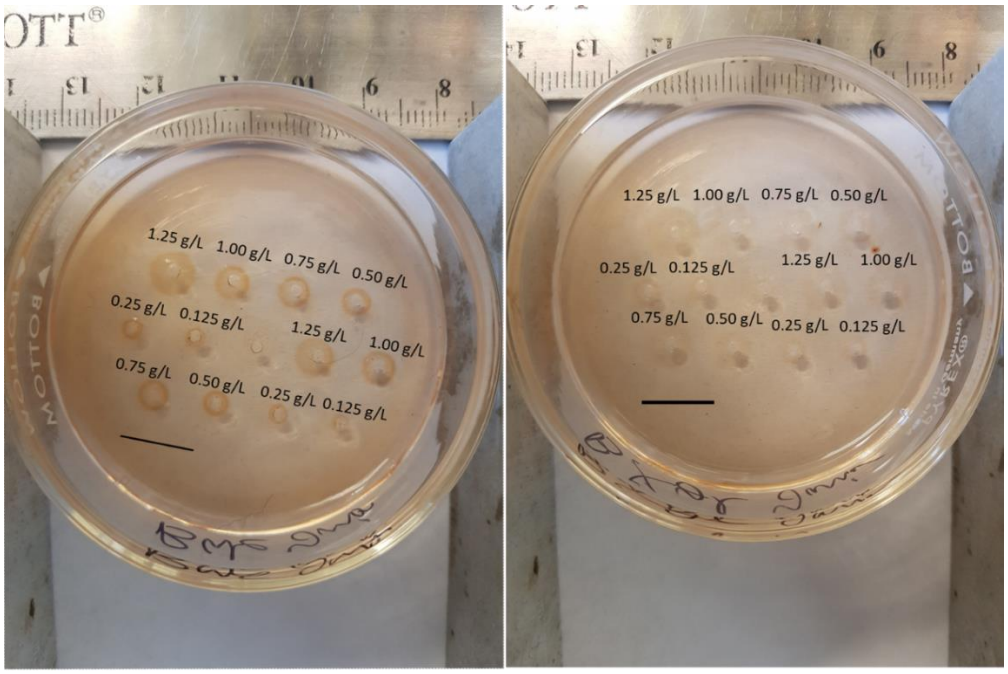

Regular gel assay containing a) β-D-Glc (**1**) b) β-D-Xyl (**3**) Yariv reagents with gum arabic AGP added to the wells. Concentration of the added AGP solutions shown above the wells Scale Bar – 1 cm

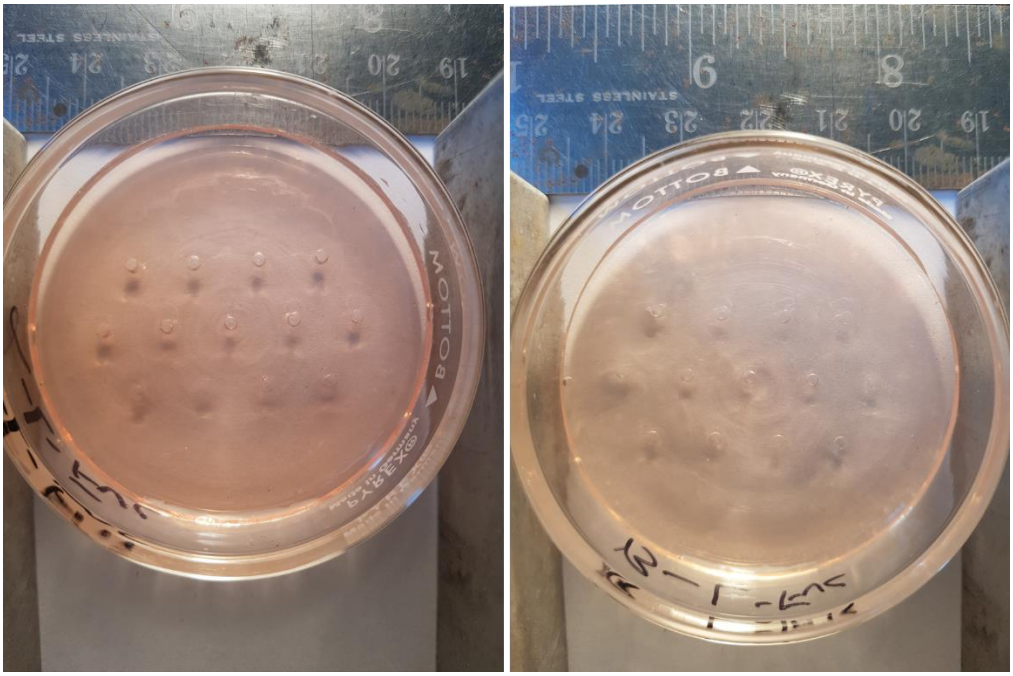

Regular gel assay containing a) α-L-Fuc (**7**) b) β-L Fuc (**6**) Yariv reagents with gum arabic AGP added to the wells

'Reverse' gel assay optimization process; βDGlc (**1**) in the wells, concentrations ranging from 2X to 8X where X=0.13 mM

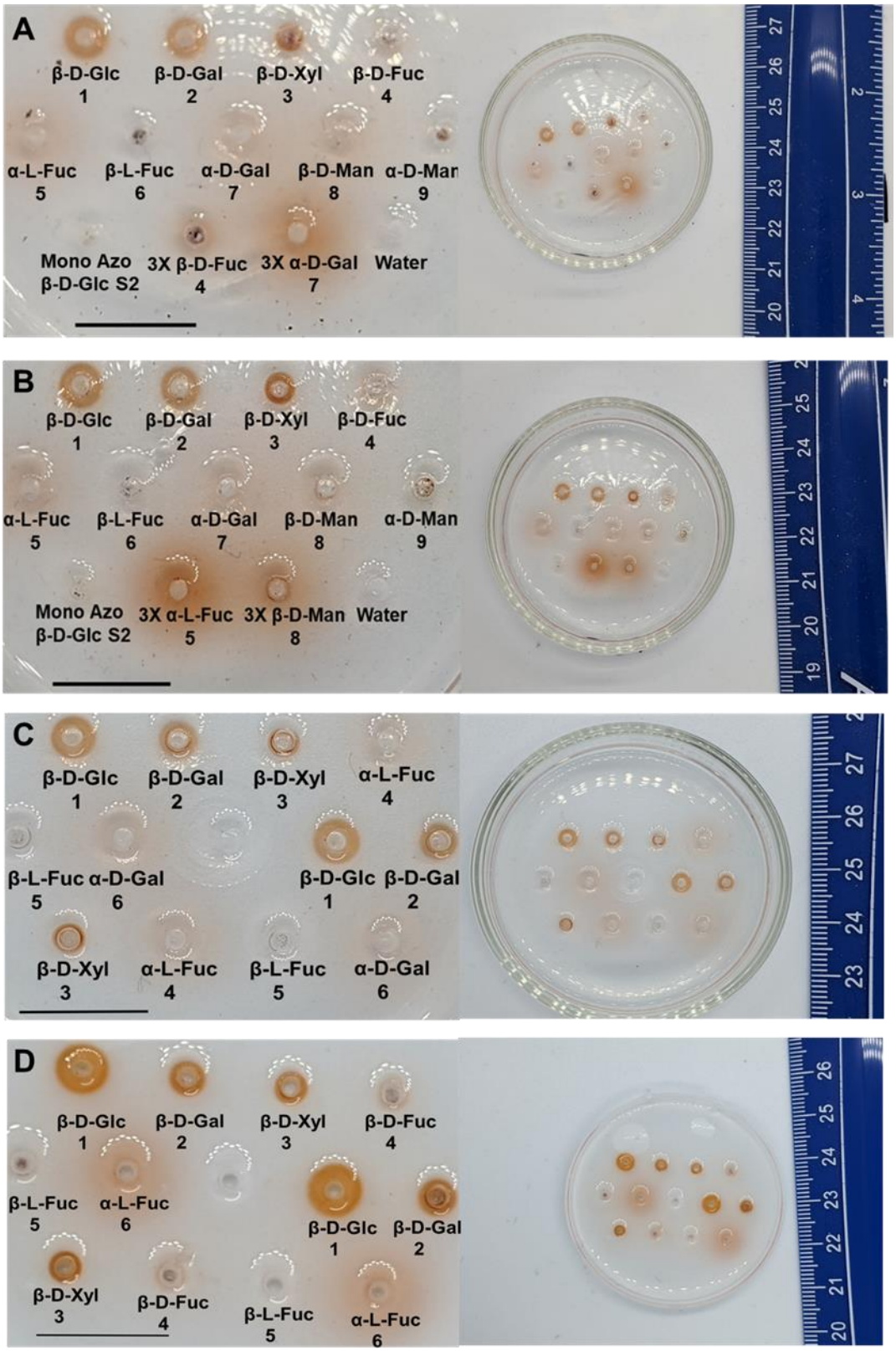

Reverse gel assay with Yariv reagents **1**-**9** and Mono Azo **11** added to individual wells. Scale bar – 1 cm

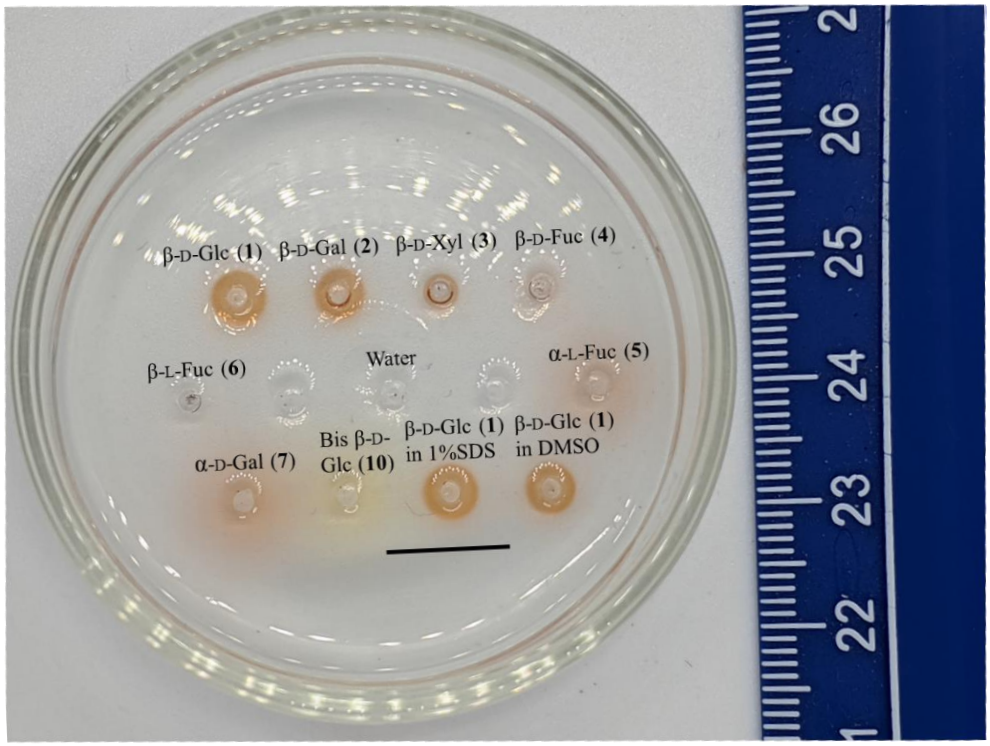

Reverse gel assay with AGP in the gel Yariv reagents added to the well; Scale bar 1- cm

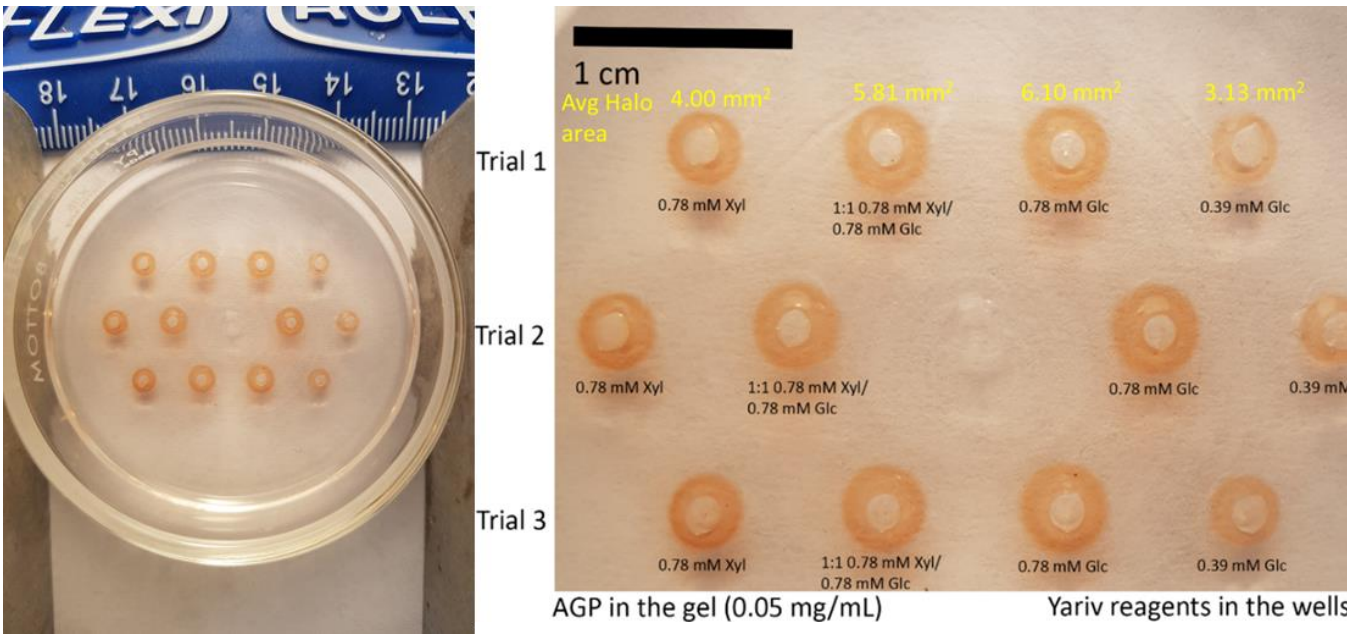

Reverse gel assay with four different kinds of samples injected into the wells

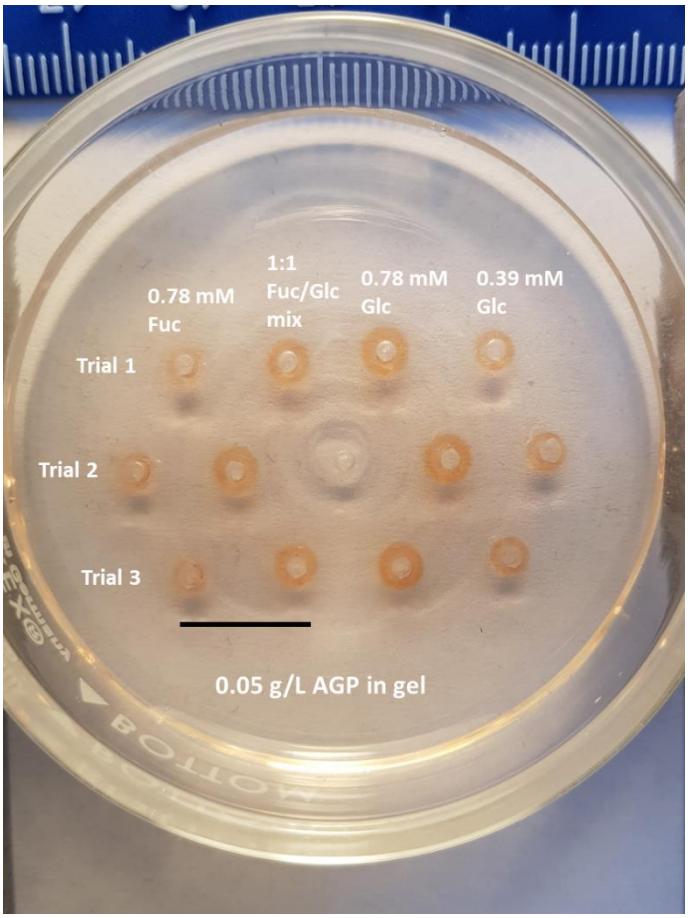

Reverse gel assay with four different kinds of samples injected into the wells. Scale Bar – 1 cm

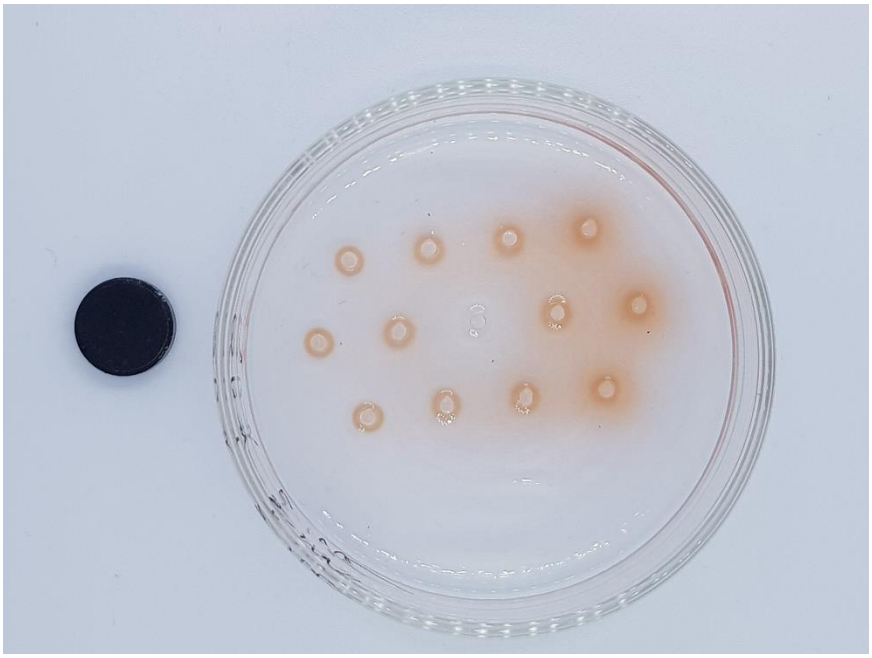
Reverse gel assay with four different kinds of samples injected into the wells Diameter of circle (Scale bar) – 1 cm